THERMODYNAMIC DATA FROM DIFFUSION COUPLES

by

Rakesh Rameshchandra Kapoor

B.Tech. METALLURGY, INDIAN INSTITUTE OF TECHNOLOGY, BOMBAY
(1985)

S.M. METALLURGY, MASSACHUSETTS INSTITUTE OF TECHNOLOGY
(1987)

SUBMITTED TO THE DEPARTMENT OF
MATERIALS SCIENCE AND ENGINEERING IN PARTIAL
FULFILLMENT OF THE REQUIREMENTS FOR THE DEGREE OF

DOCTOR OF SCIENCE in METALLURGY
at the
MASSACHUSETTS INSTITUTE OF TECHNOLOGY
September 1989

© Rakesh Rameshchandra Kapoor, 1989

The author hereby grants to MIT permission to reproduce
and to distribute copies of this thesis document in whole or part.

Signature of Author .....
Department of Materials Science and Engineering
August 11, 1989

Certified by .....
Thomas W. Eagar
Leaders for Manufacturing Professor of Materials Engineering
Thesis Supervisor

Accepted by .....
Linn W. Hobbs
Chairman Departmental Committee on Graduate Students

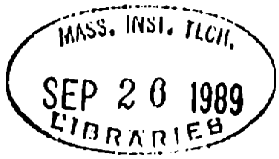

Thermodynamic Data From Diffusion Couples

by

Rakesh Rameshchandra Kapoor

Submitted to the Department of Materials Science and Engineering
on August 11, 1989 in partial fulfillment of the requirements
for the degree of
Doctor of Science in Metallurgy

ABSTRACT

The goal of this investigation was to use the information available from a binary metallic diffusion couple to compute the solution thermodynamics (activity composition relationship) for isomorphous binary metallic systems.

Using a linearly constrained, non linear least squares based algorithm that was developed during this investigation, it is now possible to compute the entire activity - composition curve for isomorphous binary metallic systems given only the interdiffusion coefficient as a function of composition (D - c data), and one additional piece of information such as the measured activity at ONE particular composition or the slope of the Henry's law line at infinite dilution.

The inherent non uniqueness of the problem leads to multiple solutions on an activity-composition diagram. The single additional piece of information (the measured activity at one composition or the Henry's law line) is used in selecting the correct solution from the set of possible solutions.

The algorithm was applied to ten isomorphous binary metallic systems for which data on the chemical interdiffusion coefficient as a function of composition was obtained from the literature. For eight out of the ten systems the algorithm located a solution that either matched the experimental data reported in the literature or exhibited a trend very similar to it. There is no experimental data for one additional system and for another system the predicted activities did not match the measured activities.

The algorithm may be easily extended to systems containing a miscibility gap.

The algorithm represents a new technique for obtaining thermodynamic data from a source that has previously never been used to generate thermodynamic information, namely a diffusion couple. It should be particularly useful for reactive and refractory metal systems for which there is currently a paucity of thermodynamic data caused by experimental difficulties. It will also check the consistency between the available data on interdiffusion coefficients and the activity data.

Thesis Supervisor : Dr. Thomas W. Eagar

Title : Leaders for Manufacturing Professor of Materials Engineering

Table of Contents

Title Page 1
Abstract 2
List of Figures 5
List of Tables 7
Acknowledgements 8

Introduction 11

Thermodynamic Data from Diffusion Couples - I 13
2.1 **Abstract** 13
2.2 **Introduction** 13
2.3 **Proposed Model** 15
2.4 **Numerical Simulations** 19
2.5 **Results And Discussion** 24
2.6 **Conclusions** 33
2.7 **Symbols** 34
2.8 **References** 35

Thermodynamic Data From Diffusion Couples - II 37
3.1 **Abstract** 37
3.2 **Introduction** 37
3.3 **Literature Review** 38
3.3.1 *Relationship between diffusivity and thermodynamics* 38
3.3.2 *Least Squares Techniques* 41
3.4 **Proposed Algorithm** 42
3.5 **Constraints On The Thermodynamic Function** $\phi(c)$ 45
3.6 **Selection Of Model Functions** 46
3.6.1 *Models for the thermodynamic term* 46
3.6.2 *Models for the function f(c)* 48
3.6.3 *Functional Model for the Interdiffusion Coefficient* 49
3.7 **Acquisition Of Interdiffusion Data** 49
3.8 **Preliminary Results** 49
3.9 **Theoretical Basis For Constrained Non Linear Least Squares** 50
3.10 **Constrained Fitting Of Diffusivity Data** 53
3.11 **Results Of Constrained Fitting** 54
3.11.1 *Obtaining a set of feasible minima* 55
3.11.2 *Selection of the Appropriate minimum* 57
3.12 **Discussion** 59
3.13 **Conclusions** 59
3.14 **Symbols** 60
3.15 **References** 62

Thermodynamic Data from Diffusion Couples - III 71
4.1 **Abstract** 71
4.2 **Introduction** 71
4.3 **Model Summary** 72
4.4 **Treatment Of Diffusion Data** 75
4.5 **Computation Results** 77
4.5.1 *CoNi system* 78
4.5.2 *CuAu system* 78
4.5.3 *PdCu system* 79
4.5.4 *CuNi system* 80

4.5.5 *PdNi system* 81
4.5.6 *AgAu system* 82
4.5.7 *PdFe system* 83
4.5.8 *AuNi system* 84
4.5.9 *NiPt system* 85
4.5.10 *NbTi system* 86
4.6 Discussion 89
4.7 Future Efforts 91
4.7.1 *Temperature variation of Activity data* 91
4.7.2 *Extensions to non isomorphous binaries* 91
4.8 Conclusions 92
4.9 Symbols 93
4.10 References 94

Improving the Calculation of Interdiffusion Coefficients 116
5.1 Abstract 116
5.2 Introduction 116
5.3 Literature Review 119
5.4 Linear Least Squares Approximation Using Splines 120
5.4.1 *Polynomial Interpolation* 120
5.4.2 *Spline Interpolation* 121
5.4.3 *Least Squares Approximation Techniques* 123
5.4.4 *Example of Spline fit* 125
5.4.5 *Software for Spline Fitting* 125
5.5 Numerical Experiments 126
5.6 Results 127
5.7 Discussion 129
5.8 Conclusions 129
5.9 Symbols 130
5.10 References 131

Conclusions 140

Future Efforts 142
7.1 Examination of other isomorphous binary systems 142
7.2 Alternate modelling functions for f(c) and $\phi(c)$ 142
7.3 Temperature Variation of Activity Data 142
7.4 Extension to systems containing several phases 142

Appendices 144
8.1 Appendix I Computed Residuals at Minimum 144
8.2 Appendix II Interdiffusivity Data 151
8.3 Appendix III Estimation of the enthalpy of solution for solid state binaries 182
8.4 Appendix IV Behavior of $(d\phi/dc)$ at terminal compositions 186
8.4.1 *Regular Solution Model* 187
8.4.2 *Henrian Solution Model* 189
8.4.3 *Conclusion* 190

Biographical Note 198

List of Figures

Figures for Paper I

Figure 1. Diffusion couple depicting two profiles 16
Figure 2. Activity-Composition-Distance Surface 18
Figure 3. Volume element highlighting relevant compositions 21
Figure 4. Outline of simulation scheme 23
Figure 5. Simulation results 25
Figure 6. Composition difference between successive profiles 26
Figure 7. Effect of rounding compositional data on curvature 28

Figures for Paper II

Figure 1. Activity coefficients for four binaries 64
Figure 2. Thermodynamic factor for five isomorphous binaries 65
Figure 3. Fitted and original diffusivity data for CoNi 66
Figure 4. Computed thermodynamic function for CoNi 67
Figure 5. Complete set of solutions for the CoNi system 68
Figure 6. Complete set of solutions for the CoNi system 69
Figure 7. Ln(gamma) as a function of mole fraction Ni 70

Figures for Paper III

Figure 1. Computed activities for the CuAu system 95
Figure 2. Ln(gamma) vs. c for the CuAu system 96
Figure 3. Computed activities for the PdCu system 97
Figure 4. Ln(gamma) vs. c for the PdCu system 98
Figure 5. Computed activities for the CuNi system 99
Figure 6. Ln(gamma) vs. c for the CuNi system 100
Figure 7. Computed activities for the PdNi system 101
Figure 8. Ln(gamma) vs. c for the PdNi system 102
Figure 9. Computed activities for the AgAu system 103
Figure 10. Ln(gamma) vs. c for the AgAu system 104
Figure 11. Computed activities for the PdFe system 105
Figure 12. Ln(gamma) vs. c for the PdFe system 106
Figure 13. Computed activities for the AuNi system 107
Figure 14. Ln(gamma) vs. for the AuNi system 108
Figure 15. Computed activities for the NiPt system 109
Figure 16. Computed thermodynamic term for the NiPt system 110

Figure 17. Computed activities for the NiPt system 111
Figure 18. Computed activities for the NbTi system 112
Figure 19. Ln(gamma) vs. c for the NbTi system 113
Figure 20. Fitted and original diffusivity data for NbTi 114
Figure 21. Fitted and original diffusivity data for NbTi 115

Figures for Paper IV

Figure 1. Raw digitized diffusivity data for the NiPt system 132
Figure 2. Least Square error vs. number of polynomial pieces 133
Figure 3. Raw and Spline fitted diffusivity data 134
Figure 5. Residual between the spline fitted and raw data 135
Figure 5. Computed diffusion profile for the AuNi system 136
Figure 6. Interdiffusion coefficient computed from profile 137
Figure 7. Diffusivity computed from noisy profile data 138
Figure 8. Diffusivity computed using noisy profile data 139

List of Tables

Table 1. Error in computed activities 28
Table I Residual at minimum for the NbTi system 87

Acknowledgements

I am thankful to my thesis advisor, Prof. T. W. Eagar, for his guidance, advice, enthusiastic encouragement, infectious optimism and friendship throughout my stay at MIT. His vision of science and engineering and his approach to research have left a permanent impression on my mind. In particular, his ability to analyze and break down complex problems into smaller and simpler portions, his persistence in seeking simple and elegant explanations for complex phenomenon as well as his insistence on quantification of all ideas and hypotheses have struck me as being worthy of emulation. He has encouraged independent and innovative thinking by setting broad goals and patiently allowing me to achieve these while making himself available for discussions and guidance. This has been backed by a well equipped and well funded laboratory wherein it has been relatively easy to convert ideas in to experiments. Finally, he has also provided ample opportunities for my overall professional growth by encouraging me to make several formal presentations, by offering several opportunities to interact with our sponsors and by providing me with the financial resources to attend several technical conferences.

I also wish to thank the faculty members on my doctoral committee, Prof. J. F. Elliott and Prof. K. C. Russell who have been very encouraging and supportive of this work. Their constructive criticism at various stages has greatly improved the quality of the final document and enhanced my appreciation for some of the subtleties involved in the treatment of thermodynamic data.

This thesis would not have been possible without the unconditional and absolute support of our sponsors, NSF, in the form of a creativity grant (Grant number 8502411-DMR) wherein we were given the freedom to first define a problem of our choice and then to solve it. A major reason for our success is the absolute freedom allowed to us by NSF. For the sake of basic research I hope more such creativity grants will be awarded to the research community in the future.

Several mathematicians have helped me improve my understanding of applied math, which was crucial for this thesis. Not all of those mentioned here were directly involved in this thesis, but I believe that their efforts have greatly contributed to the thesis. I would particularly like to thank the following people: Prof. L. N. Trefethen, MIT, for two superbly taught and enlightening courses in numerical methods, for sparing time for the several discussions pertaining to this thesis and for his general advice on numerical methods; Prof. Y. Agnon, MIT, for carefully going over the preliminary model as well as for his advice and helpful discussions; Prof. Carl de Boor, University of Wisconsin, firstly for authoring an excellent treatise on splines and secondly for his generous help in explaining and debugging some of the Fortran source code; Eric Grosse and Jack Dongarra for their efforts in setting up the NetLib facility on Internet, which proved to be a reliable source of high quality public domain software; Profs. Gill, Murray and Wright, Stanford, for authoring an excellent book on optimization and for developing the relevant portion of the NAG software which proved to be invaluable in this investigation; Dr. P. V. Prakash of the MIT Ocean Engineering Design Laboratory for initial help with splines and general advice on numerical methods.

My colleagues in the office have helped by way of discussions and general encouragement. Their friendship has also sustained me during periods when the results from this investigation were less than encouraging. For this I would like to thank Dr. Y. S. Kim, Lt. D. J. Peters, Dr. E. W. Kim, Mr. S. T. Eickhoff, Mr. R. J. Bowers, Dr. M. A. Khan, Dr. J. W. Elmer and Mr. C. Calva. Thanks are due also to Dr. C. D. Sorensen for his help in checking the preliminary model development. I would particularly like to thank Dr. M. A. Khan for his willingness and enthusiastic participation in several brainstorming sessions as well as for the several long hours that he devoted in debugging some of the source code. Dr. C. Allemand provided preliminary advice on solving coupled nonlinear equations and Mr. S. T. Eickhoff patiently read several drafts of the thesis proposal. Ms. H. Shapiro, who was initially involved with this project, was helpful in the literature review portion of this investigation. The efforts of my UROP assistant, Ms. M. Sequeira in digitizing some of the diffusivity data are also appreciated.

Dr. G. G. Krishnamurthy (Chemical Process Metallurgy Laboratory) asked insightful questions that forced me to redirect some of our efforts in more fruitful directions. In addition I am thankful to him and to Dr. I. Majid (grain boundary group) for carefully reading and checking the preliminary copy. Prof. Dilawari (mathematical modelling group) verified the physics of the preliminary model.

Mr. I. M. Puffer, who has taught me most of what I know about vacuum systems, and Mr. B. Russell were both very supportive and helpful in the welding laboratory. Mr. Mike Drooker of the Ocean Engineering Design laboratory offered extensive help on both the hardware and software aspects of setting up the MicroVAX systems on which some of the computations were carried out. Mr. L. Sudenfield in the SEM lab and Ms. L. Shaw in the surface analysis laboratory have both taught me much about the practical use of electron optical instruments. I am grateful to all of them for their time, effort and friendship.

The staff at Project Athena operations and consulting office are to be thanked for providing friendly and exhaustive assistance (both on line and over the phone) to any problems encountered in the use of the workstations or the software. I also wish to thank Ms. A. Lavin (Project Athena accounts) for setting up a software locker to house most of the software.

Finally, I would like to thank my family for their love, support and encouragement. My parents have made many sacrifices to provide us with the very best of education. They have also set very high examples for learning and for self improvement. I firmly believe that without their guidance, love, and inspiration I would not have reached this far in life.

This thesis is dedicated to my wife, Anuradha, who has cheerfully made many personal sacrifices in allowing me the freedom to pursue my education. She has throughout been, and remains, a constant source of moral support and the anchor of my life. I hope that the completion of this document brings to her as much satisfaction as it does to me.

To my wife
Anuradha

Introduction

The science of thermodynamics and an understanding of the diffusion process together provide much of the basis for the current understanding of materials. Hence there is a large demand for basic data in both fields. This is particularly true for the newer classes of materials which are already in use but for which basic data is still lacking. For some of these materials it is difficult to conduct conventional experiments due to the high temperatures involved or the extreme reactivity of the materials. Novel techniques must therefore be developed that will permit estimation of basic thermodynamic parameters by exploiting available data on other physical quantities. Such techniques, if developed, would provide new sources for thermodynamic data. In addition they would check the consistency of currently available data on the physical quantity with the available thermodynamic data.

The main premise of this investigation was that information on the free energies of mixing must be implicitly contained in a diffusion couple since diffusion occurs under the influence of a chemical potential gradient. The thermodynamicist who experimentally obtains activity data for a particular system and the transport phenomenologist who experimentally obtains interdiffusivity data for the same system are both fundamentally perturbing the identical system (same set of atoms and lattices) in making their measurements. Further, since the diffusion process involves mixing of two materials it stands to reason that the two experiments (measurement of activities and interdiffusivities) must be interrelated. This is more transparent when one considers that the interdiffusion coefficient is determined in part by the thermodynamics of the solution.

This thesis has been organized as four papers ready for submission to a journal. It is recommended that papers one through three be read serially. Paper four is independent of the others.

Paper one describes the preliminary efforts that analyzed the dynamic behavior of a diffusion profile and confirmed that activity data was implicitly contained in a diffusion couple. However the preliminary efforts also indicated that it was more fruitful to seek activity data by modelling the variation of the interdiffusion coefficient as a function of composition instead of analyzing a diffusion profile.

Paper two describes the linearly constrained non linear least squares based model that was developed to compute activity data given interdiffusivity data whereas paper three applies the model to ten isomorphous binary systems and compares the computed activities for each system with the experimentally measured activities obtained from the literature.

Paper four presents least squares spline interpolation as a reliable and reproducible technique for estimation of the slope of a diffusion profile and for filtering out the noise in the profile data. Use of splines is expected to reduce the numerical errors associated with the calculation of interdiffusion coefficients from raw diffusion profile data using the Boltzmann Matano treatment.

Thermodynamic Data from Diffusion Couples - I

2.1 ABSTRACT

A model aimed at computing activity-composition data by analyzing two successive diffusion profiles for isomorphous binary metals is presented. Simple numerical simulations were performed to check model validity on hypothetical alloy systems that possessed a constant diffusivity but variable chemical potential - composition relationships. Results indicate that it is possible to compute activity data if the mobility function is known a priori. Extension of the model, to real alloy systems, wherein the mobility and chemical potential are coupled, is not possible since in a real system the number of unknowns exceeds the available information. Hence in real systems one must resort to least squares techniques that do not provide analytical solutions.

2.2 INTRODUCTION

The science of thermodynamics and an understanding of the diffusion process together provide much of the basis for the current understanding of metallurgy. Hence, there is a large demand for basic data in these fields. Traditionally, metallurgical thermodynamic data has been obtained using calorimetric techniques, wet chemical methods, vapor pressure measurements or electromotive force measurements[1,2,3] while solid state diffusion data has been generated from diffusion couples[4,5].

The Fickian laws of diffusion relate the flux and depletion rate of a diffusing species to the slope and curvature of the diffusion profile. Einstein later clarified that diffusion was in fact driven by gradients in chemical potential. Thus the Nerst-Einstein relationship which relates mobility and diffusivity firmly established the link between thermodynamics and diffusion[4]. This was experimentally

demonstrated by Darken in his well known uphill diffusion experiment[6]. Other investigators have related the chemical potential to elements of the diffusion matrix[7-11]. Excellent reviews covering the literature on solid state diffusion and the associated phenomenological theory of irreversible processes are available[11-21]. However, despite the understanding that diffusion is driven by chemical potential gradients, it is the Fickian description of diffusion (comprising of diffusivities and concentration gradients) that is more popular. One reason for this is that concentrations are relatively straightforward to measure experimentally whereas chemical potentials are not.

Since diffusion is driven by chemical potential gradients, it is reasonable to expect that the diffusion profile contains information about chemical potentials. This is the main premise of the current investigation, which is aimed at obtaining the free energies of mixing (chemical potentials) from diffusion experiments. For the most part the investigation will focus on isomorphous binary systems and later attempt to extend the treatment to binary systems containing two phases.

This is the first of four papers covering this investigation. This paper describes the preliminary efforts which resulted in the development of a simple mathematical model that was intended to permit one to back out chemical potentials by using the composition-distance data from two diffusion profiles. Numerical simulations conducted on hypothetical alloy systems to check the validity of the model confirmed the hypothesis that activity data could be obtained from consideration of the diffusion profiles. However, it will be shown that although this model was consistent with the thermodynamics of real alloy systems, it could not be used to calculate activities in a real system since the total number of unknowns constituting the model exceeded the available equations. This motivated the development of a least squares based algorithm that permits one to compute the activity-composition relationship for a real alloy given the variation of the interdiffusion coefficient with composition. The least squares based algorithm is described in the second paper. The third paper presents the results of the least squares based algorithm as applied to ten isomorphous

binary systems. The interdiffusion data for these ten systems was obtained from the literature. The fourth paper discusses least squares spline interpolation techniques and their application in computing the interdiffusion coefficient by use of the Boltzmann-Matano treatment. It will be shown that spline interpolation techniques can lead to significant improvements in the accuracy of the diffusivities computed using the Boltzmann-Matano treatment.

Thus the overall thrust of this work is the establishment of new techniques for obtaining thermodynamic data by manipulating diffusion data. The main advantage of such techniques would be the ability to obtain thermodynamic data for metallic systems where it is not feasible to conduct conventional thermodynamic experiments. Examples would include reactive and refractory metal systems. Apart from providing new data, these techniques will also aid in checking the accuracy and consistency of the data already available. Finally it is hoped that this study will lead to a better appreciation of the link between thermodynamics and solid state diffusion.

2.3 PROPOSED MODEL

The proposed model is based on the following assumptions: (i) The system is assumed to be isothermal; (ii) The density is assumed to be constant across the entire range of composition, i.e. the volume change on mixing is negligible; (iii) Vacancies are assumed to be in local thermal equilibrium.

The diffusional process is governed by two factors, the driving forces (chemical potential gradients, concentration gradients) and the coefficients (mobility, diffusivity). A complete range of compositions from 0% B to 100% B is found in an infinite diffusion couple between two metals A and B. The current problem involves obtaining the activity of B in A over this entire range of compositions. Since one desires information on the forces (chemical potentials) that drive the diffusion profile, one needs to observe the dynamic behavior of this profile by perturbing it. In other words one needs to allow the system to diffuse for a further time (dt) and

then to consider both profiles, the one at t and the one at t + dt, simultaneously. This is outlined in figure 1, which also depicts a typical volume element V_1, which is "dx" in extent.

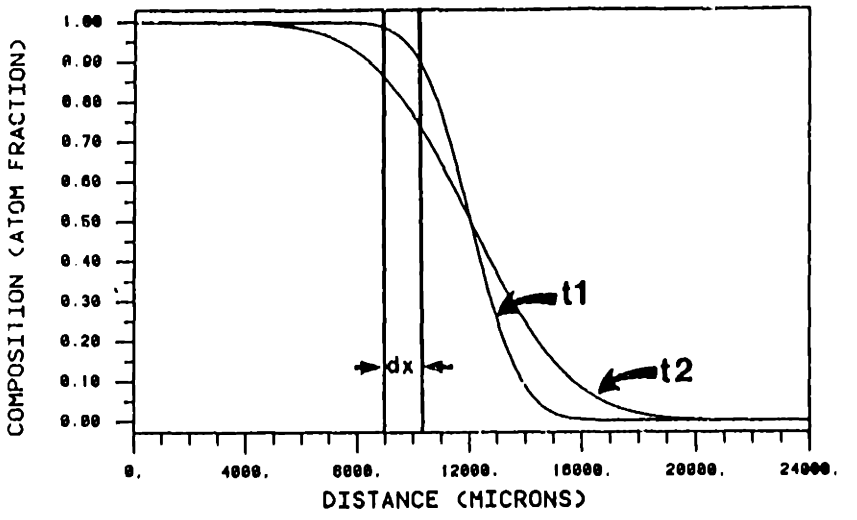

Figure 1. Diffusion couple depicting two successive diffusion profiles.

Applying Ficks second law to the volume element:

$$\left(\frac{\partial c}{\partial t}\right)_{t_1} = -\left(\frac{\partial J_x}{\partial x}\right)_{t_1} \qquad [1]$$

$$\left(\frac{\partial c}{\partial t}\right)_{t_2} = -\left(\frac{\partial J_x}{\partial x}\right)_{t_2} \qquad [2]$$

If the time interval 'dt' is small then the average rate of accumulation ($\dot{q}$), over the time interval t_2-t_1, may be approximated by averaging the accumulation rates at times t_1 and t_2 leading to the following equation:

$$-\dot{q} \cong \frac{1}{2}\left(\left(\frac{\partial J}{\partial x}\right)_{t_1} + \left(\frac{\partial J}{\partial x}\right)_{t_2}\right) \qquad [3]$$

whereas the change in concentration may be expressed as:

$$\Delta c = c_{t_2} - c_{t_1} \qquad [4]$$

By using a finite difference approximation to the local depletion rate one may combine all of these equations as follows:

$$q \cong \frac{\Delta c}{\Delta t} \qquad [5]$$

$$-2\left(\frac{\Delta c}{\Delta t}\right) \cong \left(\frac{\partial J}{\partial x}\right)_{t_1} + \left(\frac{\partial J}{\partial x}\right)_{t_2} \qquad [6]$$

One may next express the instantaneous depletion rate in terms of a mobility function and a chemical potential gradient:

$$J = -M\left(\frac{\partial \mu}{\partial x}\right) \qquad [7]$$

$$\frac{\partial J}{\partial x} = -\frac{\partial}{\partial x}\left(M\left(\frac{\partial \mu}{\partial c}\right)\left(\frac{dc}{dx}\right)\right) \qquad [8]$$

$$-\left(\frac{\partial J}{\partial x}\right)_t = \left(\frac{\partial M}{\partial c}\right)_t\left(\frac{\partial \mu}{\partial c}\right)_t\left(\frac{dc}{dx}\right)_t^2 + M_t\left(\frac{\partial^2 \mu}{\partial c^2}\right)_t\left(\frac{dc}{dx}\right)_t^2 + M_t\left(\frac{\partial \mu}{\partial c}\right)_t\left(\frac{d^2 c}{dx^2}\right)_t \qquad [9]$$

In deriving these equations*, the unknown quantities** M and μ have been differentiated with respect to concentration rather than distance. Fundamentally both these quantities depend only on composition, their dependence on distance comes about only as a result of the dependence of the concentration on distance. Hence, the desired quantities (M and μ) are independent of any particular diffusion profile. This is clarified in figure 2 which depicts a diffusion profile onto which the activity-composition diagram has been superposed. Each point (i.e. composition) on the profile has a unique activity associated with it (plotted at right angles to the plane of the profile). Together all the points and associated activities map out a curve in distance-composition-activity space. Each profile (at a certain time) has associated with it one such curve, but the projection of all such curves onto the activity-composition plane (at right angles to the composition-distance plane) is

* The composition, c, is a function of the spatial variable, x, and the temporal variable, t. Since equation [9] represents the depletion rate at a fixed time the use of the total derivative (dc/dx) instead of the partial derivative ($\partial c/\partial x$) is justified.

** The phenomenological mobility function, M, used here possesses units of (gm-moles)$cm^{-3}sec^{-1}$ and differs from the conventional definition of mobility.

identical and this projection represents the activity-composition diagram for the particular alloy. It then follows (fig. 2) that if the activity were known for a particular composition on any profile, it would be known at that composition on any other profile. This point will be re-emphasized later.

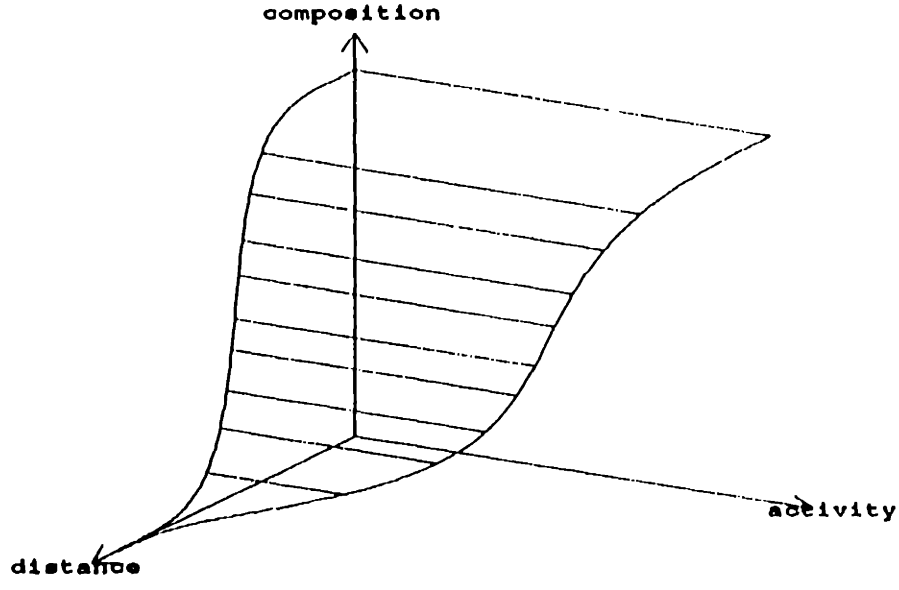

Figure 2. Activity-Composition-Distance surface associated with a diffusion couple.

One can now combine equations 6 and 9 to yield :

$$\frac{2\Delta c}{\Delta t} = \left(\frac{\partial M}{\partial c}\right)_{t_1}\left(\frac{\partial \mu}{\partial c}\right)_{t_1}\left(\frac{dc}{dx}\right)^2_{t_1} + M_{t_1}\left(\frac{\partial^2 \mu}{\partial c^2}\right)_{t_1}\left(\frac{dc}{dx}\right)^2_{t_1} + M_{t_1}\left(\frac{\partial \mu}{\partial c}\right)_{t_1}\left(\frac{d^2 c}{dx^2}\right)_{t_1}$$
$$+ \left(\frac{\partial M}{\partial c}\right)_{t_2}\left(\frac{\partial \mu}{\partial c}\right)_{t_2}\left(\frac{dc}{dx}\right)^2_{t_2} + M_{t_2}\left(\frac{\partial^2 \mu}{\partial c^2}\right)_{t_2}\left(\frac{dc}{dx}\right)^2_{t_2} + M_{t_2}\left(\frac{\partial \mu}{\partial c}\right)_{t_2}\left(\frac{d^2 c}{dx^2}\right)_{t_2} \quad [10]$$

This equation constitutes the model for computing chemical potentials. It relates measurements made at two different times in a diffusion couple to the chemical potential, its derivatives and to the mobility (M) and its derivative.

It was decided to carry out some simple numerical simulations to test the validity of equation [10] and perhaps gain an understanding into the sensitivity of

any proposed calculation to the measured quantities. To simplify the analysis, it was decided to assume that the quantity M varied linearly with composition. The proportionality constant was taken to be the diffusion coefficient. This is precisely what one would expect for an ideal alloy or an alloy exhibiting Henrian behavior.[22,23] Hence one may write the following equation:

$$M = Dc \qquad [11]$$

Equation 11 may be substituted into the model equation 10 to yield:

$$\frac{2\Delta c}{D\Delta t} = \left(\frac{\partial \mu}{\partial c}\right)_{t_1}\left(\frac{dc}{dx}\right)^2_{t_1} + c_{t_1}\left(\frac{\partial^2 \mu}{\partial c^2}\right)_{t_1}\left(\frac{dc}{dx}\right)^2_{t_1} + c_{t_1}\left(\frac{\partial \mu}{\partial c}\right)_{t_1}\left(\frac{d^2c}{dx^2}\right)_{t_1}$$
$$+ \left(\frac{\partial \mu}{\partial c}\right)_{t_2}\left(\frac{dc}{dx}\right)^2_{t_2} + c_{t_2}\left(\frac{\partial^2 \mu}{\partial c^2}\right)_{t_2}\left(\frac{dc}{dx}\right)^2_{t_2} + c_{t_2}\left(\frac{\partial \mu}{\partial c}\right)_{t_2}\left(\frac{d^2c}{dx^2}\right)_{t_2} \qquad [12]$$

Thus for a system exhibiting an M-c relationship akin to that of an ideal alloy, and possessing a constant diffusivity, a diffusion experiment such as that outlined above (with two profiles) would yield the slopes and curvatures of the curves at both the times and also the left hand side term in the above equation. For such an alloy the only remaining unknowns would be the slopes and curvatures of the chemical potential at the two times, t_1 and t_2. The subscripts in equation [12] refer to the fact that these quantities were evaluated at the composition corresponding to each specific location at each time.

2.4 NUMERICAL SIMULATIONS

It was decided to numerically simulate a series of hypothetical alloy systems (with mobility M=Dc) and to use the resultant diffusion profiles as input to the model (eqn. [12]). This would serve as a simple test of the model. Two additional concerns needed to be addressed before any computations could be performed. Firstly, the simplified equation [12] involved two sets of three terms one from each profile. Each set of three terms taken together represents a second order ordinary differential equation. This implies that if the terms corresponding to one profile (either time t_1 or time t_2) were known from a boundary condition or from prior calculation then

one could solve for the chemical potential terms corresponding to the other profile. Secondly, assuming that it is possible to obtain the three terms (corresponding to one profile) there still remain two additional pieces of information (boundary conditions) which must be known to uniquely solve the second order ordinary differential equation. The second concern is addressed first, i.e. that of finding two boundary conditions.

Appropriate boundary conditions may be found on examining the solution behavior of real metallic alloys[2]. It is well known that above a certain limiting concentration (99%, or 95% depending on the alloy system) all solutions behave ideally. This implies that one may write the following equations to describe solution behavior above the limiting concentration (taken to be 99% for these simulations):

$$a = c \qquad \mu = \mu_o + RT \ln c$$

$$\frac{d\mu}{dc} = \left(\frac{RT}{a}\right)\left(\frac{da}{dc}\right) = \frac{RT}{c} \qquad \frac{d^2\mu}{dc^2} = -\left(\frac{RT}{c^2}\right) \qquad [13]$$

Knowledge of these boundary conditions suggests the following algorithm. Consider a volume element V_1 in the 'tail' region of the diffusion couple where the computation may be initiated (Figure 3). Figure 3 highlights a band of compositions in excess of 99% where the boundary conditions determine the chemical potential. If the volume element is infinitesimally small, then the slope, curvature and composition at point C_{11}^{m} may be taken to represent the composition, slope and curvature of profile 1 across the entire volume element V_1. Since all compositions corresponding to profile 1, in the volume element V_1, lie in a composition range that exceeds 99%, it follows that the three terms corresponding to time t_1 in equation [12] are completely known (eqn. 13). Further note that the composition of point 'A_1' of profile 2 in figure 3, also exceeds 99%. Hence the same boundary conditions apply to point 'A_1', where one knows the chemical potential, as well as its derivatives with respect to composition. Then one may substitute into equation [12] for the three

terms corresponding to time t_1 and obtain the following second order ordinary differential equation :

$$Q = X\left(\frac{d\mu}{dc}\right) + Y\left(\frac{d^2\mu}{dc^2}\right) \qquad \text{where} \qquad [14]$$

$$Q = \frac{2\Delta c}{D\Delta t} \qquad X = \left(\frac{dc}{dx}\right)^2_{t_2} + c_{t_2}\left(\frac{d^2c}{dx^2}\right)_{t_2} \qquad Y = c_{t_2}\left(\frac{dc}{dx}\right)^2_{t_2}$$

Solution of the ordinary differential equation (by use of the boundary conditions at A_1) provides one with knowledge of the chemical potential, its slope and second derivative (with respect to composition) at the point 'C_1' in figure 3.

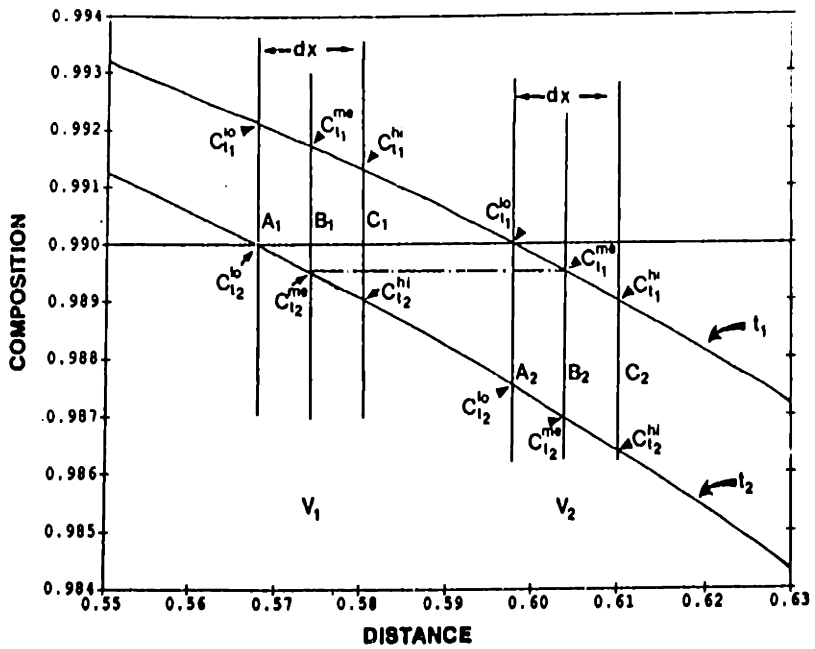

Figure 3. Volume elements highlighting compositions relevant to the computation scheme.

The computation can be continued by defining a new volume element that extends from point 'C_1' to a lower composition. The process may be iterated several times. Each such computation extends the range of compositions over which the chemical potential and its derivatives are known. For the first few volume elements the composition of all the points corresponding to profile 1 in volume element V_1 will remain in excess of c=0.99. However, beyond a certain point, when $c_{t_1}^{me} < 0.99$,

it will no longer be valid to assume that the solution behaves ideally. Therefore one needs an alternative method of obtaining the three terms corresponding to t_1 in equation [12]. It will be next shown that it is possible to compute these three terms using chemical potential data obtained during previous calculations.

Consider the volume element V_2, in figure 3, for which c_{f1}^{m*} is less than 0.99. One notes that the composition c_{f1}^{m*} in volume element V_2 is actually the composition c_{f2}^{m*} of some earlier volume element (V_1 in this case). This implies that in an earlier computation the chemical potential (and its derivatives) for this composition (c_{f1}^{m*}) had been obtained. Since the chemical potential is a function only of the composition (in an isothermal experiment) it is possible to utilize the information from an earlier computation in calculating the three terms corresponding to time t_1 in equation [12]. This is equivalent to stating that the projections of the various operating curves (each corresponding to a unique diffusion profile) onto the activity-composition plane are identical. All of this implies that the three terms corresponding to time t_1, in volume element V_2 are known and that the computation may be carried out further.

The computation can proceed in this manner up to the Matano interface. At the Matano interface the two profiles crossover and hence the computation may be continued further but with the roles of profiles 1 and 2 exchanged. In other words, beyond the Matano interface, the three terms corresponding to profile two are known and one computes for the terms involving profile one since profile one is at a lower composition.

To test the validity of the arguments presented above and thereby test the model, the one dimensional simulation scheme depicted in figure 4 was implemented. An equidistant finite difference grid was used. The initial conditions of the diffusion profile were specified along with the mobility function ($M = Dc$). The chemical potential function was assumed to obey a regular solution model and the regular solution parameter was varied. Diffusion profiles corresponding to various isothermal

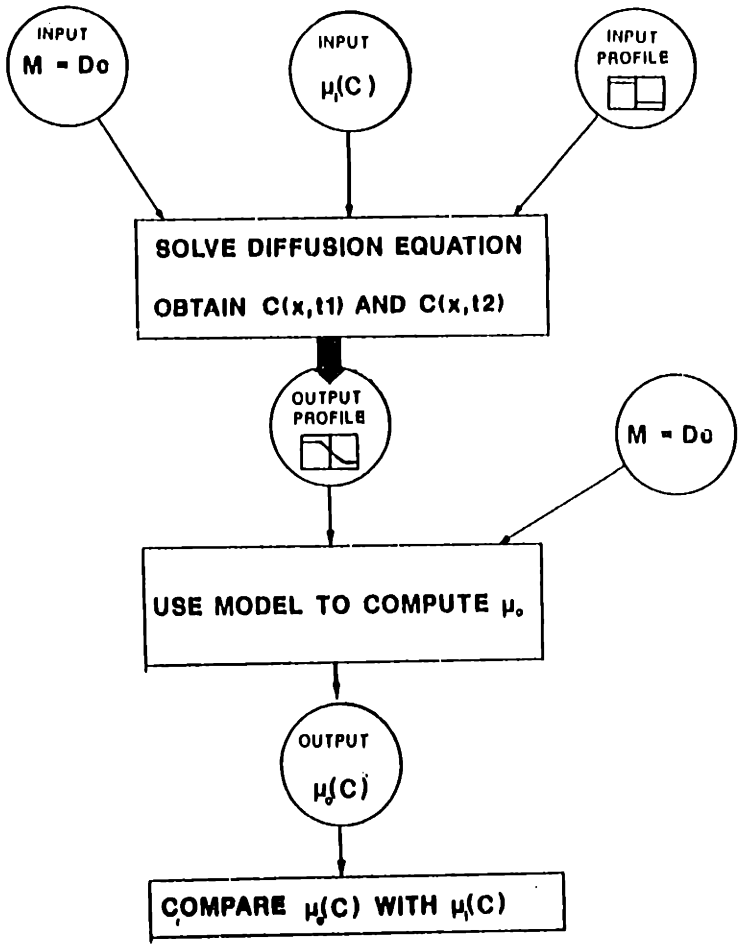

Figure 4. Outline of Simulation Scheme.

annealing times were computed using a first order finite difference approximation to the phenomenological description embodied in equation [7]. Using the computed diffusion profiles, and knowing the mobility function explicitly, an attempt was made to compute chemical potentials in the manner outlined above (i.e. by using the simplified equation 12). The computed chemical potentials were later compared with the chemical potentials input in step 1. Several cases were tested, each corresponding

to a different value of the regular solution parameter. In this manner, the chemical potential was varied while keeping the mobility function constant (M = Dc, with D constant).

It should be noted that in a real alloy system one would not be able to vary both the chemical potential and the mobility independently since they are inter-related by the Nerst-Einstein equation. In other words one may easily note (by comparing fluxes in the Fickian and phenomenological descriptions) that the following equation must hold:

$$D = M\left(\frac{d\mu}{dc}\right) \qquad [15]$$

Nonetheless, the present computation scheme will test whether the model equations are valid.

2.5 RESULTS AND DISCUSSION

Several simulations were conducted in the manner outlined above. The regular solution parameter, α was allowed to take on the following values: -1.5, 0, +0.5, 1.0 and 1.5 . Profiles were computed by solving the diffusion equation 7, with insulating boundary conditions (zero flux at either end of the couple; also termed Von Neumman boundary conditions) and using Eulers method in the time dimension. An artificially high, constant diffusivity, D = $10^{-5}cm^2/s$ was used to compute the mobility function. In stage 3 (figure 4) the model was used to compute chemical potential (activities) from the profiles generated. The mobility function (M=Dc) was known explicitly*. A Runge-Kutta-Nystrom technique was used to solve the resultant second order ordinary differential equation. Care must be taken to ensure that the step size in the solution of the ordinary differential equation is small to avoid a numerical instability. Results for these simulations are depicted in Figure 5.

* Since the mobility function was constant and the chemical potential was varied the simulations in effect decouple the system's transport properties from the system's thermodynamics. Hence the present simulations are representative of hypothetical alloys rather than real alloys.

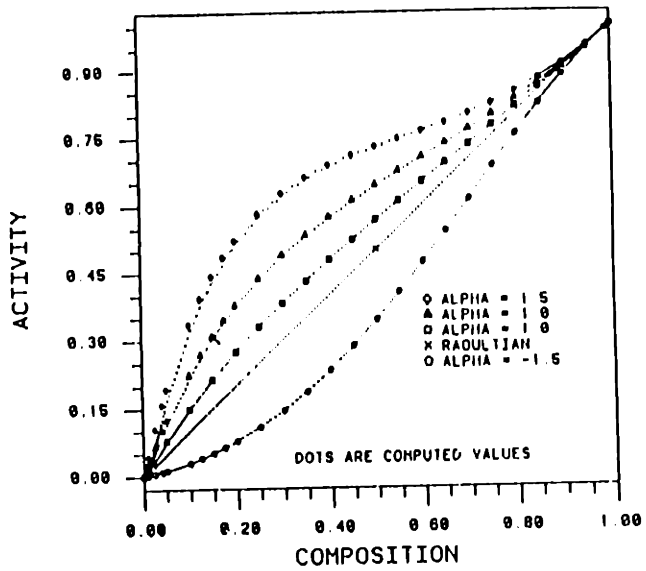

Figure 5. Simulation results for the proposed computational scheme.

In figure 5, the dots represent the values computed by the model whereas the solid symbols indicate the input activity data. It is clear from the figure that for the present simulation conditions ($D=10^{-5}cm^2/s$, $t_1=4000sec$, $t_2=4100sec$)** there is an excellent agreement between the computed activities and the activities used as input in computing the diffusion profile. This excellent agreement indicates that the proposed model (eqn [12]) is capable of extracting activities if the mobility function is known explicitly, as in the present simulations.

Although encouraging, the results from these preliminary calculations also raised several critical questions regarding the feasibility of this approach for real systems. Some of these are discussed next.

1. For the simulation conditions used, the composition difference between the two profiles was very small as seen from figure 6 (maximum composition difference < 0.25%). In a numerical simulation, the composition data is available

** The general conclusions from these simulations are not dependent on the numerical value of the diffusivity. A smaller diffusivity would lead to longer annealing times to attain the same profile.

to 8 digit (or 16 digit) precision but in a real experiment, which typically would rely on an electron microprobe, one would not expect the compositional sensitivity to be any better than 0.1%-0.2% (assuming several standard samples were used). Thus the compositional difference, Δc , may be lost in the noise associated with the measurement. Clearly *a noise reduction technique*, is needed before the proposed model can be used with a real experiment.

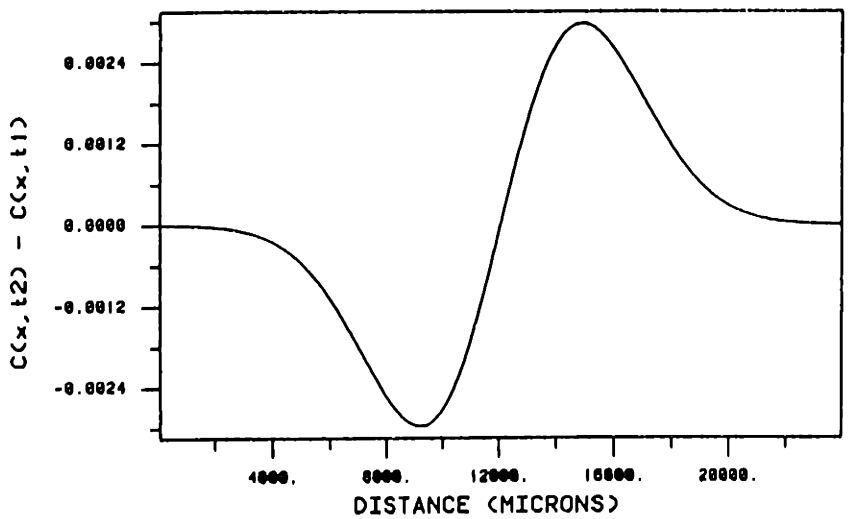

Figure 6. Compositional difference between two successive diffusion profiles.

2. One solution to overcoming the problem discussed above would be to increase the time difference 'dt' between the two profiles. But increasing 'dt' would mean that the approximations underlying the model (eqns. 3,6) would begin to break down and cause larger errors ϵ , where ϵ may be expressed as follows:

$$\epsilon = \frac{\Delta C}{\Delta t} - \frac{1}{2}\left[\left(\frac{\partial J}{\partial x}\right)_{t1} + \left(\frac{\partial J}{\partial x}\right)_{t2}\right]$$

Clearly, there was a need to study the effect of increasing ϵ on the error in the computed activity data.

3. Upto this point, in all simulations the mobility function had been known explicitly and had been decoupled from the chemical potential function. Since these conditions are not valid for a real alloy system, the major concern at this stage was *whether a scheme could be developed that would simultaneously compute both the mobility and the chemical potential.*

It will be shown next that concerns 1 and 2 do not pose a major problem but that concern 3 above is a likely stumbling block.

To address concern 1, it was decided to simulate real data by rounding the computed profile to 3 digits. The rounding operation did not significantly contaminate the C-x data but the $\left(\frac{dc}{dx}\right)-x$ and $\left(\frac{d^2c}{dx^2}\right)-x$ data, which were computed using finite difference approximations to the C-x data, exhibited the presence of high wavenumber noise (figure 7). This a direct consequence of the rounding operation. This high wavenumber noise led to numerical instabilities in the computations. To overcome this, the rounded compositional data were fitted with a sixth order least squares spline (see accompanying paper on splines for details). This filtered out the noise from the data while ensuring that four derivatives of the C-x data were continuous. The least squares spline is obtained by minimizing the least squares error between the polynomials comprising the spline and the data points. The final interpolant does not pass through the data points exactly thereby avoiding the high wavenumber noise. When the simulations were run with the spline fit data, the resultant activity data agreed well with the initial data. Thus it is believed that by using splines it is possible to compute activity data with only 3 digit data as input.

To address concern 2, a series of simulations were run wherein the time interval between two successive diffusion profiles was increased and the error in the computed activities was monitored as a function of the error in the assumptions (ϵ). It was possible to compute ϵ since the actual $\left(\frac{\partial J}{\partial x}\right)$ data were available from the initial program (in stage I of figure 4) that computed the diffusion profiles. Table I plots the error in the computed activity data as a function of the error in the assumptions ϵ.

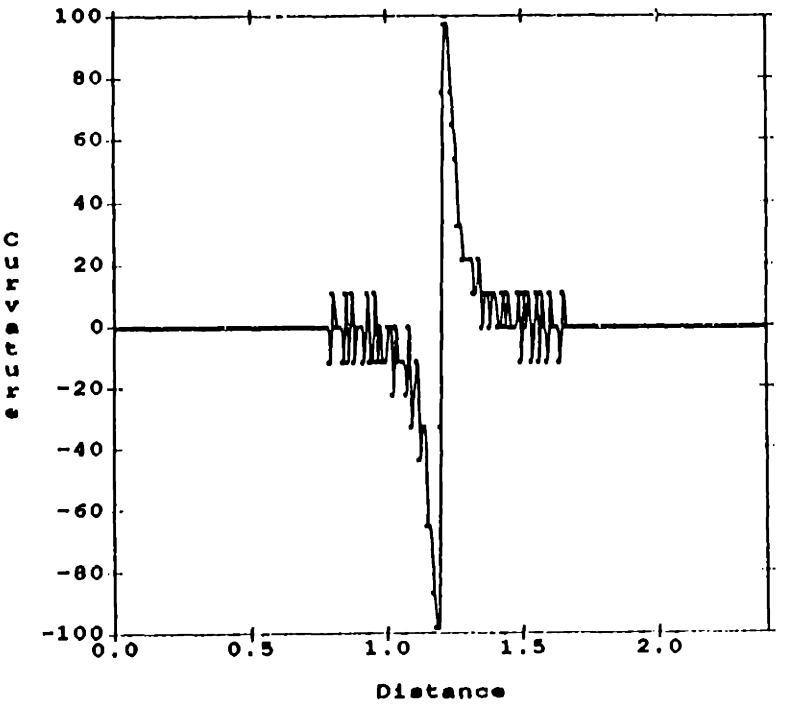

Figure 7. Effect of rounding compositional data to three digits on the curvature of the diffusion profile computed using second order finite difference approximations.

Table I Error in the computed Activities as a function of the Error in Model Approximations

ϵ	Relative error in a-c data	max Δc between 2 profiles
2%	<1%	0.8%
2.75%	<1%	1.89%
6.58%	<1%	3.45%
17.51%	<1%	5.88%
30.12%	<1%	7.76%
108%	2.8%	13.54%

It is clear from Table I that the error in the a-c data is extremely insensitive to the error in the model approximations, at least when M=Dc and when M is known during the computation. It is also clear that only small errors accrue in the computed activities even when the maximum compositional difference between the two profiles is large. In turn this implies that the time difference between two successive profiles can be increased (until the composition difference between the two profiles is significant enough to be measured with an electron microprobe) without affecting the accuracy of the computed activity data.

Thus the preliminary simulations were very encouraging. However, as stated earlier these simulations were conducted on hypothetical alloy systems since the mobility and the chemical potential had been artificially decoupled. A computational scheme was next proposed that would permit simultaneous evaluation on the mobility and chemical potential given diffusion profiles from a real experiment. Instead of conducting a diffusion experiment, it was decided to compute diffusion profiles for a real system using measured D-c data taken from the literature. It was hoped that this would serve as a quick check of the proposed scheme.

Computation of the diffusion profiles required knowledge of the variation of the interdiffusion coefficient as a function of composition. Accordingly, the literature was scanned for data describing the variation of the chemical interdiffusion coefficient as a function of composition for isomorphous binary alloys. A useful compilation of this data is found in the book by Borovskii[12]. The Au-Ni system, investigated by Cohen et. al.[24,25,26], was chosen for the initial simulations. The raw data were digitized at approximately 100 points and fitted with a fourth order least squares spline (i.e. a cubic spline). Details on spline fitting procedures are found in the companion paper[27]. The spline representation was used for all further computations. Using the interdiffusivity data, the diffusion equations (in the Fickian description) were solved on a one dimensional equidistant finite

difference grid using Eulers method in the time dimension and finite difference approximations to the spatial derivatives[28]. The resultant profiles were used as input to the model in an attempt to compute the chemical potential.

The availability of spline fitting techniques made it possible to compute the slope of the diffusivity data, $\left(\frac{\partial D}{\partial c}\right)$. This suggested a simplification of the model from a two profile model to a single profile model. If the diffusivity and its slope are known then in Fickian coordinates one may express the depletion rate as follows:

$$-\frac{\partial J}{\partial x} = D\nabla^2 c + \left(\frac{\partial D}{\partial c}\right)(\nabla c)^2 \qquad [16]$$

In the original model (eqns. 1-12), two profiles were considered in order to obtain an approximation to the depletion rate by considering the change in concentration between time t_1 and t_2 (eqns. 3, 5). This was necessary since measurement of a diffusion profile does not yield information on the instantaneous depletion rate. However with the aid of spline interpolation techniques, eqn. 16 can be used to compute $\left(\frac{\partial J}{\partial x}\right)$. The simplified model is then obtained by equating the depletion rates in the Fickian and phenomenological descriptions (ref. equations 16 and 17). This leads to :

$$D\nabla^2 c + \left(\frac{\partial D}{\partial c}\right)(\nabla c)^2 = \left(\frac{\partial M}{\partial c}\right)\left(\frac{\partial \mu}{\partial c}\right)(\nabla c)^2 + M\left(\frac{\partial^2 \mu}{\partial c^2}\right)(\nabla c)^2 + M\left(\frac{\partial \mu}{\partial c}\right)(\nabla^2 c) \qquad [17]$$

The simplified model embodied in equation 17 is more transparent than the two profile model of equations 10 and 12. The basis for the proposed model is now clear: invariance of the instantaneous depletion rate with respect to the choice of variables (Fickian or phenomenological). The coupling between the mobility, M, and the chemical potential, μ is also apparent. It is also clear that additional information is needed to solve equation 17. Hence one equates the fluxes in the two descriptions to obtain :

$$J_{Fickian} = J_{phenomenological} \quad [18]$$

$$-D\nabla c = -M\nabla\mu \quad [19]$$

$$M = \frac{D}{\left(\frac{\partial\mu}{\partial c}\right)} \quad [20]$$

Thus the model now reduces to equations 17 and 20. Viewed in this manner (single profile model), a major limitation of the proposed scheme becomes apparent. To solve equation 17 one needs M and $\left(\frac{\partial M}{\partial c}\right)$ This information must be computed *simultaneously* with the chemical potential information. One initial suggestion for obtaining $\left(\frac{\partial M}{\partial c}\right)$involved differentiating eqn. 20 and then solving the resultant equation (21) simultaneously with equations 17 and 20. Differentiation of equation [20] leads to the following expression :

$$\left(\frac{\partial M}{\partial c}\right) = \frac{\left(\frac{\partial D}{\partial c}\right)\left(\frac{\partial\mu}{\partial c}\right) - D\left(\frac{\partial^2\mu}{\partial c^2}\right)}{\left(\frac{\partial\mu}{\partial c}\right)^2} \quad [21]$$

Attempts to solve equations 17, 20 and 21 simultaneously will not work since equations 17, 20 and 21 are linearly dependent. This can be seen by substituting equations 20 and 21 into 17. Clearly, one has too many unknowns and not enough equations.

The linear inter-dependence of equation 17, 20 and 21 implies that equations 17 and 20 are equivalent (since equation 21 is obtained by differentiating 20). This seemingly trivial observation has profound implications. Firstly, this means that one may obviate the model equation [17] and concentrate instead on equation 20 to obtain chemical potential information. This implies that information on chemical potentials is implicitly contained in the variation of the interdiffusion coefficient with composition. This in itself is no surprise since the theories proposed by Darken[7], Manning[10], Kirkaldy[11], Howard and Lidiard[9], all lead to expressions that explicitly relate the chemical interdiffusion coefficient to the system thermodynamics. What is more interesting to note is that knowledge of the slope of the diffusivity $\left(\frac{\partial D}{\partial c}\right)$, led to simplification of the model from 2 profiles to a single profile and now

examination of the simpler model (eqns. 17, 20 and 21) leads one to conclude that one need not explicitly examine *any* profile. Instead all one requires is the dependence of D on composition. However, it should be noted that the variation of D with composition is itself obtained by subjecting the diffusion profile to a Boltzmann-Matano treatment. One only needs the diffusion profile explicitly to obtain the variation of the diffusivity with composition but not to compute chemical potentials from a diffusion couple. Once the diffusivity is known (as a function of composition), additional experiments (multiple diffusion profiles) do not yield any new information.

In other words, the diffusion profiles (C-x data) are physical manifestations of the D-c relationship. Therefore one may think in terms of a D-c-x space along with an M-c-x space, similar to the μ-c-x space presented in figure 2. Since M, D, and μ are interrelated and all of these depend fundamentally on composition alone, it is clear that the task of looking for μ-c data in C-x data is more complex than looking for μ-c data in D-c data. The spatial variable, x, is an intermediate variable. It is intuitively appealing, since it is a physical variable, but it is not really helpful in obtaining chemical potential information. All of this implies that one must focus on equation 20 to obtain chemical potential information from diffusivity data.

Examination of eqn. 20 indicates an additional problem; one knows only the interdiffusivity D and one wishes to compute both μ and M. Clearly, an analytical solution yielding both chemical potential and mobility from the interdiffusivity is not possible unless additional information on the concentration dependence of M is made available from some other measurement (preferably a non transport measurement). This implies that additional assumptions must be made regarding the functional form of μ and M. These ideas and a non linear least squares technique for computation of M and μ are the subject of the following paper.

2.6 CONCLUSIONS

The main conclusions from this part of the investigation may be summarized as :

(i) Chemical potential information is available from a diffusion couple. By simulating a series of hypothetical alloys which possess a mobility akin to that of an ideal alloy it has been shown that it is possible, in theory, to compute chemical potentials from a diffusion profile if the mobility is known a priori.

(ii) Observation of the dynamic behavior of a diffusion profile, or examination of multiple profiles, does not provide any additional information. The requisite information is available in the equation relating mobilities, chemical potentials and diffusivity.

(iii) It is not possible to extract an analytical solution to the chemical potential directly from the interdiffusion coefficient without knowledge of the mobility function. Computation of both μ and M demands additional assumptions regarding the functional form of the variation of these quantities with composition.

2.7 SYMBOLS

c	:	composition gm/cm^3
t_1, t_2	:	time sec
J	:	Flux $gm/(cm^2 - sec)$
x	:	spatial cordinate cm
$\dot{q}$	:	average rate of accumulation $gm/(cm^3 - sec)$
$-\frac{\partial J_x}{\partial x}$	:	instantaneous rate of depletion $gm/(cm^3 - sec)$
Δc	:	change in concentration $gm/(cm^3)$
M	:	phenomenological coefficient or mobility $(gm - moles)/(cm^3 - sec)$
μ	:	chemical potential $(gmcm^2 sec^{-2} gm - mole^{-1})$
a	:	activity *dimensionless*

2.8 REFERENCES

1. Carl Wagner, *Thermodynamics of Alloys*, Addison Wesley, (1962).

2. D. R. Gaskell, *Introduction to Metallurgical Thermodynamics*, McGraw Hill, (1973).

3. C. H. P. Lupis, *Chemical Thermodynamics of Materials*, North Holland, (1983).

4. P. G. Shewmon, *Diffusion in Solids* J. Williams Book Co., (1983).

5. Crank, *The Mathematics of Diffusion*, Oxford Press (1975).

6. L. S. Darken, *Trans. AIME*, **180**, pg 430, (1949).

7. L.S. Darken, *Trans. AIME*, **174**, pp. 184-201, (1948).

8. L. S. Darken, in *Atom Movements* ASM, (1950).

9. R. E. Howard and A. B. Lidiard, *Rep. Prog. Phys.*, **27**, 161, (1964).

10. J. R. Manning, *Diffusion Kinetics for Atoms in Crystals*, D. Van Nostrand, (1968).

11. J. S. Kirkaldy and D. J. Young, *Diffusion in the Condensed State*, The Institute of Metals, (1987).

12. I. B. Borovskii, K. P. Gurov, I. D. Marchukova and Y. E. Ugaste, *Interdiffusion in Alloys*, Nauka Publishers, NTIS Document PB86-245495, (1986).

13. S. R. de Groot, *Thermodynamics of Irreversible Processes*, North Holland Publishing Company, (1963).

14. K. G. Denbigh, *Thermodynamics of the Steady State*, John Wiley & sons (1951).

15. I. Prigogine, *Introduction to the thermodynamics of Irreversible Processes*, John Wiley and Sons, (1961).

16. J. C. Baker and J. W. Cahn, *Solidification*, ASM, pp. 23-58, (1970).

17. Lars G. Onsager, *Physical Review*, **37**, pp. 405-426, (1931).

18. Lars G. Onsager, *Physical Review*, **37**, pp. 2265-2279, (1931).

19. B. D. Coleman and C. Truesdell, *The Journal of Chemical Physics*, **33**. No. 1, pp. 28-31, (1960).

20. W. W. Mullins and R. F. Sekerka, *Scripta Metallurgica*, **15**, pg. 29 (1981).

21. J. S. Kirkaldy, *Scripta Metallurgica*, **19**, No. 11, (1985).

22. J. P. Stark, *Metallurgical Transactions A*, **Vol. 11A**, 1797-1798 (1980).

23. J. P. Stark, *Metallurgical Transactions A*, **Vol. 11A**, 1793-1795 (1980).

24. A. D. Kurz, B. L. Averbach and Morris Cohen, *Acta Metall.*, **Vol.3**, 442-446, (1955).

25. J. E. Reynolds, B. L. Averbach and Morris Cohen, *Acta Metall.*, **Vol. 5**, 29-40, (1957).

26. L. L. Seigle, B. L. Averbach and Morris Cohen, *Journal of Metals*, 1320-1327 (1952).

27. Rakesh R. Kapoor, *Thermodynamics Data from Diffusion Couples*, Paper IV, Sc.D thesis, MIT, (1989).

28. V. Vemuri and W. J. Karplus, *Digital Computer Treatment of Partial Differential Equations*, Prentice Hall, (1981).

Thermodynamic Data From Diffusion Couples - II

3.1 ABSTRACT

A non linear least squares based strategy is presented to compute activity-composition data from measured interdiffusivity - composition data for isomorphous binary metals. The interdiffusion coefficient is modelled as a product of two functions, one representing the contributions of the system thermodynamics and the other representing the contributions of the phenomenological coefficients. Since both functions are unknown and only their product (the interdiffusion coefficient) is known there exists an inherent non uniqueness to the problem. Hence, the proposed solution scheme leads to multiple sets of coefficients which on an activity-composition diagram correspond to solutions exhibiting positive and negative deviations from ideality. One additional piece of information, such as the experimentally measured activity at a particular composition or the slope of the Henry's law line at infinite dilution, is needed to pick the correct set of coefficients. The scheme was applied to the CoNi system for which the activity data computed from the interdiffusivity data showed excellent agreement with the experimentally measured activity data.

3.2 INTRODUCTION

This is the second of four papers covering an investigation aimed at obtaining chemical potential information from diffusion couples. In the previous paper a preliminary model had been proposed that analyzed the dynamic behavior of a diffusion profile in an attempt to extract chemical potential information. However, the preliminary model led to a larger number of unknowns than the number of available equations. A careful analysis of the preliminary model had shown that

instead of analyzing the dynamic behavior of a profile, it is more fruitful to focus on obtaining chemical potential directly from the variation of the interdiffusion coefficient with composition. Thus it was shown that the starting point for computing chemical potentials is the following equation:

$$M = \frac{D}{\left(\frac{\partial \mu}{\partial c}\right)} \qquad [1]$$

This paper begins by examining various theories in the literature interrelating the chemical interdiffusion coefficient to the system thermodynamics and to the phenomenological (Onsager) coefficients.

3.3 LITERATURE REVIEW

3.3.1 *Relationship between the diffusivity and the system thermodynamics*

The phenomenological theory of irreversible processes expresses the flux of a diffusing species as a linear combination of all driving forces[1-4]. In the case of solid state diffusion, the driving forces are the gradients in chemical potential of the diffusing species. The following equation expresses the phenomenological relationship between fluxes and forces:

$$J_i = \sum_{k=1}^{k=n} L_{ik} X_k \qquad [2]$$

whereas the entropy production rate is given by :

$$\Delta \dot{S} = \frac{1}{T}\left(\sum_k J_k X_k\right) \qquad [3]$$

The earliest atomistic theory relating the interdiffusion coefficient to the system thermodynamics is attributed to Darken[5]. There were two major assumptions in Darken's analysis. Firstly, Darken assumed that the off diagonal Onsager coefficients were negligible and secondly he assumed that vacancies were in local equilibrium in the diffusion couple. Darkens analysis led to the following expression:

$$\tilde{D} = (D_1^* N_2 + D_2^* N_1)\left(1 + \frac{d\ln\gamma}{d\ln N}\right) \qquad [4a]$$

In Darken's theory, the phenomenological coefficients were related to the tracer diffusivities by the following expression:

$$L_1 = c_1 D_1^* \qquad [4b]$$

$$L_2 = c_2 D_2^* \qquad [4c]$$

From these expressions it is clear that the phenomenological expressions are strong functions of composition.

Subsequently, Howard and Lidiard[6], Manning[7], and Kirkaldy[4] modified Darken's treatment to include the effect of non-zero off diagonal Onsager coefficients. By considering a quaternary A-A*-B-B* system and assuming that the vacancies were in local equilibrium, they arrived at the following expression:

$$\frac{\tilde{D}}{\left(1+\frac{\partial \ln \gamma}{\partial \ln c}\right)} = (D_1^* c_2 + D_2^* c_1) + \frac{kT}{N}\left(\frac{X_B}{X_{A^*}} L_{AA^*} + \frac{X_A}{X_{B^*}} L_{BB^*}\right) \qquad [5]$$

In equations 4a and 5 the thermodynamic factor $\phi(c)$ provides a complete description and embodies the thermodynamics of the system. Knowledge of the function $\phi(c)$ completely defines the solution behavior of the alloy system.

It has been estimated[4] that the additional term in equation [5] leads to an error of around 5% over equation [4] in the computed interdiffusion coefficient for isomorphous binary alloys and an error of up to 28% in the measurement of the marker velocity. Since measurements of interdiffusion coefficients often contain as much as 25% errors, it is not possible to detect the contribution of the additional term in equation [5] by measurement of the diffusion coefficient alone.

Experimentally, the interdiffusion coefficient is obtained as a function of composition by subjecting the measured diffusion profile data to the Boltzmann-Matano treatment[4,8,9]. This treatment is embodied in the following expression:

$$D(c) = \left(\frac{-1}{2t}\right)\left(\frac{1}{\left(\frac{dc}{dx}\right)}\right)\int_0^c \{x(c) - x_m(c)\}dc \qquad [6]$$

Crank[10] and Balluffi[11] have modified the Boltzmann-Matano treatment to account for the volume change of mixing. The correction is small for isomorphous binary alloys, which exhibit small changes in molar volume. Hence this effect will be neglected in the present investigation.

It should be noted that Darken's theory (eqn. 4a) and the theory proposed by Howard and Lidiard[6], Manning[7] and Kirkaldy[4] (eqn. 5) differ only in the number and functional form in which the phenomenological coefficients contribute to the interdiffusion coefficient. Darken's theory calls for two independent phenomenological coefficients whereas the theory proposed by Howard and Lidiard, Manning and Kirkaldy calls for five independent phenomenological coefficients to completely describe binary diffusion under the assumption that the vacancies are in local equilibrium. Despite these differences, it is important to note that both theories predict an identical dependence of the interdiffusion coefficient on the system thermodynamics (eqns. 4a and 5). Both treatments express the diffusivity in the following general form:

$$\tilde{D} = f(c)\left(1 + \frac{\partial \ln \gamma}{\partial \ln c}\right) \qquad [7]$$

where f(c) is a function of the phenomenological coefficients and the alloy composition and hence depends on the theory being considered (eqns. 4a and 5).

It is clear from equation 7 that the interdiffusion coefficient is a very strong function of the thermodynamics of the system. Borovskii[12] has provided several examples to illustrate this point effectively. For example, in the U-Zr system (binary isomorphous) one would expect the interdiffusion coefficient to increase with increasing contents of U (the lower melting point metal). However, diffusivity measurements indicate that the diffusion coefficient first decreases (0-25% U), remains fairly constant (25-60%) and then begins to increase sharply. This unexpected behavior is attributed to the influence of the thermodynamic term on the interdiffusion coefficient.

Thus as far as the present investigation is concerned, the main point to be noted is that the interdiffusion coefficient is related to the system thermodynamics by equation 7. The exact functional form of f(c) is of little concern since one is interested in the system thermodynamics.

3.3.2 *Least Squares Techniques*

This section provides a brief introduction on the philosophy underlying least squares techniques since such techniques are central to the proposed computational scheme. Least squares techniques are often used to fit functions to experimentally measured data. There are two main advantages in doing this. Firstly one is able to filter out the noise in the experimental data and secondly the resultant function is a useful way of representing the data since it can be evaluated, differentiated and integrated with ease. A review of the main stages in least squares fitting is presented next.

Assume that one is attempting to measure some physical quantity as a function of an independent variable for several systems. Examples would include density as a function of composition for several alloy systems or thermal expansion coefficient as a function of temperature. The experimental data would consist of data pairs of the measured quantity and the independent variable. Further, assume that there are theoretical reasons to believe that the variation of the measured physical quantity with respect to the independent variable can be expressed by a generic class of mathematical functions. For example it is generally accepted that the diffusivity for any substitutional metallic solute in any metallic solvent can be expressed by the following generic function; $D = A[Exp(-Q/RT)$. The right hand side of this expression is the mathematical model and the quantities A and Q are two variables which differ from one solute to the other. For each solute one computes A and Q by subjecting the measured diffusivity data to a least squares analysis. Thus the first stage in least squares analysis is defining the mathematical function that will represent the physical quantity.

In the second stage a least squares error function is defined which geometrically corresponds to the sum of the squares of the distance between each data point and the mathematical function. The third stage involves minimizing the least squares error function to obtain the variables that define the mathematical function (A and Q in the present case). Geometrically this amounts to minimizing the distance between the mathematical function and the measured data.

3.4 PROPOSED ALGORITHM

The proposed scheme relies on the following assumptions: (i) The molar volume is invariant with composition, (ii) The system is isothermal and (iii) Vacancies are in local equilibrium everywhere in the diffusion couple.

The proposed scheme involves fitting a non linear least squares function to the isothermal interdiffusion data, that is, one attempts to model the isothermal variation of the interdiffusion coefficient with alloy composition. It is known that the interdiffusion coefficient is a product of two functions: f(c) and $\phi(c)$(equation [7]). To conduct a least squares fit to the interdiffusion coefficient one must begin by choosing mathematical models to represent both quantities f(c) and $\phi(c)$ The product of the mathematical models chosen to represent f(c) and $\phi(c)$will yield the function which can be used to model the interdiffusion coefficient. The mathematical models for f(c) and $\phi(c)$ will be defined in terms of unknown coefficients. One would use the product of the two functions and the experimental interdiffusion data to conduct the least squares fit. The least squares fitting process will provide numerical values of the unknown coefficients that constitute the model functions chosen for f(c) and $\phi(c)$for a certain alloy. Knowledge of the numerical values of the variables that constitute the mathematical function representing $\phi(c)$will permit one to compute $\phi(c)$. Knowledge of $\phi(c)$is equivalent to knowing the thermodynamics of the system since one can integrate $\phi(c)$ to obtain the $\gamma - c$ relationship for the alloy and from it the activity-composition data. With this general overview in mind, one may next examine the details of the proposed computational scheme.

It is clear from equation 7 that to obtain the chemical potential (or equivalently, the function $\phi(c)$) from the interdiffusion coefficient, demands knowledge of the function f(c), which is related to the Onsager phenomenological coefficients. Since f(c) is not known a priori, an analytical solution of the $\phi(c)$ function cannot be obtained. Hence additional assumptions must be made regarding the nature of the functions f(c) and $\phi(c)$. Clearly an important first step is the selection of appropriate functional forms for f(c) and $\phi(c)$

Assume that the functional forms of the two functions f(c) and $\phi(c)$are known a priori.* Further assume that f(c) is being modelled by a function of 'n' variables, $(\tau_1, \tau_2, \ldots\ldots, \tau_n)$ whereas $\phi(c)$ is being modelled as a function of 'm' variables $(\tau_{n+1}, \ldots\ldots, \tau_{m+n})$. This implies that the interdiffusion coefficient is being modelled as a function of 'm+n' variables:

$$D = f(\tau_1, \tau_2, \ldots\ldots, \tau_n)\phi(\tau_{n+1}, \ldots\ldots, \tau_{m+n}) \qquad [8]$$

The mathematical functions chosen to represent f(c) and $\phi(c)$are presumed to possess sufficient degrees of freedom (free variables) to adequately model the quantities they represent. In other words, given a real, metallic, isomorphous, binary alloy system there exists at least one set of real values for the variables $\tau_1, \ldots\ldots, \tau_{m+n}$ such that the resulting function $\phi(c)$adequately represents the solution behavior of the alloy system.

Further, assume that the interdiffusion coefficient has been measured at several discrete compositions over the entire range from 0-100% solute. This may be regarded as the input data, comprising of several sets of points $(C_i, D_i, i=1,k)$ say 'k' sets where 'k' is presumed to be a large number of the order of 100. The diffusivity data is presumed to have been generated during a prior diffusion experiment. One proposes to conduct a non linear least squares fit to the measured diffusivity data. The least squares analysis will yield values of the parameters $\tau_1, \ldots, \tau_{m+n}$ which minimize the

* Later in the paper a discussion is presented to help deduce such functional forms

least square error between the measured data points and the product of the proposed model functions for f(c) and $\phi(c)$. The parameters $\tau_1 \ldots \tau_{m+n}$ will define the functions $\phi(c)$ and f(c), and thereby provide an estimate of the thermodynamics of the system.

Implementation of a least squares solution demands the definition of a least squares error function (sometimes referred to as the chi squared function). In the present case this may be expressed as :

$$E^2 = \sum_i (w_i)^2 \{D_i - [f_i(\tau_1, \ldots, \tau_n)\phi_i(\tau_{n+1}, \ldots, \tau_{m+n})]\}^2 \qquad [9]$$

The non linear least squares estimation process amounts to searching an 'n+m+1' dimensional space for a minimum. At the minimum, the numerical value of the least squares error function, E^2 is 'small' but not necessarily zero. The numerical value of E^2 at the minimum is termed the residual and is a measure of the goodness of fit.

There are two major problems when least squares analysis is applied to a function that is a product of two other functions (f(c) and $\phi(c)$). Firstly, there is no guarantee that the space spanned by E^2 and the m+n unknown variables (τ_i) contains only a unique minimum, rather the possibility of multiple minima is very strong. Secondly, there is the possibility that the two functions ($\phi(c)$ and f(c)) are correlated.

The term correlated refers to the possibility that the two functions may be mathematically similar and hence indistinguishable. As an extreme example of two completely correlated functions consider two polynomials. If a product of two polynomials was taken, then it would be impossible to deduce the coefficients of the original polynomials given only the functional form of their product. In the present case correlation effects arise due to the inherent non uniqueness of the problem wherein one is attempting to compute two functions knowing only their product.

From the preceding arguments it is clear that the choice of functions to model the term f(c) and $\phi(c)$ in equation [8] should consider the possibility of correlation and of multiple solutions.

3.5 CONSTRAINTS ON THE THERMODYNAMIC FUNCTION $\phi(c)$

It is appropriate to examine some properties of the function $\phi(c)$. One may begin with its definition :

$$\phi(c) = \left(1 + \frac{\partial \ln \gamma}{\partial \ln c}\right) \qquad [10]$$

Firstly, it should be noted that for equilibrium conditions, $\phi(c)$ is always positive*, otherwise D(c) would be negative. Alternately one may regard the requirement for $\phi(c)$ to be positive as arising from the intrinsic thermodynamic stability criterion[13,14], $\partial\mu/\partial c > 0.0$, which must hold true for all isomorphous binary systems at equilibrium. For ideal alloys the function $\phi(c)$ is identically unity at all compositions; for alloys exhibiting positive deviation $\phi(c) < 1.0$, and for alloys exhibiting negative deviations from ideality $\phi(c) > 1.0$. Hence one may summarize:

$$\begin{aligned} 0.0 < \phi(c) < 1.0 &\quad \text{positive deviation} \\ 1.0 = \phi(c) &\quad \text{ideal alloy} \\ 1.0 < \phi(c) &\quad \text{negative deviation} \end{aligned} \qquad [11]$$

In addition to the above restrictions, $\phi(c)$ tends to unity as the composition tends to zero or to unity. In other words :

$\phi(c) \to 1$ as $c \to 0$ or as $c \to 1$

This is more transparent when $\phi(c)$ is expressed as follows:

$$\phi(c) = \left(1 + \frac{c}{\gamma}\frac{\partial \gamma}{\partial c}\right) \qquad [12]$$

---

* $\phi(c)$ assumes a negative value only in non equilibrium situations. As an example consider a system that possesses a spinodal in the phase diagram. If a solution is quenched from a temperature in excess of the critical point into the spinodal region then the solution is not stable and hence transforms by a spinodal transformation. $\phi(c)$ is negative during the spinodal transformation, and hence the interdiffusion coefficient is actually negative leading to the well known phenomenon of uphill diffusion.

As $c \to 0$ $\frac{c}{\gamma}\frac{\partial \gamma}{\partial c} \to 0$ hence $\phi(c) \to 1$

whereas

as $c \to 1$ $\frac{\partial \gamma}{\partial c} \to 0$ hence $\phi(c) \to 1$

The restrictions embodied in equations [11] and [12] will be referred to later in the paper.

3.6 SELECTION OF MODEL FUNCTIONS

This section explains how appropriate functions to model f(c) and $\phi(c)$ were selected.

3.6.1 Models for the thermodynamic term

Five isomorphous binary alloy systems were selected; one of these exhibited ideal solution behavior (Co-Ni), two systems exhibited positive deviations from ideality (Au-Ni and Cu-Ni) and two systems exhibited negative deviations from ideality (Ag-Au and CuAu). Isothermal, activity-composition data and activity coefficient-composition ($\gamma - c$) data were obtained for each of these alloys from the handbook by Hultgren et. al.[12].

It should be noted that the function $\phi(c)$ is usually not tabulated in most handbooks, since it is not a popular means of describing the system thermodynamics. Hence to evaluate the function $\phi(c)$ it was necessary to obtain not only the activity coefficient as a function of composition but also its slope with respect to composition. Since the slope $(\partial\gamma/\partial c)$ is not available from the handbooks, it was decided to fit the available activity coefficient - composition ($\gamma - c$) data with simple functions such as polynomials or exponentials and then use the fitted functions (and their derivatives) to evaluate the function $\phi(c)$

Curve fitting routines from the RS/1 package[15] were utilized in fitting functions to the raw $\gamma - c$ data. Polynomials of increasing order (upto fourth order) and exponential functions were successively tried in order to obtain a reasonable fit to the data. The data from Hultgren[12] et. al. was available at ten

3.6.2 Models for the function f(c)

Since Darken's theory and the theory proposed by Howard and Lidiard result in less than a 5% difference in the interdiffusion coefficient, it was decided to use Darken's equations to estimate the function f(c) for the five isomorphous binary systems chosen earlier. It should be noted that Darkens theory *does not* underlie the current algorithm but that it was used only to obtain an initial estimate of the function f(c). This initial estimate of f(c) was helpful in choosing an appropriate functional form for f(c).

Consideration of equation [4], indicates that an estimation of the function $f(c) = (D_1^* N_2 + D_2^* N_1)$, requires knowledge of the variation of the tracer diffusivities as a function of the composition. Hence, the literature was scanned to locate tracer diffusivities for each of the five isomorphous binary systems selected earlier. However, only the tracer diffusivity data for two systems, AuNi[16,17] and Ag-Au[18,19] could be obtained. The tracer diffusivity data for these systems was available at a temperature different from the temperature at which Hultgren et. al. report the activity data. Nonetheless it was felt that the general functional behavior of the D^*-c data could be studied.

Since exponential functions had been chosen to represent the function $\phi(c)$, some other functions had to be chosen to represent the tracer diffusivities (i.e. the functions f(c)) in order to avoid the possibility of correlation. Based on several attempts at curve fitting the tracer diffusivity data, it was concluded that second order polynomials could adequately model the variation of tracer diffusivities as a function of composition. From eqn. [4] this implied that the function f(c) could be adequately modelled by a cubic polynomial.

It may be argued that the choice of a functional form for f(c) was based on data from two alloy systems only and hence may not be representative of tracer diffusivities in general. This is certainly true, and modifications to the

functional form may be called for at a later stage. However, these are relatively straightforward to incorporate. Hence for the present one may assume that f(c) is well represented by a cubic polynomial.

3.6.3 Functional Model for the Interdiffusion Coefficient

Since f(c) was modelled by a cubic polynomial (P_3) and $\phi(c)$ was modelled by the function $\exp(P_5)$, it follows from equation 7 that the interdiffusion coefficient may be represented by the function $(P_3)(\exp(P_5))$. This function possesses 10 degrees of freedom which implies searching a chi squared space that is eleven dimensional. Clearly the possibility of multiple minima is a strong one.

3.7 ACQUISITION OF INTERDIFFUSION DATA

Data describing the variation of the interdiffusion coefficient with composition for the five isomorphous binary systems (AuNi, CuAu, CoNi, CuNi and AgAu) were obtained from the text by Borovskii[9]. The curves drawn by the authors were magnified and digitized at approximately 100 points. The data were then fitted with a fourth order spline (cubic spline) using a linear least squares approximation approach. Least squares spline fitting splits the interval of interest (in this case [0,1]) into several subintervals and fits a piecewise polynomial over each subinterval ensuring that several derivatives of the interpolant stay continuous at the boundaries between two intervals[20]. Details on spline fitting are available in a separate publication[21].

After fitting the raw digitized data with a spline, the diffusivity was obtained at 100 evenly spaced points on the interval (0,1], by evaluating the spline at each of the 100 points. This interpolated data were used as input for further calculations. Appendix II presents the raw digitized data and the spline interpolated data for reference purposes.

3.8 PRELIMINARY RESULTS

The interpolated diffusivity data were fit with the function $(P_3)(\exp(P_5))$ using the unconstrained non linear least squares (NLLS) routines from the RS/1 package. An unconstrained method was used initially to determine whether there was any

need to expend the additional effort in incorporating the constraint functions ($\phi(c=0) = 0$; $\phi(c=1) = 0$). A good fit was obtained to the D-c data. However examination of the $\phi(c)$function revealed that it was continuously increasing with concentration and that it violated the constraint that $\phi(c=1) = 1$. This is a clear example of the non-uniqueness problem alluded to earlier. In the present case, a set of functions $f_1(c)$ and $\phi_1(c)$ have been computed such that their product represents the D-c data, but the function $\phi_1(c)$ violates the requirements for the $\phi(c)$function. The problem occurred because the fitting routines did not incorporate the constraints embodied in equations [11] and [12].

Thus it is clear that one must choose an algorithm that permits the specification of constraints in the non linear least squares (NLLS) fitting process. The theoretical framework for accomplishing such a task is presented next.

3.9 THEORETICAL BASIS FOR CONSTRAINED NON LINEAR LEAST SQUARES

Since solution of the least squares problem (linear and non linear) demands the minimization of the least squares error function (equation 9), it is appropriate to examine the mathematical basis underlying the general problem of minimizing a given function. There are several excellent treatises available on this topic[22-25], the present discussion is based on the book by Gill et. al [22].

The non linear constrained problem (NCP) is defined as follows[22] :

$$\text{minimize} \quad F(x)$$

$$x \in R^n$$

$$\text{subject to :} \quad c_i(x) = 0 \qquad i = 1,2,\ldots m'$$

$$c_i(x) \geq 0 \qquad i = m'+1,\ldots,m \qquad [13]$$

where F(x) is the function being minimized and c_i are the various constraints (equality and inequality constraints). For sake of brevity only the conditions that must be satisfied at the minimum of the objective function are presented. Details of the algorithms for locating a minimum are found in the standard references[22].

The simplest example of a minimization problem is the unconstrained minimization of a univariate function. From basic calculus it is known that if the function possesses a minimum then at the minimum (x^*) the following conditions hold :

$$f'(x^*) = 0$$
$$f''(x^*) \geq 0 \qquad [14]$$

In the multivariate case these conditions are replaced by their multivariate equivalents:

$$|g(x^*)| = 0$$
$$G(x^*) \text{ is positive definite} \qquad [15]$$

There exist several popular algorithms to solve multivariate minimization problems[22]. In the non linear case these are necessarily iterative in nature and may be classified according to the amount of information used to locate the minimum in the chi squared space. Some methods use only repeated function evaluations to arrive at the minimum while first order methods use the gradient, and second order methods use the Hessian in addition to both the gradient and the function. In general the higher the order of the method, the better its convergence rate.

The multivariate case is more complex than the univariate case. Firstly, in the multivariate case, the algorithm must choose an appropriate search direction from the current point and secondly it must choose a step length along the chosen direction. In contrast, in the univariate case there is no ambiguity in regard to the search direction.

The situation is further complicated by the addition of constraints. Constrained minimization problems are usually classified based on the type of constraints imposed. Thus one distinguishes between linear equality constraints, linear inequality constraints and non linear constraints. In each case the conditions for a minimum to exist differ as do the solution schemes.

Linear equality constraints are usually expressed as a set of equations:

$$\text{minimize} \quad F(x) \quad \text{subject to} \quad Ax = b \qquad [16]$$

The matrix A contains the coefficients corresponding to each constraint. One next defines a matrix Z, the columns of which form a basis for all vectors 'p' satisfying the condition that $Ap = 0$. This condition defines all feasible search directions 'p' from a given feasible point. At the minimum, the following conditions hold :

$$(i) \quad Ax^* = b$$

$$(ii) \quad Z^T g(x^*) = 0 \quad \text{or equivalently} \quad g(x^*) = A^T\lambda^*$$

$$(iii) \quad Z^T G(x^*) Z \quad \text{is positive definite} \qquad [16]$$

The quantities, λ_i are termed the Lagrange multipliers. Solution of a linear equality constraint problem (LEP) with 't' constraints in 'n' unknowns is equivalent to solving an unconstrained problem in n-t dimensions. In essence the equality constraints reduce the dimensionality of the problem. All solution algorithms first locate an initial feasible point (i.e. one that satisfies the constraints) and then search for the minimum by moving away from the current feasible point along feasible directions only (i.e along the vectors 'p' defined earlier).

In the case of linear inequality constraints ($Ax \geq b$) there exists one restriction in addition to the conditions expressed in equation 16. The additional restriction demands that all the Lagrange multipliers be strictly positive. The popular solution scheme utilized is termed *the active set method* wherein a subset of the inequality constraints is determined. All the constraints in this subset are *binding constraints*, i.e. the condition $Ax = b$ is exactly satisfied for these constraints. Such a set of constraints is termed as the active set or working set. Once an active set has been determined the solution scheme is very similar to that for the non linear equality problem.

A recurring theme in algorithms for minimization is the modelling of the objective function F(x) by a quadratic function :

$$F(x) \approx g^T(x^*) + \frac{1}{2}x^{*T}Gx^* \qquad [17]$$

Equation 17 can be derived by expanding F(x) as a Taylor series about $x=x^*$ and neglecting the terms higher in order than the second order term. Clearly such an approximation is local, i.e. it holds only close to the minimum. In practice it is found that iterative schemes usually do converge to the minimum even when the initial point is far from the minimum.

3.10 CONSTRAINED FITTING OF DIFFUSIVITY DATA

Earlier in this paper it was decided that the function $\exp(P_5)$ would be used to model the quantity $\phi(c)$ In itself, the chosen function $\exp(P_5)$ only ensures that $\phi(c)$is positive but does not satisfy the constraints of equation 12. In order to satisfy the constraint, $\phi(c=0) = 0$, the constant term in the polynomial P_5 must be set to zero. Hence the function used to represent $\phi(c)$must be modified to read as follows:

$$\phi(c) = \mathrm{Exp}(\tau_5 c^5 + \tau_6 c^4 + \tau_7 c^3 + \tau_8 c^2 + \tau_9 c) \qquad [18]$$

where τ_i are the unknown parameters that constitute the model and c is the composition, i.e. c ranges over the interval [0,1].

Thus the imposition of the constraint $\phi(c=0) = 1$ reduces the dimensionality of the problem to 9 variables. Similarly the constraint $\phi(c=1) = 1$ leads to the following constraint on the parameters :

$$\sum_{k=5}^{k=9}\tau_k = 1 \qquad [19]$$

Thus the diffusivity was modelled by the following function :

$$h_i(c) \approx \left(\sum_{j=1}^{4}(\tau_j c_i^{4-j})\right)\left(\mathrm{Exp}\left(\sum_{k=5}^{9}(\tau_k c_i^{10-k})\right)\right) \qquad [20]$$

and was subject to the constraint embodied in equation [19].

During the fitting process the data were weighed to reflect the fact that the absolute uncertainty in each data point was identical. Hence the weights were selected as the reciprocal of the absolute value of the ordinate of the data. Based on all of the above, the least squares error function may be defined as follows :

$$E^2 = \sum_{i=1}^{i=100} \{(D_i - h_i)w_i\}^2 \qquad [21]$$

where, h_i is given by equation 20 and $w_i = 1.0/D_i$

The NAG [25] fortran library subroutine E04UAF and E04VCF were used to locate the minimum. E04UAF uses a sequential augmented Lagrangian method[22] coupled with the Quasi Newton method[22]. Since the method does not utilize the gradient or the Hessian of the objective function, its convergence rate is very slow.* In contrast, the subroutine E04VCF uses a sequential quadratic programming algorithm wherein the search direction is the solution of a quadratic programming problem[22]. Since this is a comprehensive routine that utilizes information about the gradient of the objective function the convergence rate is very rapid**. In addition E04VCF makes it easier to monitor the progress of the minimization process.

3.11 RESULTS OF CONSTRAINED FITTING

The salient features and results from the attempts at constrained fitting will be highlighted by discussing the Co-Ni system in detail. Diffusivity data for this data were obtained at 1356°C. Results for the other systems will be presented in the following paper. Throughout this discussion the term *original diffusivity data* will refer to the data obtained by interpolating the spline approximation to the raw digitized diffusivity data.

Figure 3 compares the fitted and original diffusivity data. The subroutine E04UAF was used for this fit and the only constraint imposed was that embodied in equation 19. From figure 3 it is clear that a good fit was obtained to the original

* A typical run took 2-3 hours on a MicroVax II.
** A typical run required 7-10 minutes on a MicroVax II.

diffusivity data. Figure 4 depicts the $\phi(c)$ function corresponding to the fit. Figure 4 suggests that the CoNi system exhibits a positive devlation from ideality. However it is known, from Hultgren[22], that the CoNi system is ideal. Therefore the chemical potential results in figure 4 are spurious, despite the fact that the computation yielded an excellent fit to the $\tilde{D}-c$ data. This is clearly a manifestation of the correlation effect which had been alluded to earlier. In the present case the product of the computed functions f(c) and $\phi(c)$ provides a good fit to the diffusivity data but the computed function $\phi(c)$ does not represent the system thermodynamics.

The correlation effect undermines the attempts to compute chemical potentials by leading to multiple solutions. Correlation effects arise since the problem at hand is intrinsically non unique. The origin of the correlation effect lies in the fact that the diffusivity is being modelled as a product of two function which are *both* unknown. Hence by making compensating errors in each function it is still possible to get a good fit to the diffusivity (since it is the product of these functions). This implies that given some diffusivity data several sets of functions $[f_i,\phi_i(c)]$ exist such that the product of each set provides a good fit to the original diffusivity data. Each such set of functions $[f_i,\phi_i(c)]$ corresponds to a minimum in the $\phi(c)-c$ space. Clearly only one of these sets represents the real alloy system while the others are spurious minima arising from the fitting procedure. Therefore the problem at hand transforms into firstly computing all the minima and then picking the correct minimum from the set of computed minima. The problem of locating and computing all possible minima is addressed first. Next a strategy is presented to pick the correct minimum from the set of computed minima.

3.11.1 Obtaining a set of feasible minima

No general mathematical technique exists for simultaneously locating all the minima of the non linear least squares problem. Hence the following iterative strategy was adopted. The algorithms were modified to incorporate additional constraints the general form of which was as follows :

$$l \leq \phi(c_i) \leq u \qquad i = 1,\ldots 10 \qquad [22]$$

These constraints were imposed at ten compositional points evenly spaced on the interval [0,1]. The lower bounds at each compositional point were identical, i.e. $l(c=0.5) = l(c=0.7) = l(c=0.9)$ as were the upper bounds. By varying the lower and upper bounds, l_i and u_i respectively, it was possible to constrain the $\phi(c)$function to different regions of the two dimensional $\phi(c)-c$ space. For each set of constraints a complete non linear least squares fit was carried out. After each such run the goodness of the fit to the original diffusivity data were examined. If a satisfactory fit was obtained then the corresponding $\phi(c)-c$ function was added to the set of possible minima. In this manner by varying the constraints, l_i and u_i, a set of possible minima was obtained. In essence, the additional constraints in equation [22] restrict the search to a subset of the $\phi(c)-c$ space. By searching several subsets of the space one ends up with the set of possible minima. It should be noted that the constraints, l_i and u_i, must be consistent with the 'natural' constraints on $\phi(c)$ which are embodied in equation 11. In other words the choice of l_i and u_i must be such that the function $\phi(c)$tends to unity at either end of the interval [0,1]. Hence a choice of $l_i=2.0$ and $u_i=4.0$ would be incorrect.

Figure 5 depicts the results of several such runs on the CoNi system. The figure plots $\phi(c)$as a function of c for different sets of upper and lower bounds. The legend in the figure corresponds to the upper and lower bounds for each computation. In each case an excellent fit to the original diffusivity data were obtained; similar to the fit depicted in figure 3. The goodness of fit can be judged from the table of residuals (refer Appendix I).

The $\phi(c)$c data in figure 5 was integrated to yield $\gamma-c$ data. Numerical integration was carried out using a fourth order Runge-Kutta-Nystrom technique[26], and the boundary condition that $\gamma = 1$ at $c=1$. The step size used was 0.0001 and the data were plotted every 2%. Using this integration scheme the activity composition curves depicted in figure 6 were generated. In this manner all the minima were obtained.

3.11.2 Selection of the Appropriate minima

From figure 6 it is clear that if the true activity were known at any one composition then one could easily pick out the correct activity composition curve from the set of possible minima. This implies that a single experimental point in conjunction with the $\bar{D}-c$ curves and the proposed computational scheme can yield the entire $\gamma-c$ curve for the particular alloy. The set of minima may be examined prior to the experiment to choose an appropriate composition range within which an experiment could be performed. For example, for the CoNi system (figure 6), one might choose to conduct an experiment in the composition range [0.35,0.55] since the various activity-composition curves exhibit the maximum separation in this range of compositions. One might also accomplish this if the slope of the activity composition curve was known at the dilute end. It will be recalled[13,14] that the slope of the activity composition curve corresponds to the Henry law line for the solution.

In the present investigation, it was decided to use the Henry's law line in picking the correct solution. The slope of Henry's law line can be easily estimated from data on heats of solution. Heats of solution for liquid binary metal systems have been theoretically estimated by Miedema[28] et. al. .

Miedema's model is atomistic and arrives at the heat of formation by modelling the contributions of the change and discontinuities in electron charge density (that occurs on alloying) to the heat of formation. Based on this model, Miedema[28] et. al. have estimated the heats of formation at infinite dilution for several liquid binary metal systems. A good match was obtained between their predictions and the measurements reported in the literature.

Although Miedema's model works well for liquids it is less applicable to solids since it does not account for the strain energy. For solids, Russell[29] has proposed a simple scheme that permits one to estimate the enthalpy of formation in the solid state knowing the latent heat of fusion of the solute, its melting

temperature and the binary phase diagram (Ref. Appendix III for details). Russell's[29] scheme leads to the following expression:

$$\Omega_s^B = \Omega_l^B + L_m^B\left(1 - \frac{T}{T_m^B}\right) + RT\ln\left(\frac{x_l}{x_a}\right) \qquad [23]$$

where Ω_s^B represents the partial molar enthalpy of formation in the solid state, Ω_l^B represents the partial molar enthalpy in the liquid state.

It was decided to utilize Miedema's theoretical predictions in conjunction with Russell's technique to estimate the slope of the Henry's law line in order to select the correct minimum from the set of possible minima (figure 6). It was hoped that at the very least a reasonable estimate of the Henry's law line could be obtained. It was further assumed that the entropy of solution at infinite dilution was ideal. The activity coefficient was computed using the following equation :

$$\Omega_s^B = -RT\ln\gamma_B \qquad [24]$$

By using this approach the Henry's law constant was estimated for the CoNi system.

For the CoNi system Miedema's data predicts that the heat of formation at infinite dilution is -1kJ/mole for Ni in liquid Co. Since Miedema et. al. did not report the temperature to which their predictions correspond, it was assumed that in each case the Ω_l^B data corresponded to the melting point of the solvent. Based on this premise and using equations 23 and 24, the Henry's constant for Ni in Co was computed to be 0.95 at 1356°C. This line has been plotted in figure 6 for comparison. Referring next to figure 6, it is seen that the solution closest to the estimated Henry's law line is the one which was computed using the bound: $0.99 \leq \phi(c) \leq 1.10$. Hence the other solutions (sets of coefficients) may be discarded as spurious minima. From figure 6 it is clear that the chosen set of coefficients predict that the CoNi system is nearly ideal which is in excellent

agreement with the experimental data reported by Hultgren et. Al[12]. This is clearer from figure 7 which plots ln(γ) as a function of composition for the selected solution.

3.12 DISCUSSION

Thus by considering the CoNi system as an example it has been demonstrated that it is possible to compute activities given interdiffusivites. The only other piece of information used was the *theoretical* predictions of the heats of formation. One may also have used the experimentally measured activity at *one particular composition.* This paper has presented the background, theoretical basis and the proposed computational scheme for obtaining thermodynamic activities from interdiffusion coefficients. The next paper discusses the results of similar computations conducted on ten additional systems. For each of the ten systems the computed activities will be compared with the experimental data presented by Hultgren[12]. These ten systems will help establish the reliability of the proposed computational scheme.

3.13 CONCLUSIONS

A non linear least squares based strategy was successfully implemented to compute activity composition data from interdiffusion data. The proposed scheme requires the $\tilde{D}-c$ data and one additional piece of information, such as the experimentally determined activity at a particular composition or the slope of the Henry's law line at infinite dilution, to compute the entire activity-composition curve. Due to its inherent non uniqueness, the scheme leads to multiple solutions. The correct solution can be picked from the possible set of solutions by using the additional piece of information. In the present paper, by using theoretical predictions of the heat of formation to estimate the slope of the Henry's law line, it was possible to pick the correct solution. The scheme was successfully demonstrated on the CoNi system which was shown to obey Raoult's law. Excellent agreement was obtained between the predicted values and the data reported in the literature.

3.14 SYMBOLS

M	-	phenomenological coefficient
D	-	diffusion coefficient
μ	-	chemical potential
c	-	composition
J_i	-	flux of species i
$L_{i,k}$	-	generalized phenomenological coefficient
X_k	-	generalized force
$\Delta \dot{S}$	-	entropy production rate
T	-	Temperature in Kelvin
D_i^*	-	Tracer diffusivity of species i
N_i	-	mole fracion
γ	-	activity coefficient
N	-	mole fraction
X_i	-	mole fraction of component 'i'
t	-	time
x_m	-	spatial cordinate of the matano interface
$f(c)$	-	function incorporating dependence of the diffusivity on the phenomenological coefficient
$\phi(c)$	-	thermodynamic function
τ_i	-	unknown variable in the least squares analysis
w_i	-	weighing function in the least squares analysis

E^2 - least squares error function

$F(x)$ - objective function being minimized

R^n - space of real numbers

f' - slope of a univariate function f

f'' - curvarture of a univariate function f

$g(x)$ - gradient of multivariate function f

$G(x)$ - Hessian of a multivariate function f

$\| \|$ - norm of a vector or matrix

λ - matrix containing coefficients of equality constraints

δ - vector of equality constraints

λ - Lagrange multiplier

h_i - function used to model the interdiffusivity

u - upper bound on $\phi(c)$

l - lower bound on $\phi(c)$

Ω_l^B - Partial molar enthalpy of solution in the liquid state

Ω_s^B - Partial molar enthalpy of solution in the solid state

T_m - melting point of solute B

L_m - enthalpy of fusion of solute B

X_a - compositon of the solid phase in equilibrium with the liquid phase

X_l - compositon of the liquid phase in equilibrium with the solid phase

3.15 REFERENCES

1. S. R. de Groot, *Thermodynamics of Irreversible Processes*, North Holland Publishing Company, (1963).

2. K. G. Denbigh, *Thermodynamics of the Steady State*, John Wiley & sons (1951).

3. I. Prigogine, *Introduction to the thermodynamics of Irreversible Processes*, John Wiley and Sons, (1961).

4. J. S. Kirkaldy and D. J. Young, *Diffusion in the Condensed State*, The Institute of Metals, (1987).

5. L.S. Darken, *Trans. AIME*, 174, pp. 184-201, (1948).

6. R. E. Howard and A. B. Lidiard, *Rep. Prog. Phys.*, 27, 161, (1964).

7. J. R. Manning, *Diffusion Kinetics for Atoms in Crystals*, D. Van Nostrand, (1968).

8. C. Wells, *Atom Movements*, ASM, pp. 26-50 (1950).

9. I. B. Borovskii, K. P. Gurov, I. D. Marchukova and Y. E. Ugaste, *Interdiffusion in Alloys*, Nauka Publishers, NTIS Document PB86-245495, (1986).

10. Crank, *The Mathematics of Diffusion*, Oxford Press (1975).

11. R. W. Balluffi, *Acta Metallurgica*, 8, pp. 871-873, (1960).

12. R. Hultgren, P. D. Desai, D. T. Hawkins, M. Glieser and K. K. Kelley, *Selected Values of the Thermodynamic Properties of Binary Alloys*, ASM, (1973).

13. C. H. P. Lupis, *Chemical Thermodynamics of Materials*, North Holland, (1983).

14. M. Modell and R. C. Reid, *Thermodynamics and its Applications*, Prentice Hall, (1983).

15. RS/1, Release 3.0, BBN Software, Cambridge, (1987).

16. A. D. Kurz, B. L. Averbach and Morris Cohen, *Acta. Met.*, 3, 442-446, (1955).

17. J. E. Reynold, B. L. Averbach and Morris Cohen, *Acta. Met.*, 5, 29-40 (1957).

18. W. C. Mallard, A. B. Gardner, Ralph F. Bass, L. M. Slifkin, *Physical Review*, 129, No. 2, 617-625, (1963).

19. H. W. Mead and C. E. Birchenall, *Trans. AIME*, Journal of Metals, 874-877, (1957).

20. Carl deBoor, *A Practical Guide to Splines*, Springer Verlag, Applied Mathematical Series, (1985).

21. Rakesh R. Kapoor, *Thermodynamic Data from Diffsuion Couples*, Paper IV, Sc.D thesis, MIT, (1989).

22. Phillip E. Gill, Walter Murray and Margaret H. Wright, *Practical Optimization*, Academic Press, (1981).

23. Yonathan Bard, *Non Linear Parameter Estimation*, Academic Press, (1974).

24. Philip R. Bevington, *Data Reduction and Error Analysis for the Physical Sciences*, McGraw Hill, (1969).

25. NAG Fortran Library Manuals, Mark 13, Numerical Algorithms Group, Downers Grove, IL, (1987).

26. Erwin Kreyszig, *Advanced Engineering Mathematics*, Wiley, (1967).

27. Butcher, *The Numerical Analysis of Ordinary Differential Equations*, Wiley (1987).

28. A. R. Miedema, F. R. deBoer and R. Boom, *Calphad*, 1, No. 4, pp.341-359, (1977).

29. K. C. Russell, *Kinetic Processes in Advanced Alloys*, Final report to Materials Laboratory, Wright Research and Development Center, Air Force Systems Command, Wright Patterson AirForce Base, OH, WRDC-TR-89-4051, (1989).

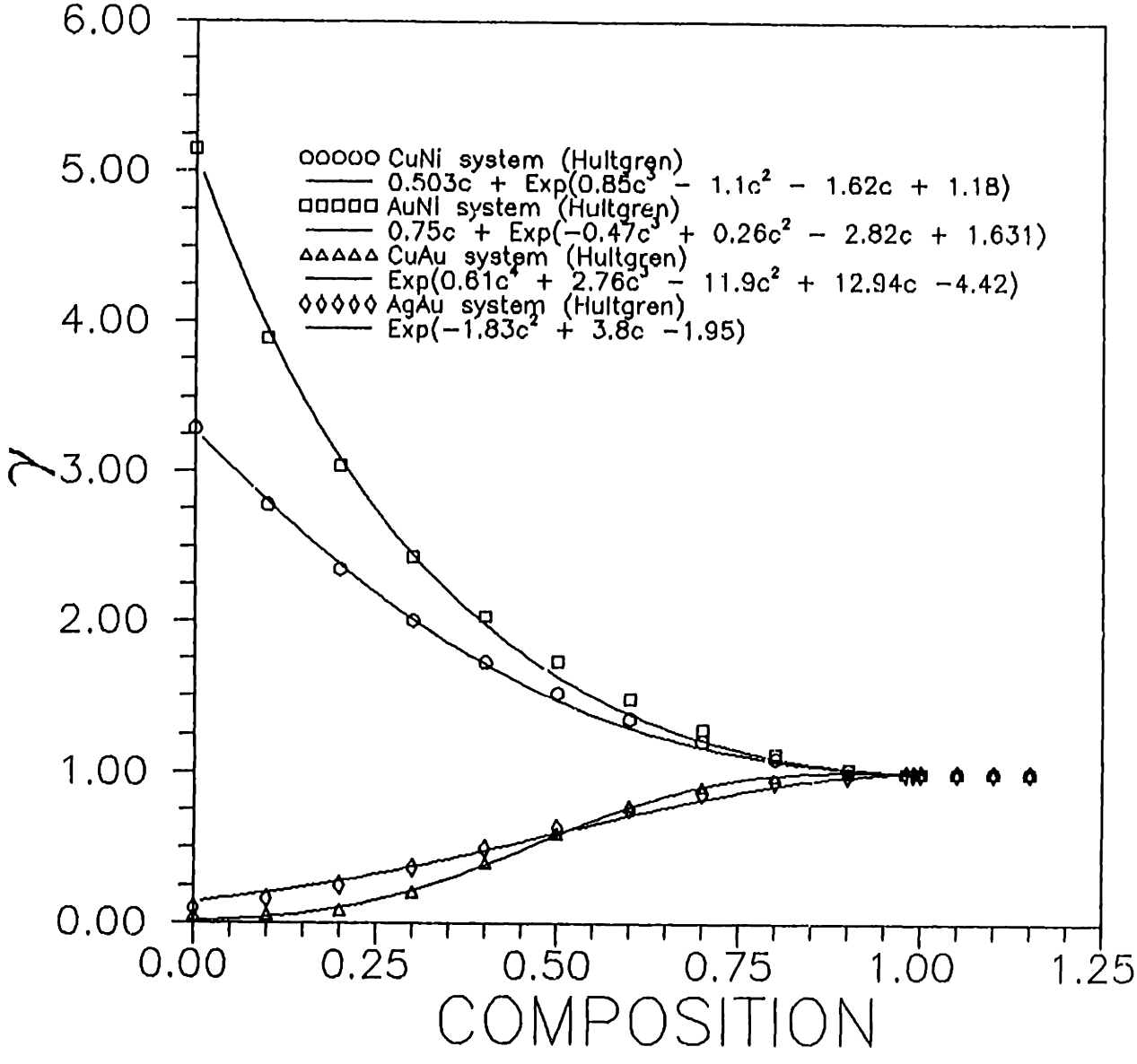

Figure 1. Activity coefficients for four isomorphous binary alloys. Solid lines represent the fitted functions.

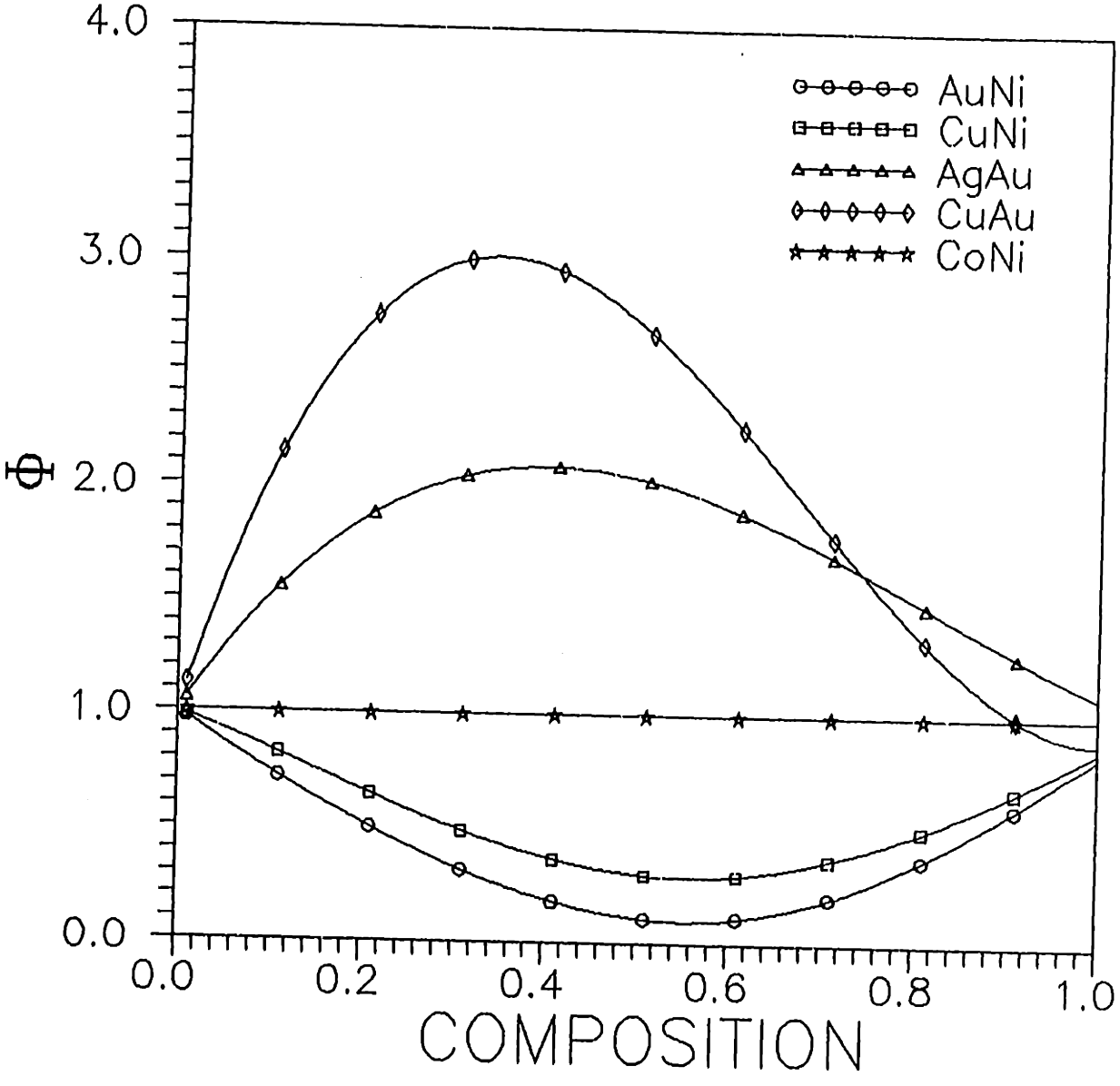

Figure 2. Thermodynamic factor for five isomorphous binaries obtained by differentiating the functions fitted to the $\gamma - c$ data depicted in figure 1.

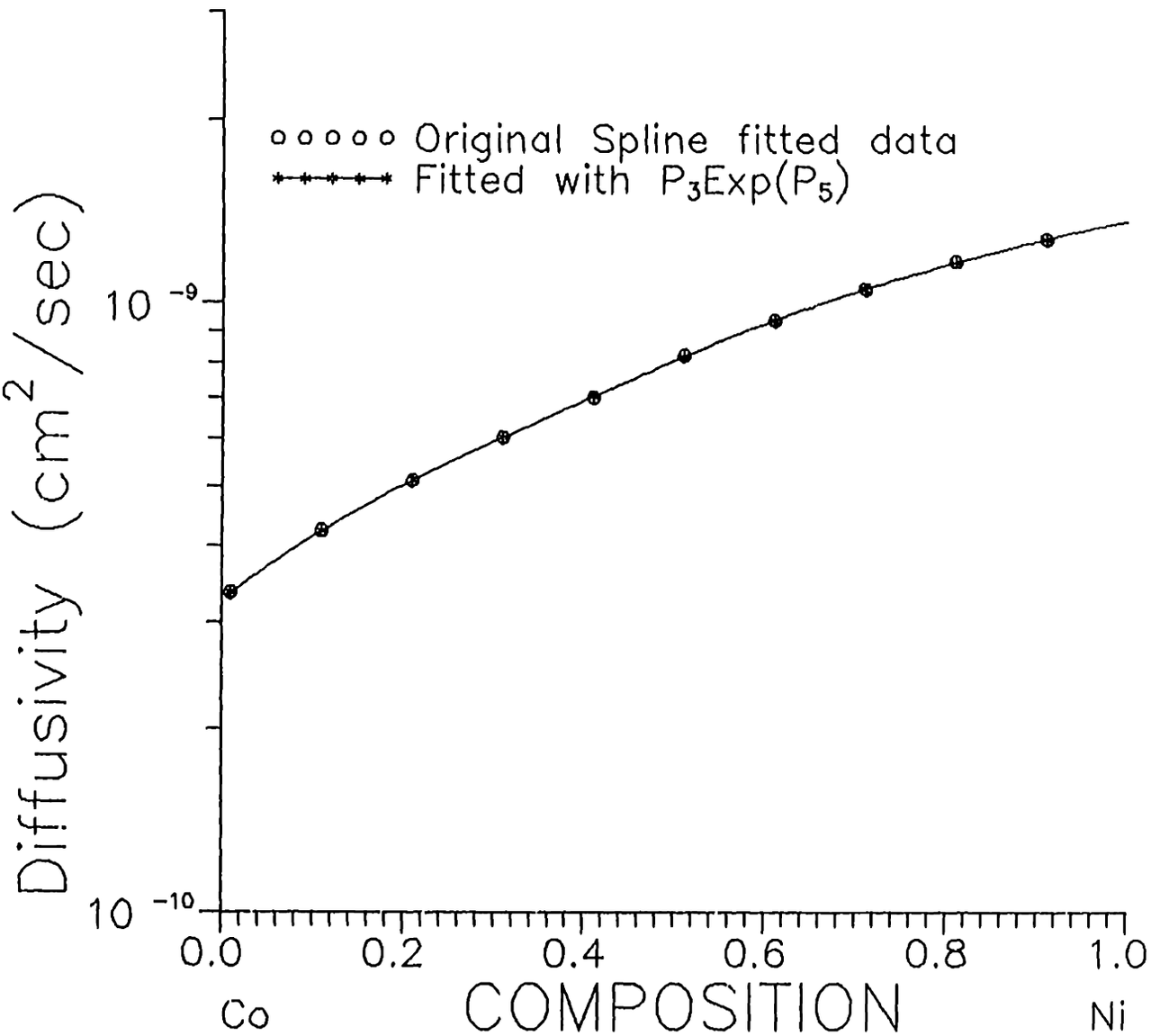

Figure 3. Fitted and original diffusivity data for the CoNi system at 1356°C. The fitting function used was $P_3[Exp(P_5)]$. The only constraints imposed were $\phi(c=0) = 0$ and $\phi(c=1) = 1$.

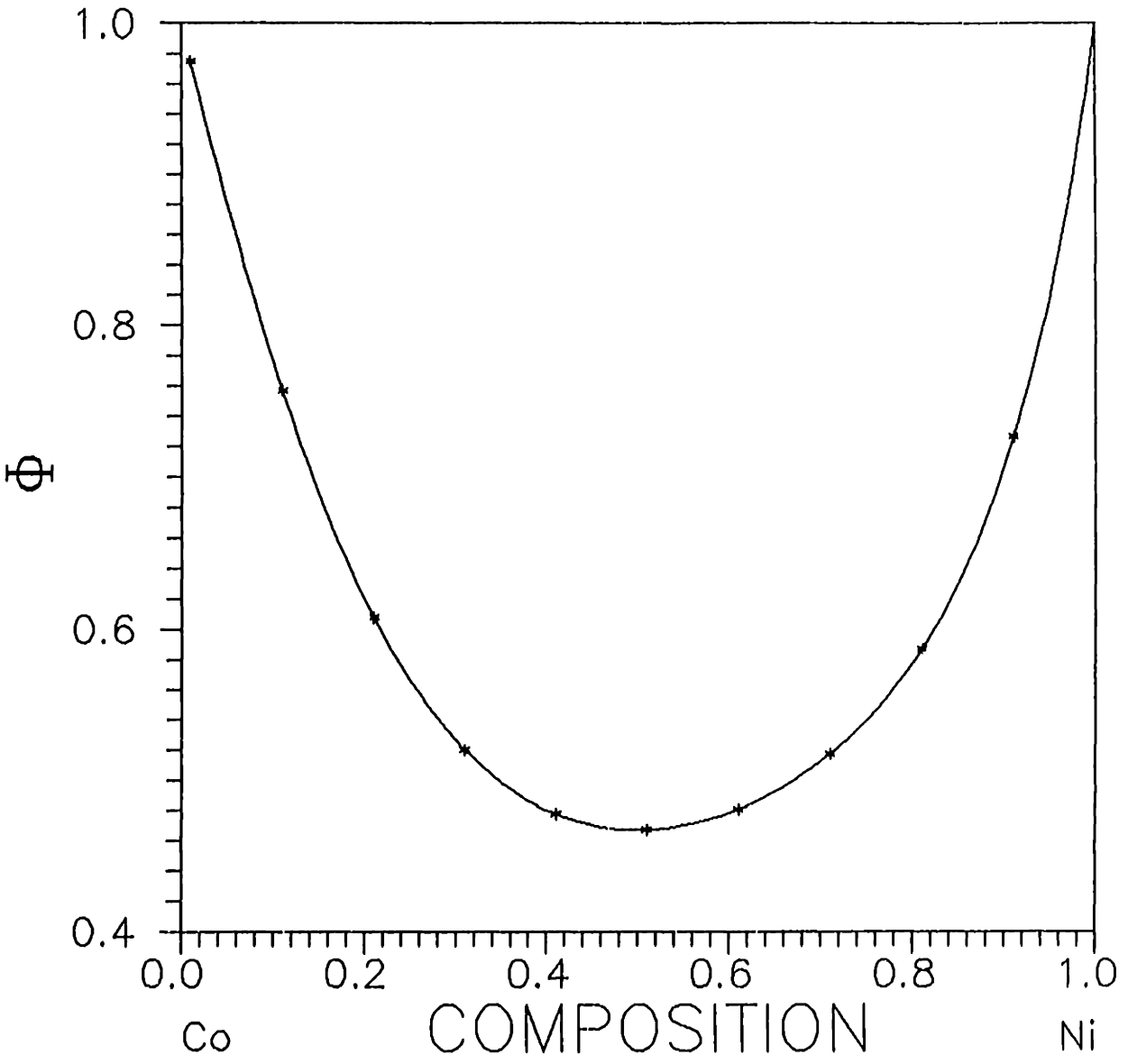

Figure 4. Computed thermodynamic function for the CoNi system at 1356°C corresponding to the fit depicted in figure 3. The only constraints imposed were $\phi(c=0) = 0$ and $\phi(c=1) = 1$.

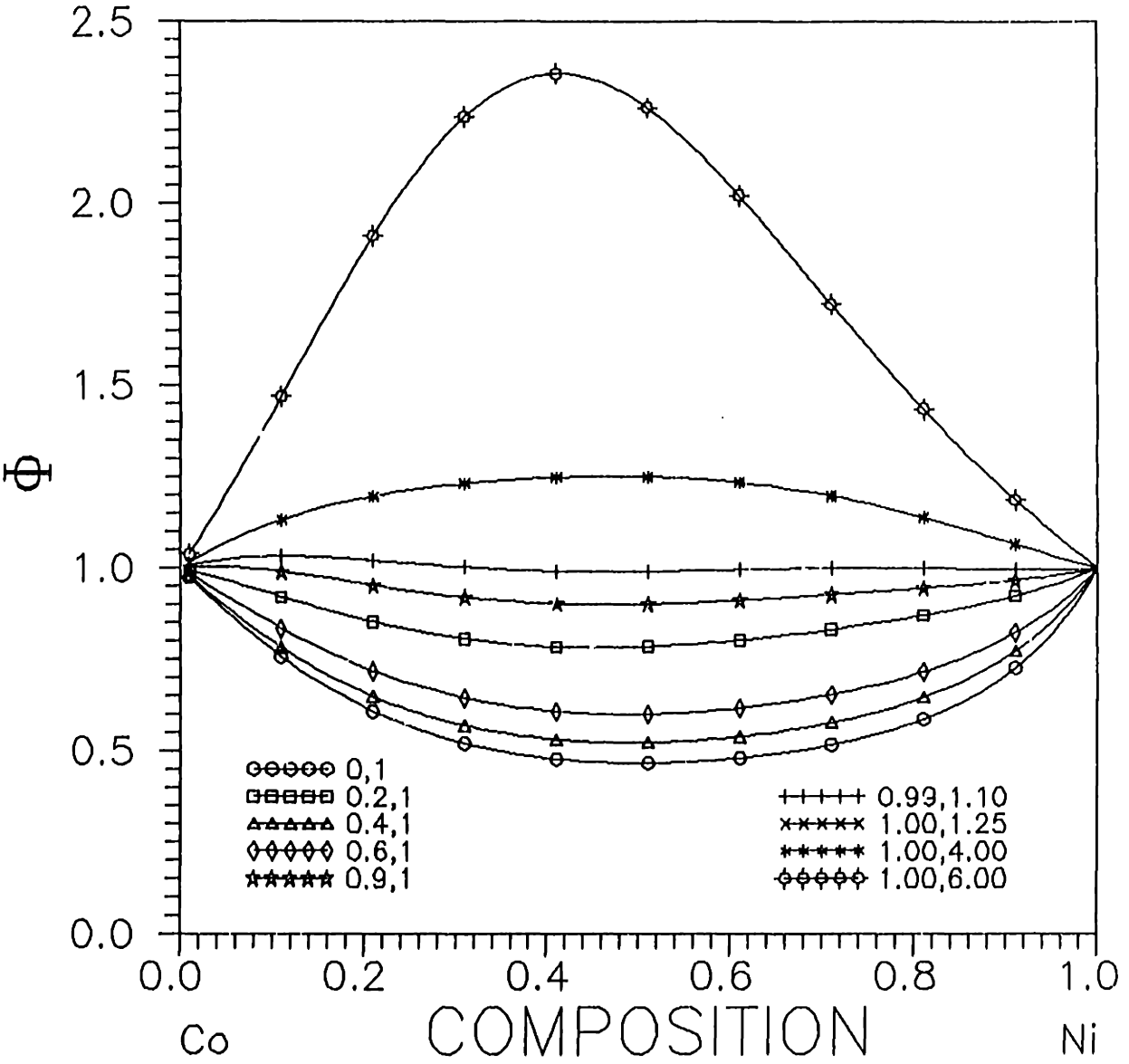

Figure 5. Complete set of feasible solutions for the CoNi binary at 1356°C on a $\phi(c) - c$ diagram. Each solution corresponds to a minimum in the $\phi(c) - c$ space. Legend in the figure refers to the upper and lower bounds imposed on $\phi(c)$ to compute each minimum. The solutions for the bounds [1,4] and [1,6] are coincident. The solution computed on imposing the bounds [0.99,1.10] was taken to represent the thermodynamics of the CoNi system.

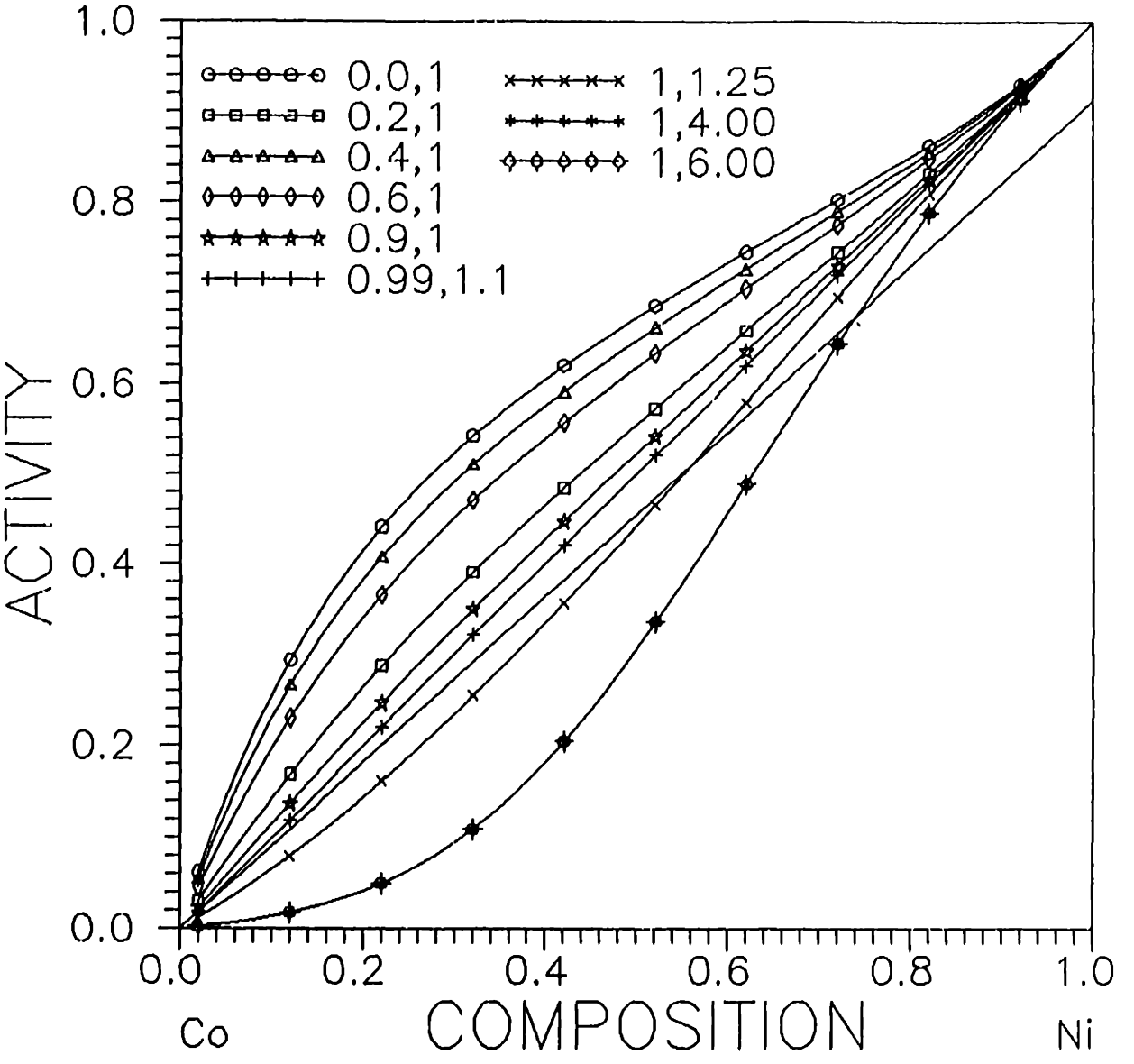

Figure 6. Complete set of [illegible] solutions for the CoNi binary at 1356°C on an activity composition diagram. This data were obtained by integrating the data in figure 5. The solutions for the bounds [1,4] and [1,6] are coincident. The solution computed on imposing the bounds [0.99,1.10] was taken to represent the thermodynamics of the CoNi system.

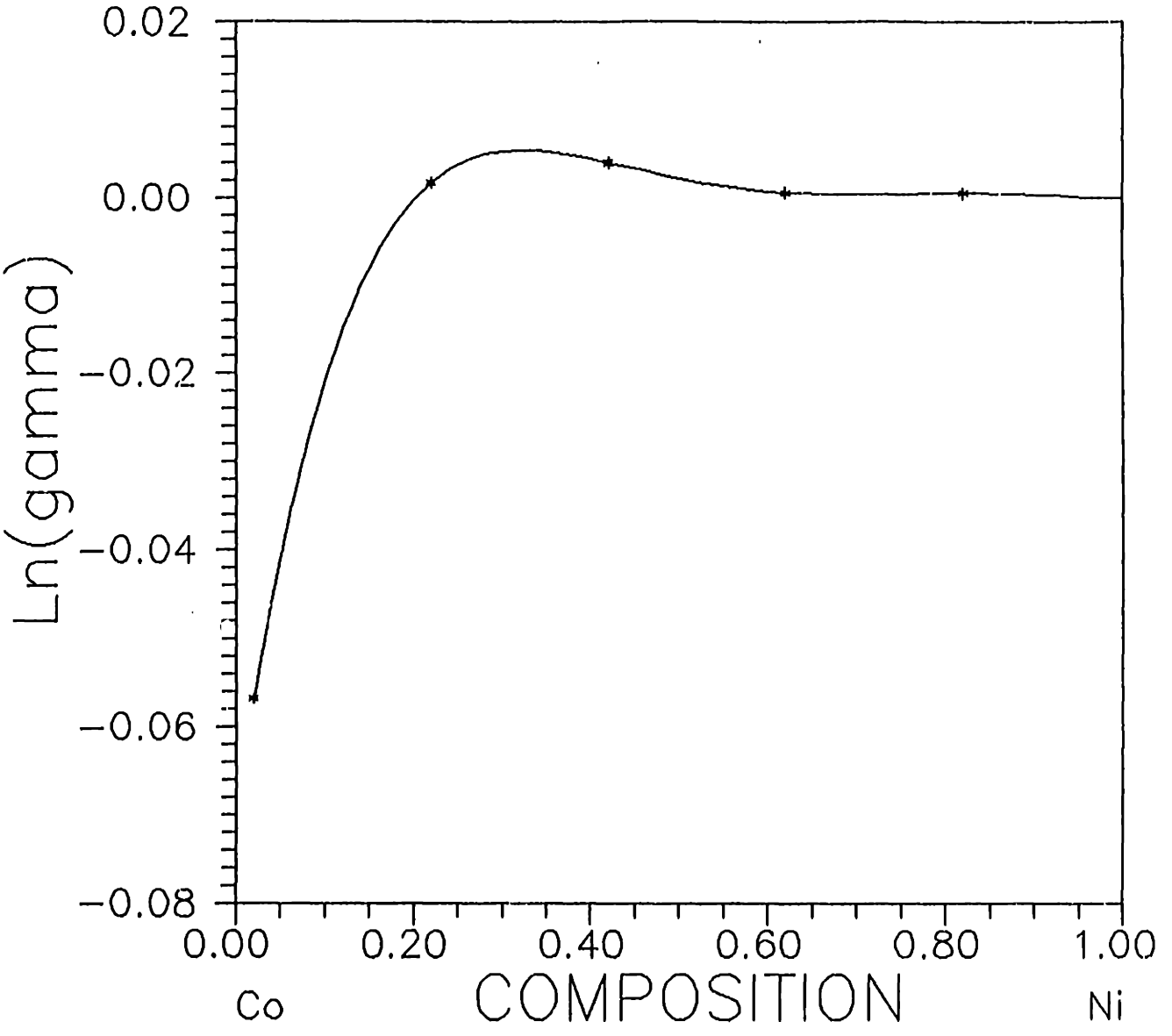

Figure 7. Ln(γ) as a function of mole fraction Ni for the CoNi system at 1356°C. This curve corresponds to the solution selected from the set of possible solutions in figures 5 and 6. The bounds used to compute this solution were [0.99,1.10].

Thermodynamic Data from Diffusion Couples - III

4.1 ABSTRACT

A non linear least squares based algorithm which permits one to compute the activity composition relationship given only the interdiffusion coefficient as a function of composition was applied to the following ten isomorphous binary alloy systems: CuAu, PdCu, CuNi, PdNi, AgAu, CoNi, PdFe, AuNi, PtNi and NbTi. Due to the inherent non uniqueness of the problem, the algorithm leads to multiple solutions. One additional piece of information such as the activity at one particular composition or the Henry's law constant at infinite dilution is needed to pick the correct solution. For eight of the ten binary systems the algorithm computed a possible solution that was close to the experimentally measured activity-composition curves confirming that it is possible to compute activities from interdiffusivities. The model may also be applied to systems exhibiting a miscibility gap.

4.2 INTRODUCTION

This is the third paper in a series of four papers covering an investigation aimed at obtaining chemical potential information from diffusion couples. In the previous paper[1] a non linear least squares approach was proposed which models the interdiffusion coefficient as a product of two functions, one arising from the thermodynamic function and the other representing the contributions of the phenomenological coefficients. In this paper the proposed computation scheme will be applied to ten isomorphous binary alloy systems. For each system data describing the variation of the interdiffusion coefficient as a function of composition was obtained from the text by Borovskii[2] et. al. . The results of the calculation were compared with the experimentally reported activity-composition data summarized in the handbook by Hultgren[3] et. al. .

4.3 MODEL SUMMARY

The proposed scheme models the interdiffusion coefficient as a product of two functions :

$$D = f(c).\phi(c) \qquad [1]$$

$$D_i \approx \left(\sum_{j=1}^{4}(\tau_j c_i^{4-j})\right)\left(\mathrm{Exp}\left(\sum_{k=5}^{9}(\tau_k c_i^{10-k})\right)\right) \qquad [2]$$

In addition the following constraints were imposed on the variables[1] :

$$\phi(c=0) = 1.0 \quad \text{and} \quad \phi(c=1) = 1.0 \qquad [3]$$

$$l_i \leq \phi(c_i) \leq u_i \quad \text{at} \quad c_i = [0.1, 0.2, \ldots\ldots, 0.9] \qquad [4]$$

Thus the diffusivity was modelled as a product of two functions: $P_3[\exp(P_5)]$. It should be noted that these functions were chosen based on preliminary analyses and that these functions may be easily changed. During this investigation it became necessary to alter the modelling function to $P_4[\mathrm{Exp}(P_6)]$. For this modelling function the diffusivity may be expressed as follows:

$$D_i \approx \left(\sum_{j=1}^{5}(\tau_j c_i^{5-j})\right)\left(\mathrm{Exp}\left(\sum_{k=6}^{11}(\tau_k c_i^{12-k})\right)\right) \qquad [5]$$

The least squares error function for these models may expressed as follows :

$$E^2 = \sum_{i=1}^{i=100}\{(D_i - h_i)w_i\}^2 \qquad [6]$$

where, h_i is given by equation [2] or equation [5] (depending on the model being used) and $w_i = 1.0/D_i$

Using the Fortran routine E04VCF from the NAG library[4] the least squares problem of equation 6 was solved subject to the constraints embodied in equations 3 and 4. Solution of the least squares problem amounts to minimizing E^2 with respect to the variables τ_i and subject to the imposed constraints (eqns. 3 and 4). Several runs were performed, each with a different set of upper and lower bounds $[l_i, u_i]$. A minimum in $E^2 - c$ space was located for each set of bounds. For each such set the

fit to the interdiffusion coefficient was checked graphically and if found satisfactory the particular minimum was accepted as a possible solution to the problem. In this manner a set of solutions was determined.

Multiple solutions are inherent to this computational scheme since one is attempting to compute two unknown functions (f(c) and $\phi(c)$) given only their product ($\tilde{D}-c$). One expects that there will be several sets of functions [$f_i(c)$, $\phi_i(c)$] such that the product of each set will provide an adequate fit to the original diffusivity data. The constraints of equation [4] restrict one of the two functions, $\phi(c)$, to a certain region of the $\phi(c)-c$ space. For each set of bounds one searches a section of the $\phi(c)-c$ space. Thus by searching different sections of the space, the entire set of feasible solutions can be easily determined.

The $\phi(c)-c$ data for each solution was then integrated to obtain $\gamma-c$ data from which a set of curves were generated on the activity-composition diagram. Integration of the $\phi(c)-c$ data was carried out using a Runge-Kutta-Nystrom technique with a step size of 0.0001. The data were plotted every 2%. Each curve corresponded to a particular solution of the problem. The next task was that of selecting the appropriate solution from the set of possible solutions.

The task of selecting the appropriate solution from the set of possible solutions demands one additional piece of information. This could be in the form of experimentally measured activity data at a single composition. If an experiment were to be performed, then observation of the set of computed solutions would suggest an appropriate composition range within which an experiment ought to be performed. The composition range selected for the experiments should be one wherein the computed solutions exhibit the maximum separation.

Alternately, one may utilize the slope of the Henry's law line at infinite dilution to select the appropriate solution from the set of solutions. In this study, theoretical model predictions of the heats of mixing at infinite dilution (by Miedema[6] et. al.) were used to compute the Henry's law line for each of the systems under consideration.

The procedural details have been presented in the earlier paper[1] (see also Appendix III). Using the theoretically predicted Henry's law line it was hoped that the correct solution from the set of feasible solutions could be picked. The selected solution was compared with the experimentally available activity data reported by Hultgren[3] et. al. to determine the reliability of the proposed computational model.

Since the objective function (E^2) is non linear in the unknown parameters (τ_i) the process of minimization is iterative and commences at an initial guess which must be provided. For all the computations conducted in this investigation the initial guess was taken to be the unit vector, i.e. $\tau_i = 1$ for all i. This initial guess is clearly not consistent with the constraints of equations [3] and [4]. However, the subroutine E04VCF, is powerful enough to locate an initial feasible point* within the first iteration. Subsequent iterations always move from one feasible point to another. With each iteration the subroutine attempts to minimize the value of the least squares error function (E^2). When no improvement is possible and the gradient of the objective function is 'small', the minimum is said to have been attained and the program terminates. At the minimum, the least squares error, E^2, is usually non-zero and is termed the residual. The numerical value of the residual is a measure of the goodness of fit. This is particularly useful in cases where two solutions are close to another. The solution with the smaller residual provides a better fit to the diffusivity data and is therefore selected as the correct solution.

The proposed scheme may fail for any of the following reasons. Firstly it is possible that an inappropriate functional form was chosen to model the thermodynamic term or the function f(c). This should manifest itself as an inability to obtain a good fit to the diffusivity data. Secondly from the proposed set of solutions one may pick the wrong solution due to inaccuracies in the estimated slope of the Henry's law line. The first problem may be easily solved by modifying the functional form of f(c) or $\phi(c)$and recomputing a new set of solutions. The second

* A feasible point is one where all the constraints are satisfied.

problem is more serious and may lead to an inability to select the correct solution from the set of possible solutions (assuming that the set of possible solutions does contain a correct solution). In such a case the additional piece of information can be obtained experimentally. These limitations should be kept in mind when reviewing the results of the computations for each of the ten systems.

4.4 TREATMENT OF DIFFUSION DATA

All of the diffusivity data for this investigation was obtained from the text by Borovskii[2] et. al. which exhaustively reviews the current literature on diffusion in alloys. As part of the review, interdiffusion data from several investigations in the literature is presented. Hence this book was used as a central source for all of the diffusion data. In certain cases the data is not available at the ends, that is, the data is reported only on the range $0.05 < c < 0.9$. For such systems the data were extrapolated to the end points*. Similarly, for some systems, diffusivity data as a function of composition is presented at several temperatures. In such cases the data for the highest temperature was chosen to avoid any errors arising from grain boundary diffusion which dominates at the lower temperatures.

The figures in Borovskii's book were magnified and digitized at approximately 100 points. The digitizing process introduces high wavenumber noise in the data. To smooth out this noise and to obtain a suitable interpolant to the data, the raw data were fitted with a fourth order linear least squares spline. Spline fitting is a process that sub divides the interval of interest into several sub intervals and fits a polynomial to the data over each sub interval such that at the boundaries of two sub intervals the derivatives remain continuous. For full details on spline fitting see the

---

* Initially it was hoped that one would be able to use the tracer diffusivity of the solute in the solvent as an approximation to the interdiffusion coefficient at infinite dilution. This is approximately valid at infinite dilution, since according to Darkens relationship the following equation holds :

$$D = (D_2^* c_2 + D_1^* c_1)\left(1 + \frac{\partial \ln \gamma}{\partial \ln c}\right)$$

Although Kirkaldy, Manning, Howard and Lidiard have modified the above expression, the difference between the modified expression and Darkens expression is of the order of 5% and the difference is less significant for dilute alloys. Hence at infinite dilution ($c_1 \to 0.0$) the interdiffusion coefficient may be approximated by the tracer diffusivity of the solute in the solvent. However when the data on tracer diffusivity was examined from the Handbook by Smithell[7], it was found to have a fairly large scatter and hence could not be used. Thus in some cases one resorted to extrapolation to obtain the interdiffusion coefficient at either end.

accompanying paper[7]. The spline fit to the diffusivity data were evaluated at 100 equally spaced points on the compositional interval [0,1]. This data served as input to the model. Appendix II graphically presents the raw digitized data as well as the spline fit diffusivity data.

The diffusivity data presented by Borovskii is depicted on a semi-log scale, that is the diffusivity is plotted on a log scale whereas the composition is on a linear scale. The data were digitized as log(D)-c data and the spline was also fit to the log(D)-c data. After spline fitting the data were converted back to D-c data. This is important because diffusivity data often varies over several orders of magnitude and hence if the spline fitting routines were provided with D-c data, rather than log(D)-c data, a poor spline fit may result.

During the subsequent computations, aimed at obtaining the thermodynamics of the system, the diffusivity data were scaled such that the smallest diffusivity in the entire range was typically of the order of unity. Scaling of the data is important to avoid loss of accuracy when performing computations on a machine with a finite precision. For the systems investigated, the diffusivity was of the order of 10^{-11} cm^2/s. In absolute terms this is a small number and is much closer to the finite precision available on a digital computer than a number such as unity. Hence if calculations were performed on unscaled data one would run the risk of an appreciable loss of accuracy. To avoid this, the diffusivity data were scaled by a constant factor (usually 10^{-11} or 10^{-10}) and then input to the model (equation 6). After the main calculations, the data were rescaled back to the original dimensions.

It has already been stressed that the proposed solution scheme leads to multiple solutions on an activity-composition diagram. In practice one is not interested in mapping out the entire $\phi(c)-c$ space, rather one would prefer to explore the space in a neighborhood of the solution. This can lead to significant savings in the time expended in solving a particular system. Thus for instance, if it were known that the solution exhibits a positive deviation from ideality there would be little point in searching the subset of the $\phi(c)-c$ space that corresponds to solutions depicting

negative deviations from ideality even though there may exist several minima in that subset of $\phi(c)-c$ space. Miedema's predictions were very helpful in defining the region of $\phi(c)-c$ space within which to concentrate the search. Thus in practice Miedema's data were first examined to decide whether the solution exhibited positive or negative deviations. For positive deviations from ideality, only the region corresponding to $0.0 \leq \phi(c) \leq 1.0$ was examined whereas for negative deviations from ideality, the region corresponding to $1.0 \leq \phi(c)$ was searched. Although the region of the $\phi(c)-c$ space is unbounded above for solutions exhibiting negative deviations from ideality, in a practical sense one may choose an upper bound of $\phi(c) \leq 8.0$ or $\phi(c) \leq 10.0$.

4.5 COMPUTATION RESULTS

The simulation results are presented in two figures, one depicting activity-composition curves and the other depicting the $\ln(\gamma)-c$ curve for the selected solution. Appendix II contains the complete set of $\phi(c)-c$ curves for each system. Several activity-composition curves are presented for each alloy system. Each curve corresponds to a different set of bounds on the function $\phi(c)$. The legend for each figure lists the bounds used for computing that curve. In addition Appendix I of this document presents tables depicting the residual for each system as a function of the bounds used in computing the particular fit. These tables are useful in comparing the goodness of fit between two computations each performed using different bounds. Similarly Appendix III contains details of the computations performed in estimating the Henry's law line for each system.

The activity composition diagram for each system also depicts the theoretically estimated Henry's law line which was used to pick the correct solution. In addition, the experimental data reported in Hultgren is also presented. In comparing the computed activities to the data presented by Hultgren, it should be noted that Hultgren's data represents a best fit to the experimental data from several investigations and does not necessarily reflect the actual experimental points. Hence

minor deviations from Hultgren's data do not necessarily imply that the proposed algorithm is incorrect since it is possible that Hultgren's data itself may contain some errors.

4.5.1 CoNi system

Results for this system were presented in the earlier paper[1]. Theoretical estimates of the Henry's law line based on Miedema's prediction (Appendix III) were in good agreement with the data in Hultgren's handbook. Both indicate that the system is ideal in its solution behavior. Several solutions were computed by applying the computational scheme outlined above to the diffusivity data from the book by Borovskii. The correct solution was picked using the theoretically estimated Henry's law line. Thus the proposed computational scheme is successful at computing the activity composition relation for the CoNi system.

4.5.2 CuAu system

Diffusivity data for this system was reported at 857°C whereas the data in Hultgren represent measurements made at 527°C. An excellent fit was obtained to the diffusivity data for all solutions (Appendix I). The solutions are depicted in figure 1 along with the estimated Henry's law line (Appendix III) and the experimental datapoints reported by Hultgren. Appendix II contains the $\phi(c)-c$ curves corresponding to the activity data of figure 1. The estimated Henry's law line appears to match Hultgren's data. Examination of the activity composition curves (figure 1) and the table of residuals (Appendix I) indicates that the solutions computed using the bounds [0,6] and [1,6] are coincident and agree well with the estimated Henry's law line. In addition the computed activity data closely follow the trend exhibited by the experimental data reviewed by Hultgren's. The computed data also lie closer to the ideal law line than Hultgren's data. This is consistent with the idea that all solutions tend to ideality at higher temperatures. Since the diffusivity data were obtained at a higher temperature than Hultgren's data, it is natural that the predicted activities will be closer to the ideal solution line than the data reported by Hultgren. Hence *the curves*

corresponding to the bounds [0,6] and [1,6] are taken to represent the thermodynamics of the CuAu system. Figure 2 plots ln(γ) as a function of composition for the selected solution computed using the bounds [0,6]. Thus it is believed that the proposed computation scheme leads to good results on the CuAu system.

4.5.3 PdCu system

Diffusivity data for this system was reported at 1019°C whereas Hultgren et. al. report activity data at 1077°C. Computational results for this system are depicted in figure 3 which depicts several activity-composition diagrams alongwith the estimated Henry's law line based on Miedema's data (Appendix III). The corresponding $\phi(c) - c$ curves are contained in Appendix II. The predicted Henry's law line was helpful in confining the search to a region of $\phi(c) - c$ space that corresponds to negative deviations from ideality. For each of the curves depicted in figure 3, an excellent fit to the original diffusivity data were obtained (Appendix I). It is clear from figure 3 that the estimated Henry's law line, although close to Hultgren's data does not match it exactly. Computations based on the diffusivity data predict two possible solutions in the region of interest. These correspond to computations performed with the bounds [1,6] and [1,3]. Based on the estimated Henry's law line, one would pick the solution corresponding to the bounds [1,3] since it is closest to Miedema's prediction at infinite dilution. From figure 3 it is also clear that this solution closely matches the experimental data reported by Hultgren although there is a slight discrepancy in the lower compositional range. The residual for the solution computed using the bounds [1,3], is 0.0072 whereas the residual for the solution computed using the bounds [1,6] is 0.041 (Appendix I). Thus examination of the residual also indicates that the correct solution is the one corresponding to the bounds [1,3]. Hence, *the solution computed using the bounds [1,3] is taken to represent the thermodynamics of the PdCu system at 1019oC.* Figure 4 plots ln(γ) as a function of composition for the selected solution. Since the temperatures of the interdiffusion data and Hultgren's

data are close, the computed activities are expected to lie close to the experimentally obtained data. Thus the proposed computational scheme yields good results when applied to the PdCu system.

4.5.4 CuNi system

Diffusivity data for the CuNi system at 1000°C was used for the computations while Hultgren et. al. report activity data at 700°C. Results for the computation (activity-composition data) are depicted in figure 5 alongwith the estimated Henry's law line based on Miedema's prediction (Appendix III). Hultgren's experimental data is also presented in figure 5. Appendix II contains the corresponding $\phi(c) - c$ curves for the CuNi system. It is clear from figure 5 that the estimated Henry's law line does not match Hultgren's experimental data. Hence use of the estimated Henry's law line will lead to selection of a spurious solution from the set of possible solutions. Nonetheless it is of interest to ascertain whether the computational scheme leads to any solutions which may be plausible. Miedema's data does suggest that the search should be confined to the region of $\phi(c) - c$ space corresponding to systems exhibiting positive deviations from ideality.

For each of the curves depicted in figure 5 an excellent fit was obtained to the original diffusivity data (Appendix I). Since the diffusivity was reported at a higher temperature than the temperature corresponding to the experimentally reported data, it is expected that the activity curve at 1000°C will lie between the experimentally determined activity curve at 700°C and the ideal alloy line. Hence the solution corresponding to the bounds [0.05,1], must be a spurious solution. However it should be noted that this is precisely the solution one would have picked based on the estimated Henry's law line.

Knowledge of solution thermochemistry suggests that the activity curve at 1000°C should lie between Hultgren's data at 700°C and the ideal alloy line since all solutions tend to ideality with an increase in temperature. Referring to figure 5, this implies that any one of the solutions that lie between the ideal alloy line and Hultgren's data may represent the thermodynamics of the system. Based on

the residual error at the minima (Appendix I) one would pick the solution corresponding to the bounds [0.2,1] since it exhibits the smallest residual at the minimum among the set of feasible solutions. These observations strongly suggest that *the solution corresponding to the bounds [0.2,1] represents the thermodynamics of the CuNi system at 1000oC.* Figure 6 plots $\ln(\gamma)$ as a function of composition for this solution. Thus the proposed computational scheme does provide the correct solution but in this case one had to rely on Hultgren's data at 700°C to guide one in selecting a plausible solution since the estimated Henry's law line was inconsistent with the experimental data.

4.5.5 PdNi system

Diffusivity data for this system at 1045°C was used for the computations whereas Hultgren et. al. report the experimental activity data at 1000°C. Miedema's theoretical prediction suggests that this system exhibits ideal solution behavior (Appendix III). This suggests that one should focus on a region of the $\phi(c)-c$ space that is relatively close to unity such as $0.5 < \phi(c) < 2.5$ rather than examining the entire space, $0.0 < \phi(c) < 8.0$ A series of simulations were conducted using the modelling function $P_3[\mathrm{Exp}(P_5)]$. However a good fit to the interdiffusion coefficient could not be obtained* in the region of interest ($0.5 \leq \phi(c) \leq 2.5$). Hence results for these preliminary computations are not presented. To obtain a better fit, the modelling function was altered and one degree of freedom was added to both f(c) and $\phi(c)$. Thus the modelling function chosen was $P_4[\mathrm{Exp}(P_6)]$. When the computations were rerun, a good fit was obtained to the diffusivity data (Appendix I). Results for these computations are depicted in figure 7 alongwith Hultgren's data at 1000°C and the estimated Henry's law line. Appendix II contains the corresponding $\phi(c)-c$ curves. From figure 7 it is seen that the estimated Henry's law line differs slightly from the experimentally measured data reported by Hultgren.

* See Appendix I for table of residuals

From figure 7 it is clear the solutions corresponding to the bounds [0.9,1.5] and [0.7,1.75] are both close to the estimated Henry's law line although neither solution matches it exactly at infinite dilution. The residual at the minima is 0.019 for the solution corresponding to the bounds [0.7,1.75] whereas for the solution corresponding to [0.9,1.5] the residual is 0.043. This suggests that *the solution corresponding to the bounds [0.7,1.75] represents the system thermodynamics as computed from diffusion data.* Comparison between the computed solutions and Hultgren's data indicates a fairly good match over most of the composition range except the low concentration range ($c < 0.3$). Figure 8 depicts $\ln(\gamma)$ as a function of composition for the selected solution. Thus for this system there is a slight discrepancy at the low composition end but the overall match between the activity data computed from the interdiffusion coefficient and Hultgren's data is fairly good.

4.5.6 AgAu system

Diffusivity data for this system was obtained at 900°C whereas Hultgren et. al. report the activity data at 527°C. The Henry law line computed from Miedema's prediction (Appendix III) matches Hultgrens's data very well (figure 9). Miedema's data suggests that one should concentrate in the section of $\phi(c)-c$ space corresponding to negative deviations from ideality ($1 < \phi(c)$). Initial computations on this system used the modelling function $P_5[\mathrm{Exp}(P_6)]$. A good fit was obtained to the diffusivity data when using this modelling function (Appendix I) but the none of the computed solutions in the region of interest were close to Miedema's prediction. Hence it was decided to rerun the computations using the more complex modelling function, $P_4[\mathrm{Exp}(P_6)]$. Results for these computations are presented in figure 9, which depicts the activity composition curves alongwith the estimated Henry's law line and Hultgren's data. The $\phi(c)-c$ curves are contained in Appendix II. A good fit was obtained to the diffusivity data in each case (Appendix I). From figure 9, it is clear that the solution corresponding to the bounds [1,6] closely matches the estimated Henry's law line.

Further it exhibits the same general trend as Hultgren's data and in fact is coincident with Hultgren's data at both the dilute end and the high concentration end. At intermediate compositions ($0.2 < c < 0.8$), the computed activities are closer to the ideal alloy line than Hultgren's data. This is precisely what one would expect, since the diffusivity data were measured at a much higher temperature (900°C) than Hultgren's data (527°C). On the basis of these results, it is believed that *the solution corresponding to the bounds [1,6] in figure 9 represents the activity-composition data for the Ag-Au binary.* Figure 10 depicts $\ln(\gamma)$ as a function of composition for this solution. Thus the proposed algorithm leads to good results when applied to the AgAu system.

4.5.7 PdFe system

Diffusivity data for this system was obtained at 1050°C whereas Hultgren et. al. report the activity at 1000°C. The $D-c$ data for this system had to be extrapolated at the ends since the data reported by Borovskii covered the composition range [0.05,0.95]. This system is peculiar in that it exhibits positive deviation for compositions in excess of 0.55 whereas for compositions below 0.55 it exhibits negative deviations from ideality. Consequently, one expects that the $\phi(c)-c$ curves will cross the line $\phi(c) = 1$ over the compositional interval [0,1]. Thus using unity as an upper or lower bound will be counter productive. It should be noted that for this system the estimated Henry's law line (Appendix III) does not match Hultgren's experimental data very well. Hence, one expects that the estimated Henry's law line would in this case mislead one in to picking the wrong solution from the set of possible solutions.

Initial computations were performed using the function $P_3[\mathrm{Exp}(P_5)]$ to model the interdiffusion coefficient. However the fit to the diffusivity data were not satisfactory. With some bounds, a reasonable fit was obtained but with others a good fit could not be achieved. Hence it was decided to change the modelling function to $P_4[\mathrm{Exp}(P_6)]$. With this function a good fit was achieved to the original interdiffusivity data. Results for these computations are depicted in figure 11

which also presents the experimental data reported by Hultgren as well as the estimated Henry's law line at infinite dilution. Appendix II contains the corresponding $\phi(c) - c$ data. From figure 11, it is clear that the estimated Henry's law line does not match Hultgren's data. It is also clear from figure 11 that the computational scheme does predict one solution which depicts a general trend similar to that exhibited by Hultgren's data although there is a some difference between the computed data and Hultgren's data over the intermediate range of compositions ($0.3 < c < 0.75$). Despite this difference, it is encouraging to note that the computed solution does in fact correctly predict that the system exhibits a positive deviation in the higher compositional range and a negative deviation in the lower compositional range. In fact there is excellent agreement between the experimental and computed data at the dilute end ($c < 0.3$) and at the concentrated end ($c > 0.8$). Figure 12 depicts $\ln(\gamma)$ as a function of composition for the selected solution. Thus, while the computational scheme yields activities that differ from the data by Hultgren over the intermediate range of compositions the scheme does predict the general trend in the data.

4.5.8 AuNi system

Diffusivity data for this system was obtained at 900°C whereas Hultgren's data represents the system thermodynamics at 875°C. The estimated Henry's law line based on Miedema's theoretical prediction (Appendix III) does not match Hultgren's data but is helpful in focussing the search to a region of $\phi(c) - c$ space corresponding to positive deviations from ideality. Preliminary attempts at fitting the diffusivity data with the model function $P_3[\mathrm{Exp}(P_5)]$ did not lead to a satisfactory fit. Hence the model was changed to $P_4[\mathrm{Exp}(P_6)]$. This resulted in an adequate fit to the data. Results of the computations are depicted in figure 13 which plots the computed activities as a function of composition. The corresponding $\phi(c) - c$ curves are contained in Appendix II. The solutions computed on imposing the bounds [0.001,1] and [0.01,1] are coincident. From figure 13, it is clear that the solution close to Miedema's prediction (i.e. the solution

corresponding to the bounds [0.02,1]) does not compare well with Hultgren's experimental data. However, the solution corresponding to the bounds [0.01,1] leads to a good match at low concentrations (c < 0.15). Thereafter it exhibits the same general behavior as Hultgren's' data but differs from it. Hence, *the solution computed on imposing the constraints [0.001,1] represents the thermodynamics of the AuNi system as computed from the diffusivity data.* Thus in this system also one notes that Miedema's prediction may misguide one into picking the wrong solution. However, the fitting process is capable of locating a solution that is similar to the actual data.

4.5.9 NiPt system

Diffusivity data were obtained at 1296°C whereas Hultgren et. al. report experimental data at 1352°C. The estimated Henry's law line based on Miedema's prediction (Appendix III) provides a good match to Hultgren's data. Miedema's prediction also indicates that the search should be confined to the region of $\phi(c)-c$ space representing negative deviations from ideality. Preliminary computations were performed on this system using the model function $P_3[\mathrm{Exp}(P_5)]$. Results for these are shown in figures 15 and 16 which depict the activity-composition curves and $\phi(c)-c$ curves respectively. A large number of runs were conducted and in each case a good fit was achieved to the diffusivity data. However none of the computed solutions were close to the estimated Henry's law line or to Hultgren's data. From figure 15 one notes that the computed solutions can be classified into two distinct families. The family corresponding to the bounds [1,6], [1,3], [1,6.25] and [1,6.32] is degenerate in that all the solutions are identical. These solutions are closer to the ideal alloy line than the estimated Henry's law line. The second family of solutions shows a far greater deviation from ideality than that predicted by Miedema. The computed solutions are also a strong function of the bounds chosen. This is best illustrated by comparing the solutions corresponding to the bounds [1,6.32] and [1,6.4].

It was decided to use the more complex modelling function, $P_4[Exp(P_6)]$, in the hope of locating solutions closer to Miedema's prediction and to Hultgren's data. Results for these computations are depicted in figure 17. The general trend is similar to the trend seen in figure 15. Once again two families of solutions emerge but none of the computed solutions are close to Miedema's prediction or to Hultgren's experimental data.

The lack of existence of any solutions close to Hultgren's data could be caused by any of the following reasons. Firstly, it is possible that the diffusion data itself contains systematic errors. It has been estimated that diffusion data may contain up to 25% error.[7] Secondly it is possible that the functional forms chosen for $\phi(c)$ and $f(c)$ (see equation [1]) are inappropriate for this particular system. This implies that one is unable to satisfactorily model the variation of the two functions although their product does model the diffusivity satisfactorily.

It is also possible that the activities in the Ni-Pt system are very strong functions of temperature and that one of the computed solutions does represent the thermodynamics of the Ni-Pt system. This solution may differ from Hultgren's data due to the strong temperature dependence of the activities on the temperature. However this is unlikely considering that the temperature difference is only 50°C. Lacking any additional data one is unable to comment further on which one of these reasons leads to a failure in computing the activities for the Ni-Pt system.

4.5.10 NbTi system

Diffusivity data for this system was reported at 1000°C. Only one investigation, that by Kuz'min et. al., has experimentally examined the thermodynamics of the Nb-Ti system[8]. Their data suggests that the system possesses a strong negative deviation from ideality. Hultgren et. al. do not tabulate activity data for this system since they consider Kuz'min's data to be unreliable. Thus for this system there is no thermodynamic data available. In sharp contrast to Kuz'min's data the theoretical predictions of Miedema et. al. indicate that the

system exhibits a positive deviation from ideality. A value of +9kJ/mole is predicted for the enthalpy of formation at infinite dilution which corresponds to a Henry's constant of $\gamma = 2.5$ (Appendix II).

Initial computations were performed using the model function $P_3[Exp(P_5)]$. Subsequently, the model function was altered to $P_4[Exp(P_6)]$. Since both model functions yielded similar results, only the results for the model $P_4[Exp(P_6)]$ are presented. These are depicted in figure 18 alongwith the estimated Henry's law line. For both modelling functions *considerable difficulty was encountered in obtaining a good fit to the diffusivity data.* For both modelling functions only one solution (the one corresponding to the bounds [0.05,1] in figure 18) led to a good fit (Appendix I) to the diffusivity data. The fit to the diffusivity data for this solution is depicted in figure 20 whereas figure 21 depicts the fit corresponding to the bounds [0.4,1]. The latter figure is representative of the difficulty in obtaining a good fit to the diffusivity data. Table I summarizes the results of the computations for the NbTi system.

Table I Results of least squares fitting for the NbTi system.

Bounds	Final Activity Curve	Residual at Minima
[0.05,1]	Strong Positive Deviation	0.82
[0.2,1.]	Positive Deviation	4.269
[0.4,1.]	Positive Deviation	12.8
[0.7,1.]	Positive Deviation	21.0
[0.7,6.]	Negative Deviation	5.06
[1.,8.0]	Negative Deviation	5.60
[1.,4.0]	Negative Deviation	8.47
[1.0,12]	Negative Deviation	5.365

Examination of table I and figures 20 and 21 would strongly suggest that the solution corresponding to the bounds [0.05,1] represents the thermodynamics of the NbTi system at 1000°C. This is the only solution for which a good fit has been achieved and it possesses the smallest residual at the minima.

Two arguments may be presented challenging the validity of this solution. Firstly the selected solution clearly contradicts Kuz'min's data. Secondly, the selected solution does not match the estimated Henry's law line based on Miedema's prediction. However, as mentioned earlier Kuz'min's data is not considered reliable by Hultgren et. al. As far as Miedema's prediction is concerned, the solution does agree with Miedema's prediction that the system exhibits a positive deviation from ideality. It has already been observed that the estimated Henry's law line can also contain errors (examples include the AuNi and CuNi systems discussed earlier). It should be recalled that Miedema's predictions were made for liquid alloys. Although some compensation has been made for the latent heat of fusion in estimating the partial molar enthalpy in the solid state (see Appendix III) one is still unable to account for the strain energy. Further the assumption of regular solution behavior which is implicit in the estimation of the Henry's law line (Appendix III) may not be correct. This and the fact that in the present case the homologous temperature of the diffusion experiment is approximately 0.5, together imply that it is quite possible that the estimated Henry's law line contains large errors. If the system does exhibit a positive deviation from ideality then one would expect this tendency to be more evident at lower temperatures, which is consistent with the observed behavior.

The discrepancy between Miedema's prediction and the computed solution can be resolved if a single bold assumption is made. If one assumes that the system contains a miscibility gap at temperatures lower than 1000°C then one would expect the system to exhibit the strong positive deviations that the calculations reveal. However, the binary phase diagram[9] for the Nb-Ti system does not reveal a miscibility gap. That in itself does not rule out the possibility

of a low temperature miscibility gap since it is quite possible that a miscibility gap does exist but has not been discovered earlier. The situation would be similar to the Fe-Ni binary, wherein recent studies[10,11,12] have revealed a low temperature miscibility gap formerly unknown. At the temperature of interest the diffusion coefficient is fairly small ($10^{-14}cm^2/sec$ for the NbTi system at the Nb rich end). Such small diffusion coefficients can serve as kinetic barriers hindering the transformation to the low temperature phases.

Finally, one must also consider the possibility that the diffusivity data for the NbTi system contains errors. Such errors may originate from two sources in the present case. Firstly, measurement of small diffusion coefficients is a process intrinsically susceptible to large errors. Secondly, the temperature of the diffusion experiment (1000°C) corresponds to a homologous temperature of 0.46 at the Nb rich end and 0.64 at the Ti rich end. It is well known that for homologous temperatures less than 0.5 grain boundary diffusion can contaminate the results of a bulk diffusion experiment. If such errors were present in the diffusivity data then they would lead to errors in the computed activities.

To summarize, the thermodynamics of the Nb-Ti system remain elusive. The computations suggest that the system exhibits a strong positive deviation from ideality and that the system possesses a miscibility gap below 1000°C. Additional experimentation is necessary to fully evaluate this system.

4.6 DISCUSSION

The computations on the ten isomorphous binaries may be summarized as follows. For eight systems the computational scheme resulted in solutions that either matched very well with the experimental data, were close to the experimental data or exhibited a trend similar to the experimental data. Among these, in four systems the estimated Henry's law line was helpful in selecting the correct solution, for the other four a plausible solution was computed but if the estimated Henry's law line were used then an incorrect solution would have been picked. For these four systems

the experimental data of Hultgren was relied on to help pick the correct solution. For one system (PtNi) the solution scheme did not compute any solution close to the experimental data. Finally in the case of the NbTi system, since no reliable experimental data exists, a comparison is not possible. The computed solution does agree with Miedema's prediction in that the system should exhibit positive deviation from ideality. *These results suggest that the proposed algorithm is able to compute a set of solutions which does contain the correct activity composition curve.*

It is also clear from the computations that the modelling function $P_3[Exp(P_5)]$ cannot be universally applied and that the function $P_4[Exp(P_6)]$ may provide a better model. It is recommended that initial computations be performed using the simpler function and if necessary the more complex function be used.

Thus the computations have successfully demonstrated that activity data can be computed from diffusivity data and that measurements of the interdiffusion coefficient can serve as a source of activity-composition data for isomorphous binaries. The main drawback to this computational scheme is the multiplicity of solutions. This necessitates that some additional information be made available that would help in selecting the correct solution. It was hoped that the estimated Henry's law line would provide that additional piece of information. However, *it is clear that the estimated Henry's law line cannot be relied on to pick the correct solution from the set of possible solutions.* Instead it is advisable to conduct a single experiment which will yield the activity at a particular composition and use the experimental data to pick the correct solution.

Despite this drawback it is believed that the computational scheme will be useful in two distinct applications. Firstly, it should be noted that the experimental activity data reported by Hultgren is usually representative of the system thermodynamics at lower homologous temperatures than the temperatures at which diffusivity data is measured. This implies that the experimental data reported in Hultgren could be used to pick the correct solution from sets of solutions representing the system thermodynamics at other temperatures. One could thereby generate

activity data for higher temperatures. Secondly the technique will serve as an aid in checking the consistency of existing thermodynamic and diffusion data. Finally it is hoped that this study will enhance the appreciation of the link between thermodynamic data and diffusion data.

4.7 FUTURE EFFORTS

There remain additional isomorphous binary systems for which diffusivity data is available. In the near future the computations will be extended to cover those systems also. In addition, there are two major directions that will be pursued in the future.

4.7.1 *Temperature variation of Activity data*

Since the diffusivity data in the literature is available at several temperatures, it is of interest to conduct these computations on data from different temperatures. This will provide information on the temperature variation of the solution behavior for these systems.

4.7.2 *Extensions to non isomorphous binaries*

The proposed algorithm may be extended to systems other than isomorphous binaries. In the case of systems exhibiting a miscibility gap this should be fairly straightforward since one knows that such systems exhibit a positive deviation from ideality. Over the composition range corresponding to the miscibility gap, the function $\phi(c)$ is negative, indicating that solutions of that composition are intrinsically unstable from a thermodynamic standpoint. Since the function $\phi(c)$ is known to be positive outside the miscibility gap, this implies that at the terminal compositions of the miscibility gap, the function $\phi(c)$ must be zero. As a result, one could split the computation into two halves. In the first half one would use the proposed scheme to compute the activity from the pure solvent to the composition corresponding to the miscibility gap. At either end of this compositional band the numerical value of the function $\phi(c)$ is known a priori to be zero. It is also known that the activities of the two compositions in equilibrium across the miscibility gap are identical. The value of the function

$\phi(c)$ is also known at c=0. Using all of this information, it should be straightforward to compute the activity-composition relationship for systems exhibiting positive deviations from ideality. For systems exhibiting negative deviations from ideality the situation is less clear.

4.8 CONCLUSIONS

The following conclusions may be drawn from this study:

(i) *Given the $\tilde{D}-c$ relationship and one additional piece of information the entire activity-composition curve can be computed.* An algorithm has been developed that permits one to compute the system thermodynamics (which is implicitly contained in the variation of the chemical interdiffusion coefficient) by using a constrained non linear least squares approach that models the diffusivity as a product of two functions.

(ii) The proposed scheme leads to multiple solutions. In order to select the correct solution it becomes necessary to use one additional piece of information. The additional piece of information may consist of the measured activity at a particular composition or the slope of the Henry's law line at infinite dilution.

(iii) The proposed computational scheme was applied to ten isomorphous binary systems. For eight of these systems the scheme was able to locate a solution close to the experimentally measured data confirming the proposition that one can compute activities from diffusivities. For four of these systems the correct solution was picked by using the theoretical predictions of the enthalpies of formation at infinite dilution. For one system there is no reliable experimental data available for comparison. For another system the scheme led to results that were not consistent with the experimental data.

(iv) The algorithm can be easily extended to binary systems exhibiting a miscibility gap.

4.9 SYMBOLS

$\tilde{D}$	:	interdiffusion coefficient
$f(c)$	:	contribution of phenomenoloical coefficients to interdiffusion coefficient
$\phi(c)$	:	Thermodynamic function representing the solution behavior
τ_i	:	unknown variable constituting the model used for least squares analysis
c_i	:	composition
l_i	:	lower bound imposed on the thermodynamic function
u_i	:	upper bound imposed on the thermodynamic function
E^2	:	Least squares error function
w_i	:	weighing function used in the least squares analysis
h_i	:	modelling function in least squares analysis
D_i^*	:	tracer diffusivity of element i
P_n	:	space of all nth order polynomials

4.10 REFERENCES

1. Rakesh R. Kapoor, *Thermodynamic Data from Diffusion Couples*, Sc.D. thesis, Paper II, MIT, (1989).

2. I. B. Borovskii, K. P. Gurov, I. D. Marchukova and Y. E. Ugaste, *Interdiffusion in Alloys*, Nauka Publishers, NTIS Document PB86-245495, (1986).

3. R. Hultgren, P. D. Desai, D. T. Hawkins, M. Gleiser and K. K. Kelley, *Selected Values of the Thermodynamic Properties of Binary Alloys*, ASM, (1973).

4. NAG Fortran Library Manuals, Mark 13, Numerical Algorithms Group, Downers Grove, IL, (1987).

5. A. R. Miedema, F. R. deBoer and R. Boom, *Calphad*, 1, No. 4, pp.341-359, (1977).

6. Rakesh R. Kapoor, *Thermodynamic Data from Diffusion Couples*, Sc.D. thesis, Paper IV, MIT, (1989).

7. C. J. Smithells, *Metals Reference Book*, 5th edition, Buttersworth, (1976).

8. A. A. Kuz'min and T. G. Moiseeva, *Fizika Metallov. Metallovedene*, **18**, 926-27, (1964).

9. Thaddeus B. Massalski, *Binary Alloy Phase Diagrams*, Vol. 1 and 2, ASM, (1986).

10. D. C. Dean and J. I. Goldstein, *Metallurgical Transactions A*, 17A, 1131-1138, (1986).

11. K. B. Reuter, D. B. Williams and J. I. Goldstein, *Metallurgical Transaction A*, 20A, 719-725, (1989).

12. K. C. Russell, F. A. Garner, *High Temperature Phase separation in Fe-Ni and Fe-Ni-Cr Invar-Type Alloys*, submitted to **Acta. Metall.**, private communication, (1988).

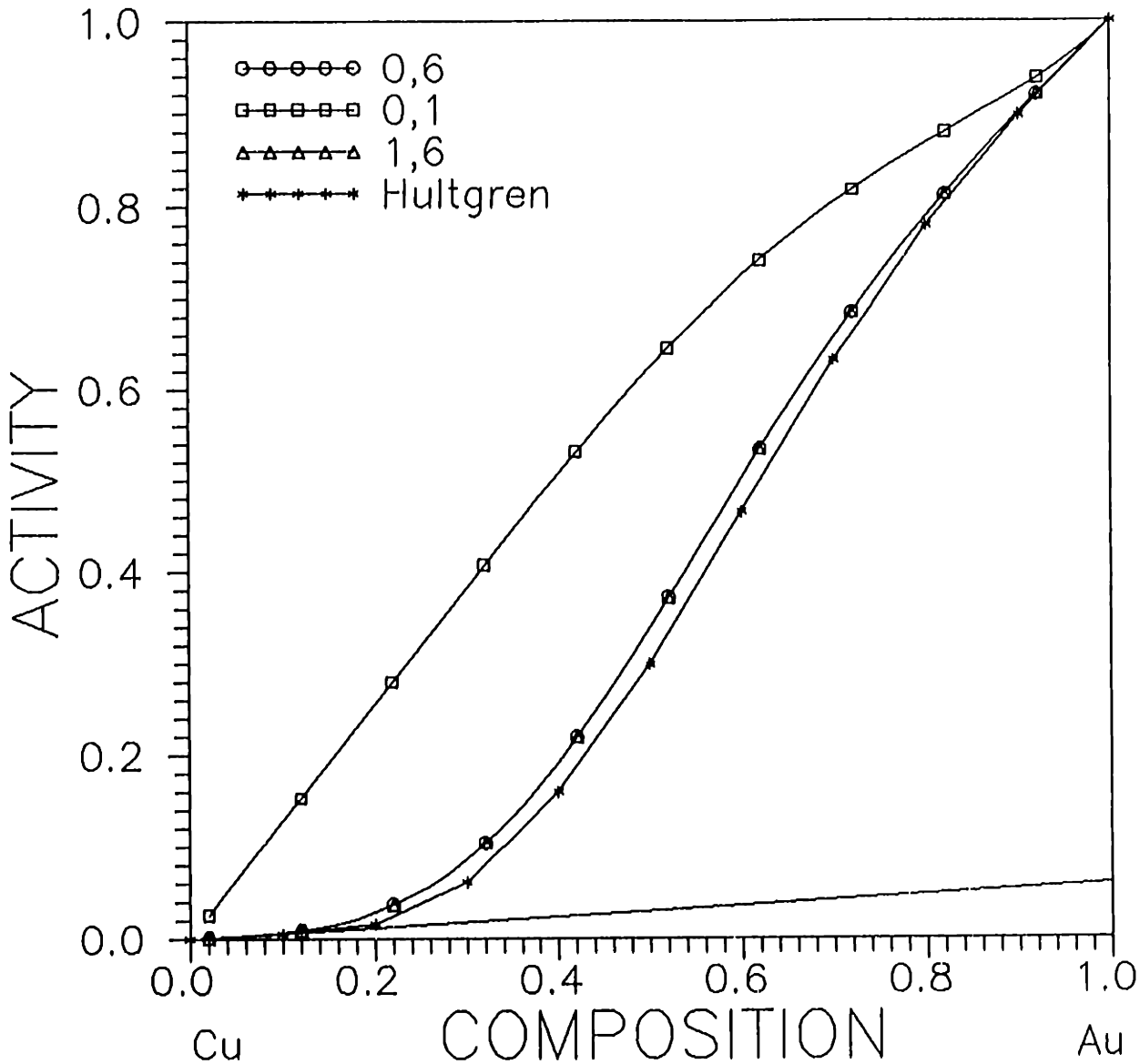

Figure 1. Computed activities for the CuAu system at 857°C using the model function $P_3[Exp(P_6)]$. The Henry's law line computed from Miedema's theoretical predictions is also depicted. The activities computed by imposing the constraints [0,6] and [1,6] are coincident and are taken to represent the thermodynamics of the CuAu system at 857°C. Experimentally determined activities from Hultgren are also presented for comparison.

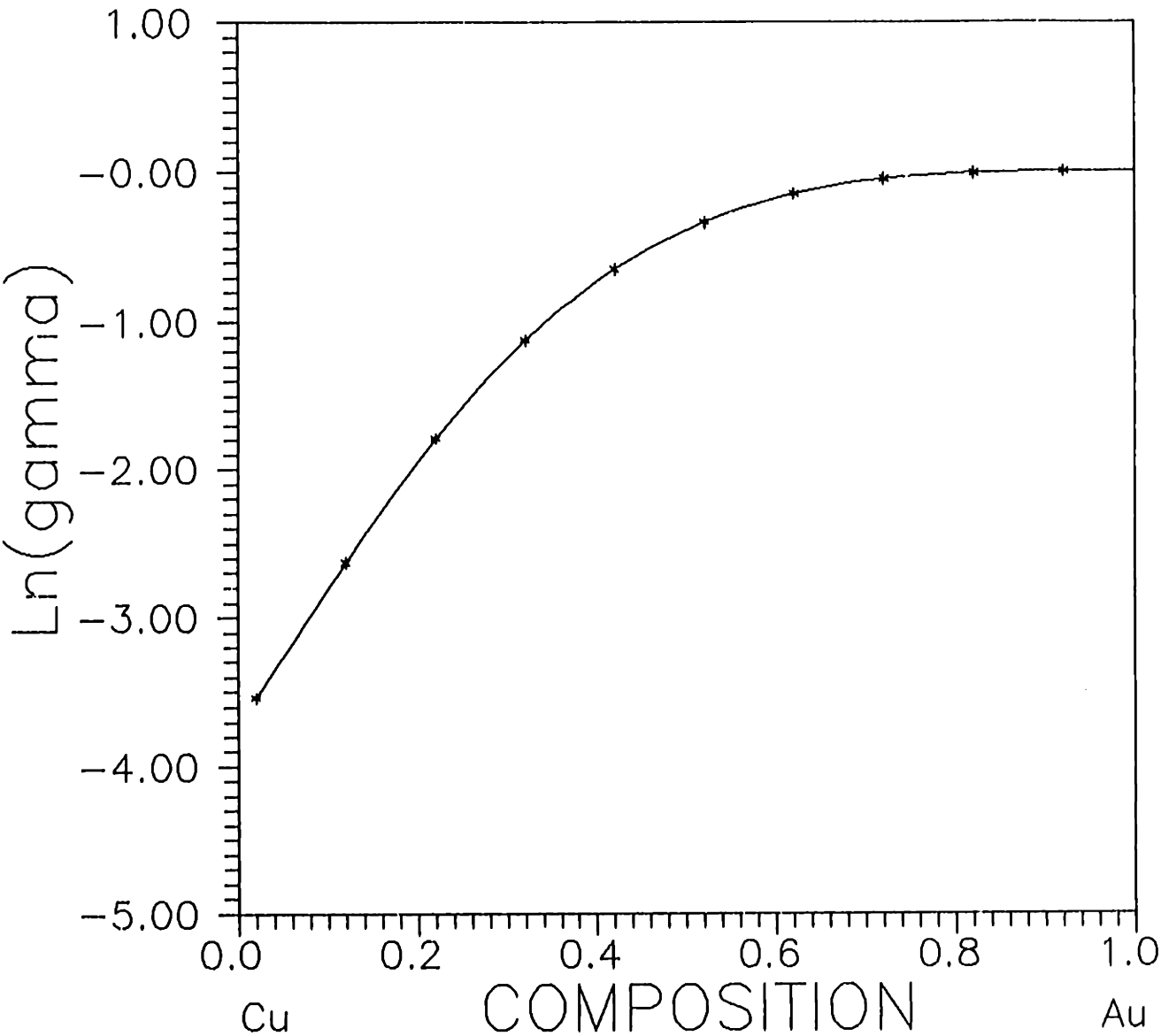

Figure 2. Computed Ln(γ)as a function of composition for the CuAu system at 857°C using the model function $P_3[Exp(P_5)]$. The selected solution was computed by imposing the constraints [0,6] on $\phi(c)$ Corresponding activities are depicted in figure 1.

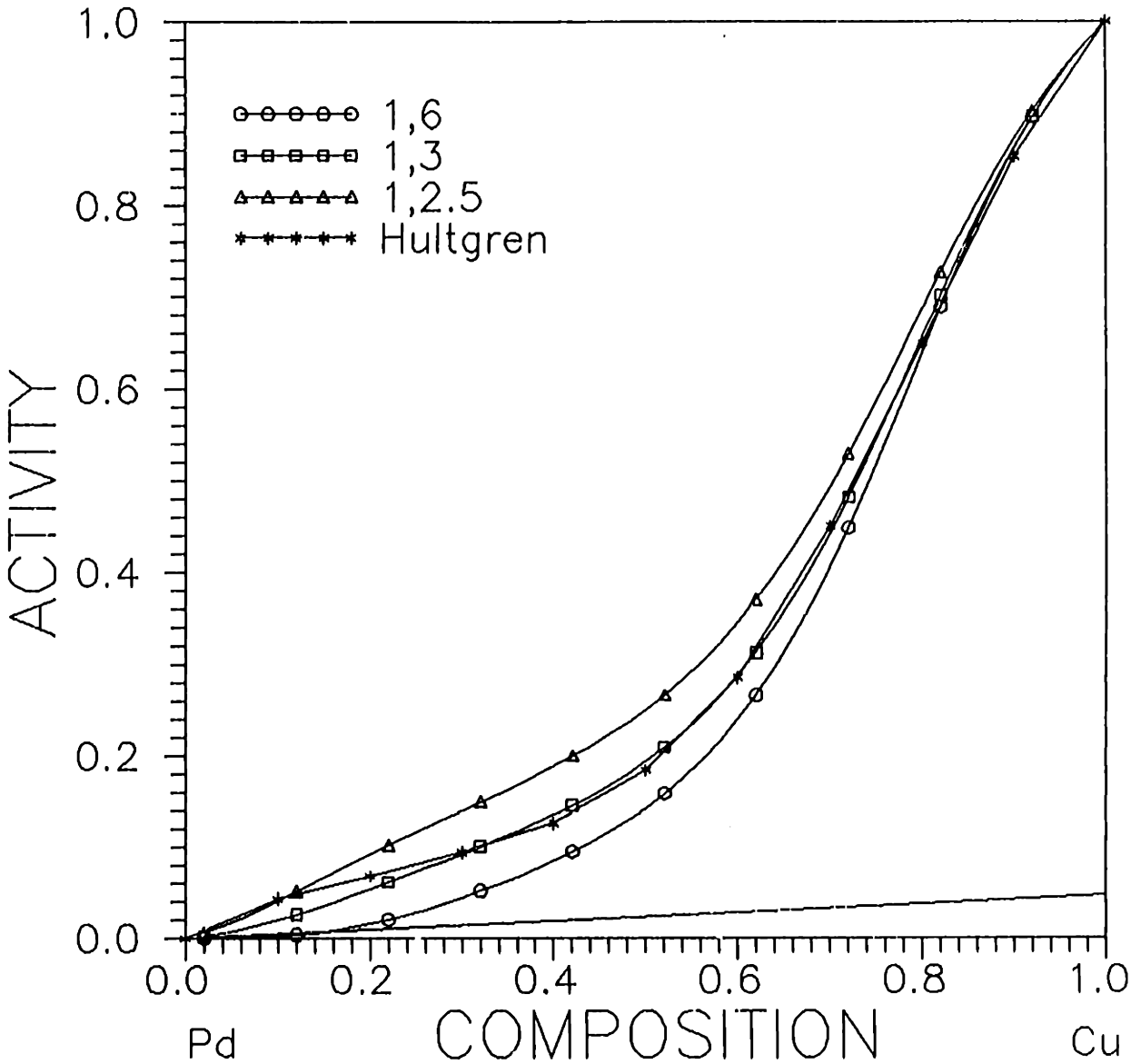

Figure 3. Computed activities for the PdCu system at 1019°C using the model function $P_3[Exp(P_6)]$. The Henry's law line computed from Miedema's theoretical predictions is also depicted. The activities computed on imposing the bounds [1,3] on $\phi(c)$ are taken to represent the thermodynamics of the PdCu system. Experimental data reported by Hultgren at 1077°C is also presented.

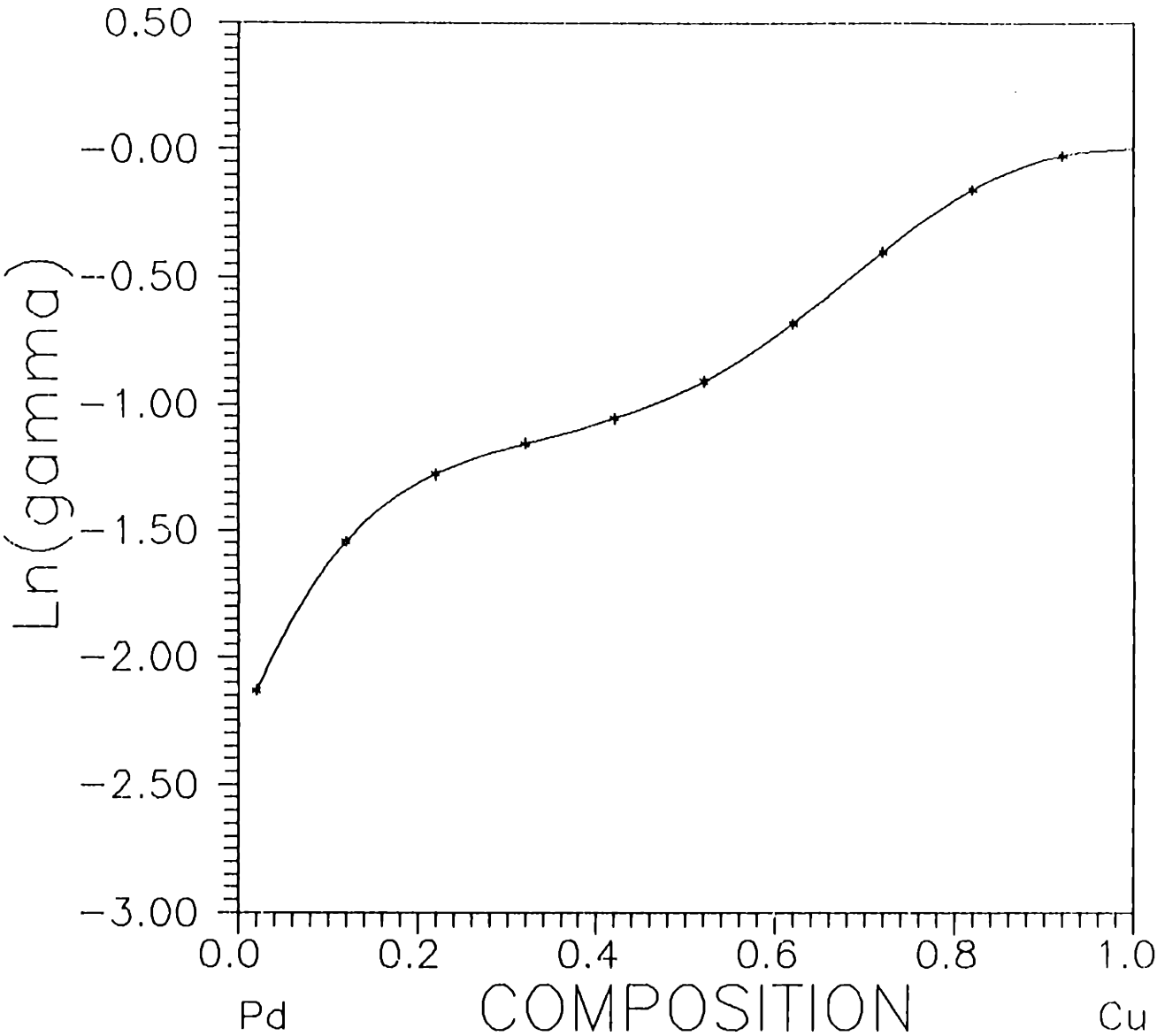

Figure 4. Computed ln(γ) as a function of composition for the PdCu system at 1019°C using the model function $P_3[Exp(P_5)]$. The selected solution was computed by imposing the constraints [1,3] on $\phi(c)$ Corresponding activities are depicted in figure 3.

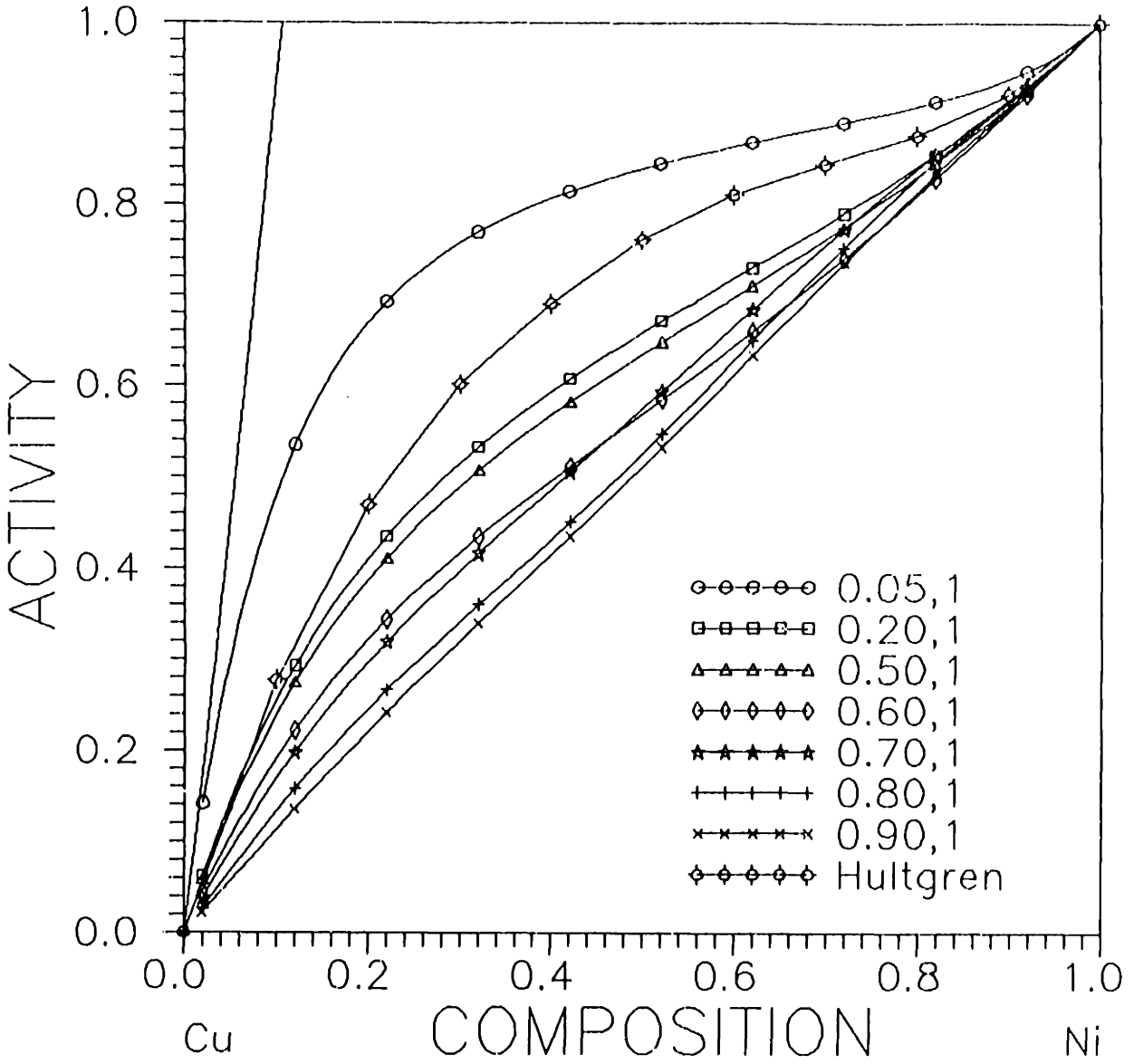

Figure 5. Computed activities for the CuNi system at 1000°C using the model function $P_3[Exp(P_5)]$. The Henry's law line computed from Miedema's theoretical predictions is also depicted. Based on the residual at minimum the activity curve computed on imposing the constraints [0.2,1] on $\phi(c)$ is taken to represent the system thermodynamics. Hultgren's data at 700°C is also depicted.

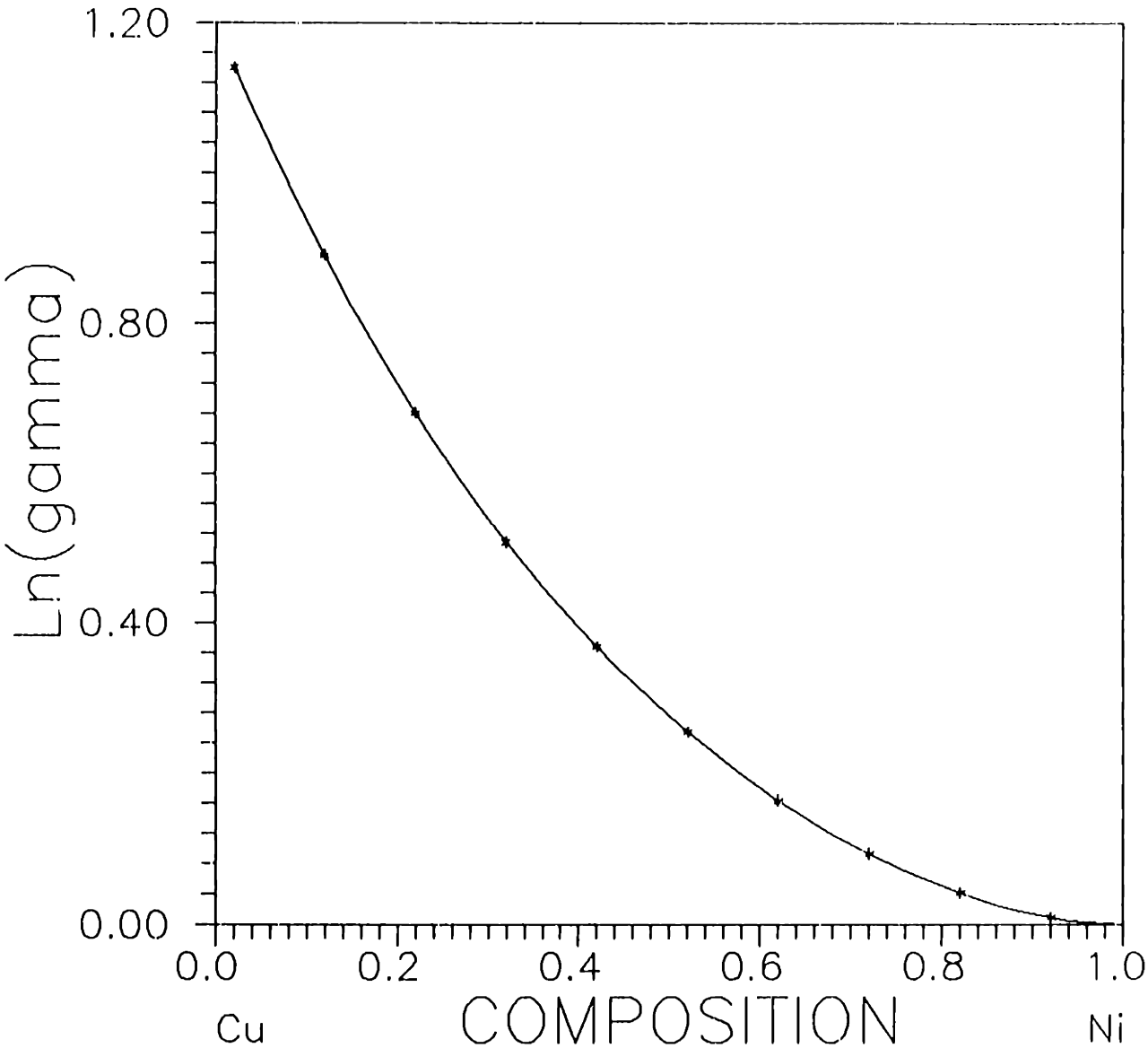

Figure 6. Computed ln(γ) as a function of composition for the CuNi system at 1000°C using the model function $P_3[Exp(P_6)]$. The selected solution was computed by imposing the bounds [0.2,1] on $\phi(c)$ Corresponding activities are depicted in figure 5.

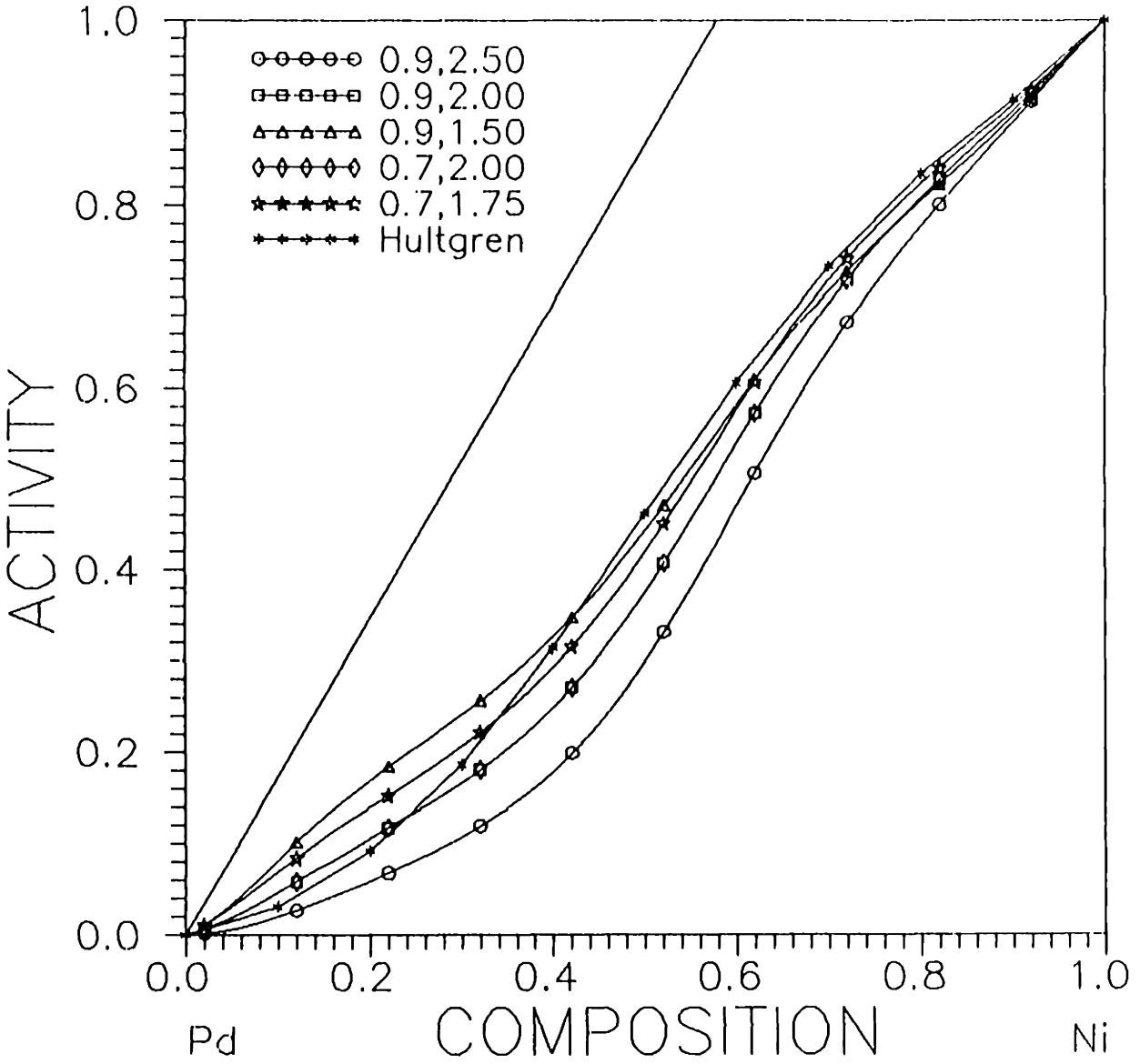

Figure 7. Computed activities for the PdNi system at 1045°C using the model function $P_4[Exp(P_6)]$. The Henry's law line computed from Miedema's theoretical prediction is also depicted. Based on the residual at minimum the activities computed on imposing the bounds [0.7,1.75] are taken to represent the system thermodynamics at 1045°C. Experimental data by Hultgren at 1000°C is also depicted.

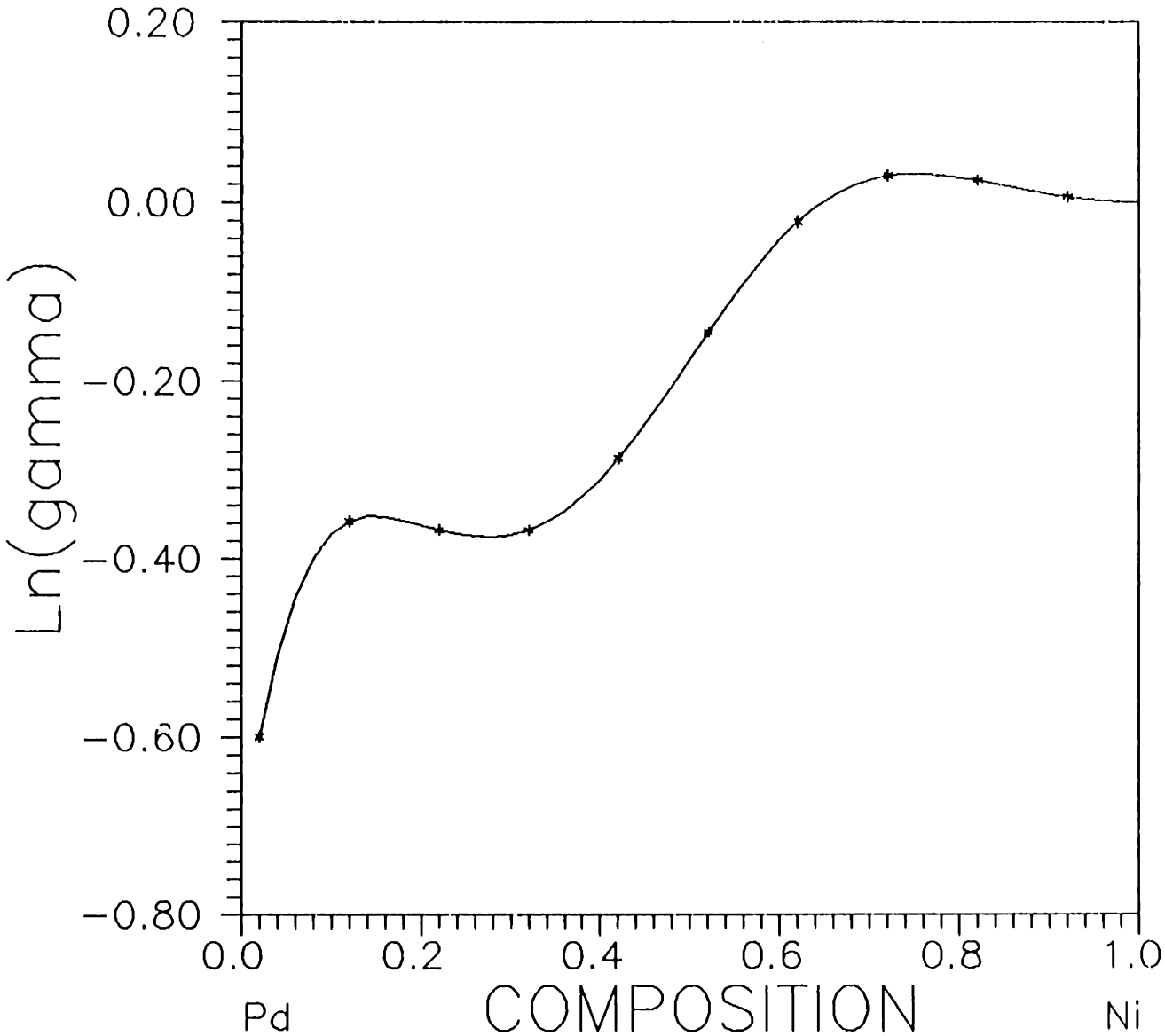

Figure 8. Computed ln(γ) as a function of composition for the PdNi system at 1045°C using the model function $P_4[Exp(P_6)]$. The selected solution was computed on imposing the constraints [0.7,1.75] on $\phi(c)$ Corresponding activities are depicted in figure 7.

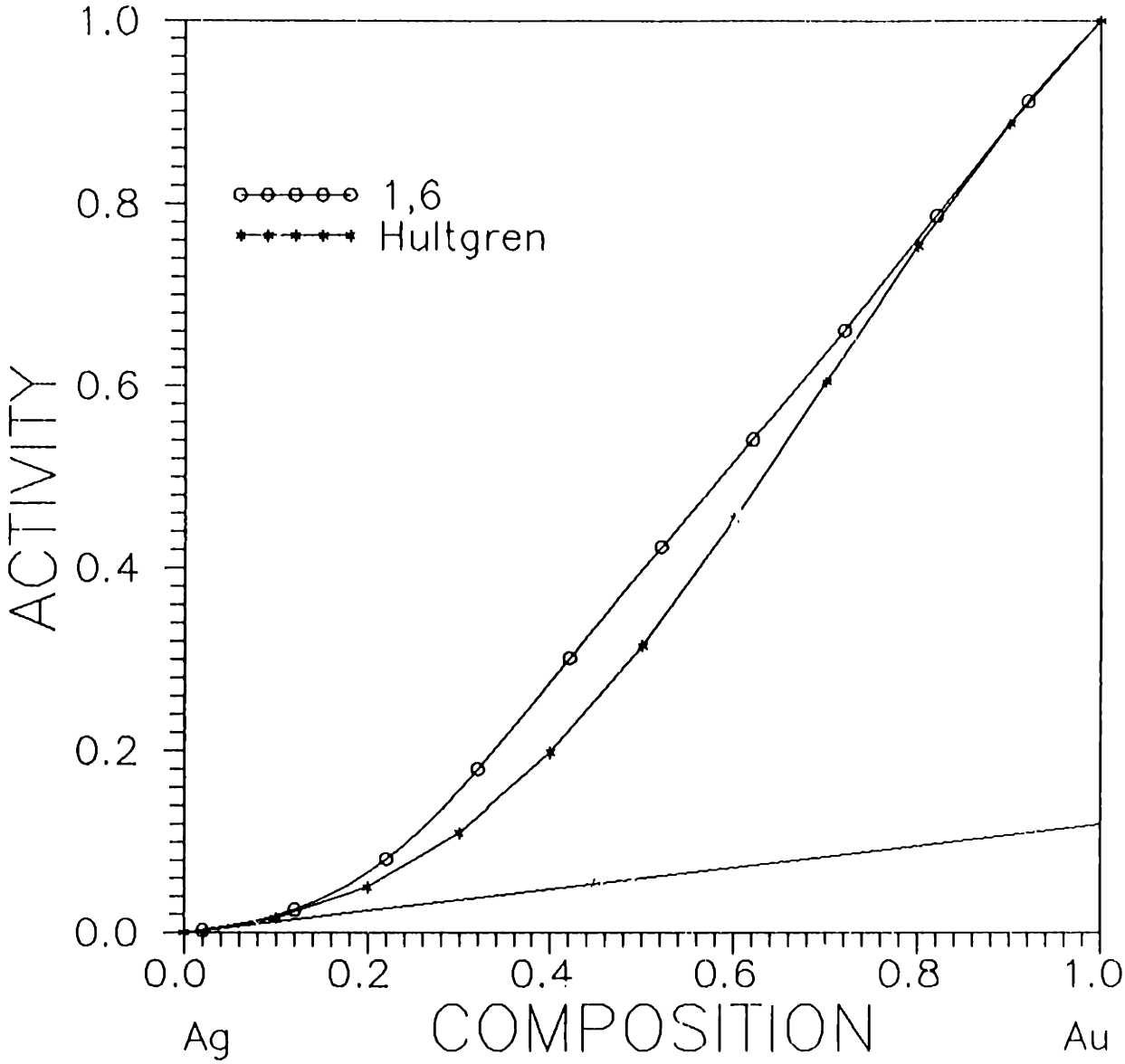

Figure 9. Computed activities for the AgAu system at 900°C using the model function $P_4[Exp(P_6)]$. The Henry's law line computed from Miedema's theoretical predictions is also depicted. The activities computed on imposing the bounds [1,6] are taken to represent the thermodynamics of the system. Hultgren's experimental data at 527°C is also depicted.

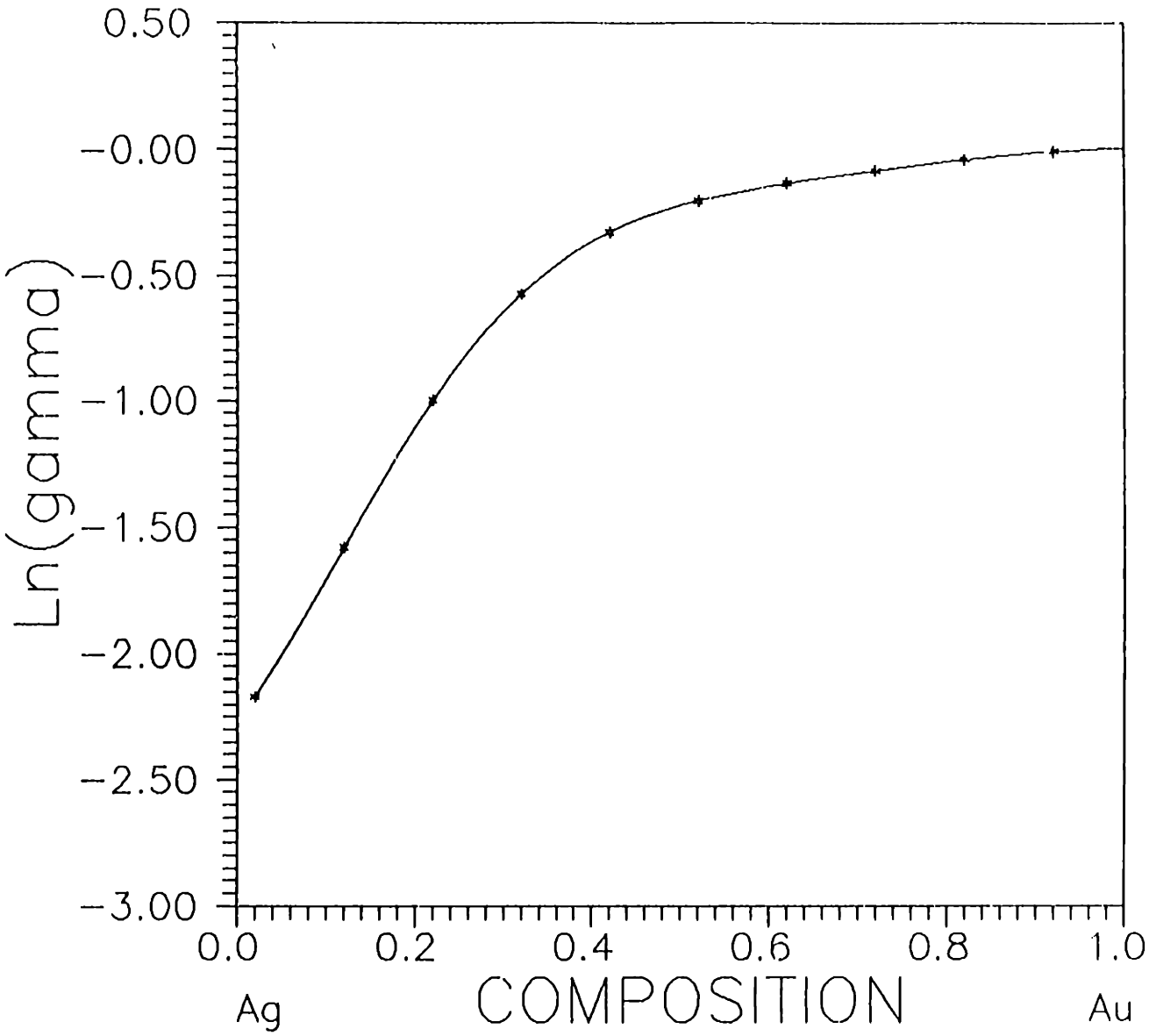

Figure 10. Computed ln(γ) as a function of composition for the AgAu system using the model function $P_4[Exp(P_6)]$. The selected solution was computed by imposing the bounds [1,6] on $\phi(c)$ Corresponding activities are depicted in figure 9.

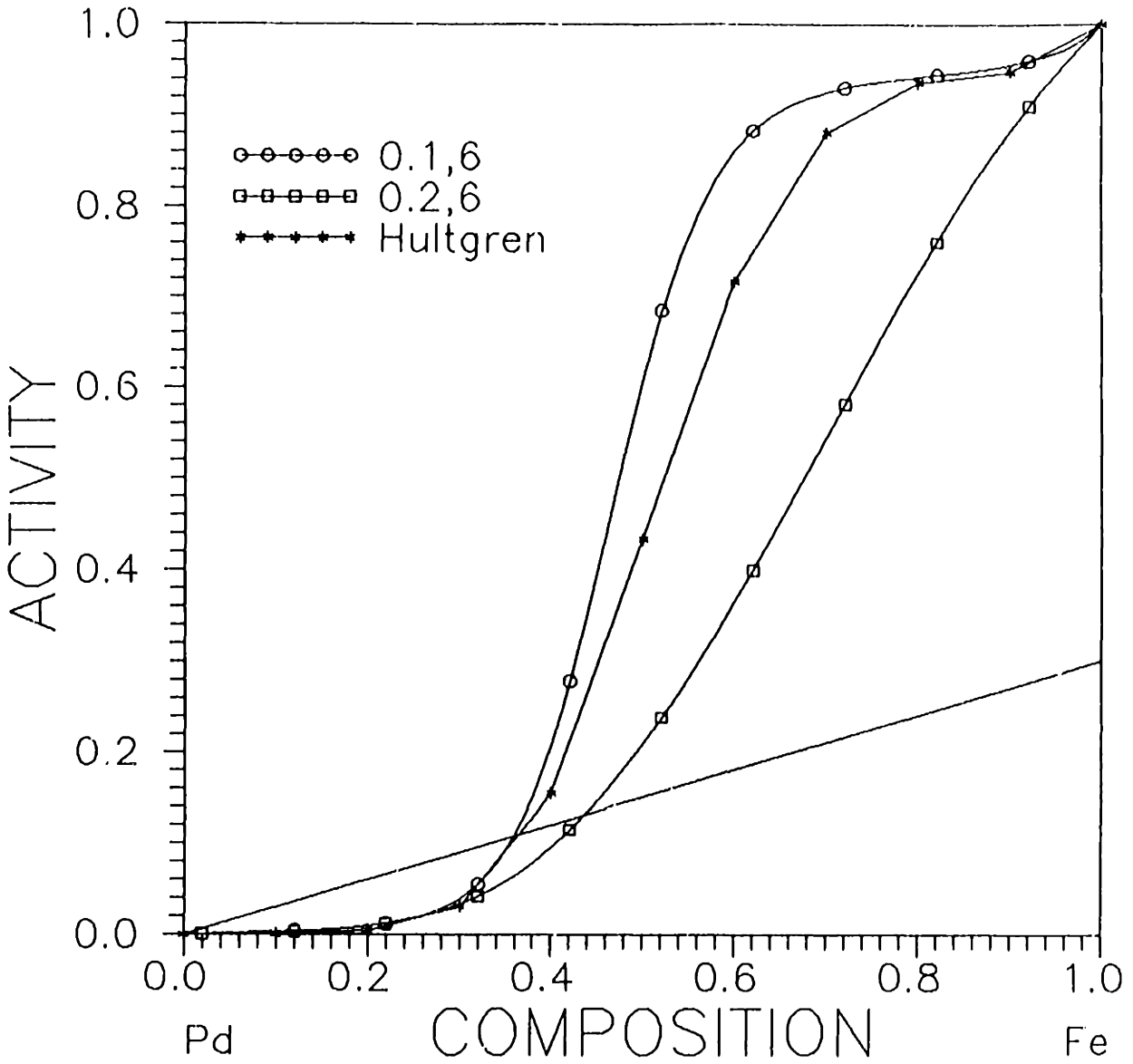

Figure 11. Computed activities for the PdFe system at 1050°C using the model function $P_4[Exp(P_6)]$. The Henry's law line computed from Miedema's theoretical predictions is also depicted. The activities computed on imposing the constraints [0,1,6] are taken to represent the system thermodynamics. Experimental data by Hultgren at 1050°C is als depicted.

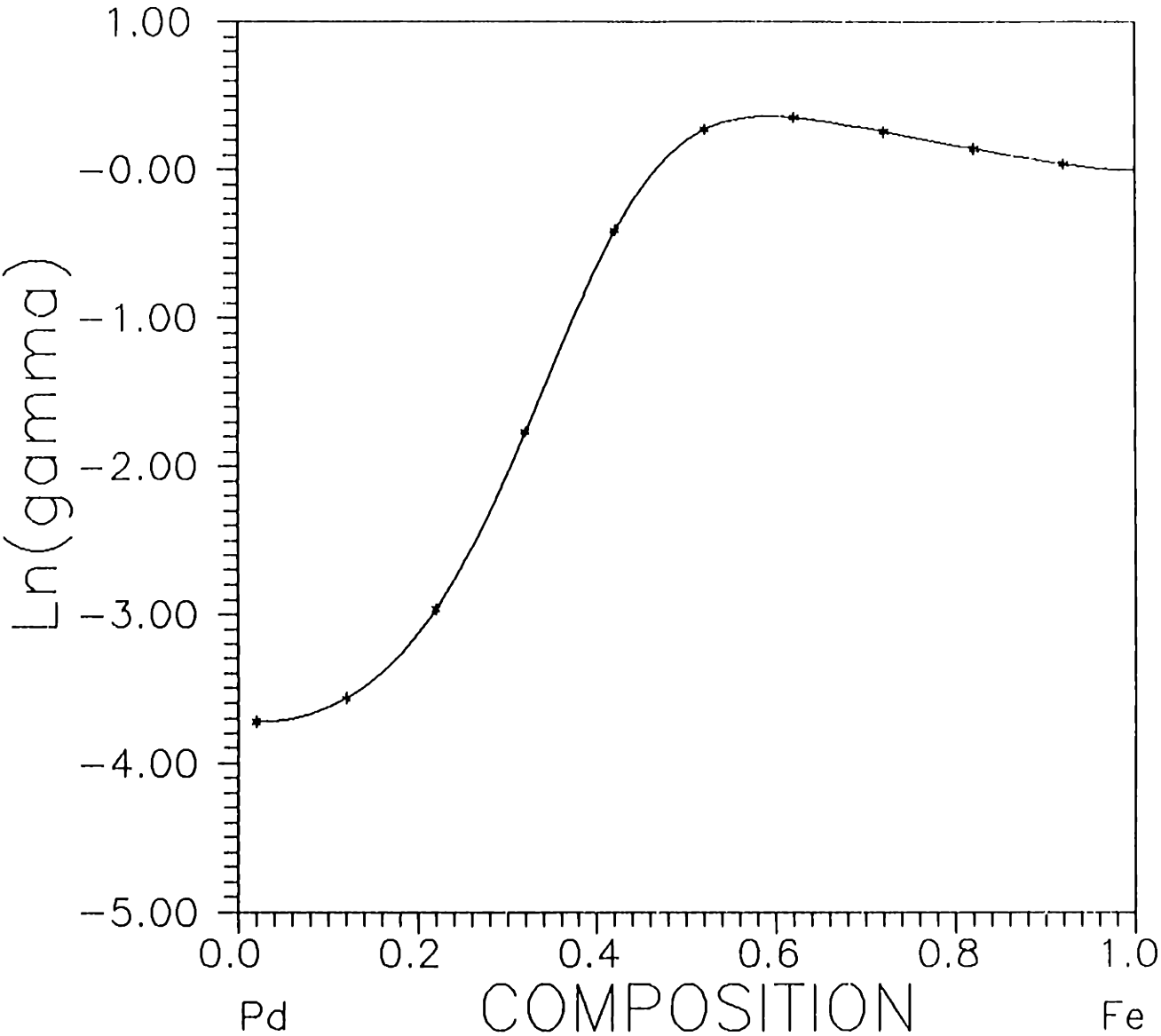

Figure 12. Computed ln(γ) as a function of composition for the PdFe system at 1050°C using the model function $P_4[Exp(P_6)]$. The selected solution was computed on imposing the constraints [0.1,6] on $\phi(c)$ Corresponding activities are depicted in figure 11.

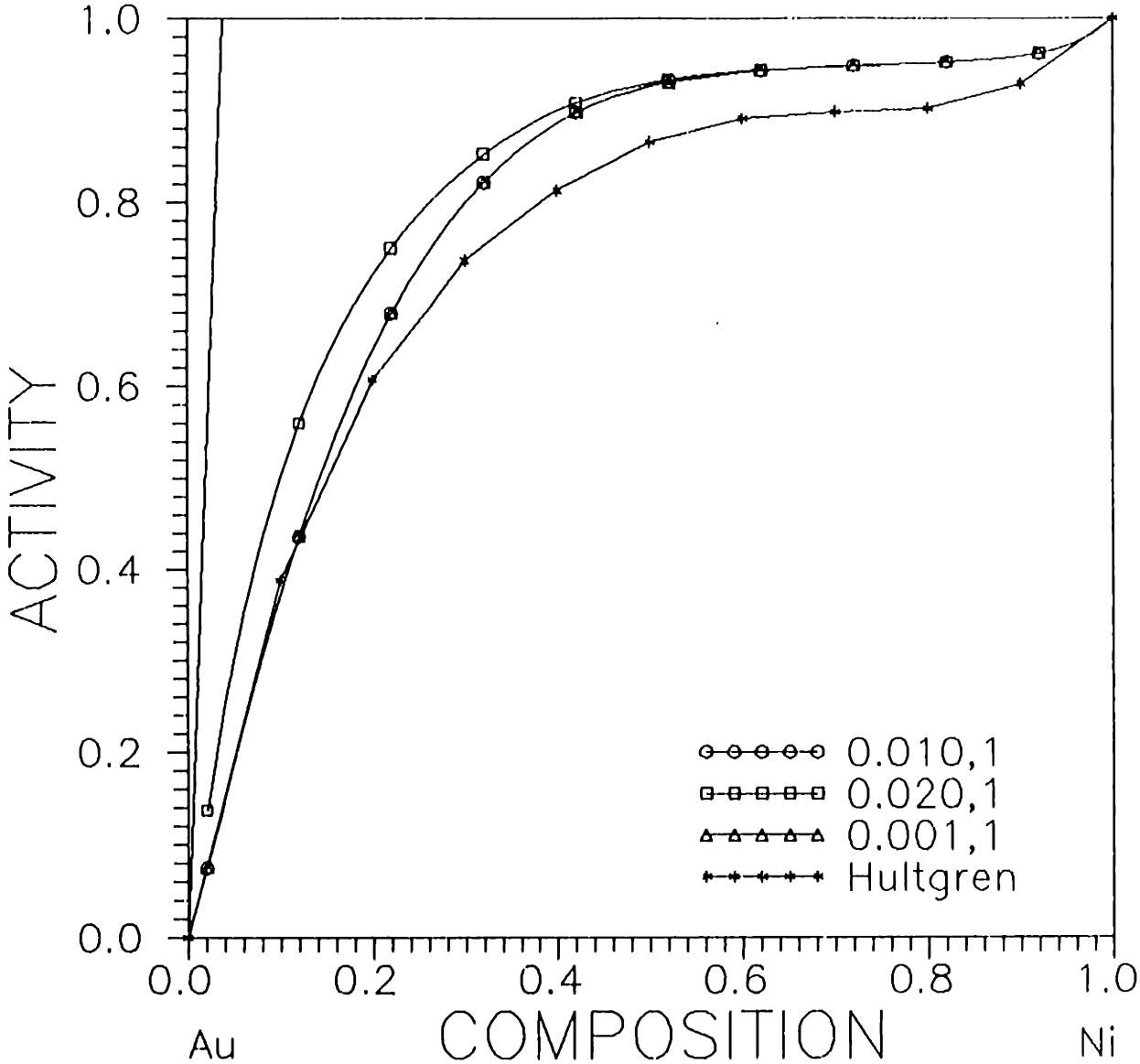

Figure 13. Computed activities for the AuNi system at 900°C using the model function $P_4[Exp(P_6)]$. The Henry's law line computed from Miedema's theoretical predictions is also depicted. The activities computed on imposing the bounds [0.01,1] and [0.001,1] are coincident and are taken to represent the system thermodynamics. Experimental data by Hultgren at 873°C is also depicted.

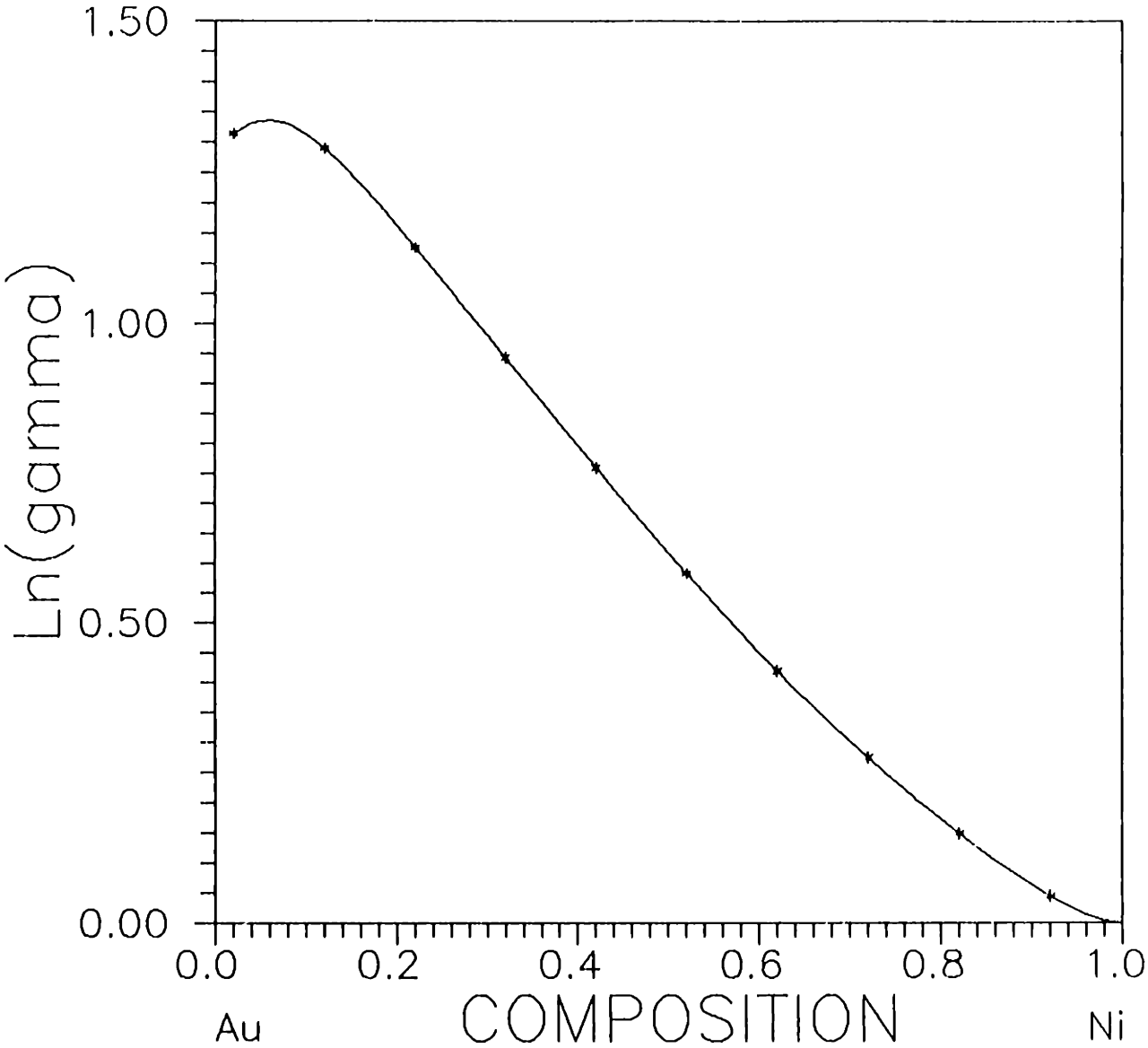

Figure 14. Computed ln(γ) as a function of composition for the AuNi system at 900°C using the model function $P_4[Exp(P_6)]$. The selected solution was computed on imposing the constraints [0.01,1] on $\phi(c)$ Corresponding activities are depicted in figure 13.

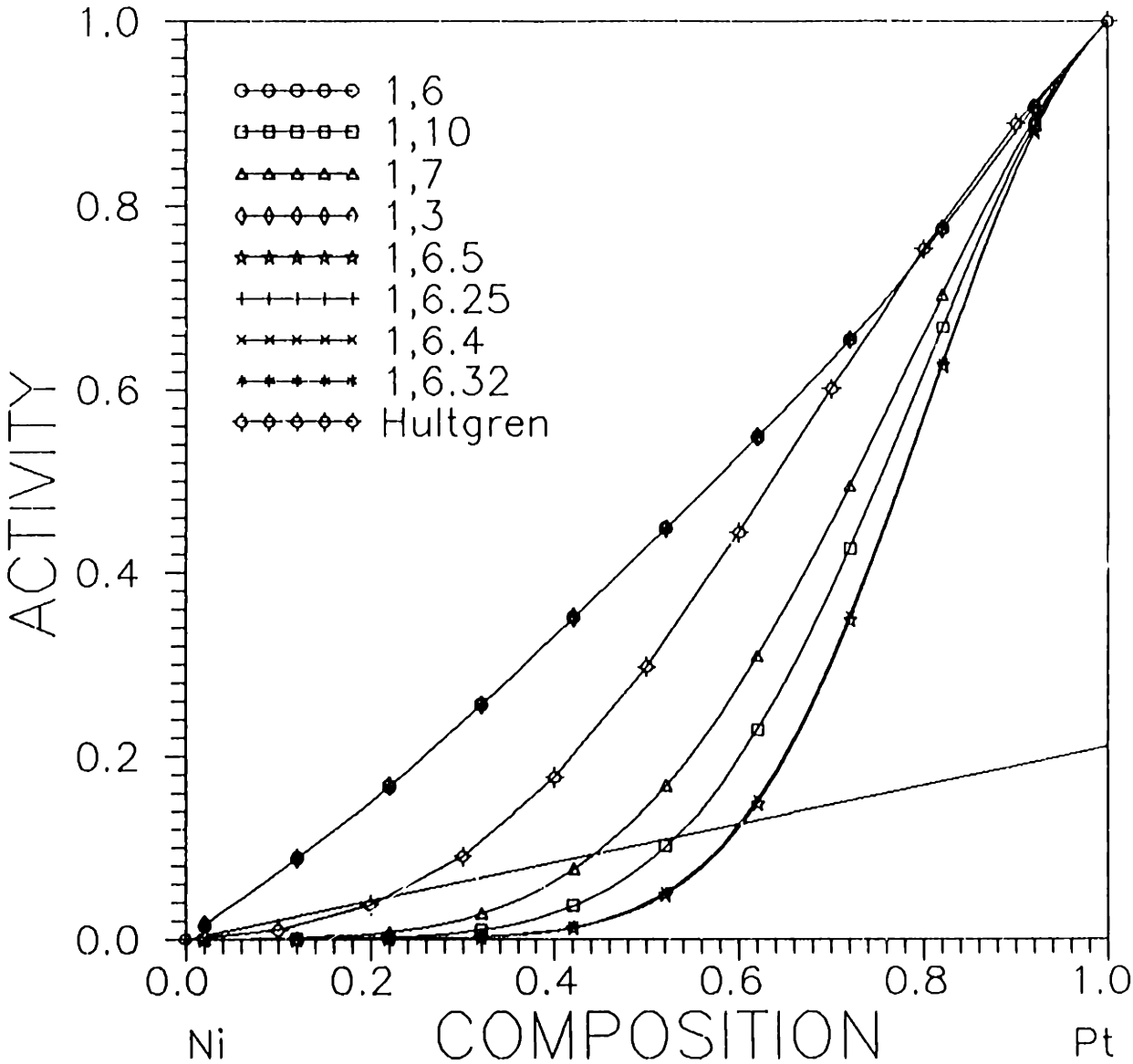

Figure 15. Computed activities for the NiPt system at 1296°C using the model function $P_3[Exp(P_6)]$. The Henry's law line computed from Miedema's theoretical predictions is also depicted. None of the computed solutions match either the predicted Henry's law line or the experimental data by Hultgren at 1352°C.

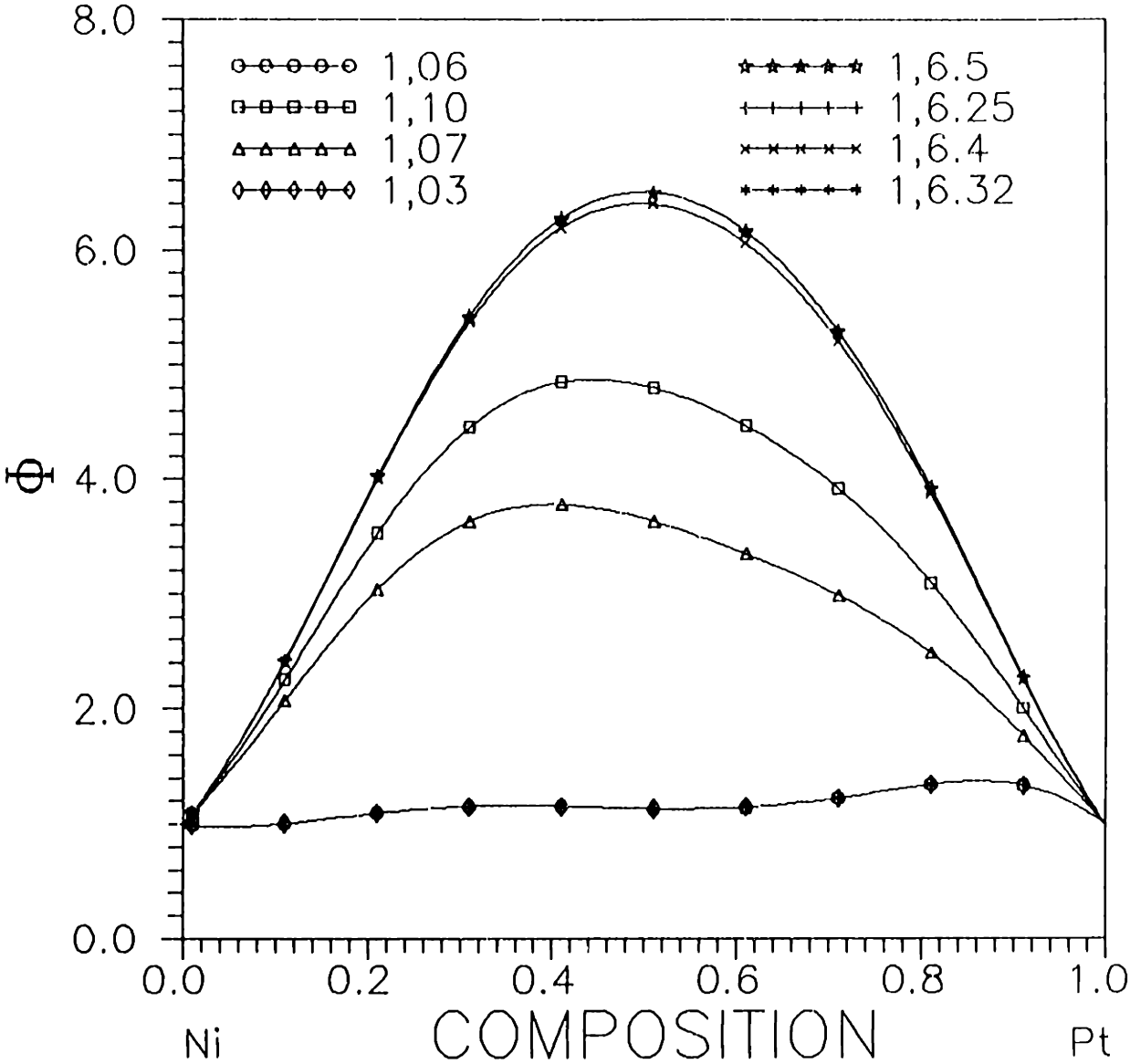

Figure 16. Computed thermodynamic term for the NiPt system at 1296°C using the model function $P_3[Exp(P_5)]$. Corresponding activities are depicted in figure 15.

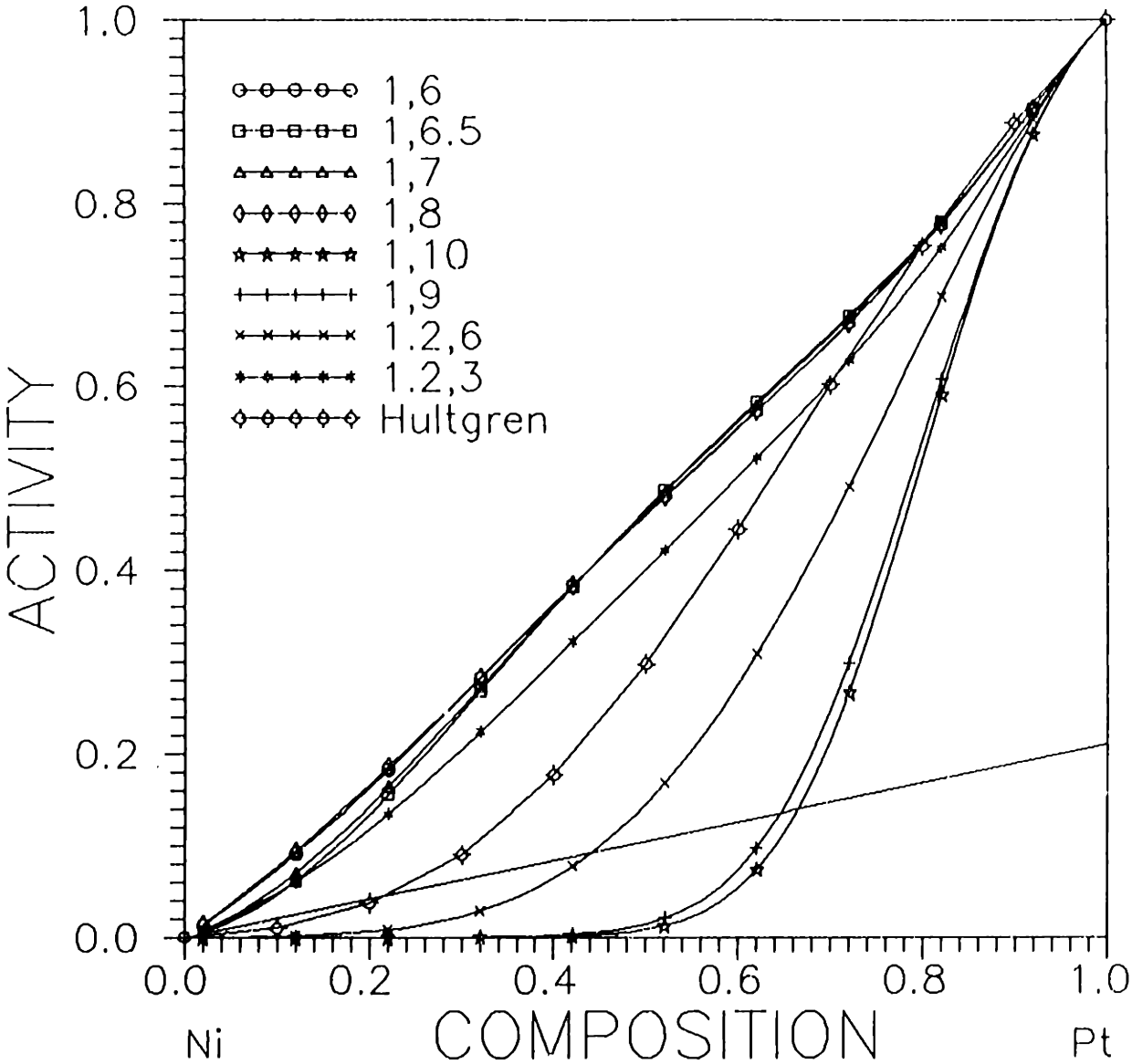

Figure 17. Computed activities for the PtNi system at 1296°C using the model function $P_4[Exp(P_6)]$. The Henry's law line computed from Miedema's theoretical prediction is also depicted. None of the computed solutions match either the predicted Henry's law line or the experimental data by Hultgren at 1352°C.

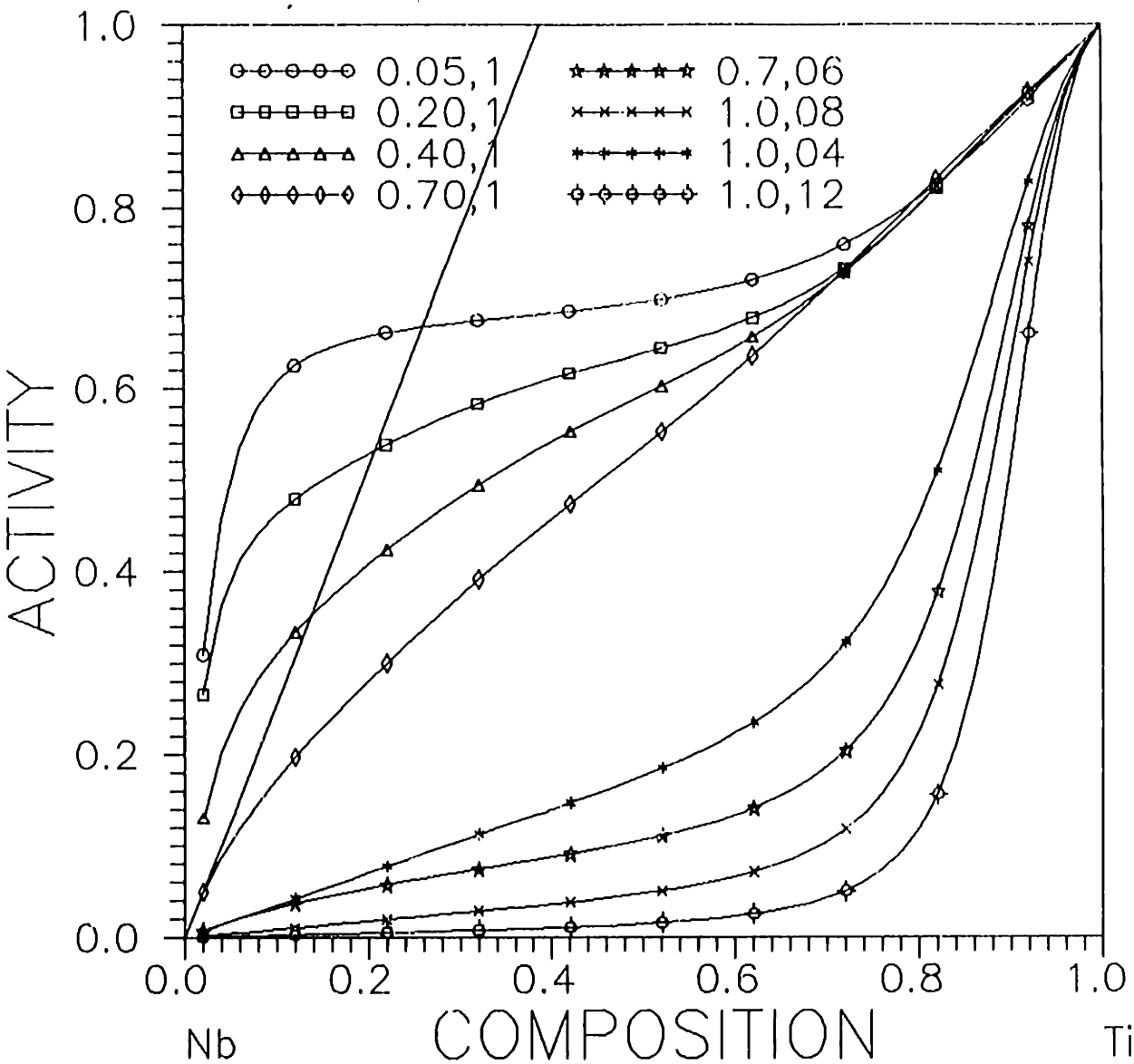

Figure 18. Computed activities for the NbTi system at 1000°C using the model function $P_4[Exp(P_6)]$. The Henry's law line computed from Miedema's theoretical prediction is also depicted. The solution computed in imposing the constraints [0.05,1] on $\phi(c)$ was taken to represent the thermodynamics of the system at 1000°C.

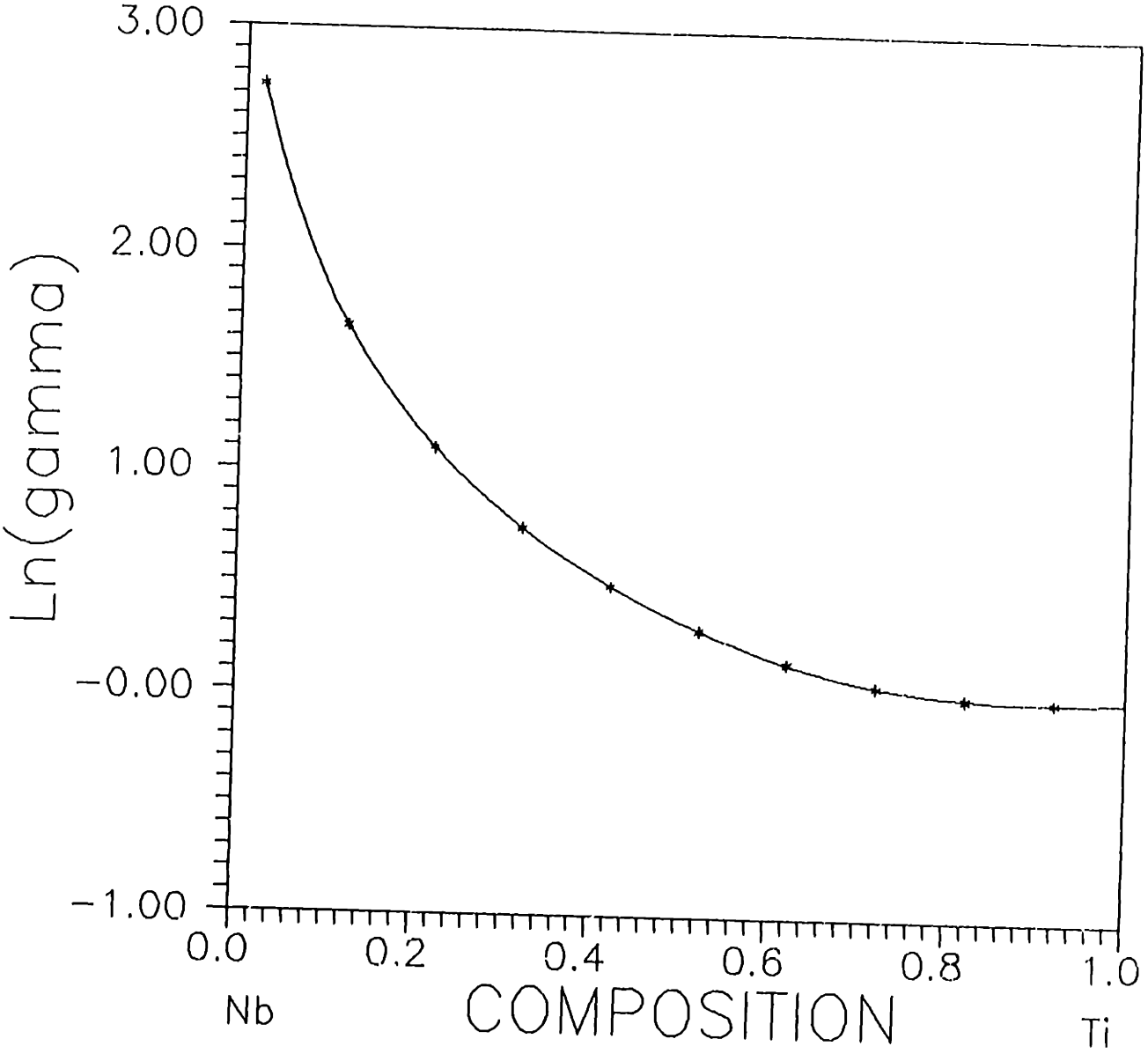

Figure 19. Computed ln(γ) as a function of composition for the NbTi system at 1000°C using the model function $P_4[Exp(P_6)]$. The selected solution was obtained on imposing the constraints [0.005,1] on $\phi(c)$ Corresponding activities are depicted in figure 18.

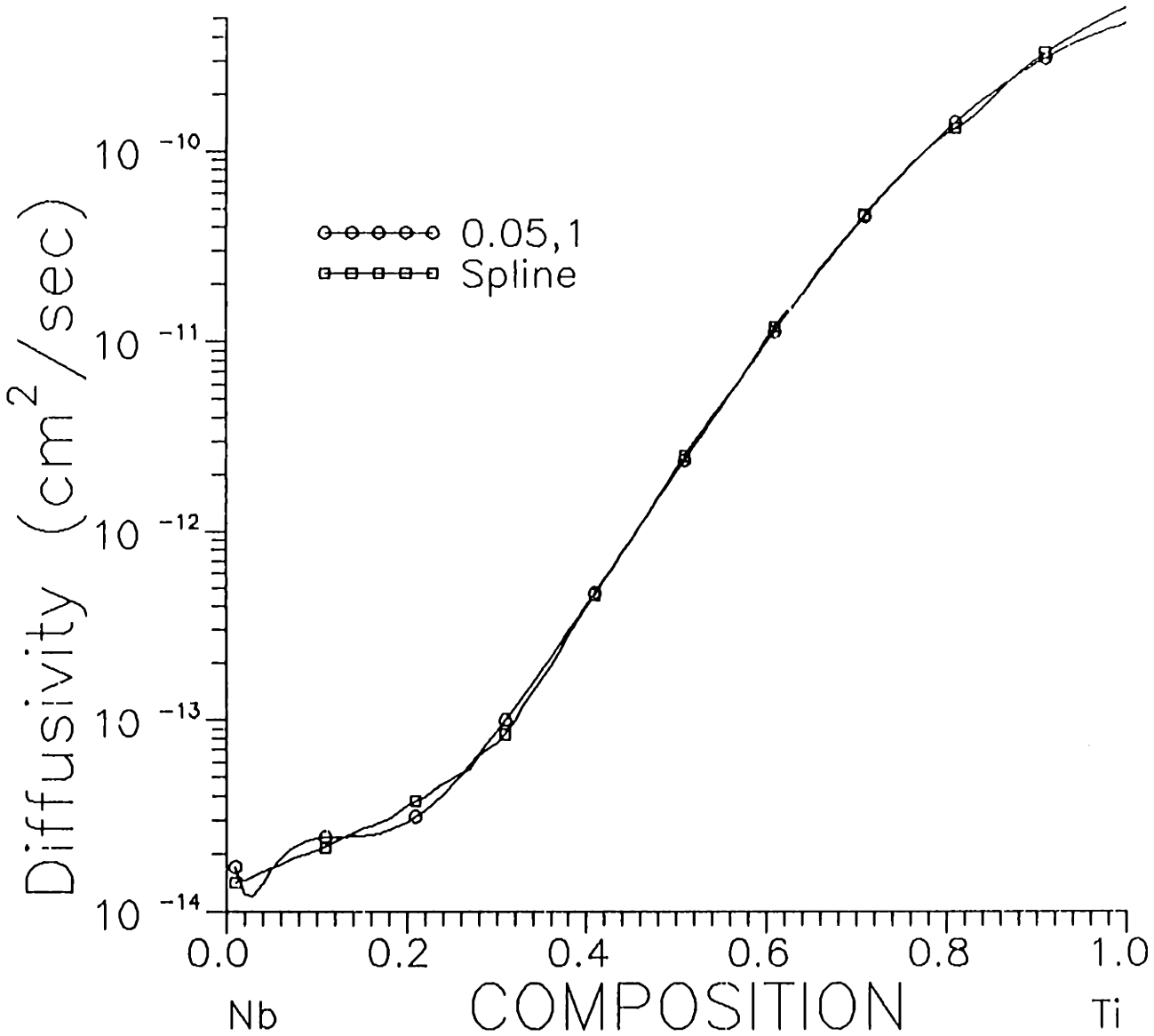

Figure 20. Illustration of a relatively good fit to the original diffusivity data for the NbTi system computed by imposing the constraints [0.05,1] on $\phi(c)$ The residual at the minimum was 0.82.

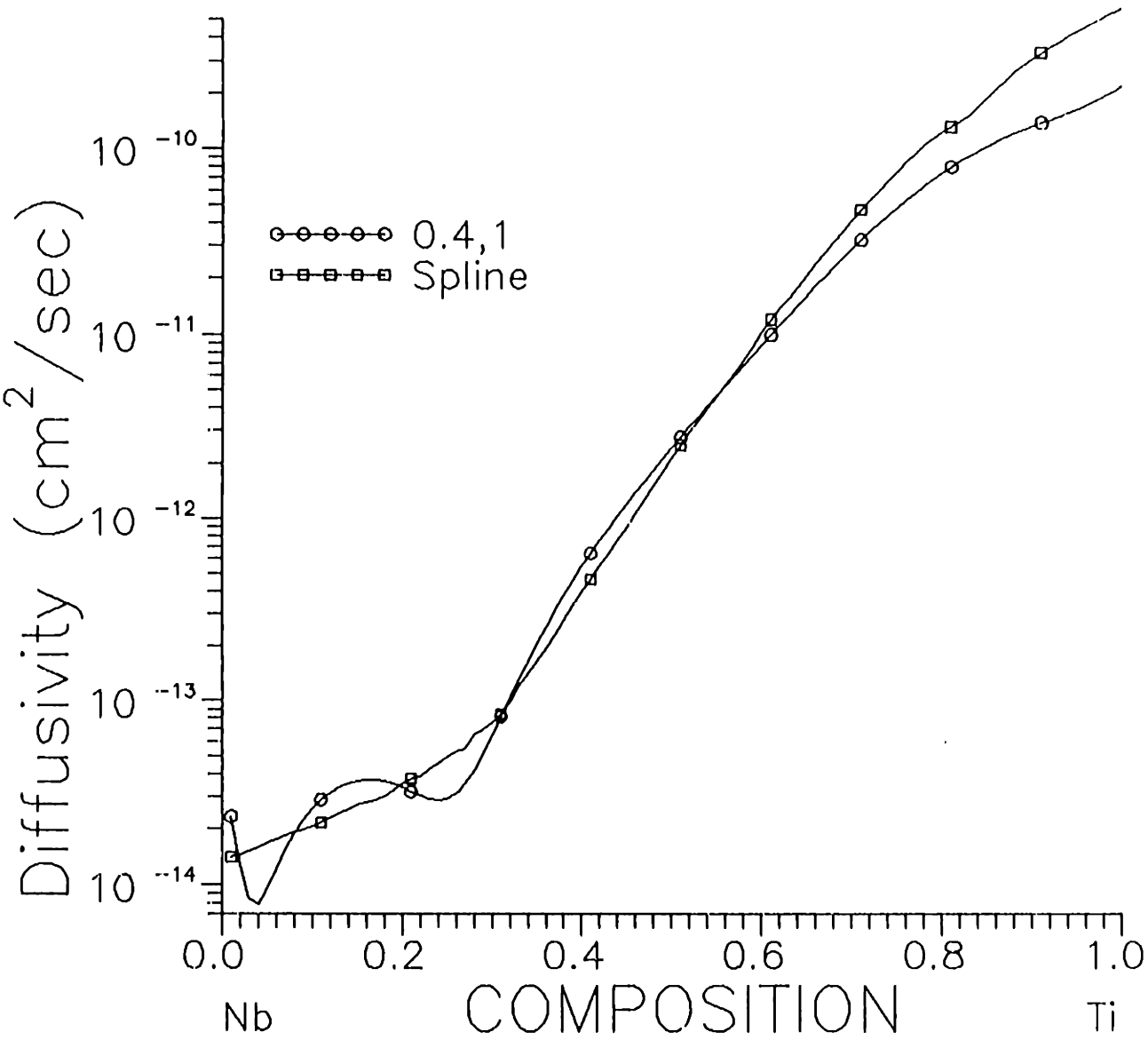

Figure 21. Illustration of a relatively poor fit to the original diffusivity data for the NbTi system computed by imposing the constraints [0.4,2] on $\phi(c)$ The residual at the minimum was 12.8.

Improving the Calculation of Interdiffusion Coefficients

5.1 ABSTRACT

Least squares spline interpolation techniques are reviewed and presented as a mathematical tool for noise reduction and interpolation of diffusion profiles. Numerically simulated diffusion profiles were interpolated using a sixth order spline. The spline fit data were successfully used in conjunction with the Boltzmann Matano treatment to compute the interdiffusion coefficient, demonstrating its usefulness as a numerical tool for such calculations. Simulations conducted on noisy data indicate that the technique can extract the correct diffusivity data given compositional data that contains only 3 digits of information and is contaminated with a noise level of 0.001. Splines offer a reproducible and reliable alternative to graphical evaluation of the slope of a diffusion profile used in the Boltzmann Matano treatment. Hence, use of splines will reduce the numerical errors associated with calculation of interdiffusion coefficients from raw diffusion profile data.

5.2 INTRODUCTION

The interdiffusion coefficient is a quantity that is useful to both researchers and to professional engineers. Improvements in the ability to measure diffusion coefficients or modifications in the numerical techniques used to obtain interdiffusion coefficients from raw diffusion data are expected to improve the accuracy of the data in the interdiffusion database. Such improvements are expected to influence basic research and practical applications in metallurgy.

Literature on diffusion currently lists two major theories that relate the interdiffusion coefficient to the system thermodynamics and to the phenomenological

coefficients. The older theory by Darken[1] is simpler since it assumes that the off diagonal phenomenological coefficients are zero and that vacancies are in local equilibrium in a diffusion couple. Darken's theory leads to the following expression :

$$\tilde{D} = (D_1^* c_2 + D_2^* c_1)\left(1 + \frac{\partial \ln \gamma}{\partial \ln c}\right) \qquad [1]$$

Similarly the theories of Howard and Lidiard[2], Manning[3], and Kirkaldy[4] lead to the following expression:

$$\frac{\tilde{D}}{\left(1 + \frac{\partial \ln \gamma}{\partial \ln c}\right)} = (D_1^* c_2 + D_2^* c_1) + \frac{kT}{N}\left(\frac{X_B}{X_{A^*}} L_{AA^*} + \frac{X_A}{X_{B^*}} L_{BB^*}\right) \qquad [2]$$

From equations [1] and [2], it is clear that the theories differ only in the additional term that is appended in equation [2]. The contribution of this term to the interdiffusion coefficient has been estimated to be of the order of 5% for isomorphous binary alloys[4]. Since the uncertainty in typical diffusion data ranges from 20%-100%, it is not possible to compute the contribution of this term for real systems. Thus, despite the availability of a more sophisticated atomistic theory, one is unable to verify it from diffusivity measurements* due to the large errors in the diffusivity data. Hence, efforts directed towards improving the overall accuracy of diffusion data are important from a theoretical standpoint.

There have been very few changes in the method of obtaining interdiffusion coefficients over the past four to five decades. The Boltzmann-Matano analysis of a diffusion profile which yields the interdiffusion coefficient as a function of composition has been extensively used[4,5]. The diffusivity is computed using the following expression :

$$D(c) = \left(\frac{-1}{2t}\right)\left(\frac{1}{\left(\frac{dc}{dx}\right)}\right)\int_0^c (x(c) - x_m)dc \qquad [3]$$

* Typically Kirkendall velocity measurements are used to discriminate between equation [2] and [1] since one may expect as much as a 28% difference in the velocities computed from Darken's theory and those computed from the theory by Manning, Howard and Lidiard and Kirkaldy.

Thus, the method relies on the slope of the diffusion profile as well as the area between the diffusion profile and the Matano interface. Both of these quantities must be estimated from discrete measurements of the diffusion profile (pairs of C-x data points). The slope is usually computed graphically[6]. At the ends of a diffusion couple the slopes are shallow and consequently more difficult to estimate graphically. In addition, the integral in equation [3] is also harder to estimate at the ends. As a result, the diffusivity data representing the terminal compositions is known to contain large errors.

In sharp contrast, considerable advances have been made in the field of numerical analysis over the past four decades. New, improved techniques have emerged for reducing noise from physical measurements; concepts of numerical accuracy and stability have emerged and have led to better algorithms for simple tasks such as estimation of areas under a curve defined by a discrete set of points. Simultaneously, powerful computing tools are now readily available.

Significant advances have also been made in the accuracy of non destructive techniques for compositional measurement. Instruments such as the electron microprobe and more recently the scanning transmission electron microscope (STEM) have improved not only the accuracy of the compositional measurement but also improved the spatial resolution of compositional measurements. Recent STEM studies on diffusion in the FeNi system[7,8] have attained spatial resolution that varied between 50nm and 400nm whereas the compositional measurements were accurate to within 0.5% or better. Since electron optical techniques are non destructive, it is possible to rescan the same area and obtain several diffusion profiles. This further improves the uncertainty in the raw data.

In light of the improvements in the quality of the raw diffusion data (compositions and spatial resolutions), it is now important that more sophisticated numerical techniques be employed for computing the diffusion coefficient from equation [3]. Estimation of slopes graphically is subject to human error and must now be superseded by other techniques which offer better reproducibility. It would

be unfortunate indeed if the progress made in compositional measurements was offset by poor computational techniques. Instead efforts must be directed to improving the computational techniques so that eventually one may reduce the overall variation in the diffusivity data, to levels that allow one to experimentally detect the differences between equation [1] and [2]. The present paper is a small step along that general direction.

The main purpose of this paper is to review an interpolation technique known as *linear least squares spline fitting* and to demonstrate its usefulness in treatment of diffusion data. Numerical experiments were conducted to test the usefulness of this technique. Results from these experiments indicate that spline interpolation techniques can be successfully used to compute the interdiffusion coefficient even in the presence of noise.

5.3 LITERATURE REVIEW

The idea of using polynomial interpolation for computing the interdiffusion coefficient has been studied earlier by Baroody[9] and later by Borovskii[10] et. al.. In both cases the raw diffusion data (C-x) was subjected to a non linear transformation involving the error function. Subsequently a single, high order polynomial was fitted to the data over the entire composition range. The final expressions directly yielded the interdiffusion coefficient as a sum of a series of polynomials. These polynomials bear a recurrence relationship among themselves.

The apprcach taken earlier suffers from two drawbacks. Firstly a single interval was chosen for interpolating the diffusion profile. Secondly, high order polynomials were used (upto order 9 or 11) which tend to oscillate between two successive datapoints. Splines, on the other hand split the interval of interpolation in to several subintervals and fit low order polynomials over each sub interval such that the derivatives of the interpolant remain continuous at the sub interval boundaries. The resultant interpolant provides a good fit to the data and does not exhibit oscillation.

The earlier investigators could not have used splines since splines were an active area of research by mathematicians when Baroody and Borovskii examined interpolation as a mathematical tool for computing diffusivities. However, today splines are well understood and the computing facilities as well the necessary software are easily accessible.

5.4 LINEAR LEAST SQUARES APPROXIMATION USING SPLINES

This section begins with a discussion on polynomial interpolation techniques thereby developing the motivation for spline fitting. Next, details on spline fitting are presented. The final topic will cover least squares approximation techniques with emphasis on least squares spline fitting. An example of the latter is presented to highlight the technique. The discussion is terse for sake of brevity. Interested readers are directed to the book by Carl de Boor.[11]

5.4.1 Polynomial Interpolation

Polynomials are attractive and popular as mathematical models for approximation because they can be evaluated, differentiated and integrated easily using basic arithmetic operations. However the use of polynomials for interpolation is not without drawbacks. For example, uniform spacing of data points (common in real experiments) can lead to large oscillations between two successive data points as the order of the polynomial increases.

Approximation theory provides precise statements about the ability of polynomials to model other functions. It can be shown that when using polynomials to model a general function g(x), which has r continuous derivatives, the error is bounded by the following upper bound:

For $g \epsilon c^{(r)}[a,b]$ and $n > (r+1)$

$$dist_{\infty}(g, P_n) \quad \leq \quad (constant)\left(\frac{b-a}{n-1}\right)^{r} w\left(g^{(r)}; \frac{(b-a)}{2(n-1-r)}\right) \qquad [4]$$

where,

g	:	measured quantity or function being modelled by a polynomial
P_n	:	the space of all polynomials of order n
$[a,b]$	:	domain of the independent variable
n	:	order of the polynomial
$w(r)$	:	modulus of continuity
$g \in C^{(r)}$	:	implies that g has r continuous derivatives on [a,b]

The important point to note here is that the error is bounded by $\left(\frac{b-a}{n-1}\right)^r$.

Thus there are two ways to reduce the error: (i) Reduce the interval length, (b-a) and (ii) Increase the order of the polynomial, n. Increasing n certainly reduces the error between the approximating polynomial and the function g. But as n increases the polynomial tends to oscillate between two successive data points. Such oscillations are often undesirable since physical quantities are not known to show numerous oscillations. Hence, to improve the approximation process one must choose a smaller interval. In other words, the main interval [a,b], should be split into several subintervals and the function should be approximated over each subinterval with a unique polynomial (usually of low order). A simple example of such an approximation scheme would be a piecewise linear approximation to a given function.

5.4.2 Spline Interpolation

Spline interpolation is subset of piecewise polynomial interpolation. The main objection to a piecewise approximation is the lack of continuity of the derivatives of the function at the boundaries between two subintervals. Often, there are physical reasons to demand that the approximation to a physical quantity possess several continuous derivatives. For example, the slope and curvature of a diffusion profile (C-x data) are related to the flux and to the instantaneous depletion rate. Therefore discontinuities in the derivatives of the

composition-distance data are undesirable. To avoid such discontinuities, one seeks an approximation process that will ensure continuity of the derivatives across subinterval boundaries. Such an approximation process is called spline-fitting, and a subset of spline fitting is least squares spline fitting.

In spline fitting terminology, the subintervals are known as 'spans' and the endpoints of each span are termed 'knots' or breakpoints. A k^{th} order spline fit to a given data set ensures the following: (i) the resultant polynomial of order k (degree k-1) interpolates (passes through) all the given data points on that span, and (ii) (k-2) derivatives of the interpolant are continuous at the breakpoints. In other words the interpolant is differentiable (k-3) times.

To construct a spline fit, one needs not only the given data set but also some additional input. Consider a data set comprising of N data points , i.e. N (x,y) pairs. In the simplest case one desires to fit a k^{th} order spline on N spans, that is one considers the distance between two successive datapoints to constitute a subinterval*. The total number of unknowns in fitting a k^{th} order polynomial on each subinterval are kN. The constraints from the interpolation conditions are: 2(N-2) + 2 = 2(N-1). Additionally continuity of (k-2) derivatives imposes (N-2)(k-2) constraints. Thus the total number of unknowns are (k-2). In other words, to uniquely specify the k^{th} order spline one needs to provide (k-2) constraints in addition to the data set. Usually these are supplied as the values of the function or one of its derivatives at either end. Often the derivatives at either end can be set to zero based on physical considerations. An example would be the fitting of a diffusion profile from an infinite diffusion couple. In this case, it is known that the slope and curvature of the diffusion profile are zero at points far from the diffusion zone.

* The result to be presented is true even when the number of spans does not coincide with the data points.

It should be noted that in the general case the breakpoints or knots are fewer in number than the total number of data points. Further the knots need not coincide with the data points. This is particularly true for least squares approximation using splines.

5.4.3 Least Squares Approximation Techniques

Measurements of physical quantities are usually contaminated by the inherent noise associated with the measuring technique. Thus the measured quantity is a sum of the noise (which is presumed to be random) and the true value of the physical property. Least-squares approximation techniques attempt to separate the noise from the true values of the physical quantity. All least squares techniques assume a certain functional form that describes the physical quantity. The mathematical model selected reflects a compromise between the accuracy of the fit and the ability to separate noise from the data. Ideally, the function chosen should possess just enough degrees of freedom to model the underlying variation of the physical quantity. Excessive degrees of freedom will certainly improve the accuracy of the fit but the function will also include some contamination from the noise.

The first step in least squares approximation involves choosing a certain mathematical model (trigonometric, polynomial, exponential etc.) to describe the variation of the physical quantity under consideration. The second step consists of defining a least-squares error function by using the mathematical model. The third step consists of backing out the necessary coefficients which constitute the mathematical model by minimization of the least-squares error with respect to the unknown coefficients. Typically the number of observations or measurements far exceeds the number of unknowns that constitute the mathematical model. This results in an overdetermined system of equations (in the linear case) from which the unknown parameters are estimated. In the non linear case the resultant error function must be minimized using an iterative procedure.

Specifically, consider a data set comprising of N data points (x_i,y_i) to which one desires to fit a model function f. Assume that 'k' parameters $(\alpha_1.....\alpha_k)$ are needed to describe the function f. The least squares error is then given by the following equation:

$$E^2 = \sum_{1}^{n} \{[y_i - f(\alpha_1.....\alpha_k, x_i)]w_i\}^2 \qquad [5]$$

where w_i, the weighing function reflects the certainty (inverse of spread) in the i^{th} data point (x_i,y_i).

By differentiating with respect to each α_k and setting the result to zero one ends up with the normal equations that must be solved for each α_k This is accomplished by standard procedures of linear algebra (Gaussian elimination, LU factorization [12]).

In the case of least squares spline fitting, one must specify a priori, the spline order, the knot sequence and the (k-2) additional unknowns. The spline function is defined in terms of the unknown coefficients, α_k, which comprise the interpolating polynomials. Thus during the minimization process one seeks the numerical values of the unknown coefficients.

It should be noted that varying the number and location of the knots (i.e. changing the number and length of the subintervals) can significantly affect the accuracy of the fit. Hence fitting schemes must incorporate an algorithm that optimizes the number and location of the knots. The spline routines used in this work accomplish this by a two step process. In the first stage the number of polynomial pieces is increased and the residual (or least square error) is monitored as a function of the number of polynomial pieces. It will be shown in the example to follow that a plot of residual as a function of number of polynomial pieces, depicts a fairly flat minimum or a plateau. The number of polynomial pieces are

chosen to correspond to the plateau on the graph. For a given number of polynomial pieces, the knot locations are selected based on examination of the k^{th} root of the k^{th} derivative of the dataset.[11]

5.4.4 Example of Spline fit

Figure 1 depicts the chemical interdiffusion coefficient in the Ni-Pt system. The data were obtained by digitizing one of the figures in reference 10. Clearly the input data is contaminated by high wavenumber noise arising from the digitizing process. It was decided to fit a spline of order 4 (cubic spline) to this data. The input to the programs included the data set depicted in figure 1 and the two breakpoints at either end of the interval (i.e. a single span).

The programs increased the number of polynomial pieces continuously and monitored the least square error. A plot of the least square error is depicted in figure 2 as a function of the number of polynomial pieces. The 'error plateau' is clearly seen. A value of 17 was selected for the number of polynomial pieces and the B-Spline coefficients constituting the fit were computed. Figure 3 depicts the fitted function along with the raw digitized data for comparison. The fit appears to be satisfactory. Also depicted in figure 3 are the locations of all the breakpoints. A more stringent evaluation of the fit involves examination of the residual at each data point. In other words one examines the difference between the fitted value and the measured (digitized) value of the function. If the fit is a good one, then the residual should represent the noise which is presumed to be random. This difference is plotted as a function of the composition in figure 4. It is clear that the residual experiences several changes in sign. This suggests that the residual is indeed random and hence may be presumed to represent noise. Hence the fit is believed to be a good one.

5.4.5 Software for Spline Fitting

Software for the implementation of splines is readily available for spline orders up to k=4, i.e. cubic splines. Popular Fortran libraries such as the NAG[13] library offer routines for cubic splines. During this research project it became

necessary to use splines which possessed a minimum order of five and sometimes even six. The book by de Boor[11] contains several programs for this purpose. The routines by deBoor allow one to increase the number of breakpoints and determine the optimum knot placement given a certain number of knots. These routines are available in the public domain and may be easily obtained by using the NetLib facility over InterNet[14].

5.5 NUMERICAL EXPERIMENTS

A numerical experiment was conducted to test the ability of spline interpolation in extracting the correct interdiffusion coefficients from noisy diffusion profile data. The experiment consisted of the following stages:

(i) Diffusivity data for an isomorphous binary system (AuNi) was obtained from the literature and fitted with a fourth order spline.

(ii) An equidistant finite difference grid was used to numerically simulate a diffusion couple between pure Au and pure Ni. Diffusion profiles were computed for various annealing times.

(iii) Random noise was added to the computed profiles using a random number generator. The amplitude of the noise was varied.

(iv) A least squares spline, of order 6, was fit to the composition-distance data.

(v) The Boltzmann Matano treatment was used to compute the interdiffusion coefficient. The computed coefficient was compared with the diffusivity data used to simulate the profile.

A minor modification was made to the Boltzmann Matano expression. The variable of integration was altered from the compositional variable to the spatial variable resulting in the following expression :

$$D(c) = \left(\frac{-1}{2t}\right)\left(\frac{1}{\left(\frac{dc}{dx}\right)}\right)\int_0^{x(c)}(x(c) - x_m)\frac{dc}{dx}dx \qquad [6]$$

The modification is advantageous since the diffusivity is now expressed as a function of the slope alone and hence all errors will arise from a single source only; that is from the slope of the diffusivity data. The slope of the diffusion profile can be easily computed from the spline fit by differentiating the piecewise polynomial comprising the spline. To compute the integral in equation [6] the integrand was computed at discrete points and a third order finite difference scheme was used to evaluate the integral. Subroutine D01GAF from the NAG[13] Fortran library was used for this purpose.

5.6 RESULTS

Figure 5 depicts the diffusion profile computed using the diffusivity data for the AuNi system. The finite difference grid used contained 800 equidistant points for a diffusion couple 2 cms in extent. Euler's method[15] was used to solve the diffusion equation with insulating boundary conditions at either end. The original interface between the two pure metals (plane of join) was chosen to correspond to a location 0.5 cms from the Ni end of the diffusion couple.* The diffusion times corresponding to the profile are astronomically large (4.32 X 10^8 secs). However such large times were necessary to ensure that the slope and the curvature of the diffusion profile do not attain very large numerical values. In a practical experiment one would split the entire compositional interval and prepare a series of diffusion couples each covering a narrow composition range**. In such a case one would obtain shallow

* Preliminary runs were conducted with a coarse grid which suggested that x=0.5 cms would be a good choice for the plane of join. The lack of symmetry in the diffusion couple is a result of the large variation of the diffusivity in the AuNi system. At the Au rich end the diffusivity is about two orders of magnitude larger than the diffusivity at the Ni rich end.

** A narrow compositional range in a diffusion couple is necessary to ensure the validity of the phenomenological expressions (derived from irreversible thermodynamics).

profiles in a realistic time span. Thus in a real experiment each diffusion couple would provide diffusivity information over a narrow range of compositions. By using a single diffusion couple in the present simulations the computational effort has been greatly reduced. However, the use of a single diffusion couple covering the entire range of composition from 0%B to 100%B not recommended for a real experiment.

The compositional profile was computed to 10 digit accuracy which is clearly unrealistic. To simulate a real diffusion couple, the data were rounded to a lower accuracy and random noise was added to the profiles. Equation [6] was then used to compute the interdiffusion coefficient.

Figure 6 depicts the diffusion coefficient computed using 10 digit diffusion profile data. Also depicted in figure 6 is the original diffusivity data for the AuNi system. The close match between the computed and the original data confirms that the modified computational scheme of equation [6] was correctly implemented.

The diffusion profile was rounded to 2 digits (in other words the compositional data varied from 0.990 to 0.010). Noise was also added to the profile by using a random number generator. The noise possessed a maximum amplitude of 0.01. Figure 7 depicts the computed and original diffusivity data for the noisy profile data. The computed diffusivity differs slightly from the original diffusivity although the general trend is preserved. In particular, the maxima and minima around X_{Ni}=0.8 are lost due to the rounding of the profile and the addition of noise.

Similarly, figure 8 compares the computed and original diffusivities for the case when the profiles were rounded to 3 digits (in other words the compositional data varied from 0.999 to 0.001) and the maximum amplitude of the noise was 0.001. In this case an excellent match was obtained between the computed and the original diffusivities. Comparison of figures 6 and 8 indicates that the least squares spline technique is able to filter out all noise with a maximum amplitude less than 0.001 when given 3 digit profile data.

5.7 DISCUSSION

The simulation results clearly indicate that spline interpolation can be successfully used in computing interdiffusion coefficients. It is also clear that three digit data with a maximum noise amplitude of 0.001 is good enough to obtain highly accurate diffusivity data. With two digit data and 0.01 level noise some loss of reproducibility is clearly seen.

In a real experiment, the accuracy of compositional measurement will vary with the composition. At very small compositions the absolute error will be smaller but the relative error will be larger[4]. The simulations presented here are a stricter test of the method since the noise added was invariant with composition. Thus for compositions less than 0.01, the 0.01 level noise will completely swamp out the compositional data. On the other hand a real experiment introduces several other errors in the data such as errors in measuring the spatial variable, porosity in the diffusion couple etc.

It is important to note that currently, a real experiment on an electron microprobe is capable of achieving much better spatial resolution than the simulation data. With proper calibration the STEM can offer compositional data good to at least two digits and possibly three digits with noise levels approximately 0.01. An example is the work of Goldstein[7,8] et. al.. Hence the experimental conditions available presently lie between the two cases investigated in this paper. Clearly, in the present situation graphical evaluation of slopes must be superseded by other more reliable techniques.

It is hoped that in the future established numerical techniques will replace graphical evaluations of the quantities used to determine diffusivities and lead to improvements in the accuracy of basic diffusion data.

5.8 CONCLUSIONS

Least squares spline fitting techniques were reviewed and presented as a technique to filter out the noise in the measured composition data. These techniques

can be successfully applied to a diffusion profile to estimate the slope of a diffusion profile which is needed to compute the interdiffusion coefficient as a function of composition. Simulation results indicate that the technique can extract the correct diffusivity data given compositional data containing only 3 digits of information and contaminated with noise levels of 0.001. Some loss of accuracy was seen on using compositional data containing only 2 digits of information and contaminated by a noise level of 0.01.

5.9 SYMBOLS

$\tilde{D}$	:	Chemical interdiffusion coefficient
D_i^*	:	Tracer diffusivity for element i
c_i	:	Chemical interdiffusion coefficient
γ	:	Activity Coefficient
c	:	Chemical composition
$L_{AA'}, L_{BB'}$	:	Phenomenological coefficient
$X_{A'}, X_{B'}, X_A, X_B$	:	Mole fraction
k	:	Boltzmann's constant
N	:	Avogadro Number
T	:	Absolute temperature
$\frac{dc}{dx}$	:	Slope of the diffusion Profile
t	:	time
x	:	spatial variable

5.10 REFERENCES

1. L.S. Darken, *Trans. AIME*, 174, pp. 184-201, (1948).

2. R. E. Howard and A. B. Lidiard, *Rep. Prog. Phys.*, 27, 161, (1964).

3. J. R. Manning, *Diffusion Kinetics for Atoms in Crystals*, D. Van Nostrand, (1968).

4. J. S. Kirkaldy and D. J. Young, *Diffusion in the Condensed State*, The Institute of Metals, (1987).

5. P. G. Shewmon, *Diffusion in Solids*, McGraw Hill, (1963).

6. C. Wells, *Atom Movements*, ASM, pp. 26-50 (1950).

7. D. C. Dean and J. I. Goldstein, *Metallurgical Transactions A*, 17A, 1131-1138, (1986).

8. K. B. Reuter, D. B. Williams and J. I. Goldstein, *Metallurgical Transaction A*, 20A, 719-725, (1989).

9. E. M. Baroody, *Journal of Metals, Trans. AIME*, 819-822, (1957).

10. I. B. Borovskii, K. P. Gurov, I. D. Marchukova and Y. E. Ugaste, *Interdiffusion in Alloys*, Nauka Publishers, NTIS Document PB86-245495, (1986).

11. Carl de Boor : '*A Practical Guide to Splines*', Applied Mathematical Sciences Series, Springer Verlag, New York, 1985.

12. Gene Golub, and Van Loan, *Matrix Computations*, John Hopkins University Press, (1983).

13. NAG Fortran Library Manuals, Mark 13, Numerical Algorithms Group, Downers Grove, IL, (1987).

14. Jack J. Dongarra and Eric Grosse, *Distribution of Mathematical Software via Electronic Mail*, Communications of the ACM, Vol. 30, No. 5, pg. 403, (1987).

15. Butcher, *The Numerical Analysis of Ordinary Differential Equations*, Wiley (1987).

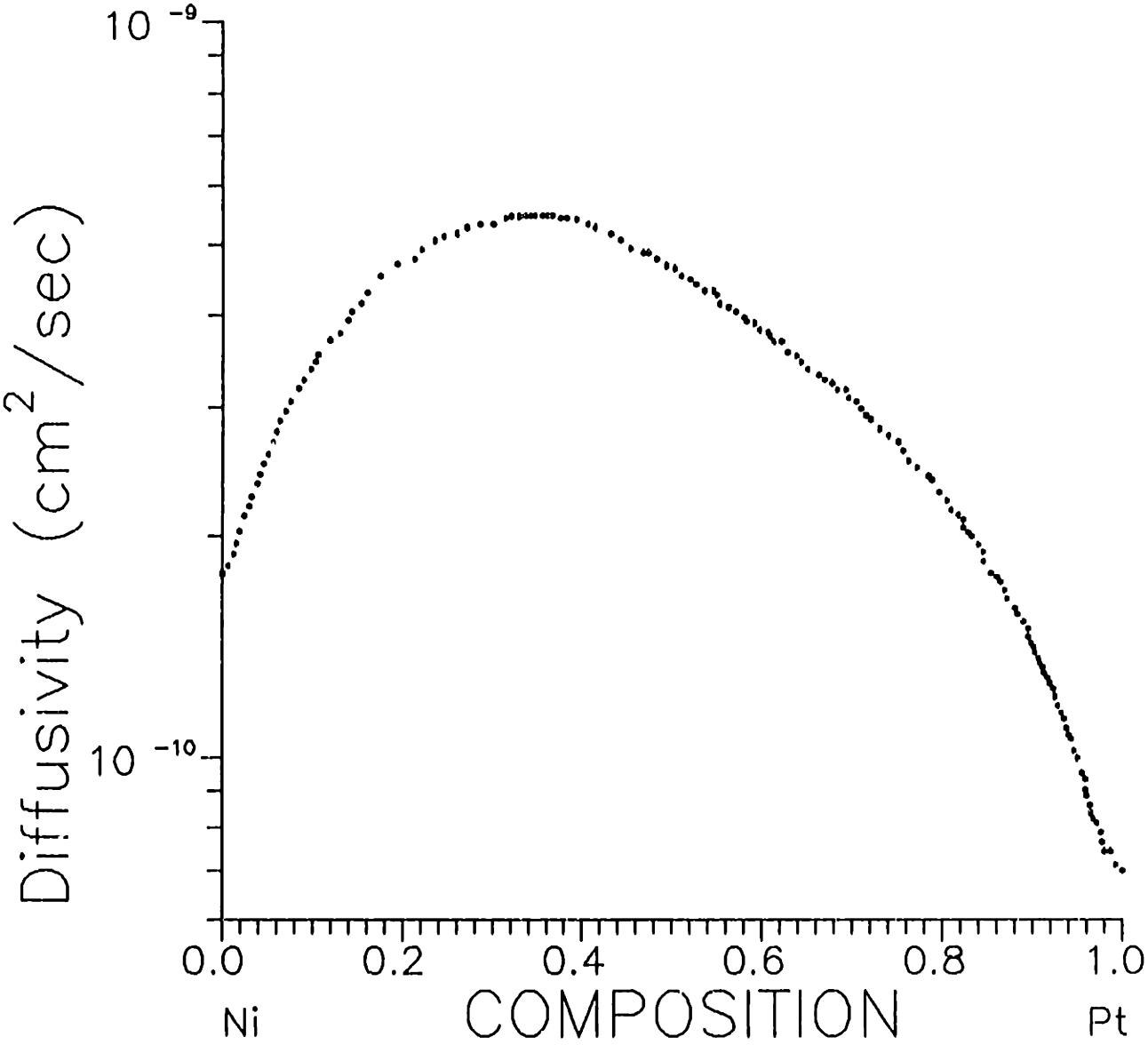

Figure 1. Raw digitized diffusivity data for the NiPt system at 1296°C.

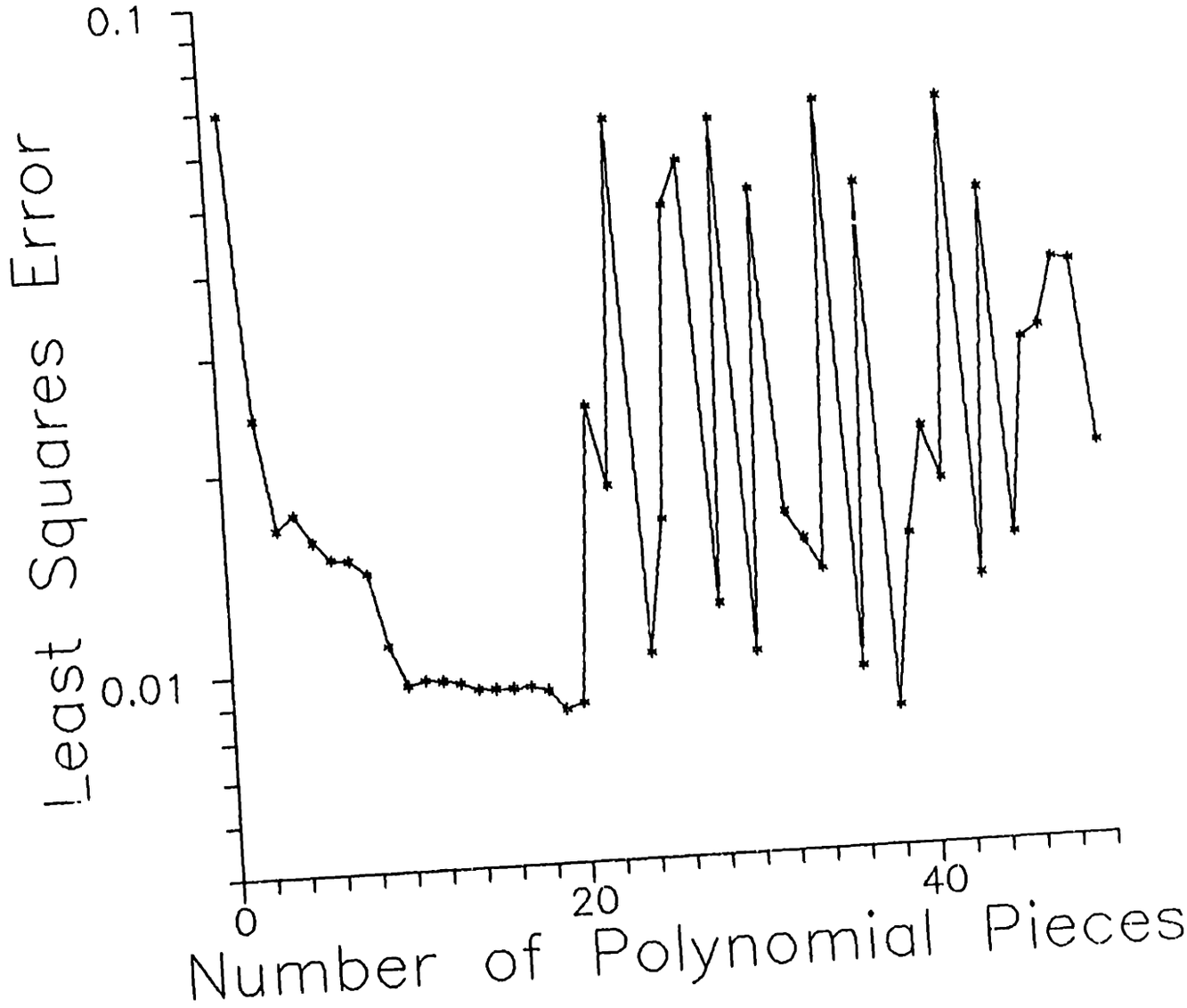

Figure 2. Least Square error as a function of the number of polynomial pieces for spline fitting the diffusivity data of figure 1. Note the error plateau in the curve.

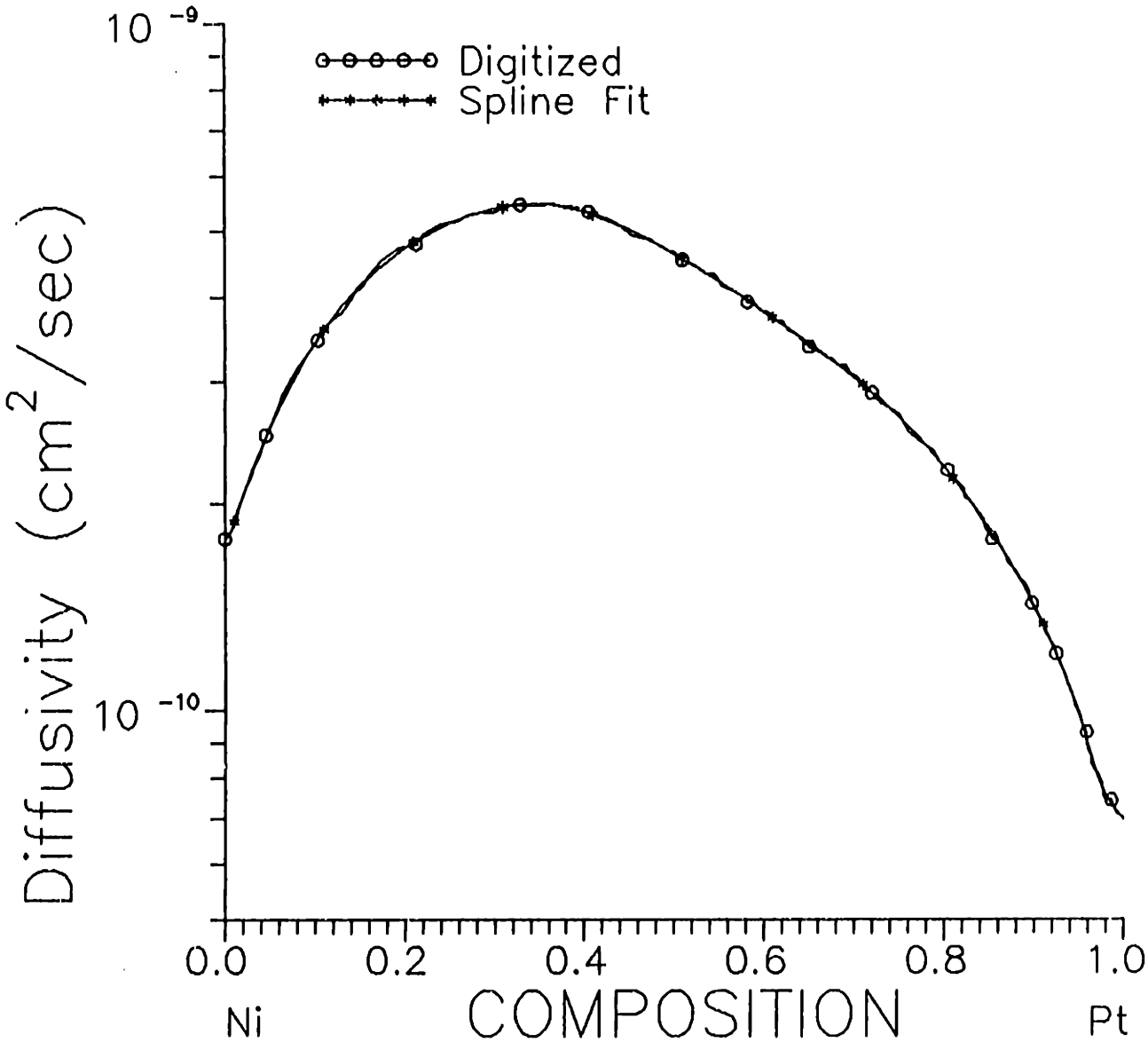

Figure 3. Raw and spline fitted diffusivity data for the NiPt system at 1296°C. The spline order was 4.

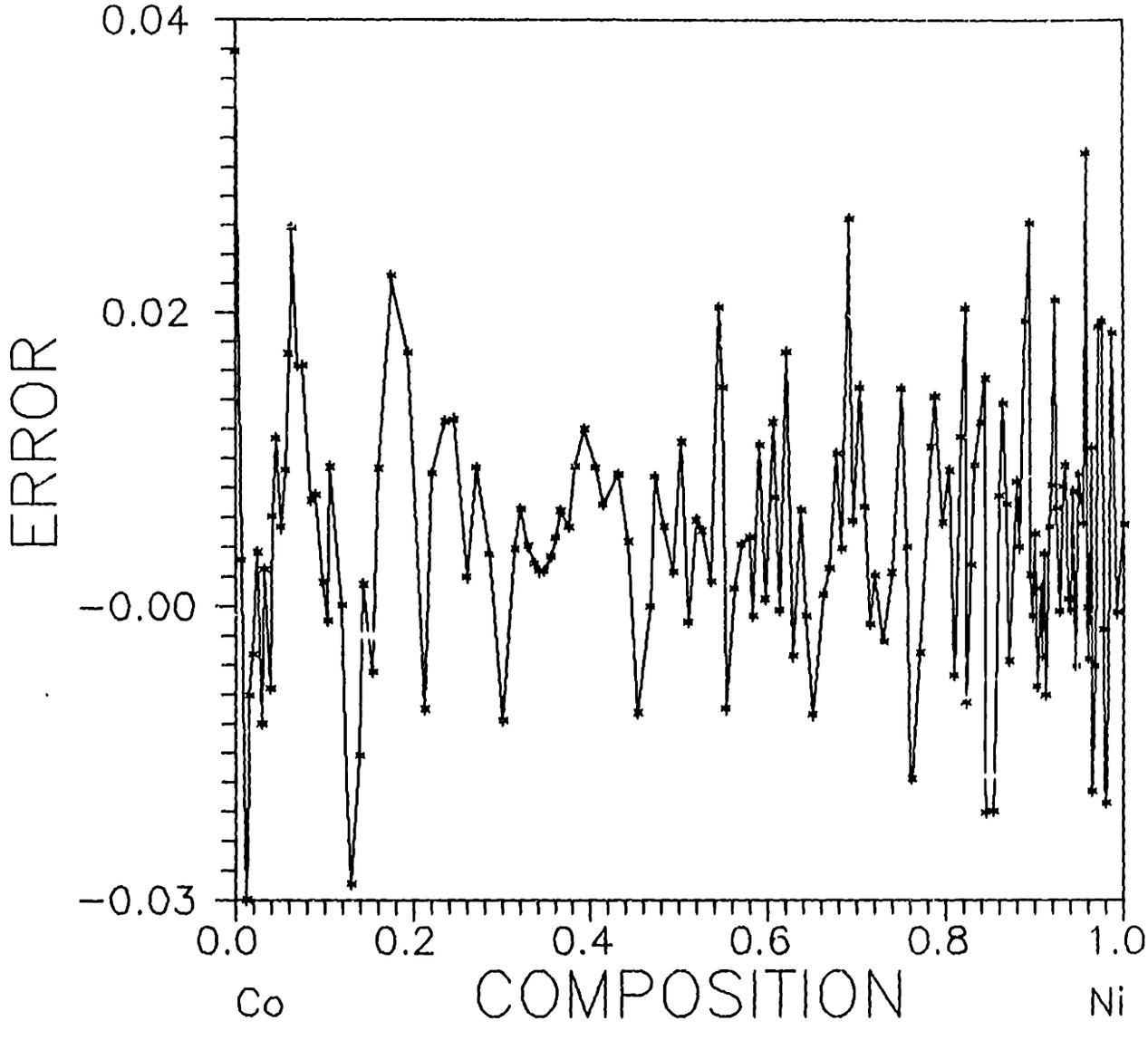

Figure 4. Difference (residual) between the raw digitized data and the spline fitted diffusivity data. The random nature of the residual is clearly evidenced in the large number of sign changes indicating that it is representative of noise.

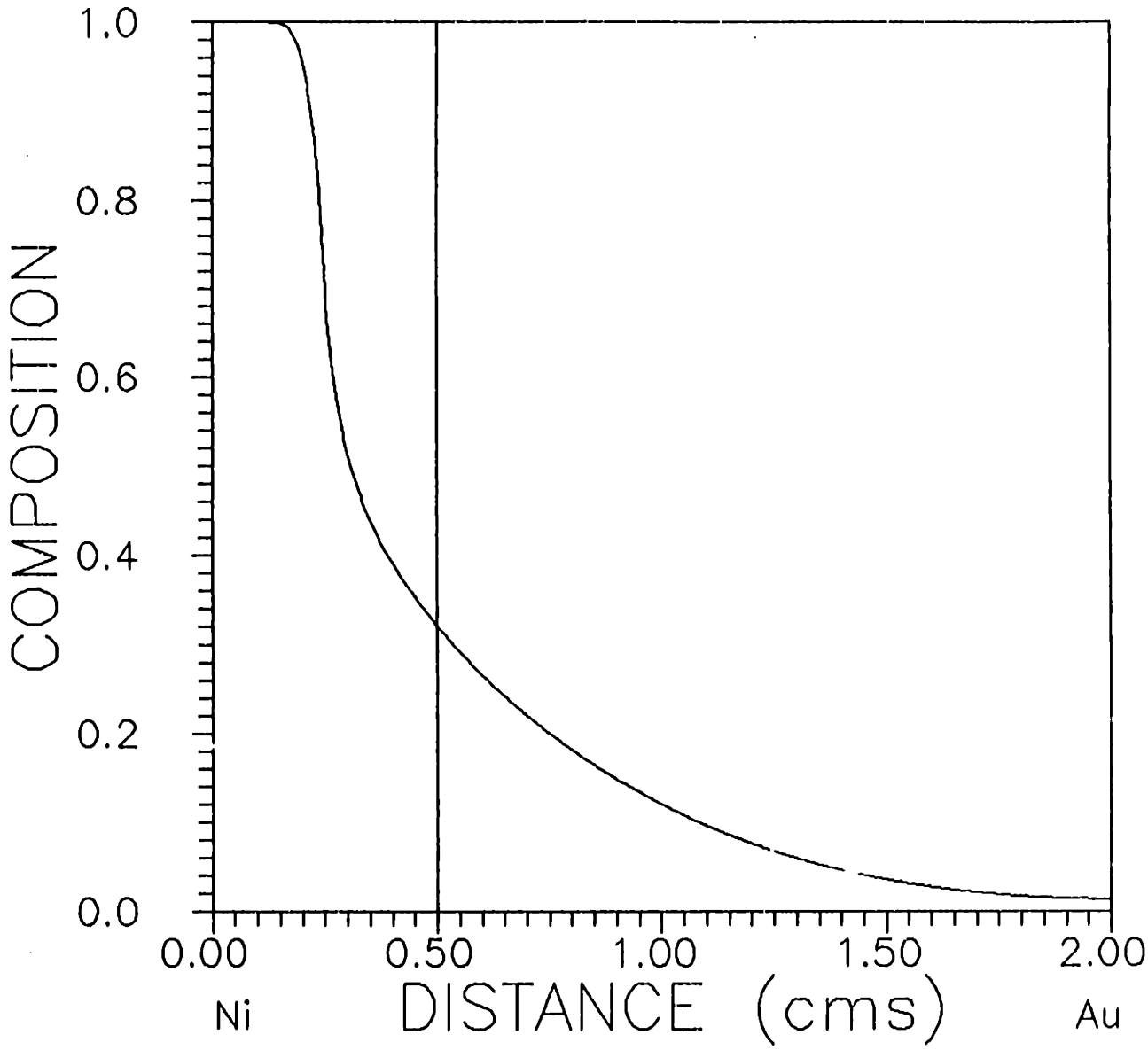

Figure 5. Computed diffusion profile for the AuNi system. The initial plane of separation corresponded to the location x=0.5 cms.

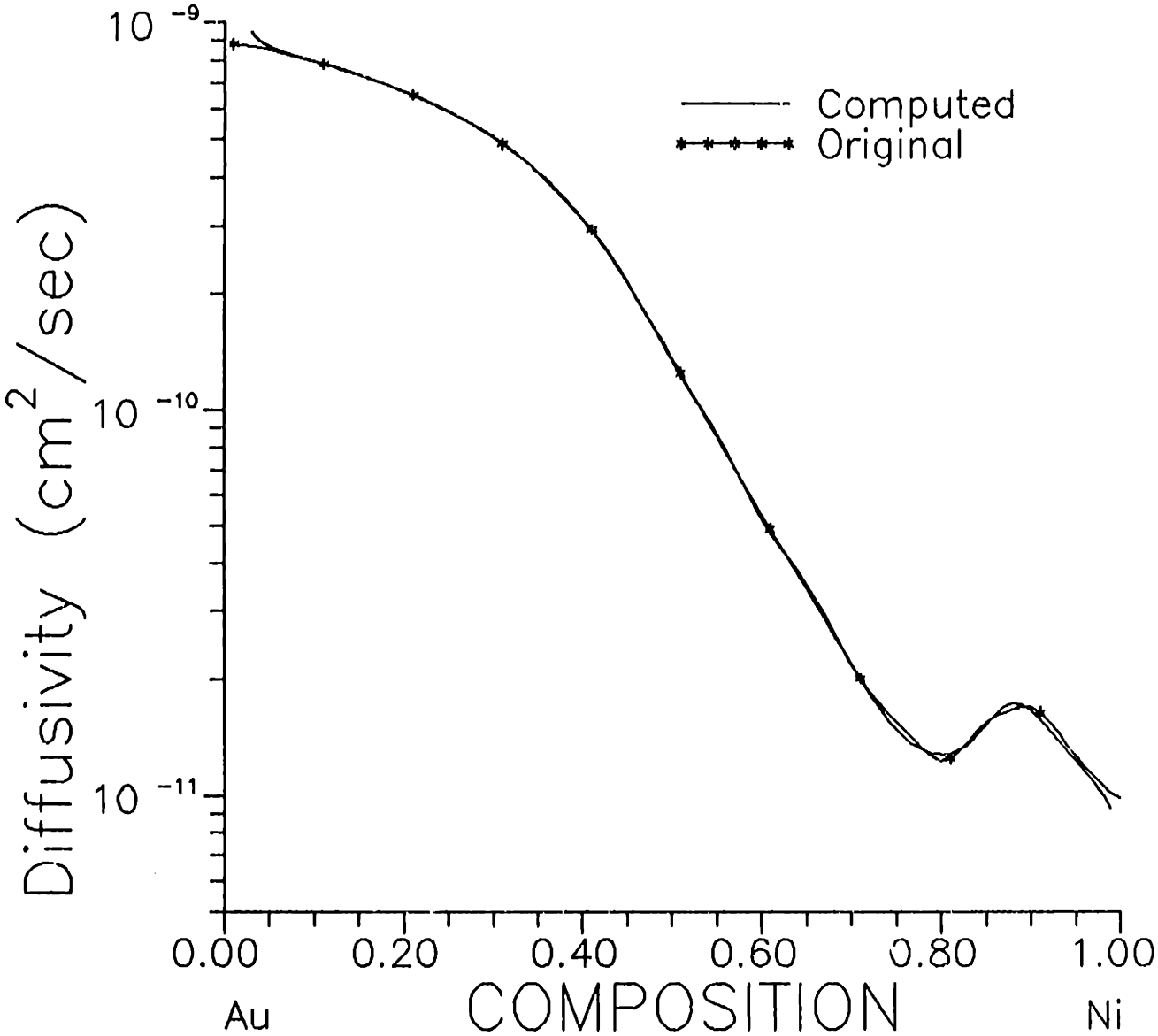

Figure 6. Interdiffusion coefficient computed by applying the modified Boltzmann Matano treatment to a noise free simulated diffusion profile. The compositional data were represented to 8 digits.

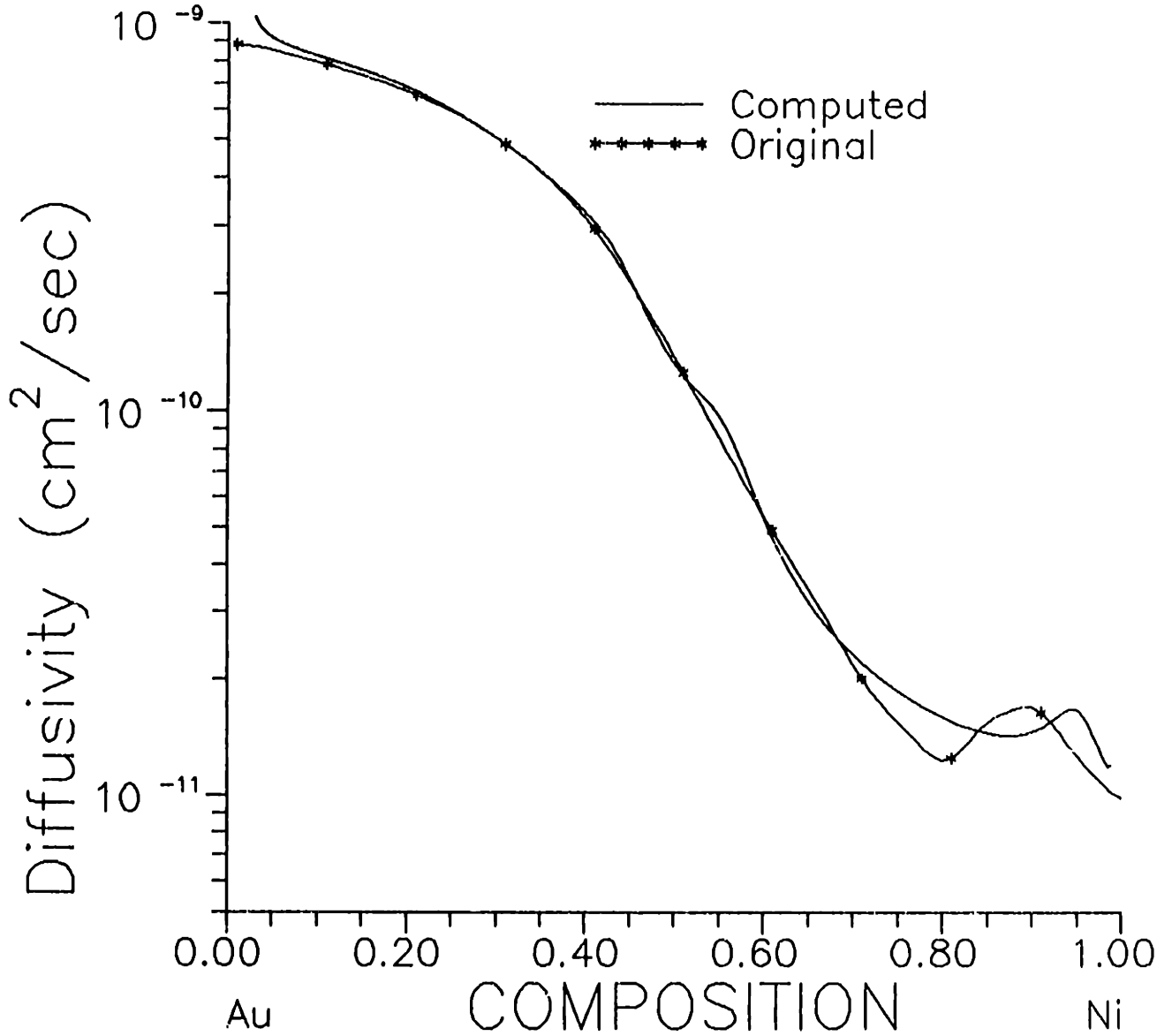

Figure 7. Diffusion coefficient computed using noisy profile data. The compositional data were rounded off to two significant digits and random noise of maximum amplitude 0.01 was superposed on the compositional data.

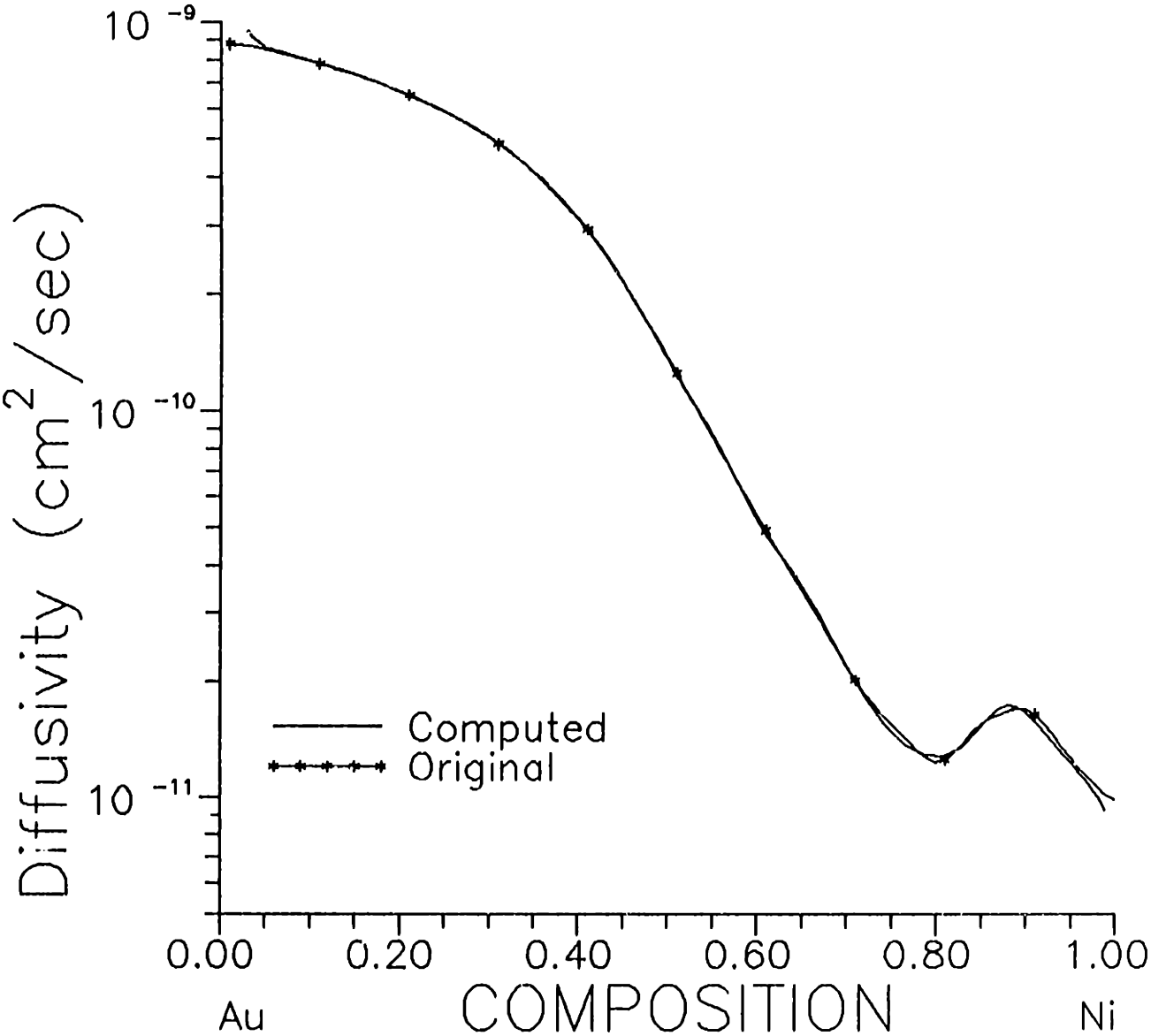

Figure 8. Diffusion coefficient computed using noisy profile data. The compositional data were rounded off to three significant digits and random noise of maximum amplitude 0.001 was superposed on the compositional data.

Conclusions

The main conclusions from this investigation may be summarized as follows:

1. *Given the interdiffusion coefficient as a function of composition ($\tilde{D}$ - c data), and one additional piece of information such as the measured activity at ONE particular composition, it is possible to compute the entire activity - composition curve for isomorphous binary metallic systems.*

2. Due to the inherent non uniqueness of the problem the proposed algorithm yields multiple solutions on an activity composition diagram. Hence one additional piece of information such as the measured activity at ONE composition or the Henry's law constant at infinite dilution is needed to pick the correct solution from the set of solutions.

3. The proposed scheme was applied to ten isomorphous binary alloy systems. For eight systems the algorithm computed solutions that were either close to the experimentally measured activities reported in the literature or followed the same general trend as that exhibited by the experimentally measured activities. For one system experimental data is not available and hence a comparison cannot be made. For another system the algorithm failed to locate a solution close to the experimentally measured activity data.

4. The algorithm can be easily extended to systems containing a miscibility gap.

5. Observation of the dynamic behavior of a diffusion profile, or examination of multiple profiles, is not helpful when seeking activity data from a diffusion couple. The requisite information is available in the equation relating the interdiffusion coefficient to the system thermodynamics and to the phenomenological coefficients.

6. Least squares spline interpolation offers a reproducible and reliable alternative to graphical evaluation of the slope of a diffusion profile. Using splines it is possible to filter out the noise in the compositional profile and accurately compute

the diffusion coefficient given compositional data containing only 3 significant digits of information and contaminated with a noise level of 0.001. Some loss of accuracy is seen in the computed interdiffusion coefficient when compositional data containing only 2 digits of information and contaminated by a noise level of 0.01 is used.

Future Efforts

There are four major areas that need further exploration.

7.1 Examination of other isomorphous binary systems

The present investigation has applied the algorithm to ten systems. There remain several additional isomorphous binary systems for which diffusivity data is available. The computations should be extended to cover these systems also. The results from the additional computations will further test the reliability of the proposed algorithm.

7.2 Alternate modelling functions for f(c) and $\phi(c)$

In this study the modelling functions $P_3Exp(P_5)$ and $P_4Exp(P_6)$ were used to represent $\phi(c)$ There is nothing sacrosanct about the particular choice of modelling functions; these were merely the first generic class of functions that appeared to meet the requirements imposed. Hence, it is very important to seek alternate modelling functions not only for $\phi(c)$but also for f(c). An alternate set of modelling functions [f(c), $\phi(c)$] may be less correlated than the present set and may also provide a better fit to the quantities being modelled.

7.3 Temperature Variation of Activity Data

For the systems investigated, diffusivity data is available at several temperatures. It is of interest to conduct the computations at different temperatures and obtain thereby the activity-composition relationships as a function of temperature.

7.4 Extension to systems containing several phases

Diffusivity data is already available in the literature for multiphase binary systems. The proposed computational scheme should be extended to cover these cases also. Paper III explored the extension of the scheme to systems exhibiting a strong positive deviation from ideality and it was shown that extending the proposed algorithm to binary systems exhibiting a miscibility gap should be fairly

straightforward. There is a need to similarly extend the treatment to systems exhibiting compound formation. Subsequently computations should be conducted on systems exhibiting compound formation and systems exhibiting a miscibility gap.

Appendices

8.1 Appendix I Computed Residuals at Minimum

This appendix will present tables that list the residual at minimum for each alloy system as a function of the bounds used in the computation. These tables are helpful in evaluating the goodness of fit to the diffusivity data.

Table I Results of least squares fitting for the CuAu system using the modelling function $P_3[Exp(P_5)]$.

Bounds	Final Activity Curve	Residual at Minima
[0.0,6.00]	Negative Deviation	0.6077×10^{-2}
[0.0,1.00]	Positive Deviation	0.4901×10^{-2}
[1.0,6.00]	Negative Deviation	0.6077×10^{-2}

Table II Results of least squares fitting for the PdCu system using the modelling function $P_3[Exp(P_5)]$.

Bounds	Final Activity Curve	Residual at Minima
[1.0,6.00]	Negative Deviation	0.4158×10^{-1}
[1.0,3.00]	Negative Deviation	0.7238×10^{-2}
[1.0,2.50]	Negative Deviation	0.1501

Table III Results of least squares fitting for the CuNi system using the modelling function $P_3[Exp(P_5)]$.

Bounds	Final Activity Curve	Residual at Minima
[0.05,1.0]	Positive Deviation	0.4015×10^{-2}
[0.20,1.0]	Positive Deviation	0.4577×10^{-2}
[0.50,1.0]	Positive Deviation	0.4593×10^{-2}
[0.60,1.0]	Positive Deviation	0.6772×10^{-2}
[0.70,1.0]	Positive Deviation	0.1055×10^{-1}
[0.80,1.0]	Positive Deviation	0.2245×10^{-1}
[0.90,1.0]	Positive Deviation	0.1948

Table IV Results of least squares fitting for the PdNi system using the modelling function $P_3[Exp(P_5)]$.

Bounds	Final Activity Curve	Residual at Minima
[0.9,2.50]	Negative Deviation	0.6244
[0.9,2.25]	Negative Deviation	1.0460
[0.9,1.50]	Negative Deviation	4.0290
[0.50,1.50]	Negative Deviation and Positive Deviation	0.9624×10^{-1}

Table V Results of least squares fitting for the PdNi system using the modelling function $P_4[Exp(P_6)]$.

Bounds	Final Activity Curve	Residual at Minima
[0.9,2.50]	Negative Deviation	0.1584×10^{-1}
[0.9,2.00]	Negative Deviation	0.1832×10^{-1}
[0.9,1.50]	Negative Deviation and Positive Deviation	0.4378×10^{-1}
[0.70,2.00]	Negative Deviation and Positive Deviation	0.1832×10^{-1}
[0.70,1.75]	Negative Deviation	0.1956×10^{-1}

Table VI Results of least squares fitting for the AgAu system using the modelling function $P_3[Exp(P_5)]$.

Bounds	Final Activity Curve	Residual at Minima
[1.0,3.00]	Negative Deviation	0.3086×10^{-2}
[1.0,2.50]	Negative Deviation	0.3086×10^{-2}
[1.0,2.25]	Negative Deviation	0.3185×10^{-2}
[1.0,2.00]	Negative Deviation	0.3580×10^{-2}
[1.0,4.00]	Negative Deviation	0.3086×10^{-2}

Table VII Results of least squares fitting for the AgAu system using the modelling function $P_4[Exp(P_6)]$.

Bounds	Final Activity Curve	Residual at Minima
[1.0,6.00]	Negative Deviation	0.3086×10^{-2}

Table VIII Results of least squares fitting for the PdFe system using the modelling function $P_4[Exp(P_6)]$.

Bounds	Final Activity Curve	Residual at Minima
[0.1,6.00]	Negative and Positive Deviation	0.8380
[0.2,6.00]	Negative Deviation	0.6974×10^{-1}

Table IX Results of least squares fitting for the CoNi system using the modelling function $P_3[Exp(P_5)]$.

Bounds	Final Activity Curve	Residual at Minima
[0.00,1.00]	Positive Deviation	0.5961 X 10-3
[0.20,1.00]	Positive Deviation	0.7657 X 10-3
[0.40,1.00]	Positive Deviation	0.6332 X 10-3
[0.60,1.00]	Positive Deviation	0.6866 X 10-3
[0.80,1.00]	Positive Deviation	Non Convergence
[0.90,1.00]	Positive Deviation	0.7753 X 10-3
[0.99,1.10]	Nearly Ideal	0.7804 X 10-3
[1.00,1.25]	Nearly Ideal	0.7844 X 10-3
[1.00,4.00]	Negative Deviation	0.6192 X 10-3
[1.00,6.00]	Negative Deviation	0.6192 X 10-3

Table I Results of least squares fitting for the NbTi system.

Bounds	Final Activity Curve	Residual at Minima
[0.05,1]	Strong Positive Deviation	0.82
[0.2,1.]	Positive Deviation	4.269
[0.4,1.]	Positive Deviation	12.8
[0.7,1.]	Positive Deviation	21.0
[0.7,6.]	Negative Deviation	5.06
[1.,8.0]	Negative Deviation	5.60
[1.,4.0]	Negative Deviation	8.47
[1.0,12]	Negative Deviation	5.365

Table X Results of least squares fitting for the NiPt system using the modelling function $P_4[Exp(P_6)]$.

Bounds	Final Activity Curve	Residual at Minima
[1.00,6.00]	Negative Deviation	0.7824×10^{-2}
[1.00,6.50]	Negative Deviation	0.8846×10^{-2}
[1.00,7.00]	Negative Deviation	0.8396×10^{-2}
[1.00,7.00]	Negative Deviation	0.7843×10^{-2}
[1.00,10.0]	Negative Deviation	0.1360×10^{-1}
[1.00,9.00]	Negative Deviation	0.1595×10^{-1}
[1.20,6.00]	Negative Deviation	0.2215×10^{-1}
[1.00,3.00]	Negative Deviation	0.9034×10^{-2}
[1.20,4.00]	Negative Deviation	0.9909×10^{-2}
[1.20,5.00]	Negative Deviation	0.9081×10^{-2}

8.2 Appendix II Interdiffusivity Data

This appendix contains interdiffusivity data for each of the ten isomorphous binary systems investigated. The diffusivity data was digitized from the book by Borovskii et. al.[1] and some of the references cited therein. The digitized data was fitted with a fourth order least squares spline. Both the digitized data and the spline fitted data are depicted graphically for comparison. The spline representation of the data is also tabulated. The tabulated data was used as input to the non linear least squares (NLLS) algorithm described in papers II and III. In addition, the appendix also contains plots of $\phi(c)$as a function of composition. These plots were generated by applying the NLLS algorithm to the tabulated diffusivity data. The $\phi(c)-c$ data was integrated to obtain the $\gamma-c$ data and the activity-composition data which were presented in papers II and III.

References

1. I. B. Borovskii, K. P. Gurov, I. D. Marchukova and Y. E. Ugaste, *Interdiffusion in Alloys*, Nauka Publishers, NTIS Document PB86-245495, (1986).

NbTi System

Table I Interdiffusion data for the NbTi system at 1000°C as a function of the mole fraction of Ti. The data was digitized from figure 6.23b in the book by Borovskii and fitted with a fourth order least squares spline. The spline representation was evaluated at 100 points to yield the data in the table.

X_{Ti}	$\tilde{D}$ cm*cm/sec	X_{Ti}	$\tilde{D}$ cm*cm/sec	X_{Ti}	$\tilde{D}$ cm*cm/sec	X_{Ti}	$\tilde{D}$ cm*cm/sec
0.01	0.1413e-13	0.26	0.5276e-13	0.51	0.2497e-11	0.76	0.8476e-10
0.02	0.1458e-13	0.27	0.5502e-13	0.52	0.2930e-11	0.77	0.9472e-10
0.03	0.1522e-13	0.28	0.6520e-13	0.53	0.3419e-11	0.78	0.1049e-09
0.04	0.1598e-13	0.29	0.6965e-13	0.54	0.3970e-11	0.79	0.1148e-09
0.05	0.1680e-13	0.30	0.7579e-13	0.55	0.4595e-11	0.80	0.1240e-09
0.06	0.1764e-13	0.31	0.8413e-13	0.56	0.5307e-11	0.81	0.1327e-09
0.07	0.1847e-13	0.32	0.9920e-13	0.57	0.6136e-11	0.82	0.1416e-09
0.08	0.1925e-13	0.33	0.1200e-12	0.58	0.7162e-11	0.83	0.1530e-09
0.09	0.1999e-13	0.34	0.1417e-12	0.59	0.8508e-11	0.84	0.1692e-09
0.10	0.2075e-13	0.35	0.1650e-12	0.60	0.1018e-10	0.85	0.1898e-09
0.11	0.2168e-13	0.36	0.1929e-12	0.61	0.1196e-10	0.86	0.2126e-09
0.12	0.2289e-13	0.37	0.2291e-12	0.62	0.1372e-10	0.87	0.2362e-09
0.13	0.2430e-13	0.38	0.2758e-12	0.63	0.1554e-10	0.88	0.2601e-09
0.14	0.2571e-13	0.39	0.3310e-12	0.64	0.1770e-10	0.89	0.2842e-09
0.15	0.2695e-13	0.40	0.3922e-12	0.65	0.2067e-10	0.90	0.3082e-09
0.16	0.2801e-13	0.41	0.4611e-12	0.66	0.2410e-10	0.91	0.3322e-09
0.17	0.2900e-13	0.42	0.5412e-12	0.67	0.2749e-10	0.92	0.3563e-09
0.18	0.3031e-13	0.43	0.6378e-12	0.68	0.3121e-10	0.93	0.3806e-09
0.19	0.3255e-13	0.44	0.7544e-12	0.69	0.3572e-10	0.94	0.4056e-09
0.20	0.3571e-13	0.45	0.8950e-12	0.70	0.4099e-10	0.95	0.4317e-09
0.21	0.3777e-13	0.46	0.1064e-11	0.71	0.4683e-10	0.96	0.4589e-09
0.22	0.3907e-13	0.47	0.1265e-11	0.72	0.5309e-10	0.97	0.4872e-09
0.23	0.4259e-13	0.48	0.1505e-11	0.73	0.5985e-10	0.98	0.5163e-09
0.24	0.4575e-13	0.49	0.1787e-11	0.74	0.6725e-10	0.99	0.5459e-09
0.25	0.4892e-13	0.50	0.2116e-11	0.75	0.7552e-10	1.00	0.5757e-09

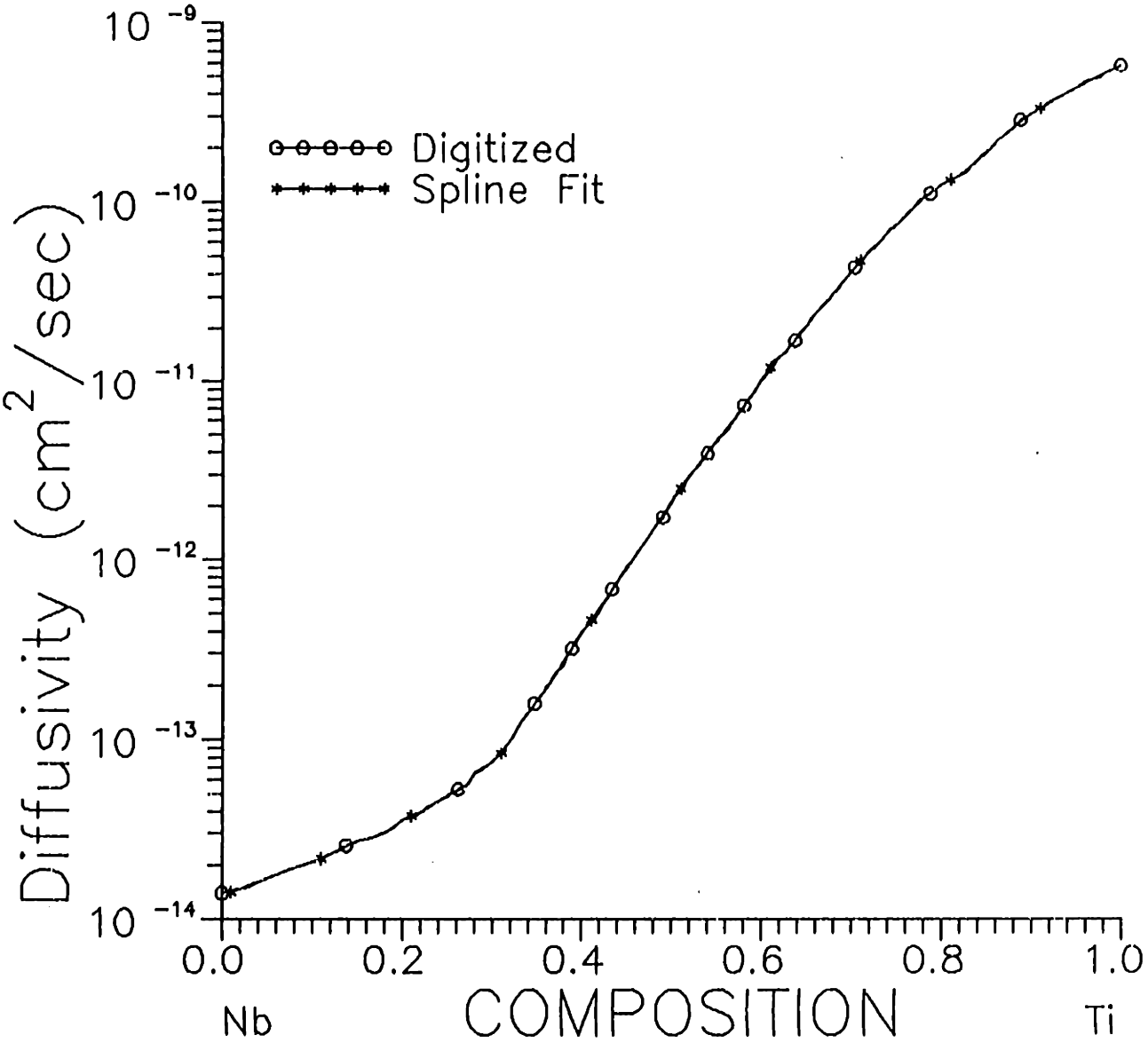

Figure 1. Raw digitized diffusivity data for the NbTi system at 1000°C. Also depicted is the spline interpolated diffusivity data after fitting the digitized data with a fourth order least squares spline. The closeness of the spline interpolated data and the digitized data is indicative of a good fit to the raw diffusivity data.

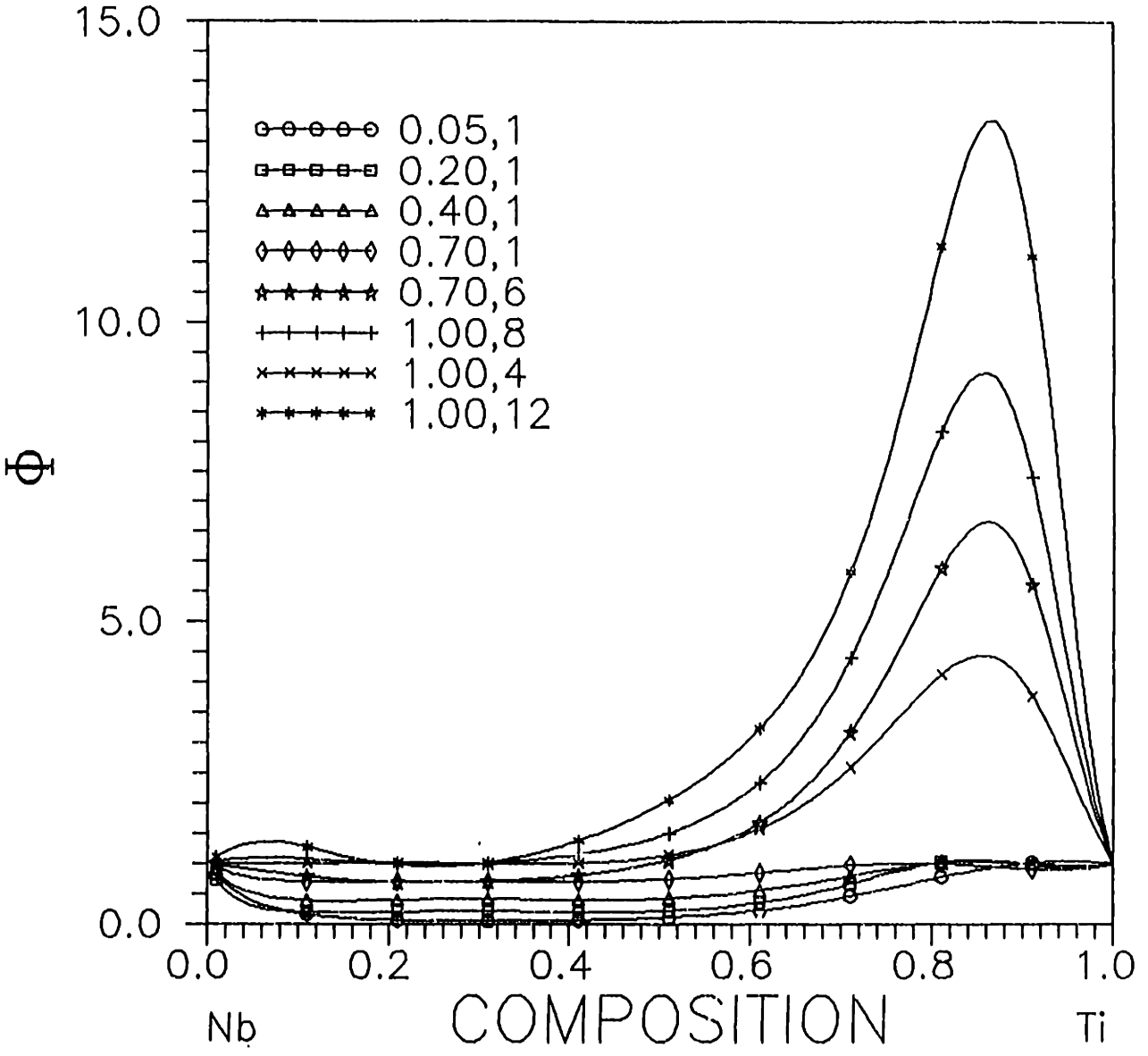

Figure 2. Computed thermodynamic term $\phi(c)$ for the NbTi system using the model function $P_4(ExpP_6)$ at 1000°C and the spline interpolated data which is tabulated in table I and graphically depicted in figure 1. Corresponding activity composition curves and the selected $\ln(\gamma)-c$ curve are presented in paper III.

NiPt System

Table II Interdiffusion data for the NiPt system at 1296°C as a function of the mole fraction of Pt. The data was digitized from figure 6.19a in the book by Borovskii and fitted with a fourth order least squares spline. The spline representation was evaluated at 100 points to yield the data in the table.

X_{Pt}	$\tilde{D}$ cm*cm/sec	X_{Pt}	$\tilde{D}$ cm*cm/sec	X_{Pt}	$\tilde{D}$ cm*cm/sec	X_{Pt}	$\tilde{D}$ cm*cm/sec
0.01	0.1886e-09	0.26	0.5194e-09	0.51	0.4555e-09	0.76	0.2593e-09
0.02	0.2056e-09	0.27	0.5253e-09	0.52	0.4471e-09	0.77	0.2513e-09
0.03	0.2229e-09	0.28	0.5306e-09	0.53	0.4387e-09	0.78	0.2432e-09
0.04	0.2404e-09	0.29	0.5352e-09	0.54	0.4304e-09	0.79	0.2349e-09
0.05	0.2579e-09	0.30	0.5393e-09	0.55	0.4220e-09	0.80	0.2265e-09
0.06	0.2754e-09	0.31	0.5426e-09	0.56	0.4137e-09	0.81	0.2181e-09
0.07	0.2927e-09	0.32	0.5451e-09	0.57	0.4055e-09	0.82	0.2095e-09
0.08	0.3098e-09	0.33	0.5469e-09	0.58	0.3973e-09	0.83	0.2009e-09
0.09	0.3264e-09	0.34	0.5477e-09	0.59	0.3892e-09	0.84	0.1924e-09
0.10	0.3427e-09	0.35	0.5477e-09	0.60	0.3812e-09	0.85	0.1838e-09
0.11	0.3584e-09	0.36	0.5468e-09	0.61	0.3732e-09	0.86	0.1754e-09
0.12	0.3735e-09	0.37	0.5449e-09	0.62	0.3654e-09	0.87	0.1671e-09
0.13	0.3881e-09	0.38	0.5420e-09	0.63	0.3576e-09	0.88	0.1588e-09
0.14	0.4019e-09	0.39	0.5383e-09	0.64	0.3499e-09	0.89	0.1505e-09
0.15	0.4151e-09	0.40	0.5339e-09	0.65	0.3424e-09	0.90	0.1421e-09
0.16	0.4276e-09	0.41	0.5287e-09	0.66	0.3349e-09	0.91	0.1335e-09
0.17	0.4395e-09	0.42	0.5230e-09	0.67	0.3275e-09	0.92	0.1248e-09
0.18	0.4507e-09	0.43	0.5167e-09	0.68	0.3201e-09	0.93	0.1162e-09
0.19	0.4614e-09	0.44	0.5100e-09	0.69	0.3127e-09	0.94	0.1080e-09
0.20	0.4715e-09	0.45	0.5029e-09	0.70	0.3053e-09	0.95	0.9927e-10
0.21	0.4810e-09	0.46	0.4955e-09	0.71	0.2979e-09	0.96	0.8946e-10
0.22	0.4899e-09	0.47	0.4878e-09	0.72	0.2903e-09	0.97	0.8102e-10
0.23	0.4982e-09	0.48	0.4800e-09	0.73	0.2827e-09	0.98	0.7578e-10
0.24	0.5059e-09	0.49	0.4719e-09	0.74	0.2750e-09	0.99	0.7234e-10
0.25	0.5130e-09	0.50	0.4637e-09	0.75	0.2672e-09	1.00	0.7000e-10

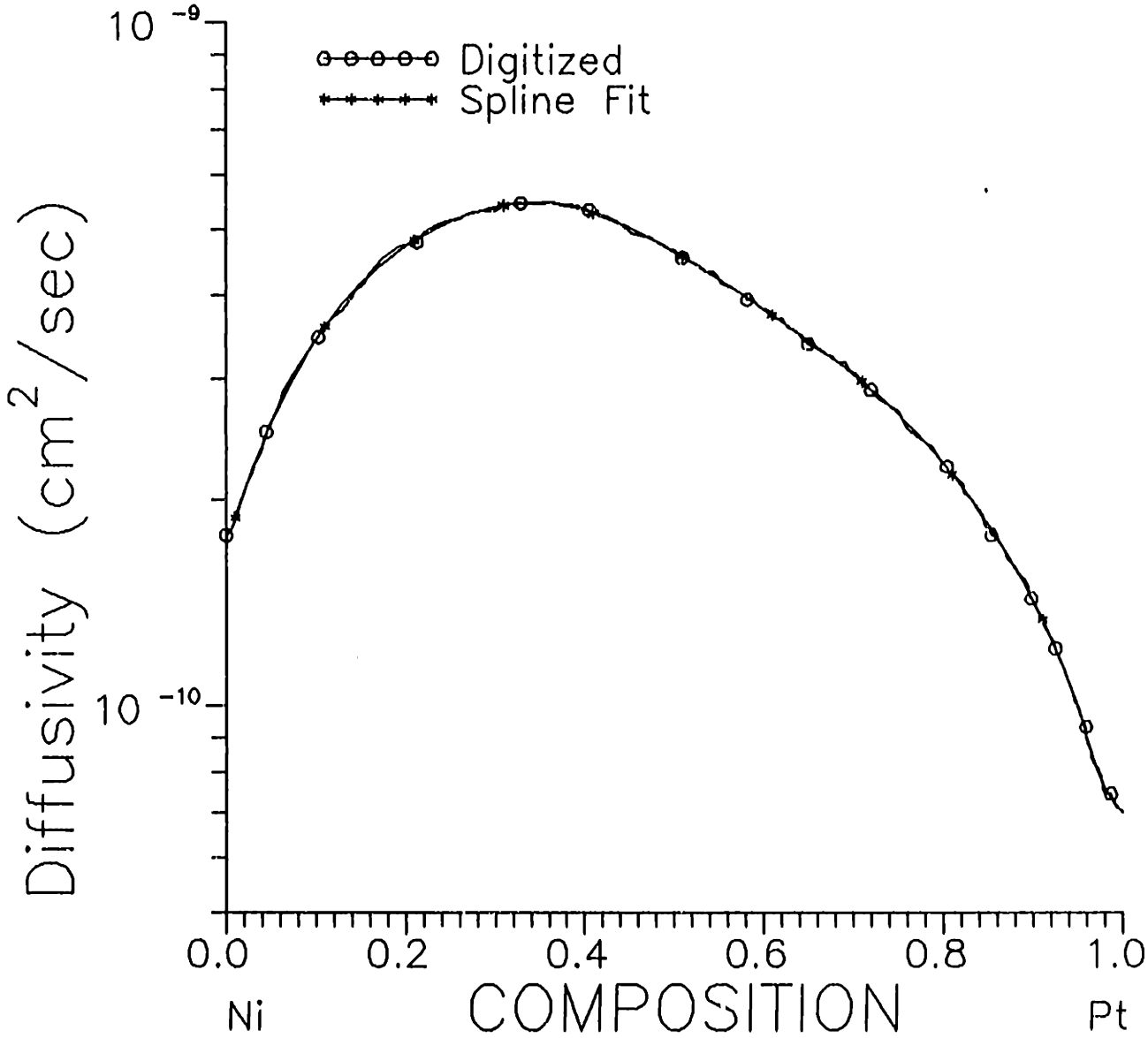

Figure 3. Raw digitized diffusivity data for the NiPt system at 1296°C. Also depicted is the spline interpolated diffusivity data after fitting the digitized data with a fourth order least squares spline. The closeness of the spline interpolated data and the digitized data is indicative of a good fit to the raw diffusivity data.

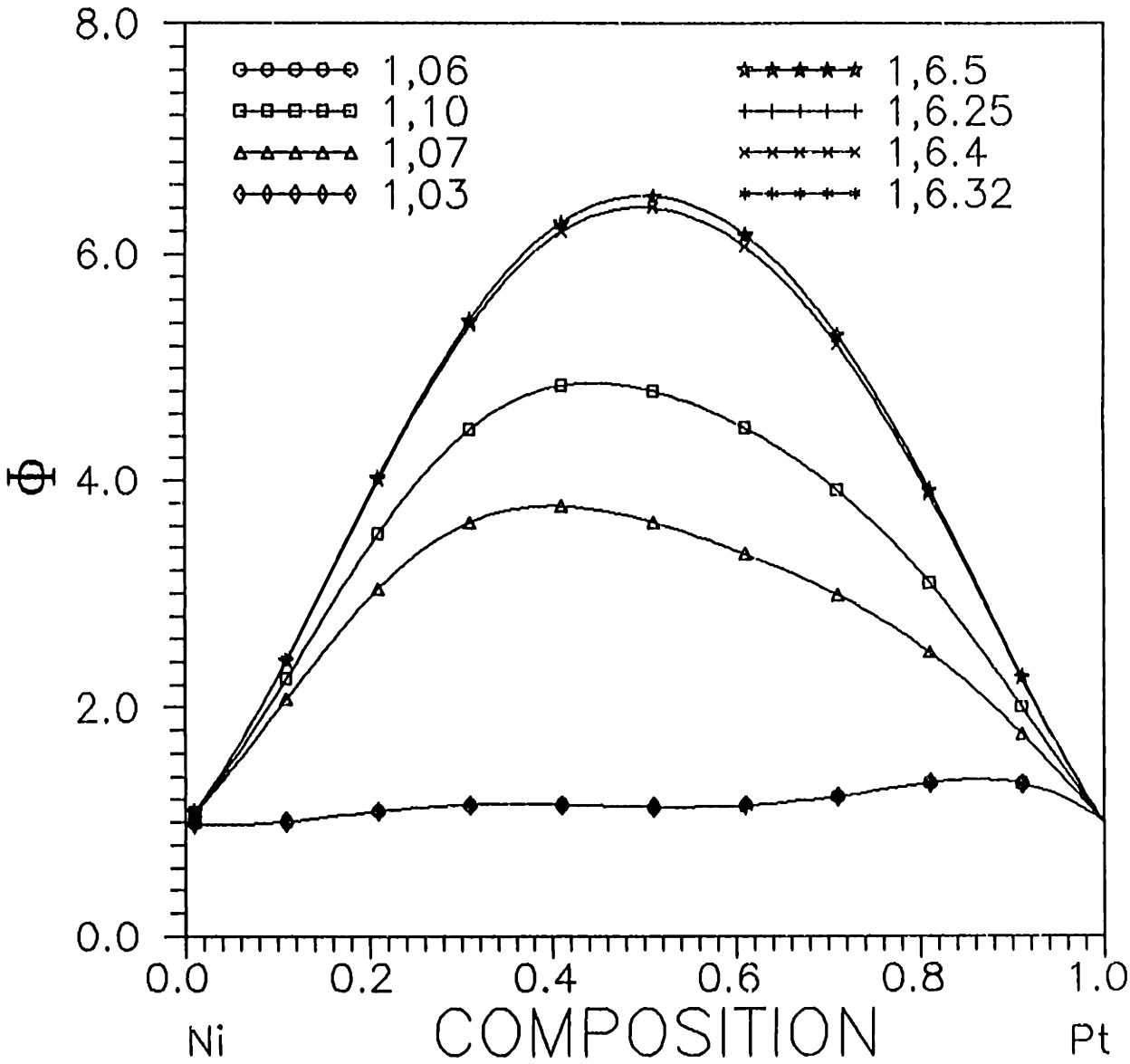

Figure 4. Computed thermodynamic term $\phi(c)$ for the NiPt system using the model function $P_3(ExpP_5)$ at 1296°C and the spline interpolated data which is tabulated in table II and graphically depicted in figure 3. Corresponding activity composition curves and the selected $\ln(\gamma) - c$ curve are presented in paper III.

Table III Diffusivity for the AuNi system at 900°C as a function of the mole fraction of Ni. The data was digitized from figure 6.6b in the book by Borovskii and fitted with a fourth order least squares spline. The spline representation was evaluated at 100 points to yield the data in the table.

X_{Ni}	D cm*cm/sec	X_{Ni}	D cm*cm/sec	X_{Ni}	D cm*cm/sec	X_{Ni}	D cm*cm/sec
0.01	0.8808e-09	0.26	0.5735e-09	0.51	0.1251e-09	0.76	0.1469e-10
0.02	0.8783e-09	0.27	0.5567e-09	0.52	0.1138e-09	0.77	0.1392e-10
0.03	0.8719e-09	0.28	0.5396e-09	0.53	0.1035e-09	0.78	0.1318e-10
0.04	0.8629e-09	0.29	0.5221e-09	0.54	0.9419e-10	0.79	0.1259e-10
0.05	0.8522e-09	0.30	0.5043e-09	0.55	0.8568e-10	0.80	0.1234e-10
0.06	0.8410e-09	0.31	0.4863e-09	0.56	0.7797e-10	0.81	0.1250e-10
0.07	0.8294e-09	0.32	0.4680e-09	0.57	0.7099e-10	0.82	0.1307e-10
0.08	0.8177e-09	0.33	0.4495e-09	0.58	0.6468e-10	0.83	0.1388e-10
0.09	0.8058e-09	0.34	0.4309e-09	0.59	0.5897e-10	0.84	0.1471e-10
0.10	0.7938e-09	0.35	0.4121e-09	0.60	0.5382e-10	0.85	0.1545e-10
0.11	0.7817e-09	0.36	0.3930e-09	0.61	0.4917e-10	0.86	0.1601e-10
0.12	0.7695e-09	0.37	0.3735e-09	0.62	0.4497e-10	0.87	0.1643e-10
0.13	0.7573e-09	0.38	0.3538e-09	0.63	0.4117e-10	0.88	0.1679e-10
0.14	0.7449e-09	0.39	0.3337e-09	0.64	0.3769e-10	0.89	0.1701e-10
0.15	0.7324e-09	0.40	0.3133e-09	0.65	0.3448e-10	0.90	0.1692e-10
0.16	0.7196e-09	0.41	0.2928e-09	0.66	0.3151e-10	0.91	0.1643e-10
0.17	0.7066e-09	0.42	0.2724e-09	0.67	0.2876e-10	0.92	0.1562e-10
0.18	0.6933e-09	0.43	0.2524e-09	0.68	0.2624e-10	0.93	0.1462e-10
0.19	0.6797e-09	0.44	0.2331e-09	0.69	0.2395e-10	0.94	0.1359e-10
0.20	0.6657e-09	0.45	0.2146e-09	0.70	0.2191e-10	0.95	0.1268e-10
0.21	0.6513e-09	0.46	0.1970e-09	0.71	0.2013e-10	0.96	0.1192e-10
0.22	0.6366e-09	0.47	0.1805e-09	0.72	0.1863e-10	0.97	0.1128e-10
0.23	0.6214e-09	0.48	0.1650e-09	0.73	0.1742e-10	0.98	0.1070e-10
0.24	0.6058e-09	0.49	0.1506e-09	0.74	0.1640e-10	0.99	0.1014e-10
0.25	0.5899e-09	0.50	0.1373e-09	0.75	0.1551e-10	1.00	0.9932e-11

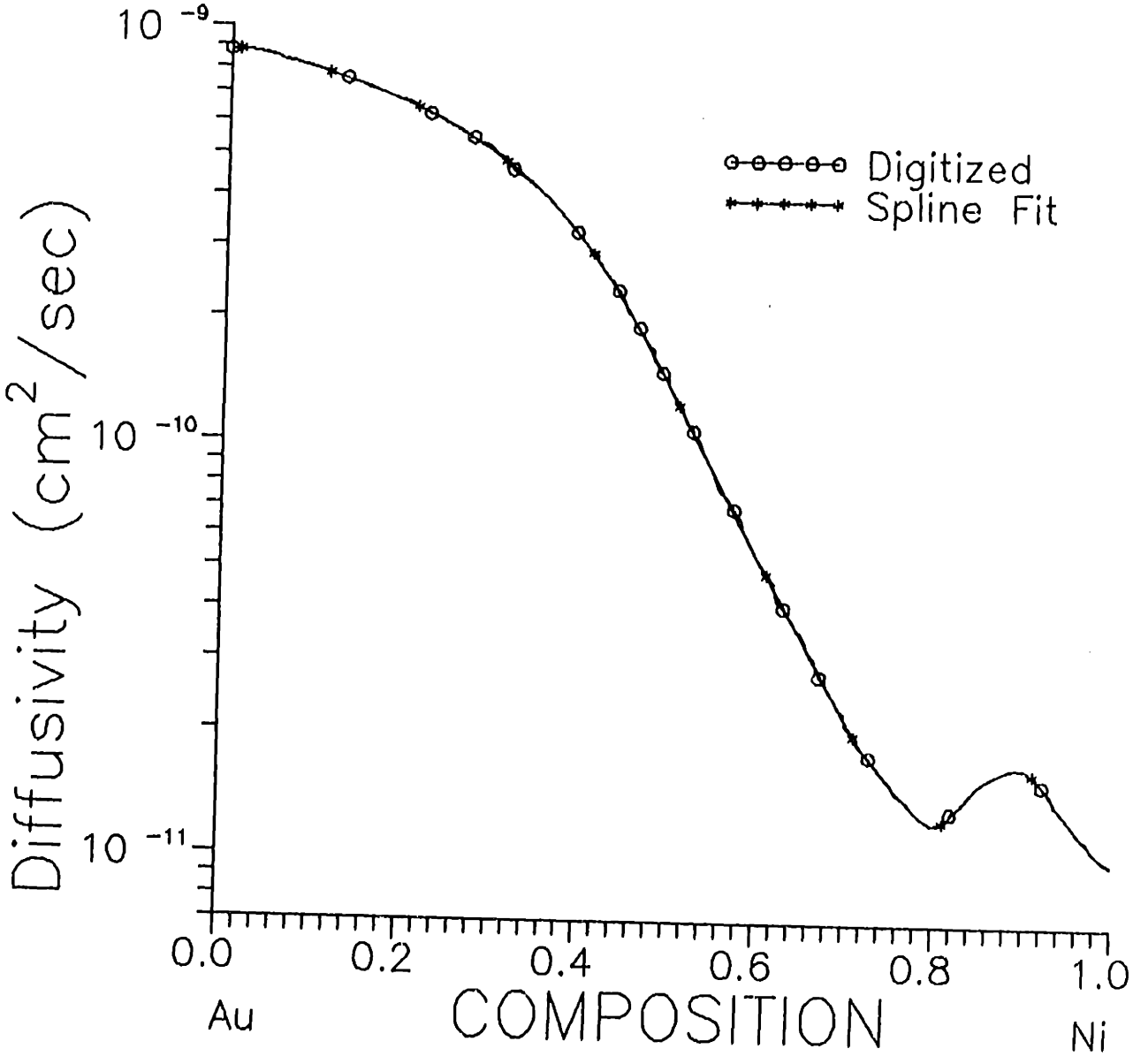

Figure 5. Raw digitized diffusivity data for the AuNi system at 900°C. Also depicted is the spline interpolated diffusivity data after fitting the digitized data with a fourth order least squares spline. The closeness of the spline interpolated data and the digitized data is indicative of a good fit to the raw diffusivity data.

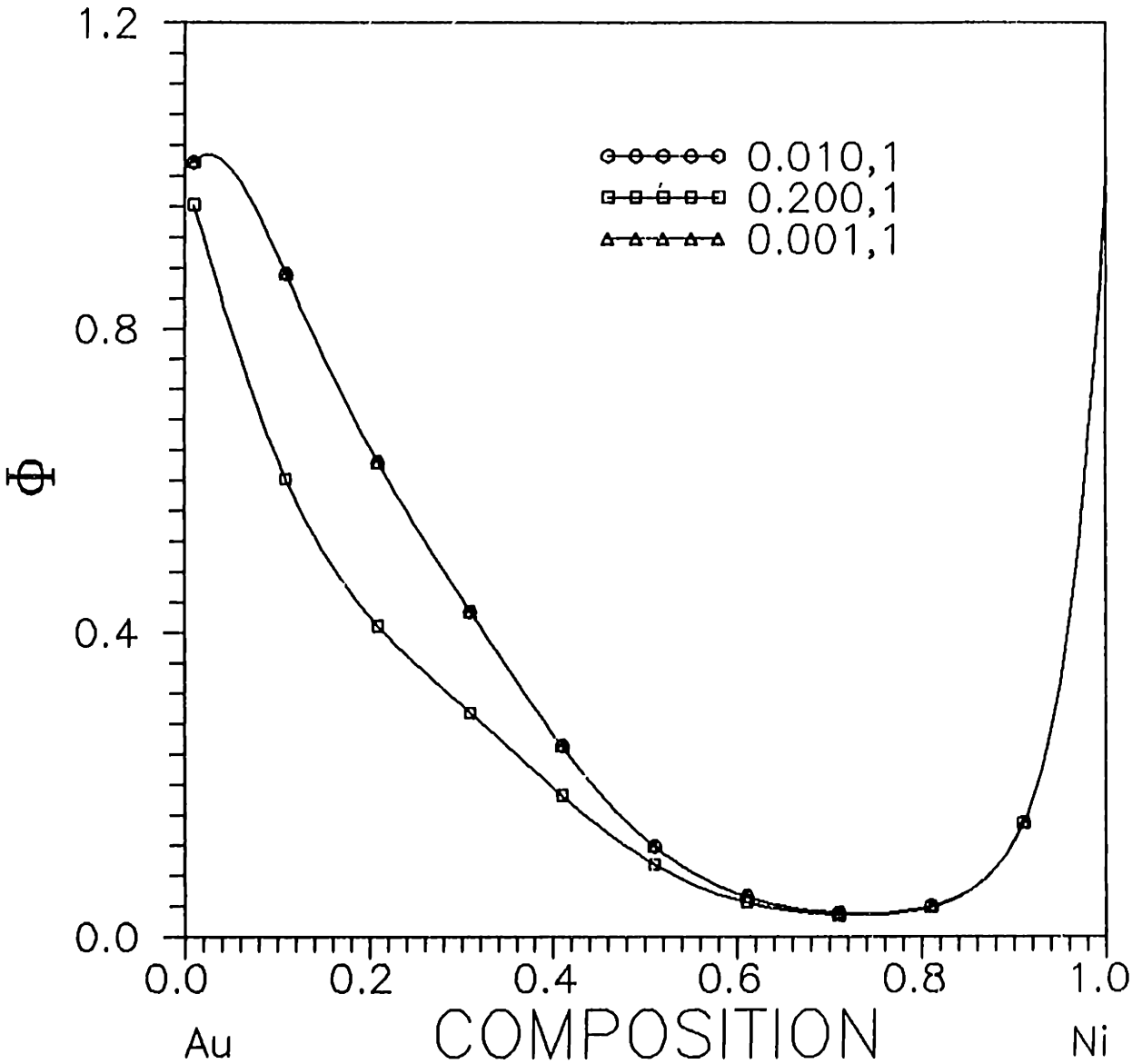

Figure 6. Computed thermodynamic term $\phi(c)$ for the AuNi system using the model function $P_4(ExpP_6)$ at 900°C and the spline interpolated data which is tabulated in table III and graphically depicted in figure 5. Corresponding activity composition curves and the selected $\ln(\gamma) - c$ curve are presented in paper III.

Table IV Diffusivity for the PdFe system at 1050°C as a function of the mole fraction of Fe. The data was digitized from figure 6.18a in the book by Borovskii and fitted with a fourth order least squares spline. The spline representation was evaluated at 100 points to yield the data in the table.

X_{Fe}	$\tilde{D}$ cm*cm/sec	X_{Fe}	$\tilde{D}$ cm*cm/sec	X_{Fe}	$\tilde{D}$ cm*cm/sec	X_{Fe}	$\tilde{D}$ cm*cm/sec
0.01	0.1780e-10	0.26	0.1269e-09	0.51	0.8184e-10	0.76	0.8248e-11
0.02	0.1959e-10	0.27	0.1301e-09	0.52	0.7704e-10	0.77	0.7156e-11
0.03	0.2162e-10	0.28	0.1329e-09	0.53	0.7198e-10	0.78	0.6886e-11
0.04	0.2390e-10	0.29	0.1352e-09	0.54	0.6663e-10	0.79	0.7012e-11
0.05	0.2647e-10	0.30	0.1371e-09	0.55	0.6106e-10	0.80	0.7283e-11
0.06	0.2935e-10	0.31	0.1386e-09	0.56	0.5570e-10	0.81	0.7612e-11
0.07	0.3256e-10	0.32	0.1396e-09	0.57	0.5093e-10	0.82	0.8059e-11
0.08	0.3612e-10	0.33	0.1401e-09	0.58	0.4698e-10	0.83	0.8696e-11
0.09	0.4006e-10	0.34	0.1402e-09	0.59	0.4374e-10	0.84	0.9495e-11
0.10	0.4438e-10	0.35	0.1398e-09	0.60	0.4092e-10	0.85	0.1039e-10
0.11	0.4908e-10	0.36	0.1388e-09	0.61	0.3832e-10	0.86	0.1131e-10
0.12	0.5414e-10	0.37	0.1373e-09	0.62	0.3578e-10	0.87	0.1226e-10
0.13	0.5952e-10	0.38	0.1352e-09	0.63	0.3321e-10	0.88	0.1331e-10
0.14	0.6516e-10	0.39	0.1325e-09	0.64	0.3053e-10	0.89	0.1452e-10
0.15	0.7098e-10	0.40	0.1293e-09	0.65	0.2778e-10	0.90	0.1594e-10
0.16	0.7688e-10	0.41	0.1257e-09	0.66	0.2504e-10	0.91	0.1757e-10
0.17	0.8277e-10	0.42	0.1217e-09	0.67	0.2252e-10	0.92	0.1936e-10
0.18	0.8858e-10	0.43	0.1175e-09	0.68	0.2050e-10	0.93	0.2126e-10
0.19	0.9427e-10	0.44	0.1132e-09	0.69	0.1876e-10	0.94	0.2325e-10
0.20	0.9979e-10	0.45	0.1088e-09	0.70	0.1679e-10	0.95	0.2533e-10
0.21	0.1051e-09	0.46	0.1044e-09	0.71	0.1570e-10	0.96	0.2750e-10
0.22	0.1101e-09	0.47	0.9996e-10	0.72	0.1269e-10	0.97	0.2975e-10
0.23	0.1148e-09	0.48	0.9550e-10	0.73	0.1165e-10	0.98	0.3207e-10
0.24	0.1192e-09	0.49	0.9100e-10	0.74	0.1022e-10	0.99	0.3441e-10
0.25	0.1233e-09	0.50	0.8646e-10	0.75	0.9045e-11	1.00	0.3670e-10

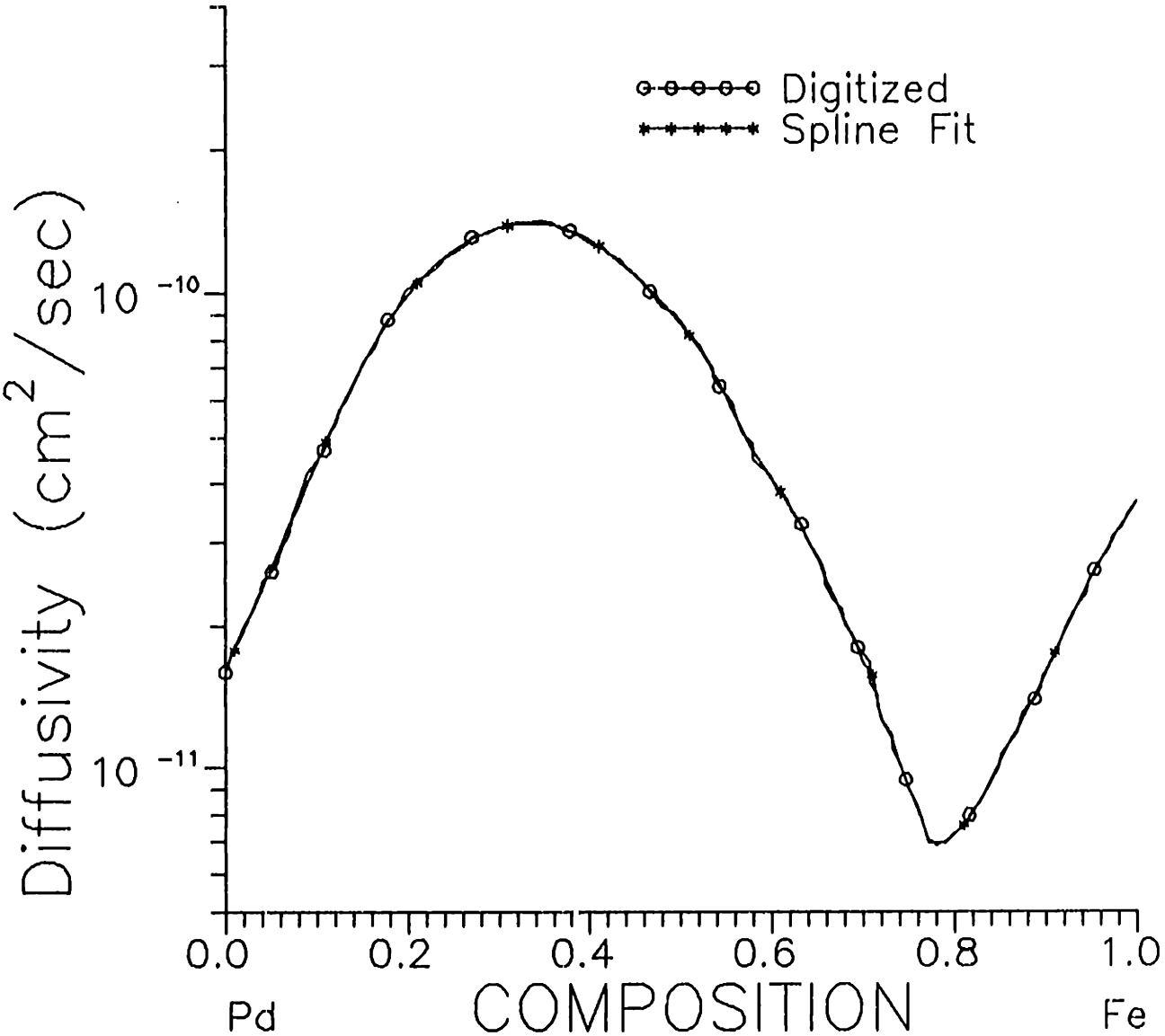

Figure 7. Raw digitized diffusivity data for the PdFe system at 1050°C. Also depicted is the spline interpolated diffusivity data after fitting the digitized data with a fourth order least squares spline. The closeness of the spline interpolated data and the digitized data is indicative of a good fit to the raw diffusivity data.

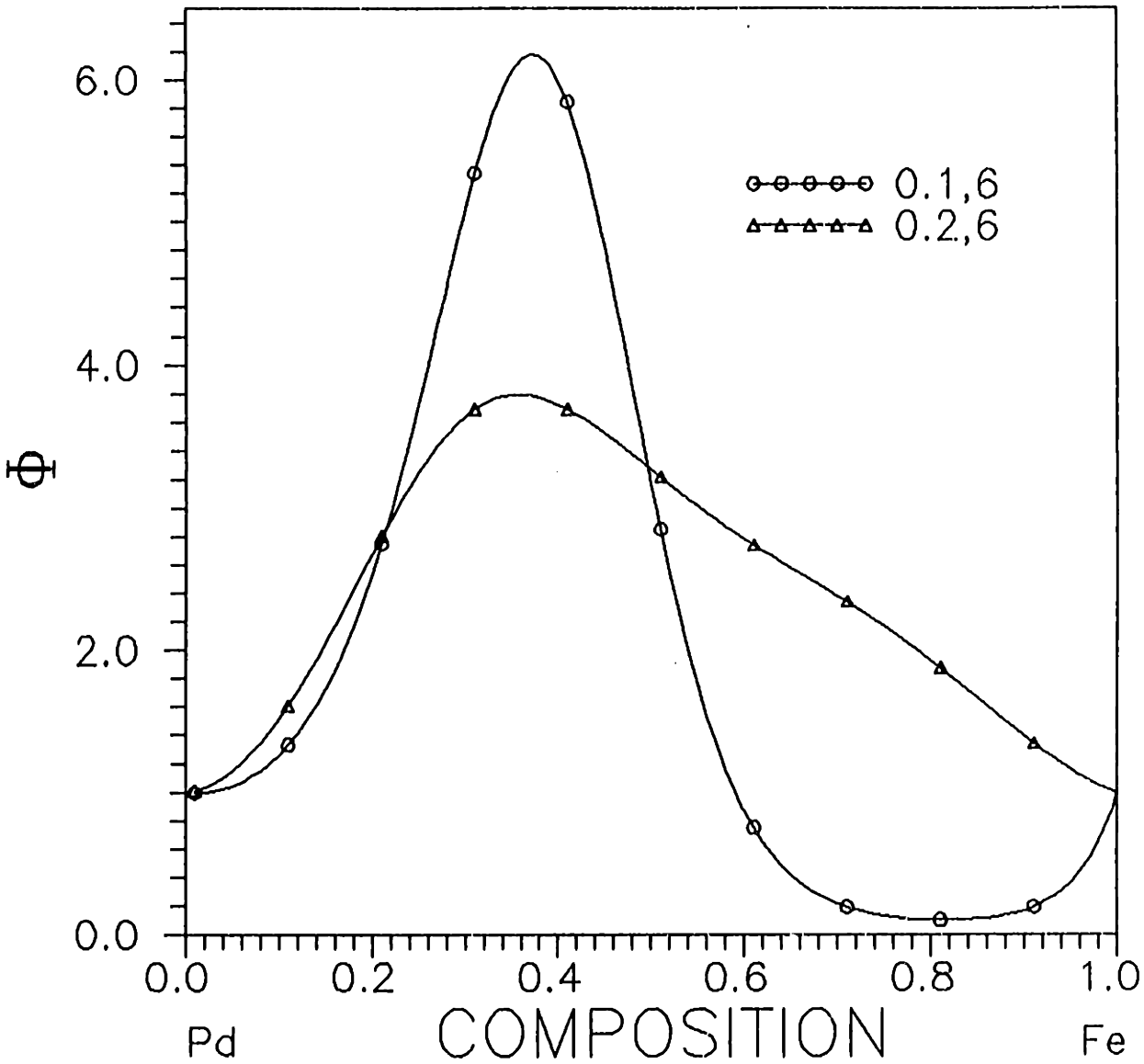

Figure 8. Computed thermodynamic term $\phi(c)$ for the PdFe system using the model function $P_4(ExpP_6)$ at 1050°C and the spline interpolated data which is tabulated in table IV and graphically depicted in figure 7. Corresponding activity composition curves and the selected $\ln(\gamma) - c$ curve are presented in paper III.

Table V Diffusivity for the AgAu system at 900°C as a function of the mole fraction of Au. The data was digitized from the figure 6.9a in the book Borovskii and fitted with a fourth order least squares spline. The spline representation was evaluated at 100 points to yield the data in the table.

X_{Au}	D cm*cm/sec	X_{Au}	D cm*cm/sec	X_{Au}	D cm*cm/sec	X_{Au}	D cm*cm/sec
0.01	0.1341e-09	0.26	0.1467e-09	0.51	0.1813e-09	0.76	0.3073e-09
0.02	0.1351e-09	0.27	0.1469e-09	0.52	0.1840e-09	0.77	0.3128e-09
0.03	0.1364e-09	0.28	0.1471e-09	0.53	0.1868e-09	0.78	0.3181e-09
0.04	0.1378e-09	0.29	0.1473e-09	0.54	0.1898e-09	0.79	0.3229e-09
0.05	0.1393e-09	0.30	0.1475e-09	0.55	0.1929e-09	0.80	0.3273e-09
0.06	0.1407e-09	0.31	0.1477e-09	0.56	0.1963e-09	0.81	0.3312e-09
0.07	0.1421e-09	0.32	0.1480e-09	0.57	0.1999e-09	0.82	0.3345e-09
0.08	0.1433e-09	0.33	0.1485e-09	0.58	0.2037e-09	0.83	0.3374e-09
0.09	0.1444e-09	0.34	0.1490e-09	0.59	0.2077e-09	0.84	0.3398e-09
0.10	0.1452e-09	0.35	0.1498e-09	0.60	0.2121e-09	0.85	0.3418e-09
0.11	0.1457e-09	0.36	0.1507e-09	0.61	0.2168e-09	0.86	0.3434e-09
0.12	0.1460e-09	0.37	0.1518e-09	0.62	0.2218e-09	0.87	0.3447e-09
0.13	0.1461e-09	0.38	0.1530e-09	0.63	0.2270e-09	0.88	0.3456e-09
0.14	0.1462e-09	0.39	0.1545e-09	0.64	0.2325e-09	0.89	0.3461e-09
0.15	0.1461e-09	0.40	0.1562e-09	0.65	0.2382e-09	0.90	0.3463e-09
0.16	0.1460e-09	0.41	0.1581e-09	0.66	0.2442e-09	0.91	0.3461e-09
0.17	0.1460e-09	0.42	0.1601e-09	0.67	0.2503e-09	0.92	0.3453e-09
0.18	0.1459e-09	0.43	0.1623e-09	0.68	0.2566e-09	0.93	0.3435e-09
0.19	0.1459e-09	0.44	0.1645e-09	0.69	0.2630e-09	0.94	0.3405e-09
0.20	0.1459e-09	0.45	0.1668e-09	0.70	0.2696e-09	0.95	0.3351e-09
0.21	0.1460e-09	0.46	0.1691e-09	0.71	0.2761e-09	0.96	0.3267e-09
0.22	0.1461e-09	0.47	0.1714e-09	0.72	0.2826e-09	0.97	0.3184e-09
0.23	0.1462e-09	0.48	0.1738e-09	0.73	0.2891e-09	0.98	0.3124e-09
0.24	0.1463e-09	0.49	0.1762e-09	0.74	0.2954e-09	0.99	0.3068e-09
0.25	0.1465e-09	0.50	0.1787e-09	0.75	0.3015e-09	1.00	0.3027e-09

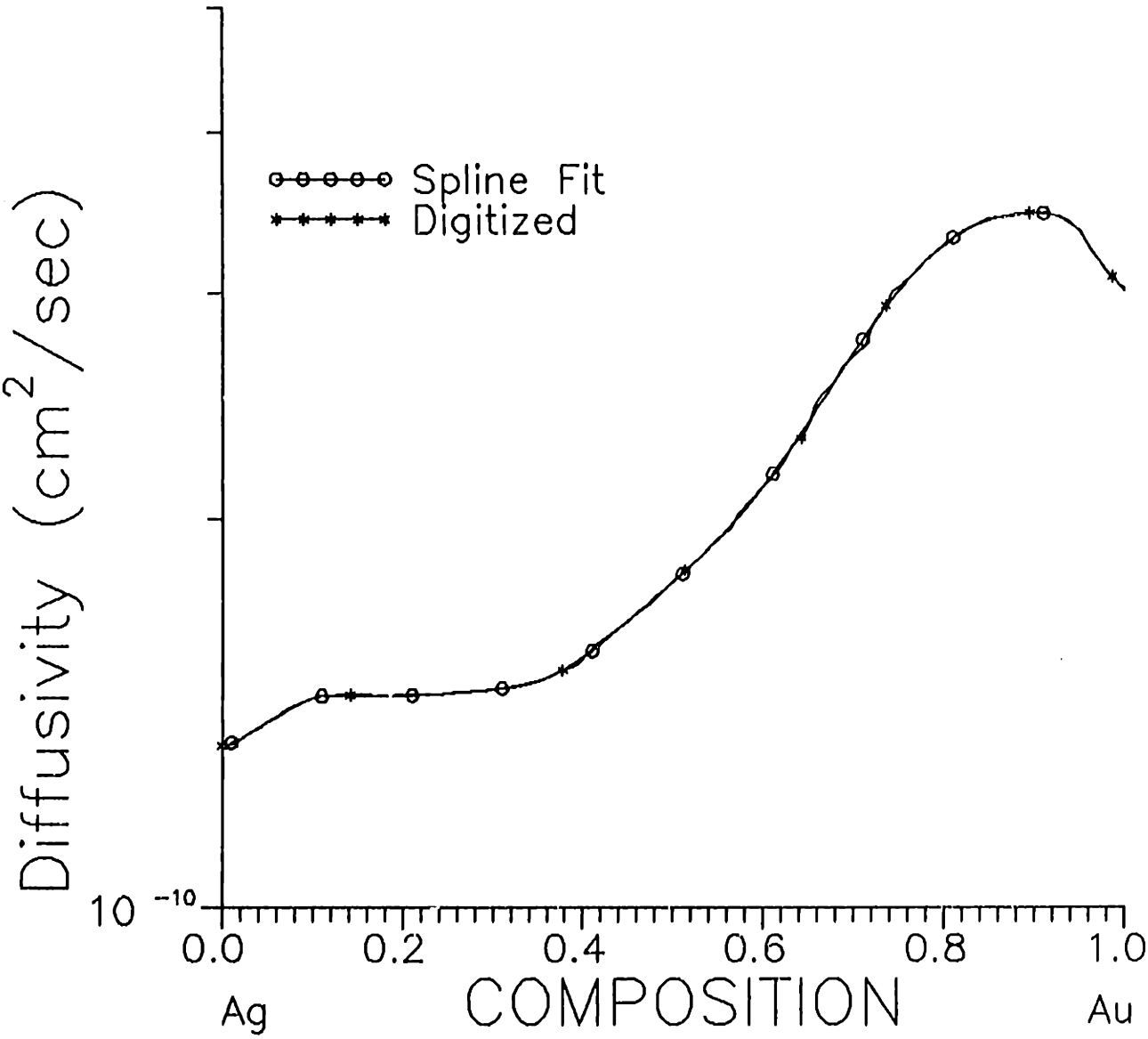

Figure 9. Raw digitized diffusivity data for the AgAu system at 900°C. Also depicted is the spline interpolated diffusivity data after fitting the digitized data with a fourth order least squares spline. The closeness of the spline interpolated data and the digitized data is indicative of a good fit to the raw diffusivity data.

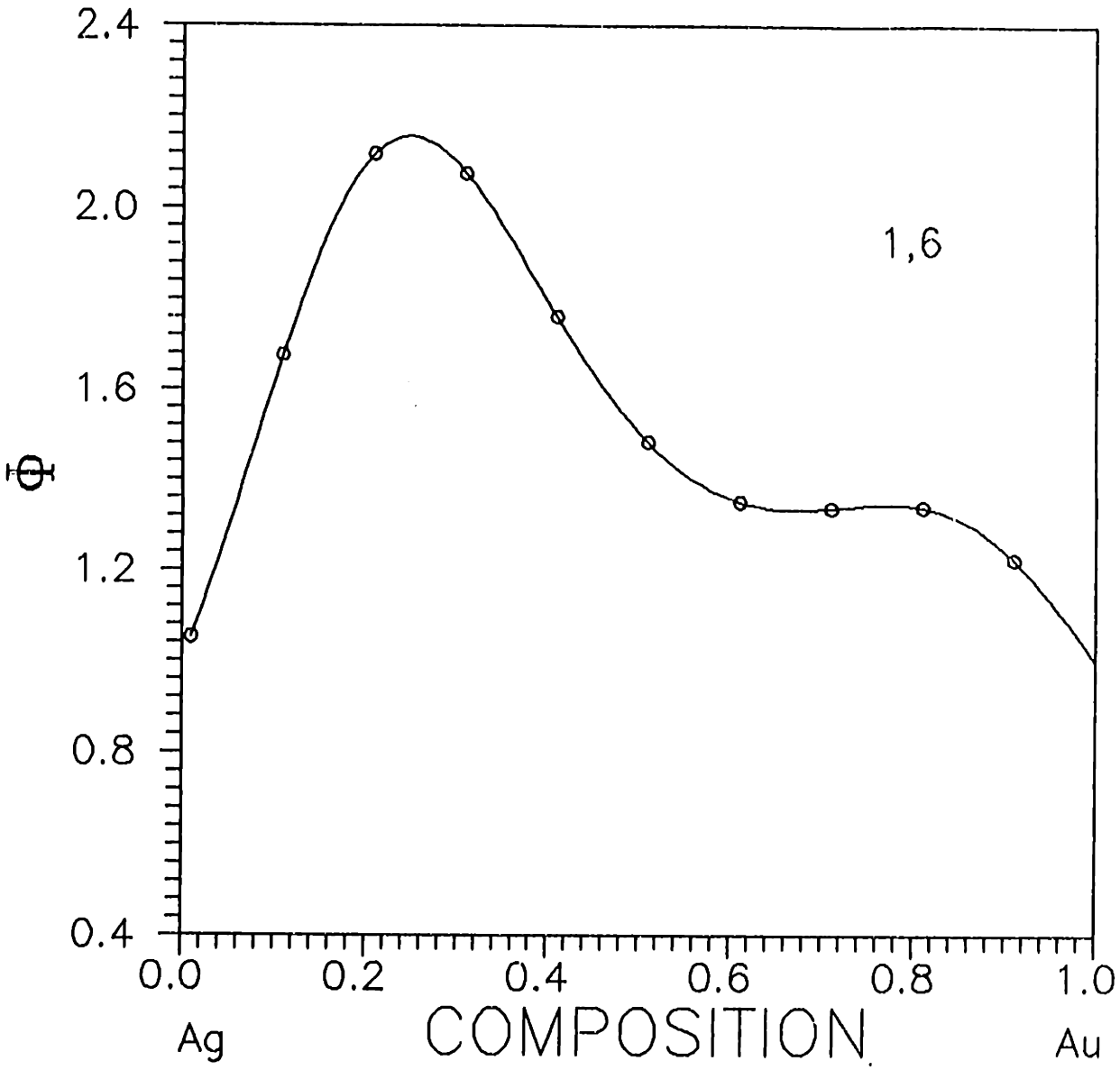

Figure 10. Computed thermodynamic term $\phi(c)$ for the AgAu system using the model function $P_4(ExpP_6)$ at 900°C and the spline interpolated data which is tabulated in table V and graphically depicted in figure 9. Corresponding activity composition curves and the selected $\ln(\gamma)-c$ curve are presented in paper III.

Table VI Diffusivity for the PdNi system at 1045°C as a function of the mole fraction of Ni. The data was digitized from figure 6.16b in the book by Borovskii and fitted with a fourth order least squares spline. The spline representation was evaluated at 100 points to yield the data in the table.

X_{Ni}	$\tilde{D}$ cm*cm/sec	X_{Ni}	$\tilde{D}$ cm*cm/sec	X_{Ni}	$\tilde{D}$ cm*cm/sec	X_{Ni}	$\tilde{D}$ cm*cm/sec
0.01	0.1623e-10	0.26	0.6373e-10	0.51	0.1851e-09	0.76	0.6912e-10
0.02	0.1675e-10	0.27	0.6743e-10	0.52	0.1861e-09	0.77	0.6474e-10
0.03	0.1782e-10	0.28	0.7137e-10	0.53	0.1870e-09	0.78	0.6061e-10
0.04	0.1919e-10	0.29	0.7554e-10	0.54	0.1877e-09	0.79	0.5672e-10
0.05	0.2043e-10	0.30	0.7992e-10	0.55	0.1881e-09	0.80	0.5305e-10
0.06	0.2154e-10	0.31	0.8449e-10	0.56	0.1878e-09	0.81	0.4961e-10
0.07	0.2259e-10	0.32	0.8923e-10	0.57	0.1864e-09	0.82	0.4638e-10
0.08	0.2365e-10	0.33	0.9416e-10	0.58	0.1837e-09	0.83	0.4335e-10
0.09	0.2477e-10	0.34	0.9934e-10	0.59	0.1794e-09	0.84	0.4052e-10
0.10	0.2600e-10	0.35	0.1048e-09	0.60	0.1736e-09	0.85	0.3787e-10
0.11	0.2736e-10	0.36	0.1107e-09	0.61	0.1662e-09	0.86	0.3539e-10
0.12	0.2885e-10	0.37	0.1169e-09	0.62	0.1578e-09	0.87	0.3307e-10
0.13	0.3049e-10	0.38	0.1236e-09	0.63	0.1494e-09	0.88	0.3091e-10
0.14	0.3228e-10	0.39	0.1305e-09	0.64	0.1416e-09	0.89	0.2890e-10
0.15	0.3423e-10	0.40	0.1376e-09	0.65	0.1342e-09	0.90	0.2703e-10
0.16	0.3632e-10	0.41	0.1447e-09	0.66	0.1273e-09	0.91	0.2529e-10
0.17	0.3855e-10	0.42	0.1517e-09	0.67	0.1204e-09	0.92	0.2366e-10
0.18	0.4090e-10	0.43	0.1584e-09	0.68	0.1138e-09	0.93	0.2216e-10
0.19	0.4335e-10	0.44	0.1644e-09	0.69	0.1073e-09	0.94	0.2076e-10
0.20	0.4588e-10	0.45	0.1696e-09	0.70	0.1010e-09	0.95	0.1946e-10
0.21	0.4850e-10	0.46	0.1739e-09	0.71	0.9502e-10	0.96	0.1825e-10
0.22	0.5122e-10	0.47	0.1774e-09	0.72	0.8929e-10	0.97	0.1714e-10
0.23	0.5407e-10	0.48	0.1801e-09	0.73	0.8384e-10	0.98	0.1610e-10
0.24	0.5709e-10	0.49	0.1823e-09	0.74	0.7866e-10	0.99	0.1514e-10
0.25	0.6029e-10	0.50	0.1839e-09	0.75	0.7376e-10	1.00	0.1425e-10

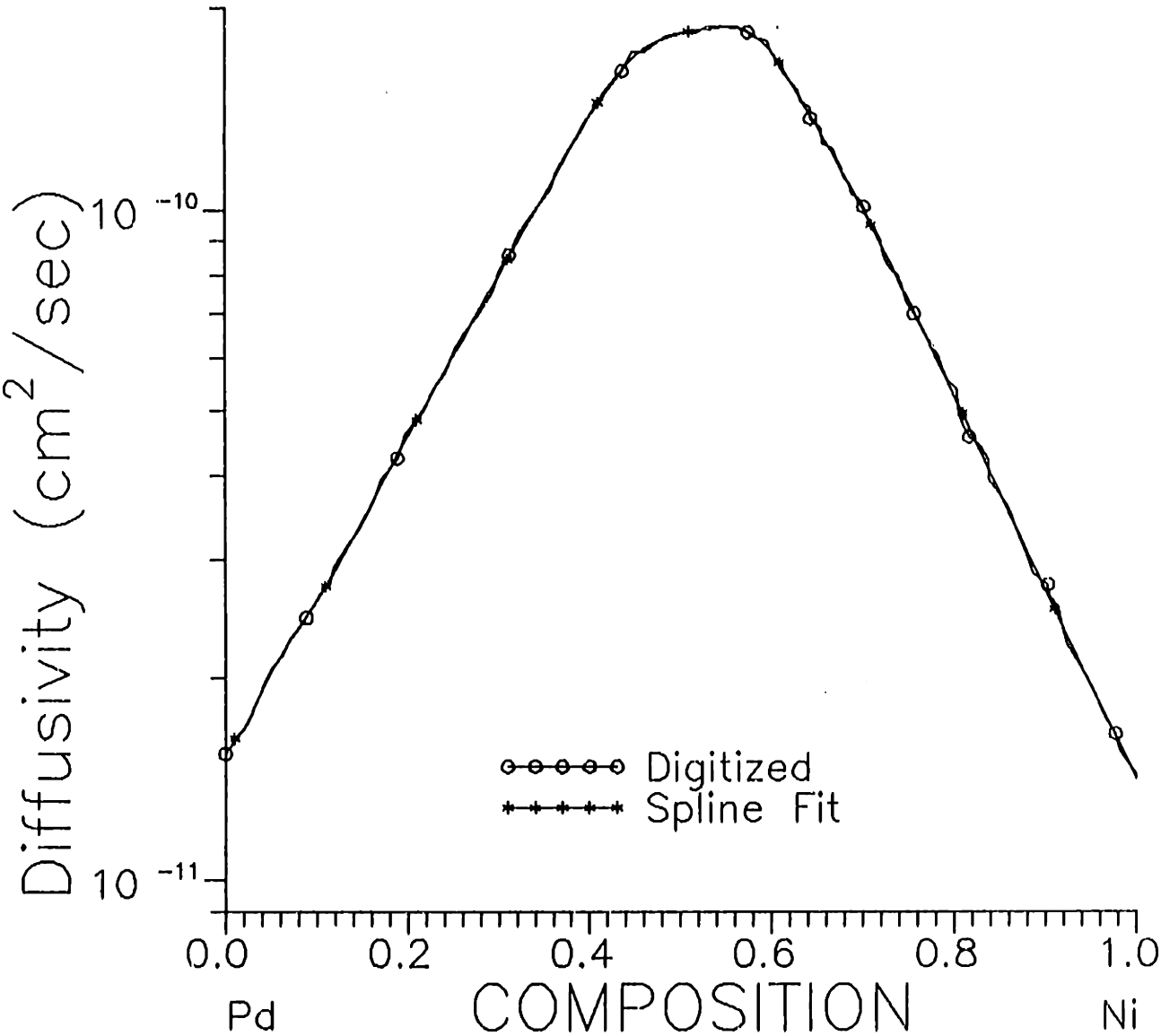

Figure 11. Raw digitized diffusivity data for the PdNi system at 1045°C. Also depicted is the spline interpolated diffusivity data after fitting the digitized data with a fourth order least squares spline. The closeness of the spline interpolated data and the digitized data is indicative of a good fit to the raw diffusivity data.

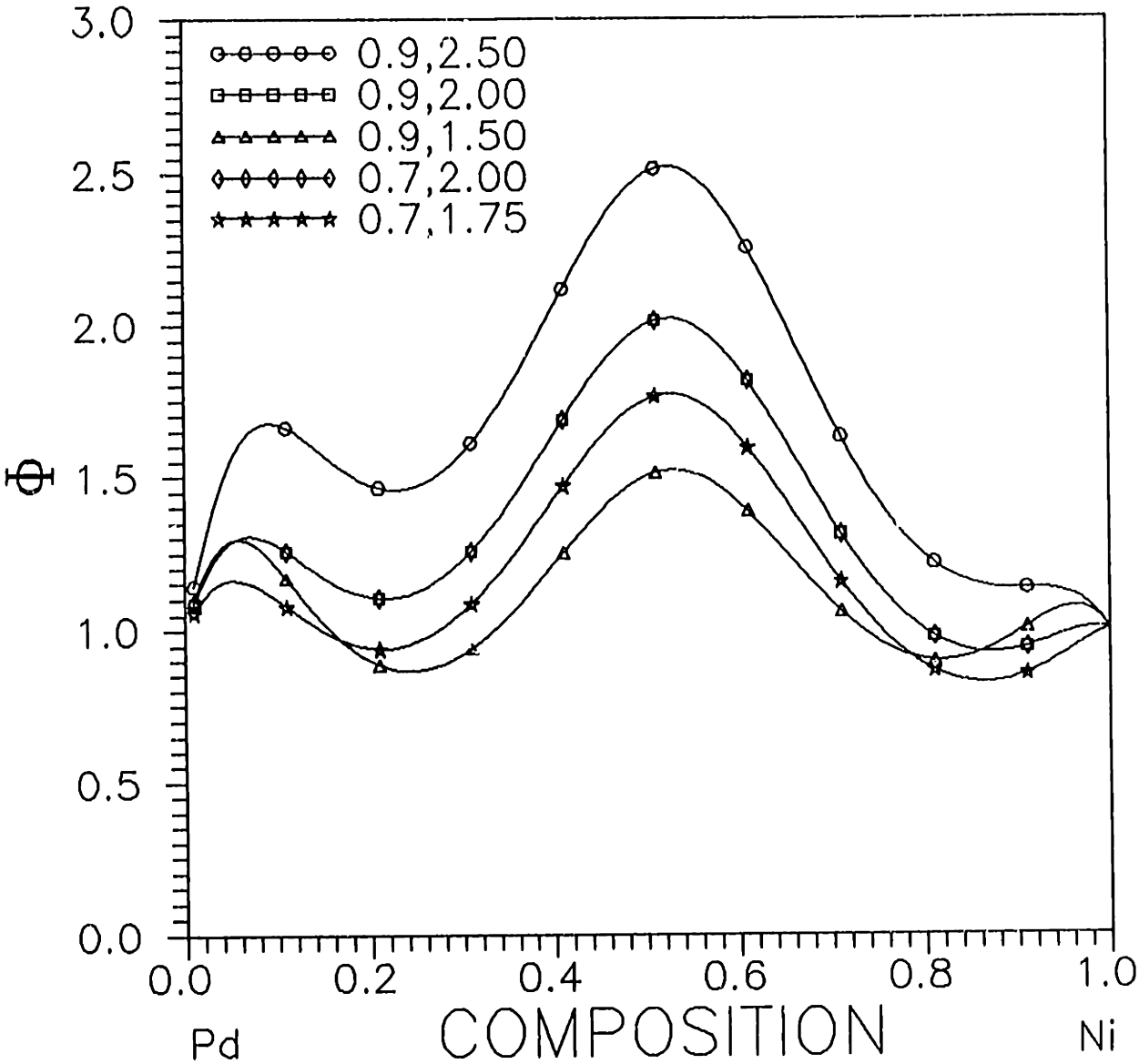

Figure 12. Computed thermodynamic term $\phi(c)$ for the PdNi system using the model function $P_4(ExpP_6)$ at 1045°C and the spline interpolated data which is tabulated in table VI and graphically depicted in figure 11. Corresponding activity composition curves and the selected $\ln(\gamma) - c$ curve are presented in paper II.

Table VII Diffusivity for the CuNi system at 1000°C as a function of the mole fraction of Ni. The data was digitized from figure 6.3b in the book by Borovskii and fitted with a fourth order least squares spline. The spline representation was evaluated at 100 points to yield the data in the table.

X_{Ni}	D cm*cm/sec	X_{Ni}	D cm*cm/sec	X_{Ni}	D cm*cm/sec	X_{Ni}	D cm*cm/sec
0.01	0.5316e-09	0.26	0.1500e-09	0.51	0.5675e-10	0.76	0.2614e-10
0.02	0.5034e-09	0.27	0.1433e-09	0.52	0.5491e-10	0.77	0.2556e-10
0.03	0.4768e-09	0.28	0.1370e-09	0.53	0.5312e-10	0.78	0.2503e-10
0.04	0.4517e-09	0.29	0.1311e-09	0.54	0.5138e-10	0.79	0.2454e-10
0.05	0.4281e-09	0.30	0.1254e-09	0.55	0.4970e-10	0.80	0.2407e-10
0.06	0.4058e-09	0.31	0.1201e-09	0.56	0.4808e-10	0.81	0.2359e-10
0.07	0.3848e-09	0.32	0.1150e-09	0.57	0.4652e-10	0.82	0.2307e-10
0.08	0.3650e-09	0.33	0.1102e-09	0.58	0.4503e-10	0.83	0.2249e-10
0.09	0.3463e-09	0.34	0.1057e-09	0.59	0.4362e-10	0.84	0.2185e-10
0.10	0.3287e-09	0.35	0.1014e-09	0.60	0.4227e-10	0.85	0.2118e-10
0.11	0.3121e-09	0.36	0.9731e-10	0.61	0.4099e-10	0.86	0.2056e-10
0.12	0.2964e-09	0.37	0.9346e-10	0.62	0.3977e-10	0.87	0.2003e-10
0.13	0.2816e-09	0.38	0.8982e-10	0.63	0.3859e-10	0.88	0.1962e-10
0.14	0.2676e-09	0.39	0.8637e-10	0.64	0.3746e-10	0.89	0.1935e-10
0.15	0.2545e-09	0.40	0.8311e-10	0.65	0.3636e-10	0.90	0.1903e-10
0.16	0.2420e-09	0.41	0.8003e-10	0.66	0.3530e-10	0.91	0.1841e-10
0.17	0.2303e-09	0.42	0.7711e-10	0.67	0.3426e-10	0.92	0.1802e-10
0.18	0.2192e-09	0.43	0.7436e-10	0.68	0.3325e-10	0.93	0.1834e-10
0.19	0.2087e-09	0.44	0.7176e-10	0.69	0.3225e-10	0.94	0.1779e-10
0.20	0.1989e-09	0.45	0.6931e-10	0.70	0.3126e-10	0.95	0.1715e-10
0.21	0.1895e-09	0.46	0.6698e-10	0.71	0.3029e-10	0.96	0.1674e-10
0.22	0.1807e-09	0.47	0.6476e-10	0.72	0.2933e-10	0.97	0.1645e-10
0.23	0.1724e-09	0.48	0.6264e-10	0.73	0.2842e-10	0.98	0.1633e-10
0.24	0.1645e-09	0.49	0.6061e-10	0.74	0.2757e-10	0.99	0.1631e-10
0.25	0.1570e-09	0.50	0.5865e-10	0.75	0.2681e-10	1.00	0.1630e-10

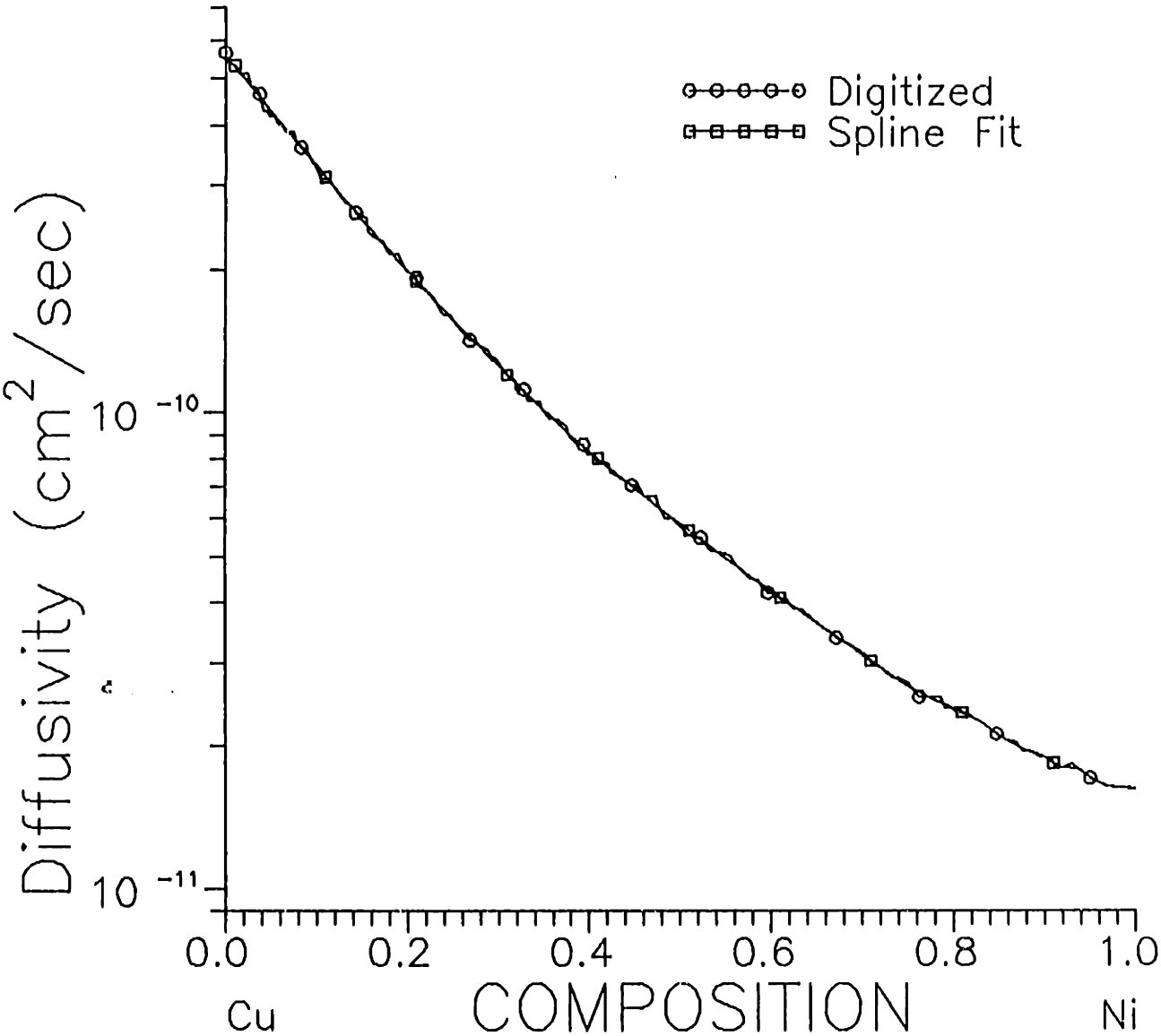

Figure 13. Raw digitized diffusivity data for the CuNi system at 1000°C. Also depicted is the spline interpolated diffusivity data after fitting the digitized data with a fourth order least squares spline. The closeness of the spline interpolated data and the digitized data is indicative of a good fit to the raw diffusivity data.

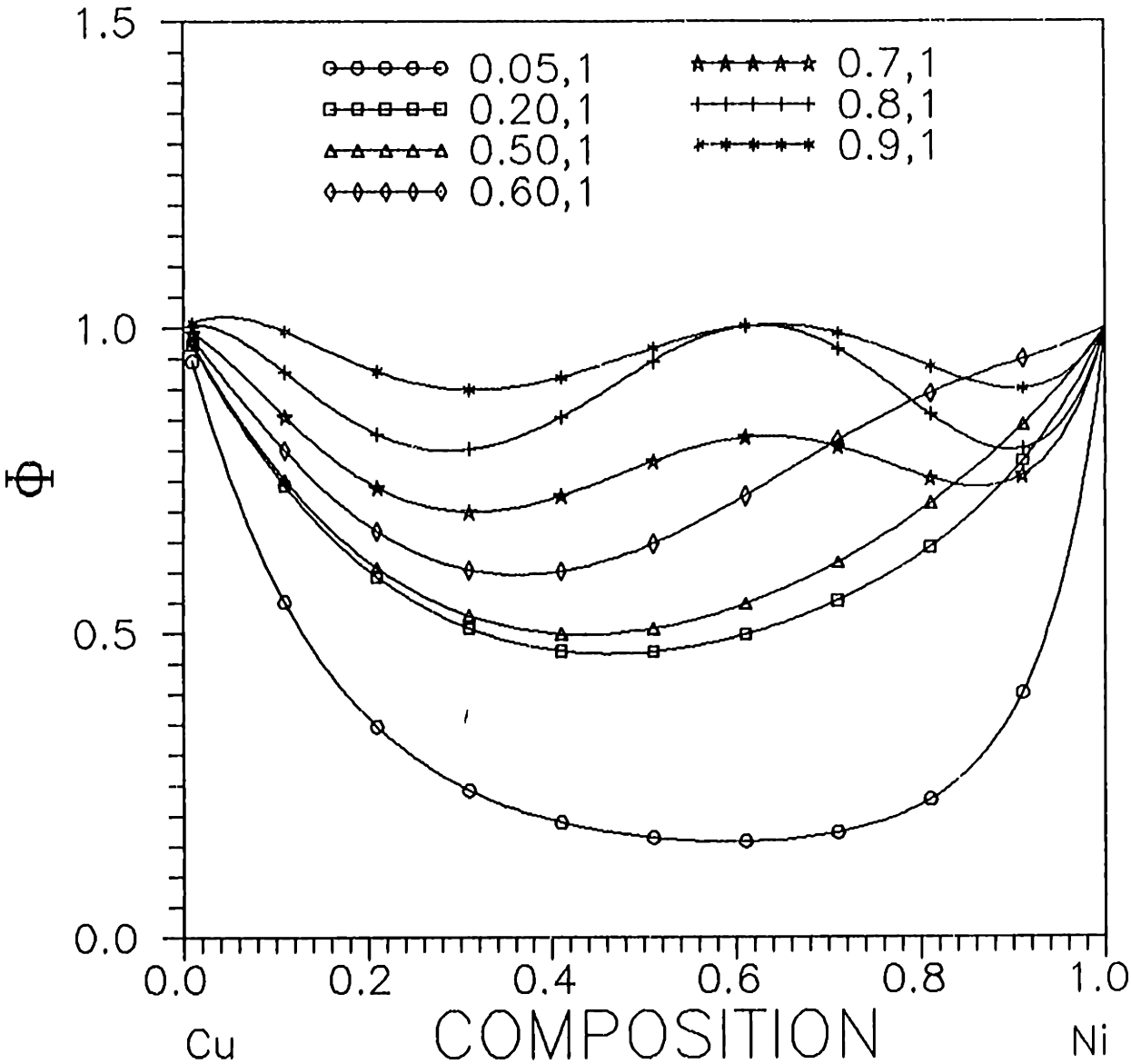

Figure 14. Computed thermodynamic term $\phi(c)$ for the CuNi system using the model function $P_3(ExpP_5)$ at 1000°C and the spline interpolated data which is tabulated in table VII and graphically depicted in figure 13. Corresponding activity composition curves and the selected $\ln(\gamma) - c$ curve are presented in paper III.

Table VIII Diffusivity for the PdCu system at 1019°C as a function of the mole fraction of Cu. The data was digitized from figure 6.15b in the book by Borovskii and fitted with a fourth order least squares spline. The spline representation was evaluated at 100 points to yield the data in the table.

X_{Cu}	$\tilde{D}$ cm*cm/sec	X_{Cu}	$\tilde{D}$ cm*cm/sec	X_{Cu}	$\tilde{D}$ cm*cm/sec	X_{Cu}	$\tilde{D}$ cm*cm/sec
0.01	0.2550e-10	0.26	0.1598e-09	0.51	0.9104e-09	0.76	0.3799e-08
0.02	0.2750e-10	0.27	0.1723e-09	0.52	0.1015e-08	0.77	0.3852e-08
0.03	0.2964e-10	0.28	0.1856e-09	0.53	0.1108e-08	0.78	0.3894e-08
0.04	0.3192e-10	0.29	0.1998e-09	0.54	0.1184e-08	0.79	0.3926e-08
0.05	0.3435e-10	0.30	0.2148e-09	0.55	0.1275e-08	0.80	0.3946e-08
0.06	0.3695e-10	0.31	0.2307e-09	0.56	0.1385e-08	0.81	0.3953e-08
0.07	0.3974e-10	0.32	0.2474e-09	0.57	0.1491e-08	0.82	0.3947e-08
0.08	0.4272e-10	0.33	0.2650e-09	0.58	0.1592e-08	0.83	0.3928e-08
0.09	0.4591e-10	0.34	0.2836e-09	0.59	0.1710e-08	0.84	0.3895e-08
0.10	0.4934e-10	0.35	0.3033e-09	0.60	0.1853e-08	0.85	0.3849e-08
0.11	0.5301e-10	0.36	0.3243e-09	0.61	0.1981e-08	0.86	0.3790e-08
0.12	0.5697e-10	0.37	0.3468e-09	0.62	0.2055e-08	0.87	0.3720e-08
0.13	0.6122e-10	0.38	0.3712e-09	0.63	0.2113e-08	0.88	0.3640e-08
0.14	0.6581e-10	0.39	0.3975e-09	0.64	0.2211e-08	0.89	0.3551e-08
0.15	0.7075e-10	0.40	0.4263e-09	0.65	0.2396e-08	0.90	0.3456e-08
0.16	0.7609e-10	0.41	0.4578e-09	0.66	0.2621e-08	0.91	0.3354e-08
0.17	0.8186e-10	0.42	0.4925e-09	0.67	0.2836e-08	0.92	0.3247e-08
0.18	0.8808e-10	0.43	0.5309e-09	0.68	0.3024e-08	0.93	0.3137e-08
0.19	0.9480e-10	0.44	0.5727e-09	0.69	0.3179e-08	0.94	0.3027e-08
0.20	0.1021e-09	0.45	0.6157e-09	0.70	0.3304e-08	0.95	0.2918e-08
0.21	0.1099e-09	0.46	0.6569e-09	0.71	0.3408e-08	0.96	0.2813e-08
0.22	0.1184e-09	0.47	0.6937e-09	0.72	0.3502e-08	0.97	0.2713e-08
0.23	0.1276e-09	0.48	0.7283e-09	0.73	0.3588e-08	0.98	0.2619e-08
0.24	0.1375e-09	0.49	0.7654e-09	0.74	0.3667e-08	0.99	0.2533e-08
0.25	0.1483e-09	0.50	0.8214e-09	0.75	0.3738e-08	1.00	0.2456e-08

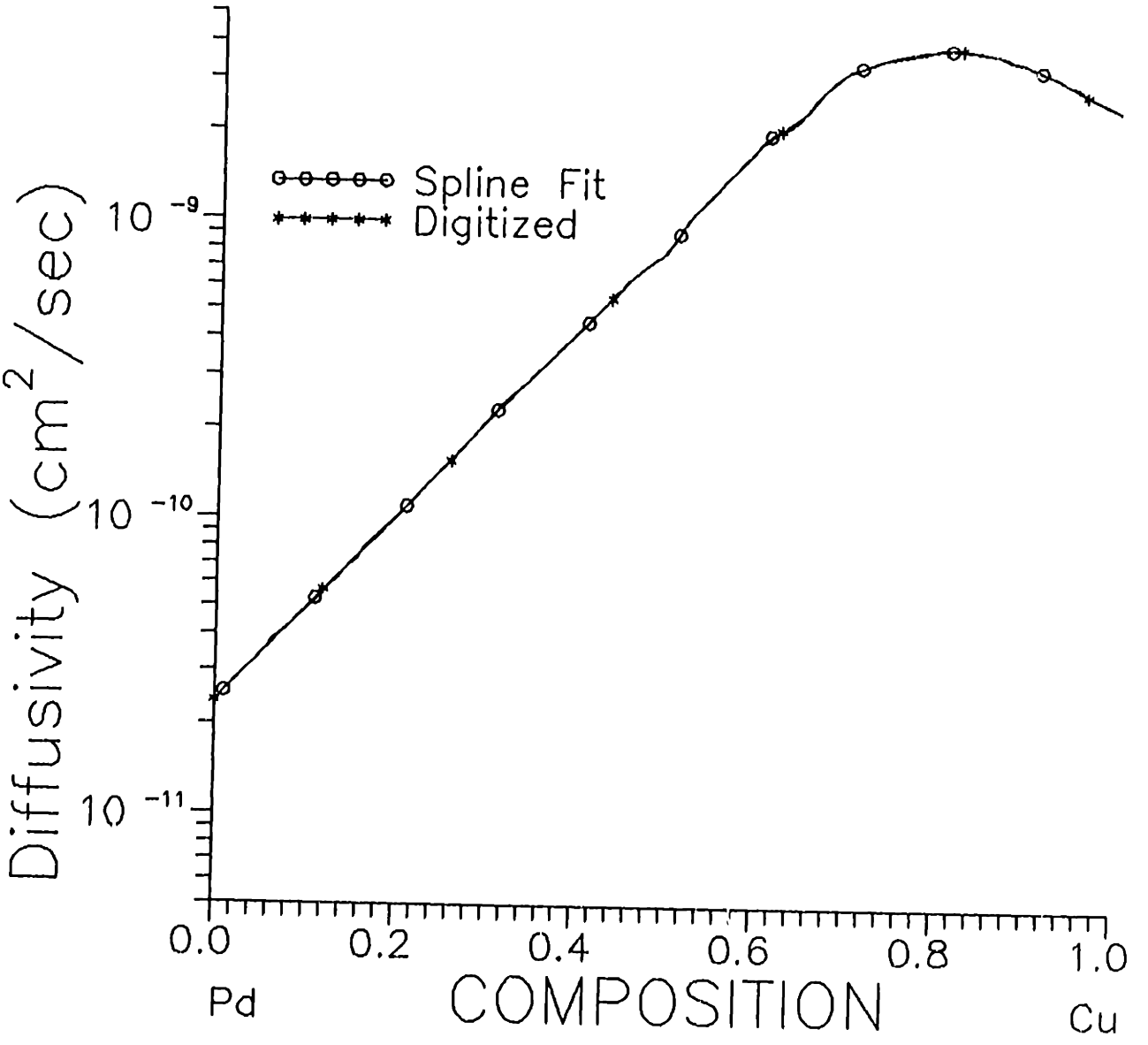

Figure 15. Raw digitized diffusivity data for the PdCu system at 1019°C. Also depicted is the spline interpolated diffusivity data after fitting the digitized data with a fourth order least squares spline. The closeness of the spline interpolated data and the digitized data is indicative of a good fit to the raw diffusivity data.

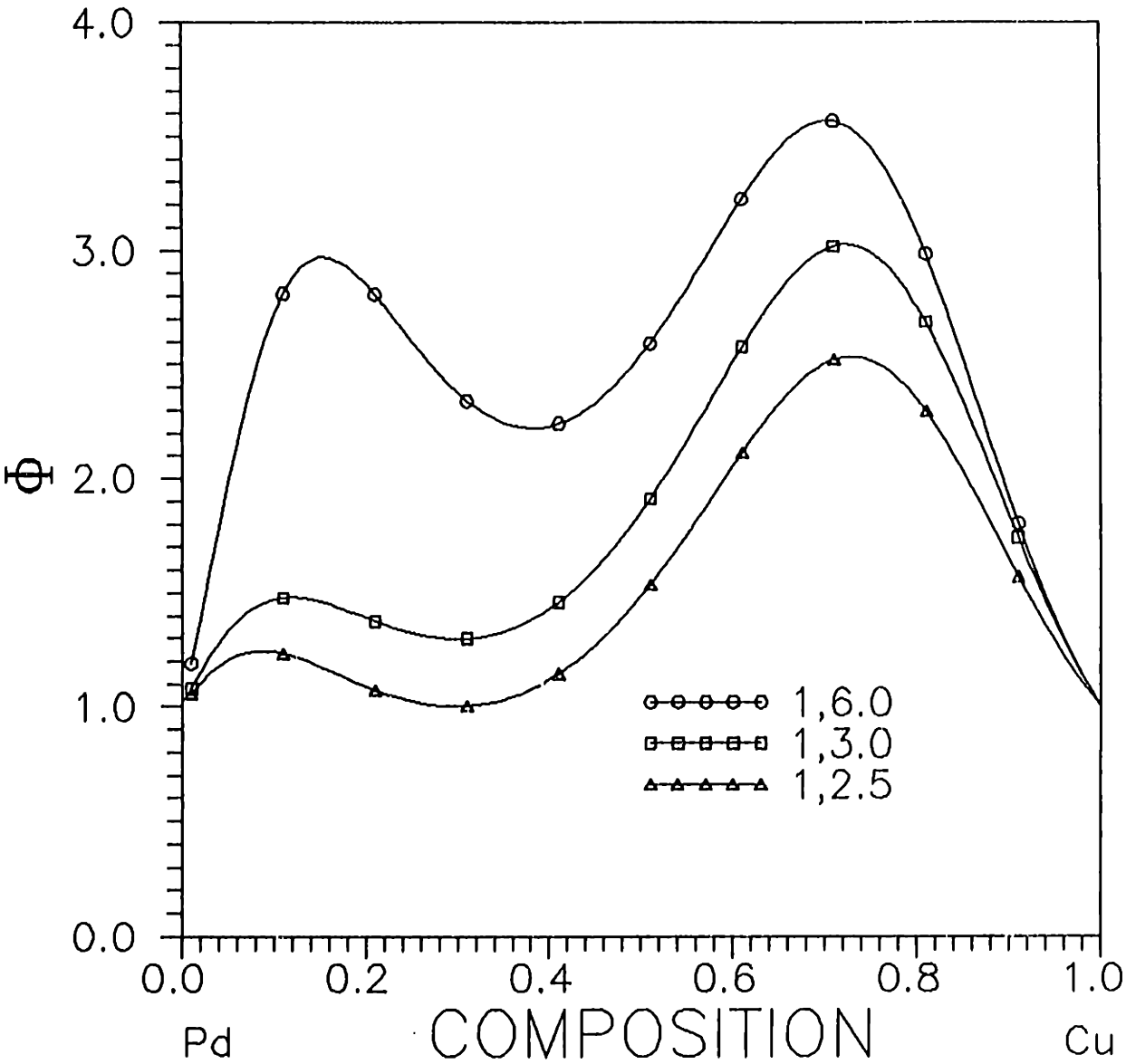

Figure 16. Computed thermodynamic term $\phi(c)$ for the PdCu system using the model function $P_3(ExpP_5)$ at 1019°C and the spline interpolated data which is tabulated in table VIII and graphically depicted in figure 15. Corresponding activity composition curves and the selected $\ln(\gamma)-c$ curve are presented in paper III.

Table IX Diffusivity for the CuAu system at 857°C as a function of the mole fraction of Au. The data was digitized from figure 6.5b in the book by Borovskii and fitted with a fourth order least squares spline. The spline representation was evaluated at 100 points to yield the data in the table.

X_{Au}	$\tilde{D}$ cm*cm/sec	X_{Au}	$\tilde{D}$ cm*cm/sec	X_{Au}	$\tilde{D}$ cm*cm/sec	X_{Au}	$\tilde{D}$ cm*cm/sec
0.01	0.2393e-09	0.26	0.1810e-08	0.51	0.3502e-08	0.76	0.2701e-08
0.02	0.2585e-09	0.27	0.1901e-08	0.52	0.3514e-08	0.77	0.2647e-08
0.03	0.2804e-09	0.28	0.1992e-08	0.53	0.3521e-08	0.78	0.2593e-08
0.04	0.3052e-09	0.29	0.2084e-08	0.54	0.3523e-08	0.79	0.2539e-08
0.05	0.3332e-09	0.30	0.2175e-08	0.55	0.3519e-08	0.80	0.2484e-08
0.06	0.3644e-09	0.31	0.2266e-08	0.56	0.3511e-08	0.81	0.2429e-08
0.07	0.3990e-09	0.32	0.2358e-08	0.57	0.3498e-08	0.82	0.2373e-08
0.08	0.4370e-09	0.33	0.2451e-08	0.58	0.3481e-08	0.83	0.2318e-08
0.09	0.4787e-09	0.34	0.2542e-08	0.59	0.3459e-08	0.84	0.2263e-08
0.10	0.5243e-09	0.35	0.2632e-08	0.60	0.3433e-08	0.85	0.2209e-08
0.11	0.5741e-09	0.36	0.2720e-08	0.61	0.3403e-08	0.86	0.2155e-08
0.12	0.6285e-09	0.37	0.2805e-08	0.62	0.3370e-08	0.87	0.2103e-08
0.13	0.6878e-09	0.38	0.2886e-08	0.63	0.3333e-08	0.88	0.2052e-08
0.14	0.7525e-09	0.39	0.2962e-08	0.64	0.3294e-08	0.89	0.2001e-08
0.15	0.8230e-09	0.40	0.3034e-08	0.65	0.3252e-08	0.90	0.1949e-08
0.16	0.8997e-09	0.41	0.3101e-08	0.66	0.3208e-08	0.91	0.1894e-08
0.17	0.9821e-09	0.42	0.3164e-08	0.67	0.3162e-08	0.92	0.1834e-08
0.18	0.1070e-08	0.43	0.3221e-08	0.68	0.3114e-08	0.93	0.1771e-08
0.19	0.1161e-08	0.44	0.3273e-08	0.69	0.3065e-08	0.94	0.1709e-08
0.20	0.1255e-08	0.45	0.3321e-08	0.70	0.3015e-08	0.95	0.1653e-08
0.21	0.1349e-08	0.46	0.3364e-08	0.71	0.2964e-08	0.96	0.1606e-08
0.22	0.1443e-08	0.47	0.3402e-08	0.72	0.2912e-08	0.97	0.1570e-08
0.23	0.1536e-08	0.48	0.3435e-08	0.73	0.2860e-08	0.98	0.1542e-08
0.24	0.1628e-08	0.49	0.3462e-08	0.74	0.2808e-08	0.99	0.1518e-08
0.25	0.1719e-08	0.50	0.3485e-08	0.75	0.2755e-08	1.00	0.1496e-08

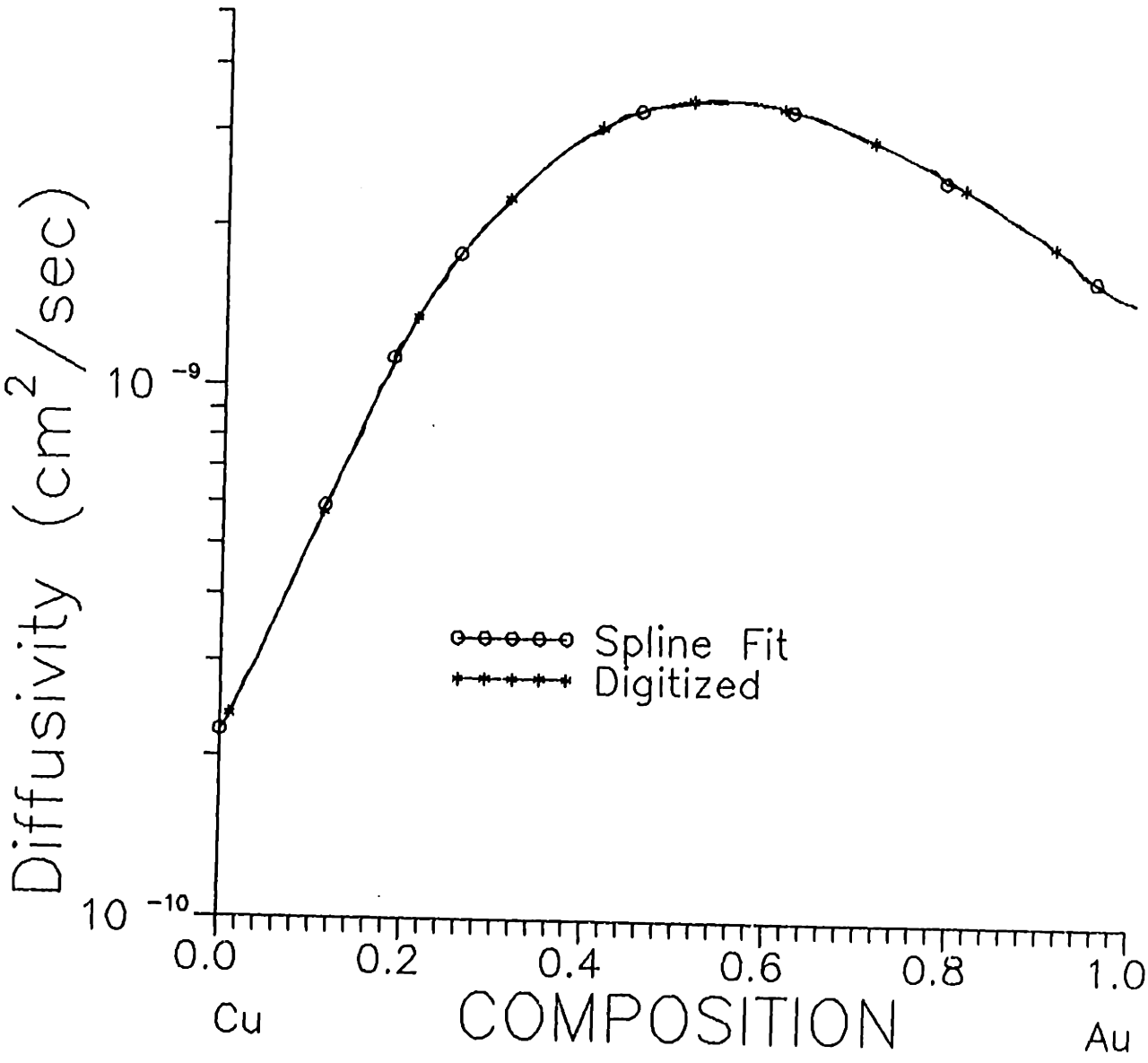

Figure 17. Raw digitized diffusivity data for the CuAu system at 857°C. Also depicted is the spline interpolated diffusivity data after fitting the digitized data with a fourth order least squares spline. The closeness of the spline interpolated data and the digitized data is indicative of a good fit to the raw diffusivity data.

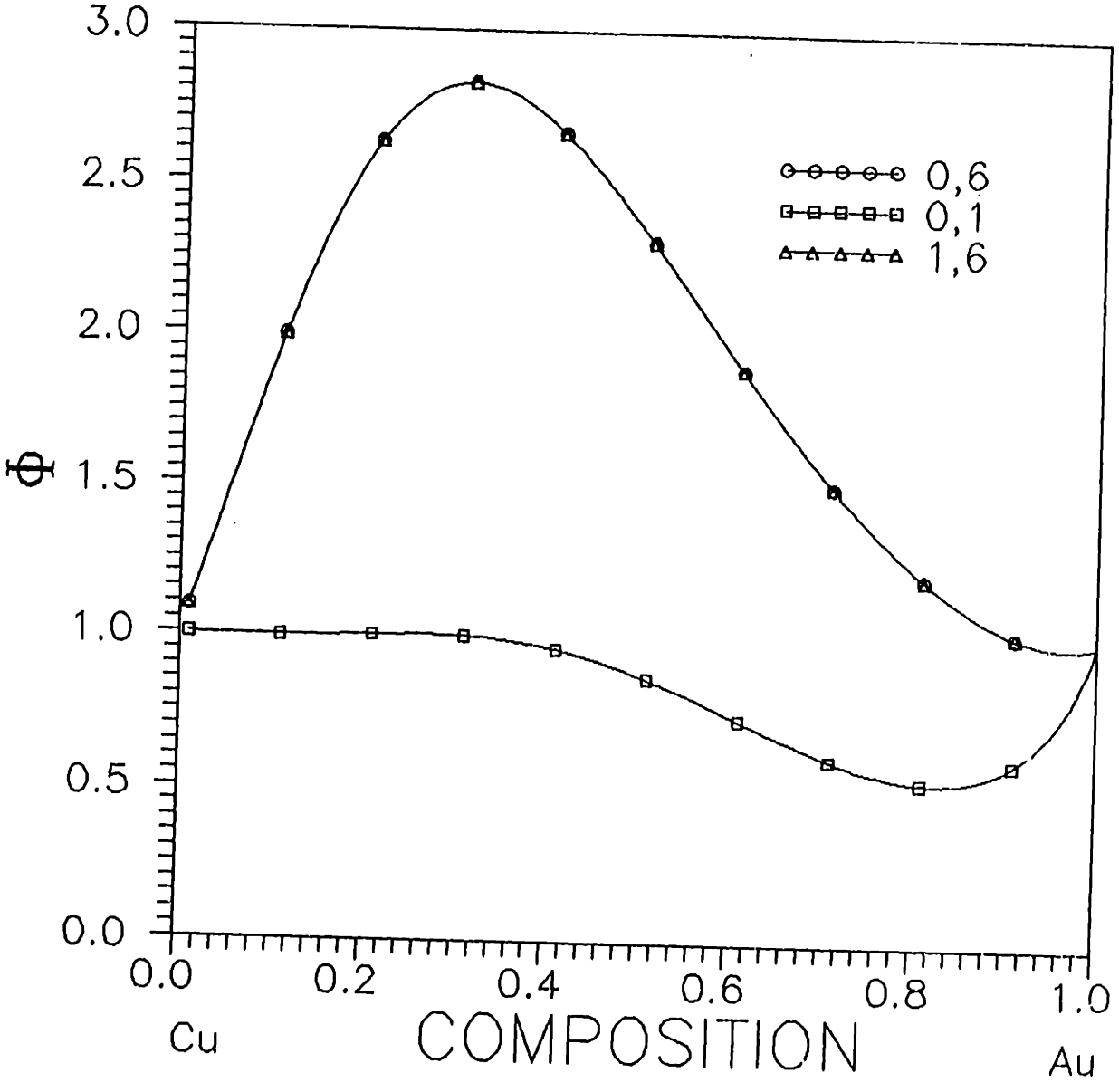

Figure 18. Computed thermodynamic term $\phi(c)$ for the CuAu system using the model function $P_3(ExpP_5)$ at 1019°C and the spline interpolated data which is tabulated in table IX and graphically depicted in figure 17. Corresponding activity composition curves and the selected $\ln(\gamma) - c$ curve are presented in paper III.

Table X Diffusivity for the CoNi system at 1356°C as a function of the mole fraction of Ni. The data was digitized from figure 6.2 in the book by Borovskii and fitted with a fourth order least squares spline. The spline representation was evaluated at 100 points to yield the data in the table.

X_{Ni}	D cm*cm/sec	X_{Ni}	D cm*cm/sec	X_{Ni}	D cm*cm/sec	X_{Ni}	D cm*cm/sec
0.01	0.3363e-09	0.26	0.5561e-09	0.51	0.8198e-09	0.76	0.1113e-08
0.02	0.3442e-09	0.27	0.5653e-09	0.52	0.8324e-09	0.77	0.1125e-08
0.03	0.3521e-09	0.28	0.5748e-09	0.53	0.8445e-09	0.78	0.1137e-08
0.04	0.3603e-09	0.29	0.5844e-09	0.54	0.8561e-09	0.79	0.1148e-08
0.05	0.3690e-09	0.30	0.5943e-09	0.55	0.8673e-09	0.80	0.1160e-08
0.06	0.3780e-09	0.31	0.6043e-09	0.56	0.8783e-09	0.81	0.1172e-08
0.07	0.3873e-09	0.32	0.6144e-09	0.57	0.8893e-09	0.82	0.1183e-08
0.08	0.3966e-09	0.33	0.6245e-09	0.58	0.9004e-09	0.83	0.1194e-08
0.09	0.4059e-09	0.34	0.6345e-09	0.59	0.9120e-09	0.84	0.1203e-08
0.10	0.4151e-09	0.35	0.6444e-09	0.60	0.9239e-09	0.85	0.1212e-08
0.11	0.4244e-09	0.36	0.6540e-09	0.61	0.9360e-09	0.86	0.1220e-08
0.12	0.4335e-09	0.37	0.6634e-09	0.62	0.9482e-09	0.87	0.1229e-08
0.13	0.4425e-09	0.38	0.6727e-09	0.63	0.9605e-09	0.88	0.1238e-08
0.14	0.4514e-09	0.39	0.6819e-09	0.64	0.9727e-09	0.89	0.1249e-08
0.15	0.4602e-09	0.40	0.6913e-09	0.65	0.9848e-09	0.90	0.1260e-08
0.16	0.4689e-09	0.41	0.7010e-09	0.66	0.9968e-09	0.91	0.1273e-08
0.17	0.4775e-09	0.42	0.7111e-09	0.67	0.1009e-08	0.92	0.1286e-08
0.18	0.4860e-09	0.43	0.7217e-09	0.68	0.1020e-08	0.93	0.1300e-08
0.19	0.4945e-09	0.44	0.7327e-09	0.69	0.1032e-08	0.94	0.1313e-08
0.20	0.5031e-09	0.45	0.7442e-09	0.70	0.1044e-08	0.95	0.1324e-08
0.21	0.5116e-09	0.46	0.7561e-09	0.71	0.1055e-08	0.96	0.1332e-08
0.22	0.5203e-09	0.47	0.7684e-09	0.72	0.1067e-08	0.97	0.1337e-08
0.23	0.5291e-09	0.48	0.7810e-09	0.73	0.1078e-08	0.98	0.1342e-08
0.24	0.5379e-09	0.49	0.7939e-09	0.74	0.1090e-08	0.99	0.1351e-08
0.25	0.5469e-09	0.50	0.8069e-09	0.75	0.1101e-08	1.00	0.1369e-08

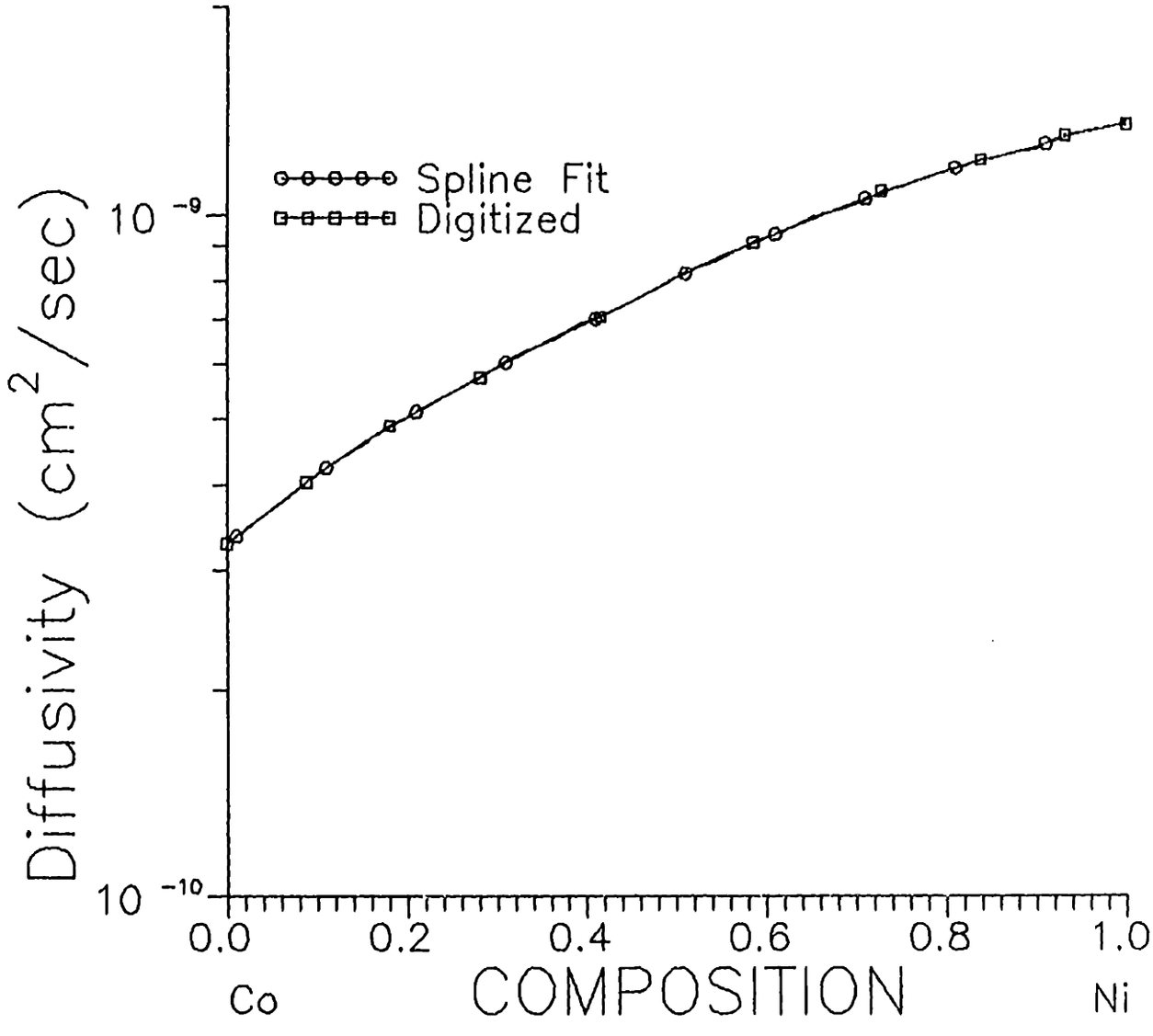

Figure 19. Raw digitized diffusivity data for the CoNi system at 1356°C. Also depicted is the spline interpolated diffusivity data after fitting the digitized data with a fourth order least squares spline. The closeness of the spline interpolated data and the digitized data is indicative of a good fit to the raw diffusivity data.

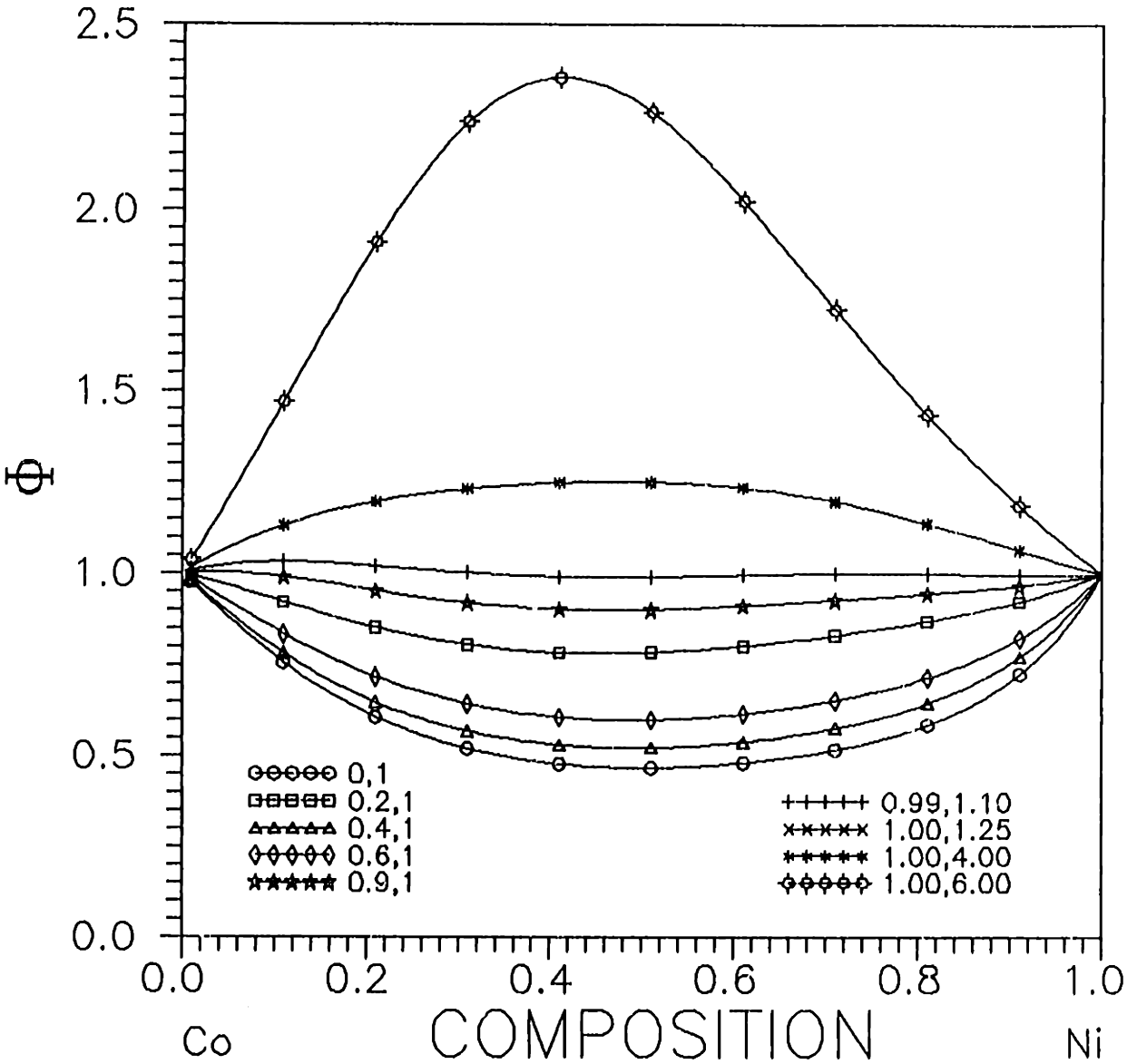

Figure 20. Computed thermodynamic term $\phi(c)$ for the CoNi system using the model function $P_3(ExpP_5)$ at 1019°C and the spline interpolated data which is tabulated in table X and graphically depicted in figure 19. Corresponding activity composition curves and the selected $\ln(\gamma)-c$ curve are presented in paper III.

8.3 Appendix III Estimation of the enthalpy of solution for solid state binaries

This appendix reviews a strategy proposed by Russell[1] to estimate the partial molar enthalpy of formation in the solid state given the partial molar enthalpy of formation in the liquid state for binary metallic systems. The heats of solution for the liquid state can be obtained experimentally or may be obtained from theoretical estimates such as those by Miedema[2].

Consider the case of a solid solution α, in equilibrium with a liquid metal, at a temperature T as shown in figure 1. Assume that the system obeys the regular solution model in both the liquid and the solid states and that the regular solution parameter is known a priori in the liquid state. Taking pure solid A and pure solid B as the standard states one may write the following equations:

$$\mu_B^l = \Omega_l(1-X_l)^2 + RT\ln(X_l) + \Delta\mu_B^\circ \qquad [1]$$

$$\mu_B^\alpha = \Omega_\alpha(1-X_\alpha)^2 + RT\ln(X_\alpha) \qquad [2]$$

where $$\Delta\mu_B^\circ = L_B\left(1 - \frac{T}{T_m^B}\right) \qquad (L_B > 0) \qquad [3]$$

Equating μ_l^B and μ_α^B one ends up with:

$$\Omega_\alpha = \Omega_l + \Delta\mu_B^\circ + RT\ln\left(\frac{X_l}{X_\alpha}\right) \qquad [4]$$

In the present investigation this scheme was used to estimate the slope of the Henry's law line for the various isomorphous binary systems at the temperature at which the diffusivity data was measured. As an illustrative example consider the NbTi system with Nb as the solvent and Ti as the solute. The regular solution parameter was estimated at 2000°C (2273K) by using the phase diagram depicted in figure 2. From the phase diagram[3] it is seen that $X_l = 0.5$ whereas $X_\alpha = 0.4$. The latent heat of fusion for Ti, obtained from the handbook by Smithells[4], was taken as 18.8kJ/mole whereas the melting temperature for Ti is known to be 1670°C. Miedema predicts a value of +9kJ/mole for the partial molar enthalpy of formation in the

liquid state at infinite dilution. Using these values, Ω_i^{Ti} was computed to be 10.02kJ/mole. Since it has been assumed that the solution exhibits regular solution behavior, it follows that Ω_i^{Ti} is independent of temperature. Hence one may compute the activity coefficient for this solution at the temperature for which the diffusivity data was reported (1000°C) by using the following equation:

$$\Omega_i^{Ti} = RT\ln(\gamma) \qquad [5]$$

Using this approach the activity coefficient was estimated to be 2.5 at 1000°C.

In a similar manner, the activity coefficients for the other alloy systems were computed. Table I lists the pertinent data used in these computations as well as the results of the computations.

References:

1. K. C. Russell, *Kinetic Processes in Advanced Alloys*, Final report to Materials Laboratory, Wright Research and Development Center, Air Force Systems Command, Wright Patterson AirForce Base, OH, WRDC-TR-89-4051, (1989).
2. A. R. Miedema, F. R. deBoer and R. Boom, *Calphad*, 1, No. 4, pp.341-359, (1977).
3. Thaddeus B. Massalski, *Binary Alloy Phase Diagrams*, Vol. 1 and 2, ASM, (1986).
4. C. J. Smithells, *Metals Reference Book*, 5th edition, Buttersworth, (1976).

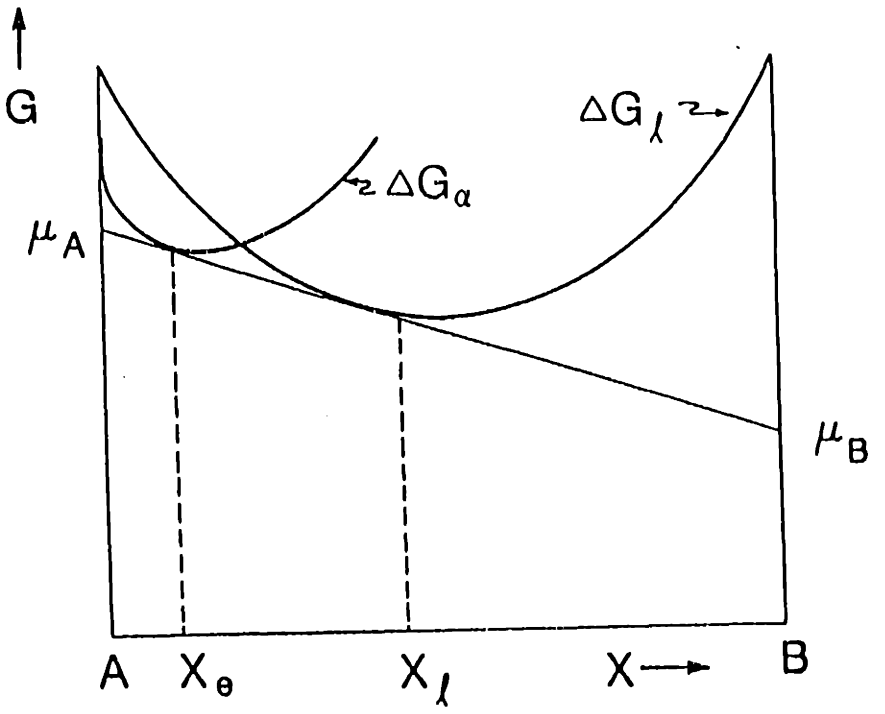

Figure 1. Free energy - composition curves depicting a liquid phase in equilibrium with a solid phase.

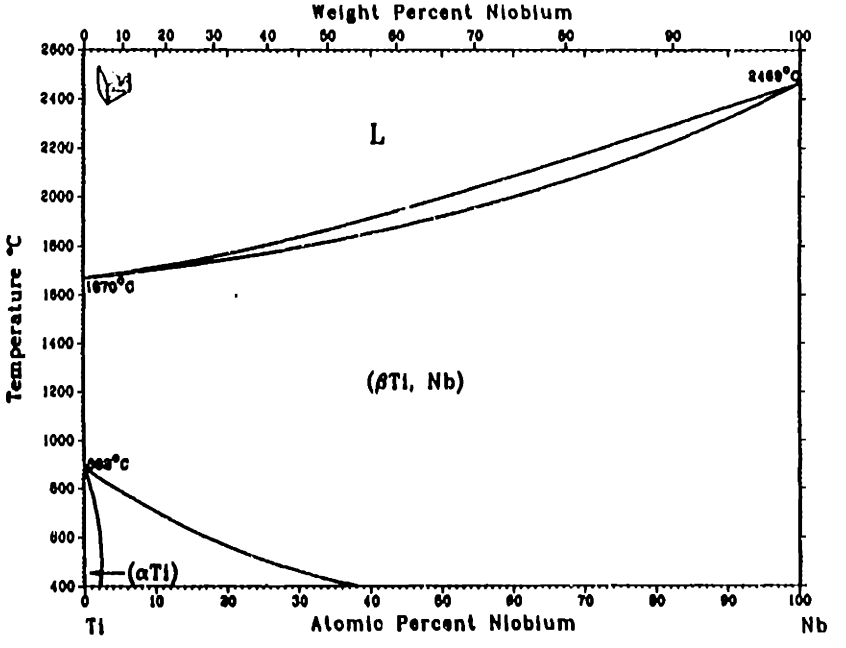

Figure 2. Phase diagram for the NbTi system taken from Massalski[8].

Table I Data used to compute Ω_s

System	Ω_l	T_m	Temperature for phase diagram analysis	X_l	X_s	L_B	Ω_s	Temperature of Diffusivity data	Activity Coefficient γ
	kJ/mole	°C	°C			kJ/mole	kJ/mole	°C	
CoNi	-1	1455	1475	50	50	17.71	-1.2	1356	0.914
CuAu	-29	1064	1000	44	36.5	12.81	-26.4	857	0.06
PdCu	-33	1084	1300	39	33.5	13.02	-33.08	1019	0.046
PdNi	0	1455	1400	20	13.5	17.71	6.03	1045	1.73
NiPt	-22	1769	1500	58	61	19.7	-20.1	1296	0.21
PdFe	-16	1539	1400	12.5	10.5	15.2	-12.4	1000	0.301
NbTi	9	1670	2000	50	40	18.8	10.02	1000	2.57
AgAu	-20	1064	1000	22.5	24	12.81	-20.06	900	0.12
AuNi	25	1455	1000	16	13	17.71	31.86	900	26.23
CuNi	26	1455	1200	22	33	17.71	23.64	1000	9.34

8.4 Appendix IV Behavior of $(d\phi/dc)$ at terminal compositions

The proposed algorithm imposes constraints on $\phi(c)$ The purpose of this appendix is to examine the behavior of the first derivative of $\phi(c)$ at the terminal compositions (c=0 and c=1) and thereby determine if any higher order constraints need to be imposed on $\phi(c)$ In particular, it is of interest to examine if the slope of $\phi(c)$ that is $(d\phi/dc)$ possesses some 'natural' constraints which hold true for all systems and can be derived from basic principles of solution behavior. For example, one may wish to determine if $(d\phi/dc)$ -> 0 as c->0 or as c->1.0 . If $(d\phi/dc)$ does indeed tend to zero at the ends or to some other finite constant that is universal for all solutions then the algorithm must impose a constraint to that effect on $(d\phi/dc)$.

To explore the behavior of $(d\phi/dc)$ one may begin with the definition of $\phi(c)$:

$$\phi(c) = \left(1 + \frac{c}{\gamma}\frac{\partial\gamma}{\partial c}\right) \qquad [1]$$

One may differentiate to obtain :

$$\frac{\partial\phi}{\partial c} = 0.0 + \frac{1}{\gamma}\frac{\partial\gamma}{\partial c} - \frac{c}{\gamma^2}\left(\frac{\partial\gamma}{\partial c}\right)^2 + \frac{c}{\gamma}\left(\frac{\partial^2\gamma}{\partial c^2}\right) \qquad [2]$$

From equation [2], it is clear that investiagtion of $(d\phi/dc)$ demands an understanding of the variation of the activity coefficient with composition (γ-c relationship). Since there is no universal γ-c relationship, one must rely on proposed models of solution behavior to investigate the behavior of $(d\phi/dc)$. Specifically, one may examine two popular models of solution behavior; the regular solution model and the Henrian model.

8.4.1 Regular Solution Model

A regular solution is defined by the following equation :

$$\ln(\gamma) = \alpha(1-c)^2 \quad [3]$$

$$\gamma = \mathrm{Exp}[\alpha(1-c)^2] \quad [4]$$

$$\frac{\partial\gamma}{\partial c} = \{-2\alpha(1-c)\}\mathrm{Exp}[\alpha(1-c)^2] \quad [5]$$

$$\frac{\partial^2\gamma}{\partial c^2} = \{-2\alpha(1-c)\}^2\mathrm{Exp}[\alpha(1-c)^2] + 2\alpha\mathrm{Exp}[\alpha(1-c)^2] \quad [6]$$

Hence for a regular solution one may plug equations 4,5,6 in to equation 2 and obtain $(\partial\phi/\partial c)$:

$$\frac{\partial\phi}{\partial c} = + \left[\frac{1}{\mathrm{Exp}[\alpha(1-c)^2]}\right][\{-2\alpha(1-c)\}\mathrm{Exp}[\alpha(1-c)^2]] - \left[\frac{c}{\{\mathrm{Exp}[\alpha(1-c)^2]\}^2}\right][\{-2\alpha(1-c)\}^2\{\mathrm{Exp}[\alpha(1-c)^2]\}^2] + \left[\frac{c}{\mathrm{Exp}[\alpha(1-c)^2]}\right]\{[-2\alpha(1-c)]^2\mathrm{Exp}[\alpha(1-c)^2] + 2\alpha\mathrm{Exp}[\alpha(1-c)^2]\} \quad [7]$$

On cancelling terms one ends up with the following:

$$\frac{\partial\phi}{\partial c} = \{-2\alpha(1-c)\} - \{c[4\alpha^2(1-c)^2]\} + \{c[4\alpha^2(1-c)^2 + 2\alpha]\} \quad [8]$$

Instead of expanding out the polynomials in 'c' and then taking the limit as c->0 one may keep each of the three terms separate in order to observe the behavior of each term in the limit.

Comparing terms between equations [8] and [2]:

$$\frac{1}{\gamma}\frac{\partial\gamma}{\partial c} = -2\alpha(1-c) \quad [9]$$

$$\frac{-c}{\gamma^2}\left(\frac{\partial\gamma}{\partial c}\right)^2 = -c4\alpha^2(1-c)^2 \quad [10]$$

$$\frac{c}{\gamma}\left(\frac{\partial^2\gamma}{\partial c^2}\right) = c[4\alpha^2(1-c)^2 + 2\alpha] \quad [11]$$

Limiting case of c->0

$$\gamma \rightarrow \mathrm{Exp}(\alpha) \qquad [12]$$

$$\frac{\partial \gamma}{\partial c} \rightarrow -2\alpha \mathrm{Exp}(\alpha) \qquad [13]$$

$$\frac{\partial^2 \gamma}{\partial c^2} \rightarrow (4\alpha^2 + 2\alpha)\mathrm{Exp}(\alpha) \qquad [14]$$

On plugging these values in one obtains :

$$\frac{1}{\gamma}\frac{\partial \gamma}{\partial c} \rightarrow -2\alpha \qquad [15]$$

$$-\frac{c}{\gamma^2}\left(\frac{\partial \gamma}{\partial c}\right)^2 \rightarrow 0.0 \qquad [16]$$

$$\frac{c}{\gamma}\frac{\partial^2 \gamma}{\partial c^2} \rightarrow 0.0 \qquad [17]$$

On adding equations 15,16 and 17 one obtains:

For c -> 0.0	$\frac{\partial \phi}{\partial c} = -2\alpha$	[18]

Limiting case of c->1

$$\gamma \rightarrow 1.0 \qquad [19]$$

$$\frac{\partial \gamma}{\partial c} \rightarrow 0.0 \qquad [20]$$

$$\frac{\partial^2 \gamma}{\partial c^2} \rightarrow 2\alpha \qquad [21]$$

On plugging these values in one obtains :

$$\frac{1}{\gamma}\frac{\partial \gamma}{\partial c} \rightarrow 0.0 \qquad p[22]$$

$$-\frac{c}{\gamma^2}\left(\frac{\partial \gamma}{\partial c}\right)^2 \rightarrow 0.0 \qquad [23]$$

$$\frac{c}{\gamma}\frac{\partial^2 \gamma}{\partial c^2} \rightarrow 2\alpha \qquad [24]$$

On adding equations 22,23 and 24 one obtains:

For c -> 1.0	$\frac{\partial \phi}{\partial c} = +2\alpha$	[25]

Equations [18] and [25] clearly show that the slope of the $\phi(c)-c$ curves is not zero at either c=0 or c=1 for a regular solution. Further, the absolute value of the slope is equal at either end for the special case of a regular solution.

To demonstrate the same graphically, some of the relevant quantities have been plotted as a function of composition for two values of the regular solution parameter, α +1.5 and α -1.5. Figures 1 through 3 plot the $\gamma-c$, $(d\gamma/dc)-c$ and $(d^2\gamma/dc^2)-c$ relationships and for the two regular solutions; α +1.5 and α -1.5. Similarly figure 4 plots the corresponding $(1/\gamma)(d\gamma/dc)-c$ relationship; figure 5 plots the corresponding $(-c/\gamma^2)(d\gamma/dc)^2-c$ relationship and figure 6 plots the corresponding $(c/\gamma)(d^2\gamma/dc^2)-c$ relationship. Thus figures 4, 5, and 6 represent the three terms in equation [2]. The sum of these three terms yields $(d\phi/dc)$ which is plotted in figure 7 for α +1.5 and α -1.5. These figures clearly depict that $(d\phi/dc)$ is non zero but finite at either end of the composition range.

8.4.2 Henrian Solution Model

A Henrian solution exhibits a linear activity composition relationship which may be expressed as follows:

$$\alpha = Kc \qquad [26]$$

$$\gamma = K \qquad [27]$$

$$\frac{\partial \gamma}{\partial c} = 0 \qquad [28]$$

$$\frac{\partial^2 \gamma}{\partial c^2} = 0 \qquad [29]$$

On substituting these into equation [2] one obtains:

$$\frac{\partial \phi}{\partial c} = 0 \qquad [29]$$

Thus for the special case of a solution obeying Henry's law $(d\phi/dc)$ is identically zero.

8.4.3 Conclusion

The lack of a non zero $(d\phi/dc)$ for regular solutions at c=0 and c=1 implies that it would be incorrect to assume *a priori* that *all* solutions must satisfy the condition that $(d\phi/dc) = 0$ at c=1 and at c=0. Hence no additional constraints should be incorporated into the algorithm.

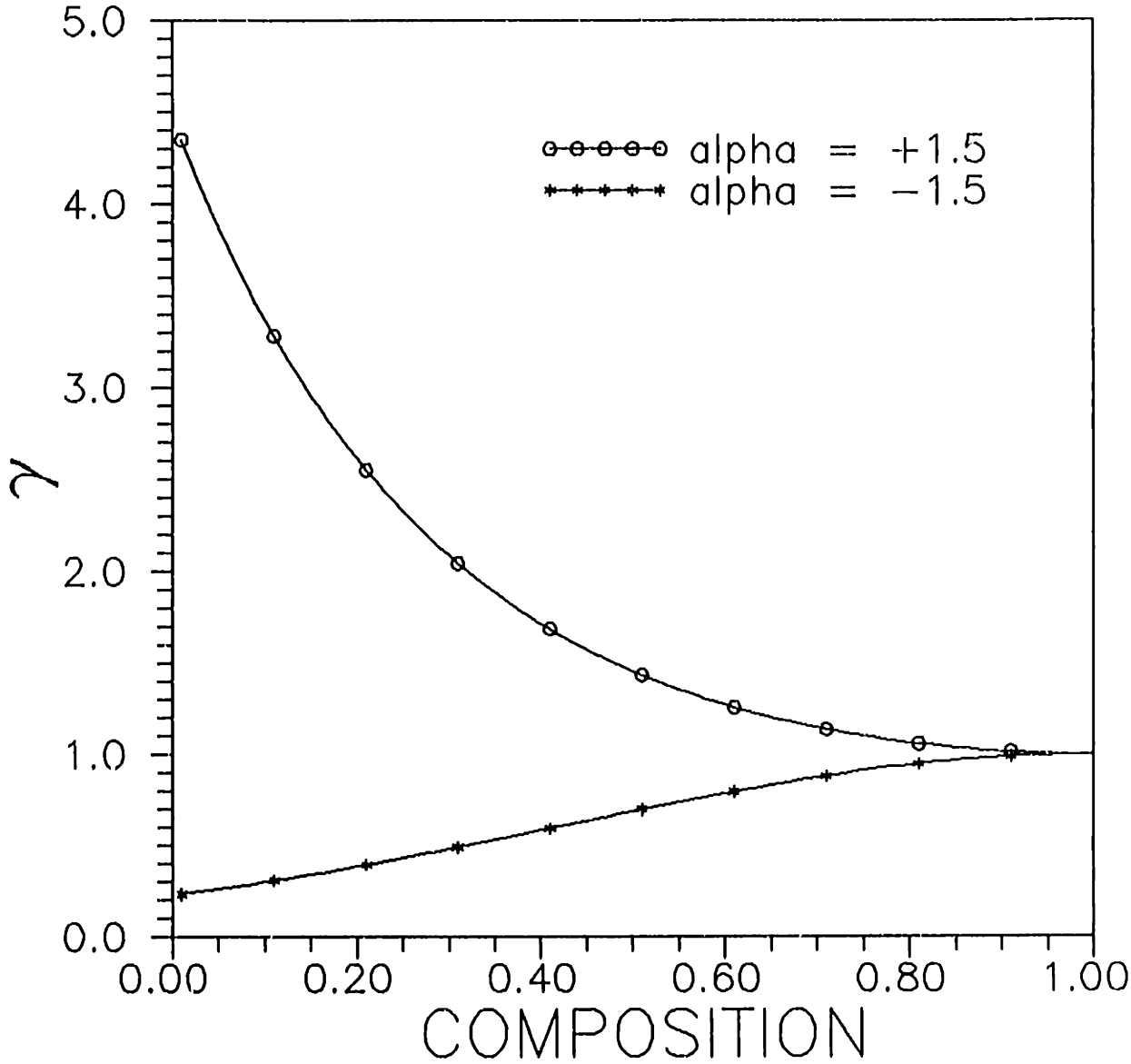

Figure 1. γ-c curves for regular solutions as a function of composition for two values of the regular solution parameter: α +1.5 and α −1.5.

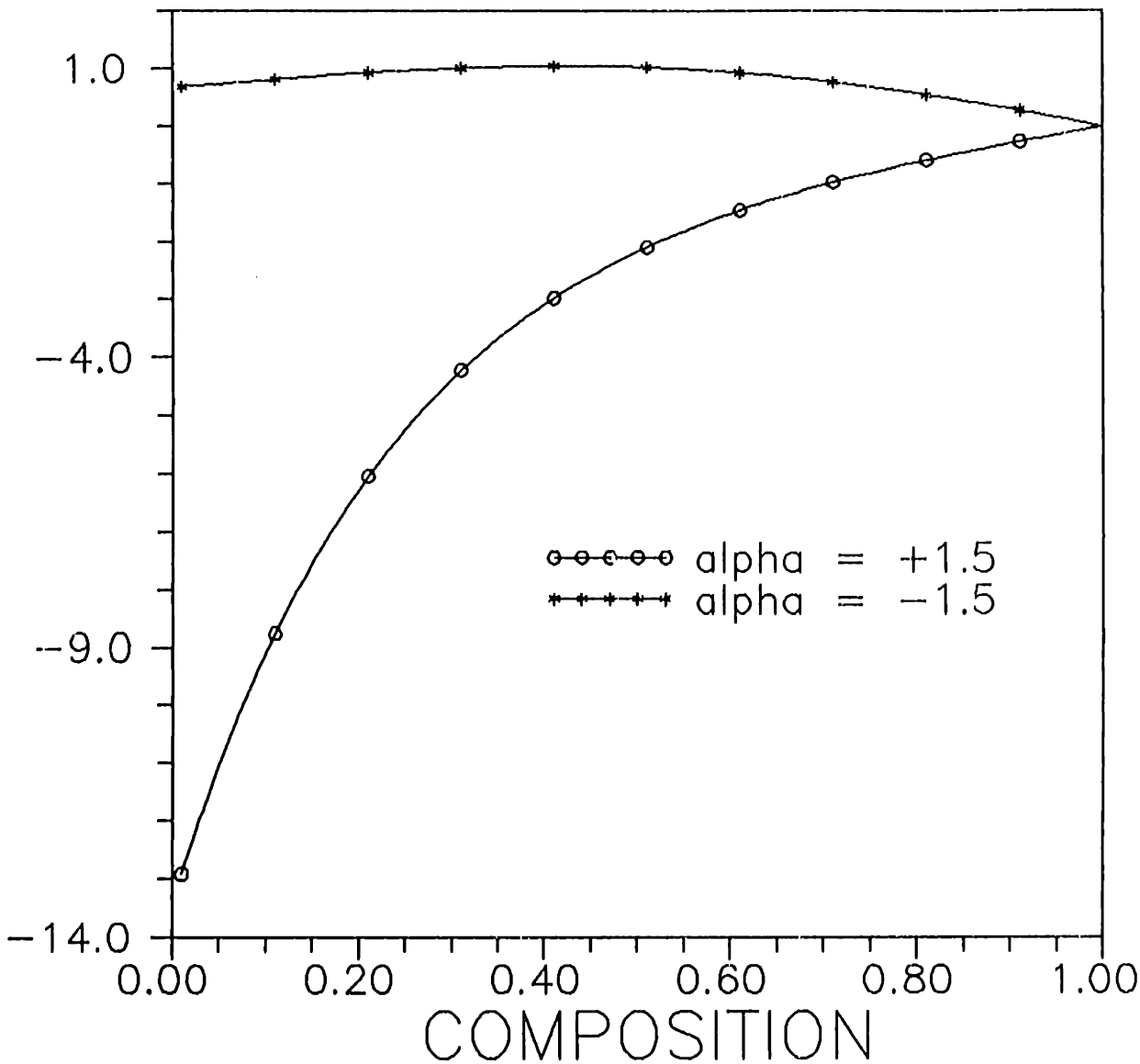

Figure 2. $(d\gamma/dc)-c$ curves for regular solutions as a function of composition for two values of the regular solution parameter: α +1.5 and α −1.5.

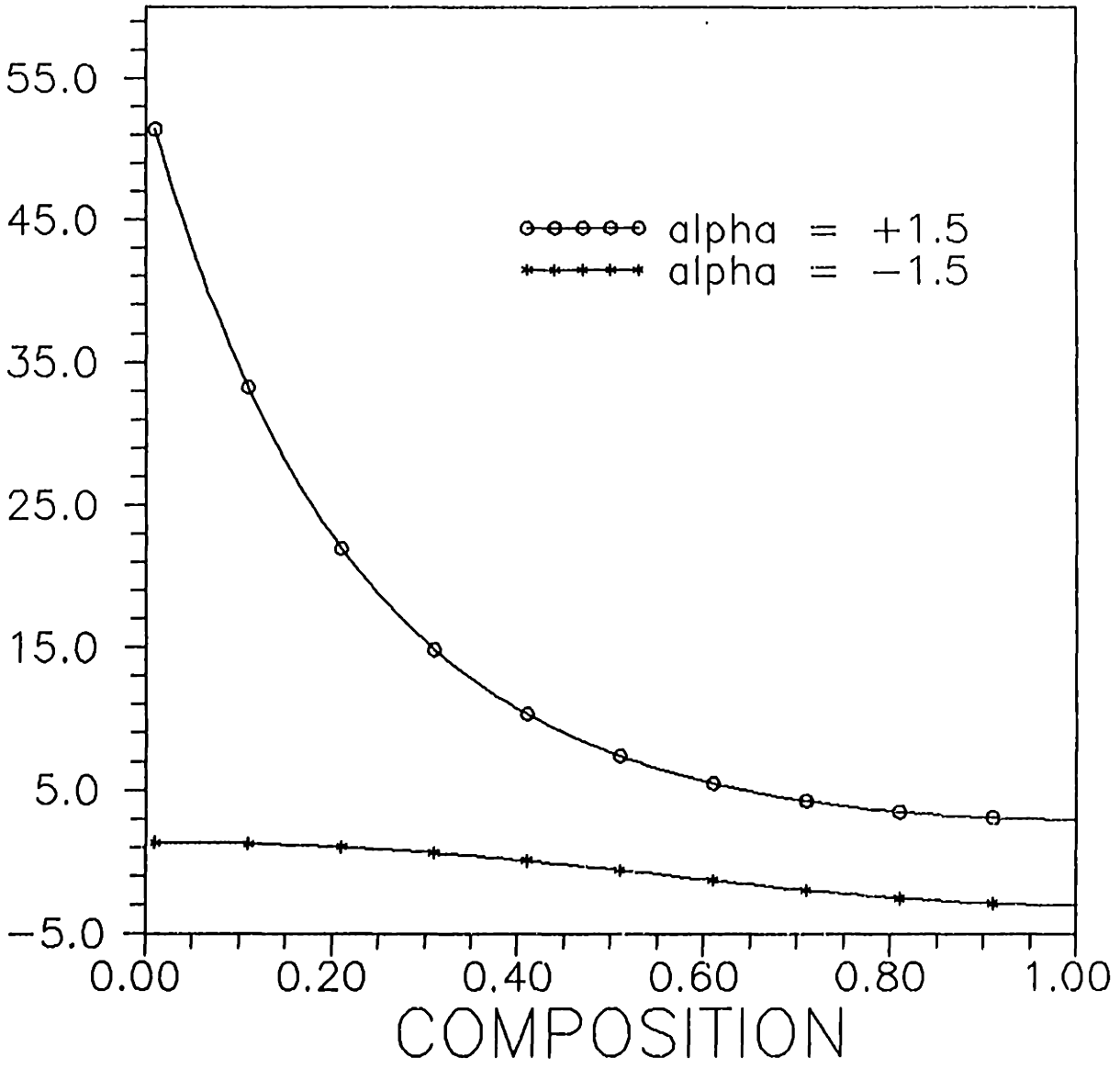

Figure 3. $(d^2\gamma/dc^2)$ - c curves for regular solutions as a function of composition for two values of the regular solution parameter: α + 1.5 and α - 1.5.

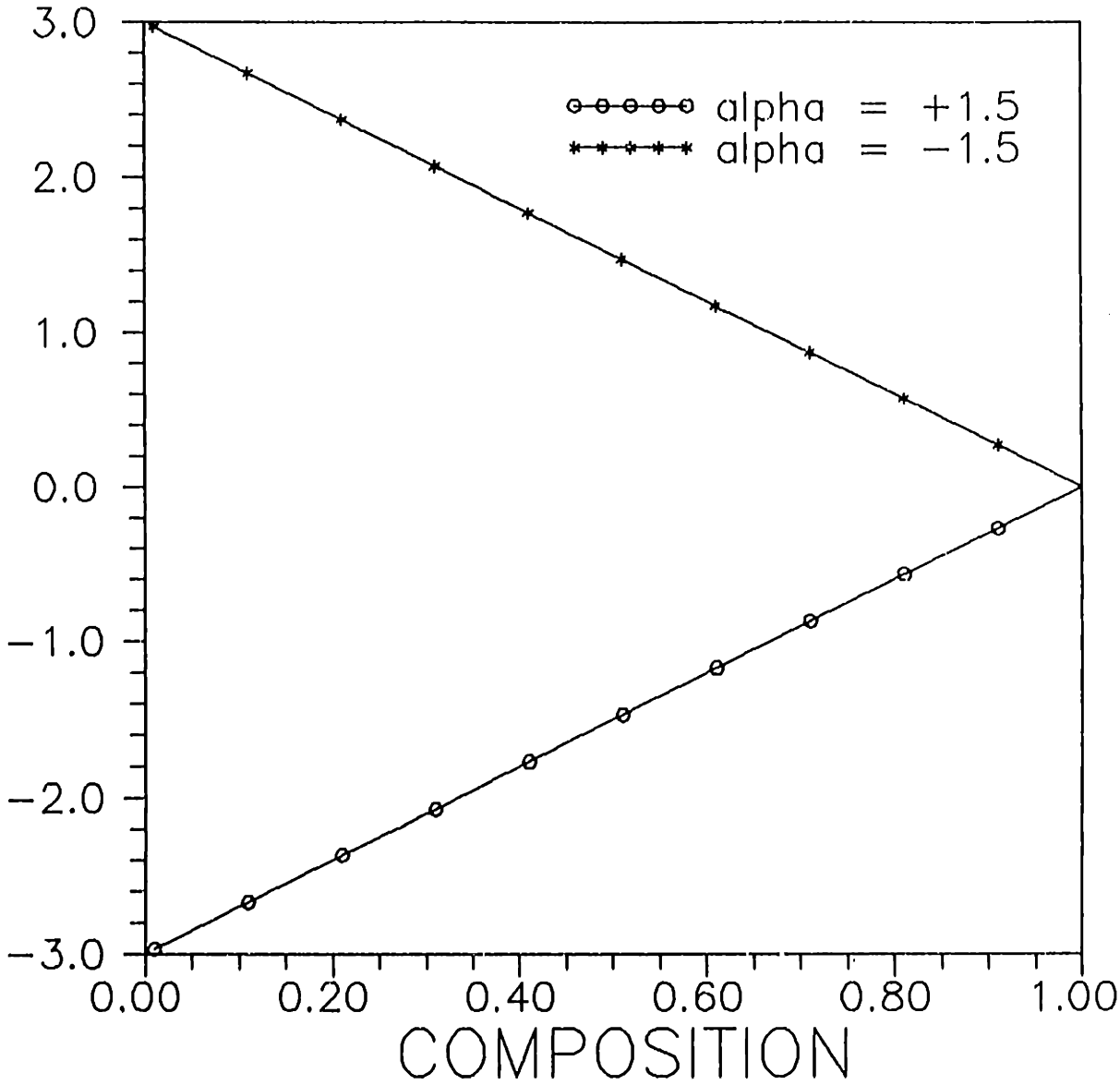

Figure 4. $(1/\gamma)(d\gamma/dc)$ - c curves for regular solutions as a function of composition for two values of the regular solution parameter: α + 1.5 and α - 1.5.

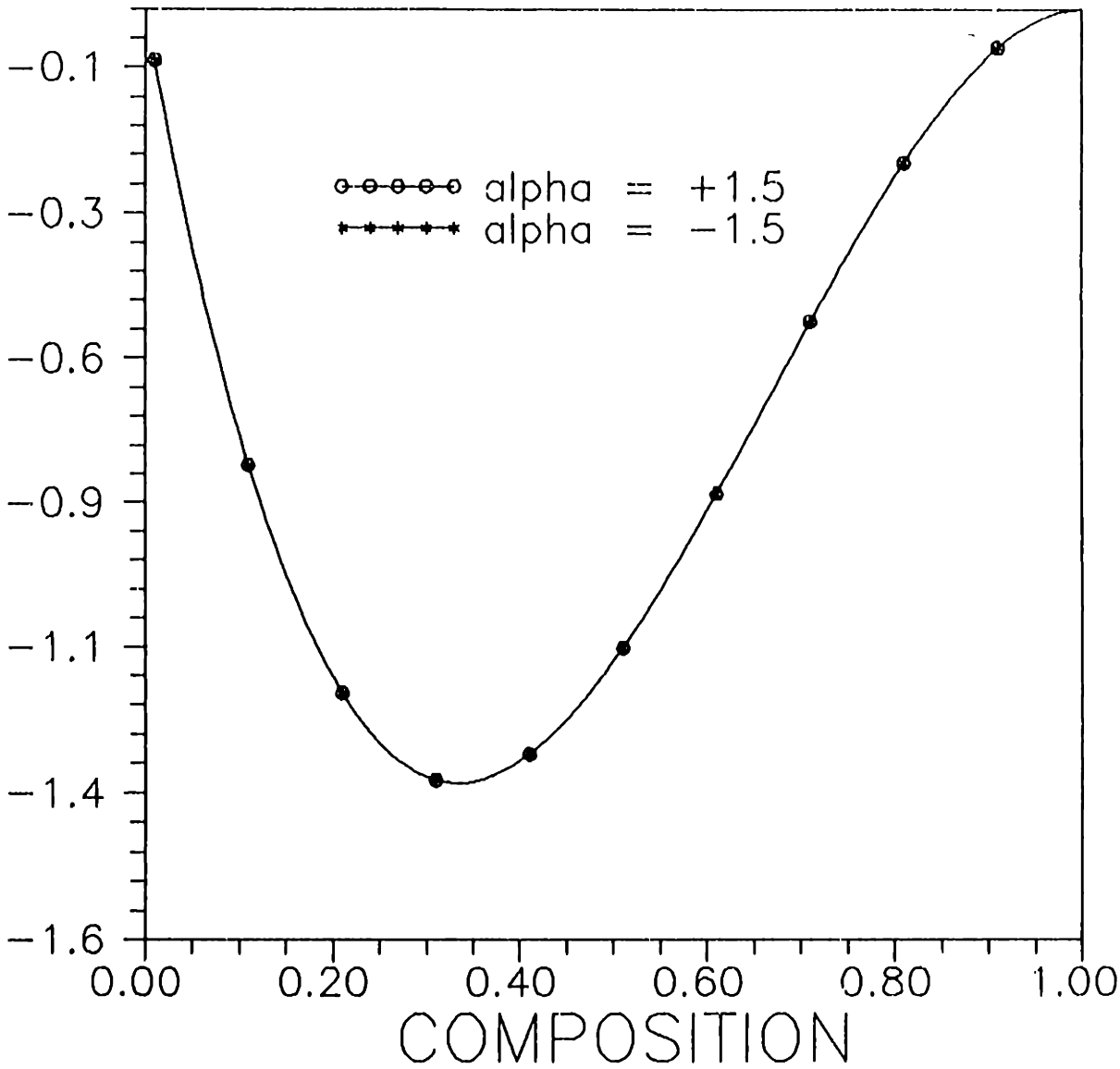

Figure 5. $(-c/\gamma^2)(d\gamma/dc)^2 - c$ curves for regular solutions as a function of composition for two values of the regular solution parameter: α + 1.5 and α − 1.5.

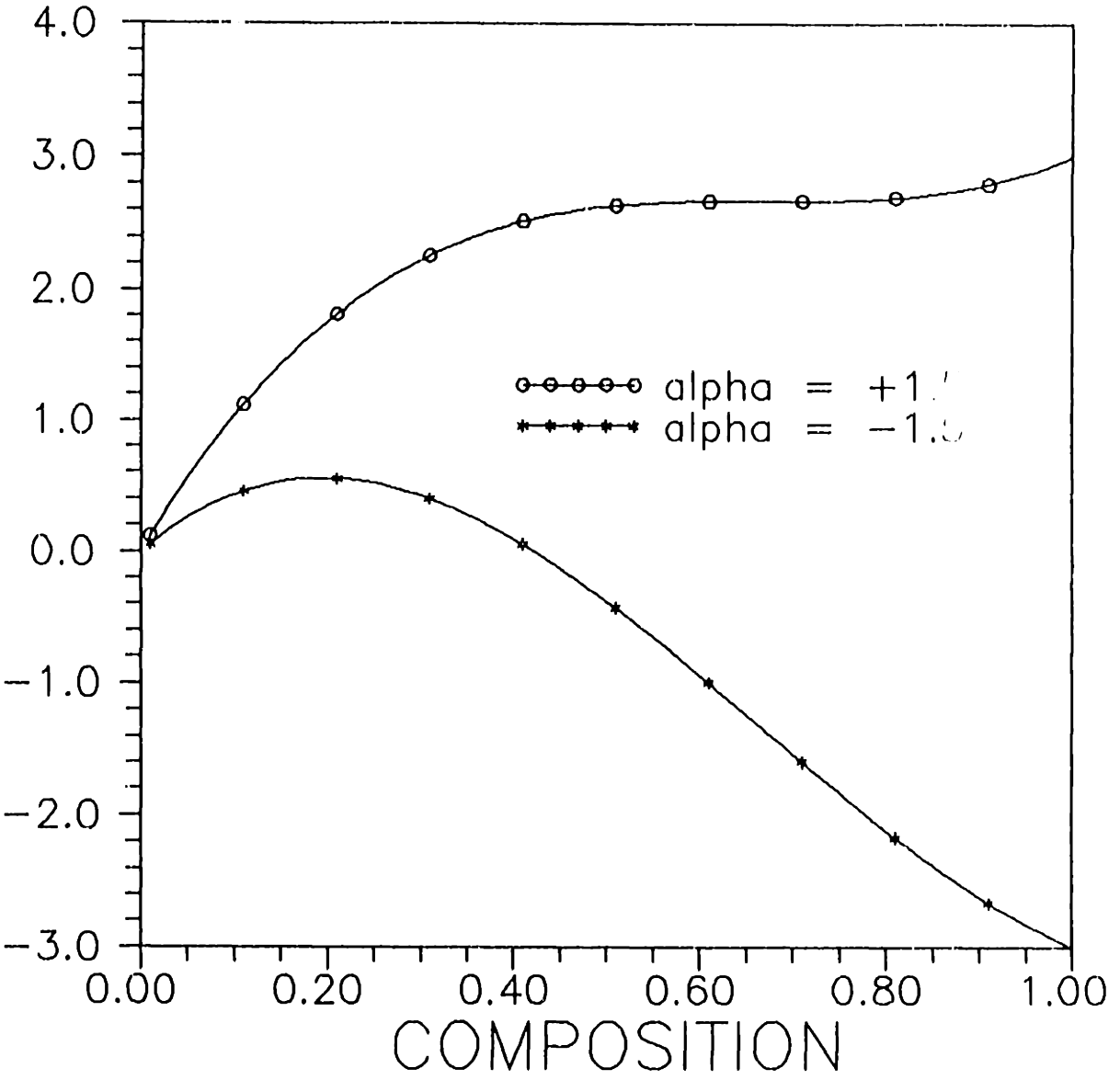

Figure 6. $(c/\gamma)(d^2\gamma/dc^2)-c$ curves for regular solutions as a function of composition for two values of the regular solution parameter: α +1.5 and α −1.5.

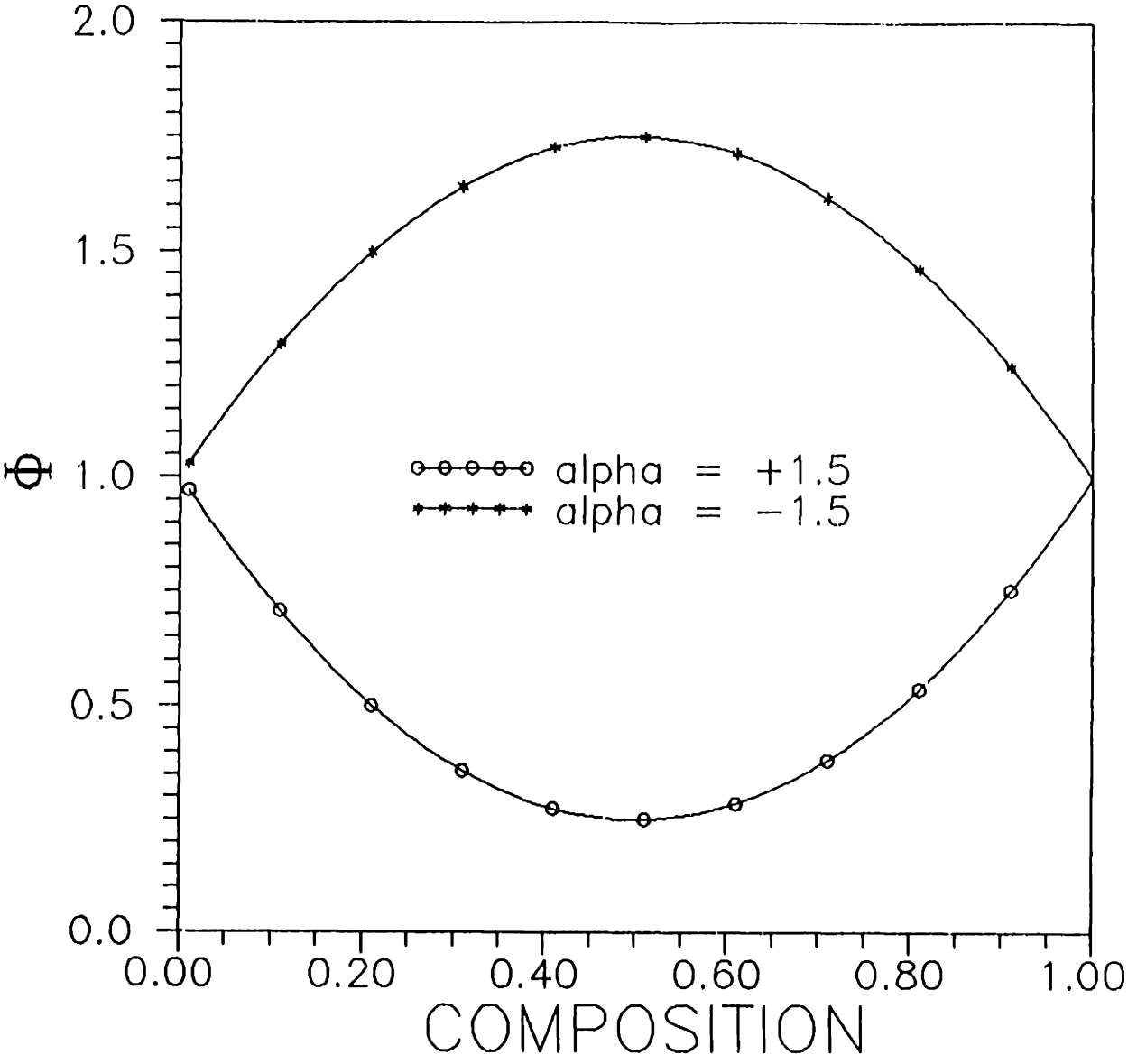

Figure 7. $\Phi(c) - c$ curves for regular solutions as a function of composition for various values of the regular solution parameter α. Note the non zero slope at either end of the curves for all curves except $\alpha = 0$ which is the degenerate case of an ideal alloy.

Biographical Note

The author was born on July 29, 1964 in Amritsar, India, to Saroj and Ramesh Chander Kapoor. He attended elementary school in the state of Punjab and later in the state of Jammu & Kashmir before moving to Bombay in 1972. After completing his secondary schooling in June 1979, from H. M. Public School he joined Mithibai Junior college for his higher secondary education in science which he completed in June 1981.

In August 1981, the author commenced his undergraduate education in metallurgical engineering at the Indian Institute of Technology (IIT), Bombay. As part of his degree requirements he spent the summer of 1984 as an engineer in training at an integrated steel plant (Tata Iron and Steel Co., India). Subsequently, he worked in a similar capacity at the heat treatment shop of an automotive plant (Mahindra and Mahindra, India). These experiences added an important practical dimension to his classroom knowledge of metallurgy. His bachelor's thesis entitled "Ferrous Powders From Machine Turnings" explored the possibility of recycling mild steel scrap for powder metallurgy applications. While at IIT, he was an active member of the mountaineering and rock climbing club. In the summer of 1983 he completed a full time course in basic mountaineering skills.

In fall 1985, the author was admitted to the Department of Materials Science and Engineering, MIT, as a graduate student under the guidance of Prof. T. W. Eagar. His masters thesis dealt with the design of brazing alloys for joining ceramics to metals. Upon completion of his masters thesis, in June 1987, he commenced work on his doctoral thesis under the guidance of Prof. T. W. Eagar. He was simultaneously engaged in research on joining of composite materials, low temperature bonding of silicon for electronic packaging applications and on oxidation behavior of brazing alloys.

Following graduation, the author intends to pursue a career in academia focussing on dissimilar materials interfaces with special emphasis on the thermodynamics and kinetics of interfaces.

The author is a member of the American Society for Metals, the Metallurgical society of A.I.M.E., American Welding Society, American Ceramic Society, Indian Institute of Metals and Sigma Xi.